

SEISMIC ISOLATION OF FOUNDATIONS
BY COMPOSITE LINERS

A THESIS SUBMITTED TO
THE GRADUATE SCHOOL OF NATURAL AND APPLIED SCIENCES
OF
MIDDLE EAST TECHNICAL UNIVERSITY

BY

VOLKAN KALPAKCI

IN PARTIAL FULFILLMENT OF THE REQUIREMENTS
FOR
THE DEGREE OF DOCTOR OF PHILOSOPHY
IN
CIVIL ENGINEERING

FEBRUARY 2013

Approval of the thesis:

SEISMIC ISOLATION OF FOUNDATIONS BY COMPOSITE LINERS

submitted by **VOLKAN KALPAKCI** in partial fulfillment of the requirements for the degree of
Doctor of Philosophy in Civil Engineering Department, Middle East Technical University by,

Prof. Dr. Canan ÖZGEN
Dean, Graduate School of **Natural and Applied Sciences**

Prof. Dr. Ahmet Cevdet Yalçiner
Head of Department, **Civil Engineering**

Prof. Dr. M. Yener ÖZKAN
Supervisor, **Civil Engineering Dept., METU**

Examining Committee Members:

Prof. Dr. Orhan EROL
Civil Engineering Dept., METU

Prof. Dr. M. Yener ÖZKAN
Civil Engineering Dept., METU

Prof. Dr. K. Önder ÇETİN
Civil Engineering Dept., METU

Prof. Dr. Tamer TOPAL
Geological Engineering Dept., METU

Assoc. Prof. Dr. S. Oğuzhan AKBAŞ
Civil Engineering Dept., GU

Date:

I hereby declare that all information in this document has been obtained and presented in accordance with academic rules and ethical conduct. I also declare that, as required by these rules and conduct, I have fully cited and referenced all material and results that are not original to this work.

Name, Last Name : Volkan KALPAKCI

Signature :

ABSTRACT

SEISMIC ISOLATION OF FOUNDATIONS BY COMPOSITE LINERS

Kalpakcı, Volkan
Ph.D., Department of Civil Engineering
Supervisor: Prof. Dr. M. Yener ÖZKAN

February 2013, 188 pages

In this research, the dynamic behavior of a seismic isolation system composed of high strength geotextile placed over an ultra-high molecular weight polyethylene (UHMWPE) geomembrane (together called as composite liner) beneath the structure is investigated experimentally. The results of the shaking table experiments which were performed on model structures both under harmonic and modified earthquake motions with and without the seismic isolation (composite liner system), are presented in the thesis. The main focus is given on the potential improvement obtained by use of the composite liner system as compared to the unisolated cases. Based on the performed experiments, it is observed that the utilization of composite liner system provides significant reduction in the accelerations and interstorey drift ratios of structures under harmonic motions while significant drop is obtained in the spectral accelerations under earthquake motions which provide noticeable improvement in the durability of structures under dynamic effects at the expense of increased translational displacements.

Keywords: Seismic isolation, earthquake, shaking table, geotextile, geomembrane

ÖZ

TEMELLERİN KOMPOZİT SİSTEMLER İLE SİSMİK İZOLASYONU

Kalpakkı, Volkan
Doktora, İnşaat Mühendisliği Bölümü
Tez Yöneticisi: Prof. Dr. M. Yener ÖZKAN

Şubat 2013, 188 sayfa

Bu çalışmada, yapı altında yüksek dayanımlı geotekstil malzemenin ultra yüksek moleküler ağırlıklı polietilen esaslı geomembran (UHMWPE) üzerine yerleştirilmesi ile oluşturulan bir sismik izolasyon sisteminin (kompozit sistem) dinamik davranışı incelenmiştir. Tez içerisinde, bahsi geçen sismik izolasyon sisteminin kullanıldığı ve kullanılmadığı durumlar için model binalar üzerinde harmonik ve uyarlanmış deprem hareketleri altında yapılan sarsma tablası deney sonuçları sunulmuştur. Bu sistemin kullanılması durumunda, kullanılmadığı duruma göre elde edilecek iyileştirme çalışmanın odak noktasını teşkil etmektedir. Deney sonuçlarına göre, test edilen sismik izolasyon sisteminin kullanılması durumunda harmonik taban hareketi altında yapıya gelen ivmelerin büyük oranda düştüğü ve görelî kat öteleme oranlarının ciddi miktarda azaldığı tespit edilmiştir. Diğer taraftan deprem hareketleri altında spektral ivmelerin önemli ölçüde düştüğü gözlemlenmiştir. Bu durum yapıların dinamik etkiler altındaki güvenilirliğini, yapının yatayda deplasman yapması karşılığında, önemli oranda artırmaktadır.

Anahtar Kelimeler: Sismik izolasyon, deprem, sarsma tablası, geotekstil, geomembran

To My Family...

ACKNOWLEDGEMENTS

The author wishes to express his sincere appreciation to his precious supervisor
Prof. Dr. M. Yener ÖZKAN
for his guidance, advice and encouragements throughout the research.

Prof. Dr. K. Önder ÇETİN
is sincerely acknowledged for his valuable support and contributions.

Mr. Alkut AYTUN
is sincerely appreciated for his technical contributions and efforts during the modification of the
shaking table used for the experiments of this study.

The author would like to specially thank
Prof. Dr. Mete ERDEMGİL
for his financial support in establishment of the experimental setup.

TÜBİTAK
is appreciated for the scholarship provided to the author during the research.

Finally, the author is grateful for the continuous support and encouragement
he has received from his family.

TABLE OF CONTENTS

ABSTRACT	v
ÖZ	vi
ACKNOWLEDGEMENTS	viii
CHAPTERS	
1. INTRODUCTION.....	1
2. LITERATURE REVIEW.....	3
2.1 Mechanical Seismic Isolators	3
2.1.1 Passive Control Systems	3
2.1.1.1 Seismic Isolation Systems.....	4
2.1.1.2 Passive Energy Dissipation Systems.....	4
2.1.2 Active Control Systems	5
2.1.3 Hybrid Control Systems.....	6
2.2 Seismic Isolators for Developing Countries	6
2.2.1 Tire Chips as Seismic Isolators.....	6
2.2.2 Use of EPS Geofoam as Seismic Buffer	9
2.2.2.1 Basic Engineering Properties of EPS Geofoam	9
2.2.2.2 Dynamic Properties of EPS Geofoam.....	11
2.2.2.3 EPS Geofoam as Seismic Buffer	12
2.2.3 Low-cost elastomers as Seismic Isolators.....	13
2.2.4 Geosynthetics as Seismic Isolators	14
3. THE EXPERIMENTAL SETUP	27
3.1 The Shaking Table	27
3.2 The Models	34
3.3 The Measurement Devices.....	36
3.4 Test Setup	39
4. THE EXPERIMENTS AND RESULTS	45
4.1 Free Vibration Tests.....	45
4.2 Tests with Harmonic Motions.....	47
4.2.1 Harmonic Tests on 3-Storey Model	47
4.2.2 Harmonic Tests on 5-Storey Model	59
4.3 Tests with Modified Ground Motion Data.....	69
4.3.1 Tests on 3-Storey Model with Modified Base Motions	71
4.3.2 Tests on 5-Storey Model with Modified Base Motions	92
5. EVALUATIONS AND CONCLUSIONS	115
5.1 Evaluations Based on Harmonic Motion Tests.....	115
5.2 Evaluations Based on Random Motion Tests	116
5.2.1 Evaluations for 3-Storey Model.....	116
5.2.2 Evaluations for 5-Storey Model.....	117
5.2.3 Evaluations for Slip Displacements	118
5.3 Conclusions.....	119
5.3.1 Experiments with Harmonic Motions	119
5.3.2. Experiments with Random Motions.....	119
REFERENCES.....	121
APPENDICES	
A. SAMPLE INPUT MOTION	123
B. SIMILITUDE CALCULATIONS.....	125
C. RESPONSE and FOURIER AMPLITUDE SPECTRA OF ORIGINAL AND FILTERED STRONG MOTIONS.....	127
D. TIME HISTORIES OF UTILIZED RANDOM MOTIONS	133
E. REDUCTIONS IN MID-STOREY ACCELERATIONS FOR 3-STOREY MODEL	151

F. ACCELERATION TIME HISTORIES FOR BASE OF 3-STOREY MODEL FOR “FB” AND “IB” CONDITIONS	153
G. RESPONSE SPECTRA FOR 3-STOREY MODEL UNDER $D = 5\%$ DAMPING.....	159
H. REDUCTIONS IN MID-STOREY ACCELERATIONS FOR 5-STOREY MODEL	169
I. ACCELERATION TIME HISTORIES FOR BASE OF 5-STOREY MODEL FOR “FB” AND “IB” CONDITIONS	173
J. RESPONSE SPECTRA FOR 5-STOREY MODEL UNDER $D = 5\%$ DAMPING.....	179
VITA.....	188

CHAPTER 1

INTRODUCTION

Today, earthquakes continue to be the most destructive disasters affecting millions of structures nearly all over the world every year. In order to provide safe living conditions, either buildings have to be designed to resist the destructive effects of earthquakes or these effects should be isolated by seismic isolators.

There are various types of seismic isolators which involve special production and installation processes. Since such applications are costly and require special staff and equipment, their use has not become a widely used practice in our country yet especially for residential and governmental (schools, hospitals, etc...) buildings are the structures that may be most responsible of loss of lives in case of collapse during an earthquake.

In this study, it is aimed to evaluate the behavior and efficiency of an easily applicable, low cost seismic isolation system which is composed of a high strength non-woven geotextile laid over an ultra-high molecular weight polyethylene (UHMWPE) geomembrane (together called as "composite liner system") which will be placed just beneath the structure. This system was studied by Yegian and Kadakal (2004) together with other options, by placing them under rigid blocks, and was evaluated to be the most stable option among others for different dynamic loading conditions, which is discussed in detail in the following chapter.

The available data in the literature about the behavior of this system were obtained by experiments on highly rigid models which had a significantly higher natural frequency " f_n " as compared to the predominant frequency " f " of the input motions. As a consequence, the results were independent of the input motion frequency. In this study, the focus is given on the behavior of this isolation system for the cases where the natural frequencies of the models are within a comparable range with the input motion frequencies. For this purpose, two models representing 3-storey and 5-storey structures were produced and accelerations at each storey level together with the base slip (for the isolated cases) were measured during the experiments. The effect of the composite liner system on model structures was investigated through shaking table tests both under harmonic and random motions. A total of 138 experiments were performed during the study. The results of these experiments are presented in a way that facilitates to evaluate the benefit of the use of the composite liner system in a comparative manner with respect to the unisolated case.

After a brief introduction in Chapter 1, a detailed literature review is presented in Chapter 2. The details of the physical modeling and the experimental setup are given in Chapter 3 and the results of the experiments are presented and discussed in Chapter 4. Finally, Chapter 5 includes the evaluations and the conclusions.

CHAPTER 2

LITERATURE REVIEW

Isolating the structures from the effects of the earthquake motion is not a new idea. There have been several attempts to achieve this goal since the beginning of the 20th century. To illustrate, German engineer J. Bechtold had suggested (Bechtold, 1907) to form a foundation filled with rounded granular material (Fig. 2.1) to design an earthquake proof building. Glicksberg (1973) and Mizuno (2000) were other examples of interesting attempts in this field.

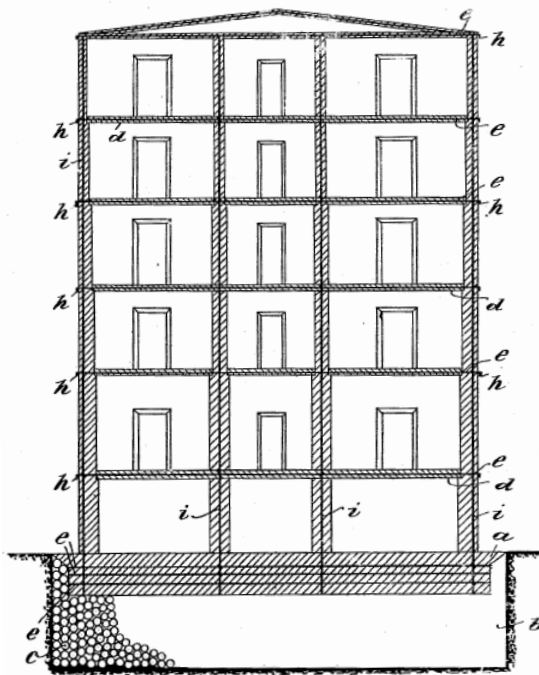


Fig. 2.1 Earthquake proof building (Bechtold, 1907)

Since that time there have been major developments in seismic isolation and several types of seismic isolators have been developed in order to protect structures from the destructive effects of the earthquakes. Some of the recent studies about seismic isolators can be listed as Jangid (2008), Wu et al. (2008), Sharma and Jangid (2009), Bucher (2009), Yuan (2009), Besa et al. (2010). The seismic response of base-isolated buildings together with the seismic soil-structure interactions were also studied by several researchers. Some recent findings about this topic can be founded in Stewart et al. (1999:I-II) and Spyrakos et al. (2009). These seismic isolators can be broadly categorized into three groups named as passive, active and hybrid control systems (USACE, 2005).

2.1 Mechanical Seismic Isolators

2.1.1 Passive Control Systems

These systems are called passive control systems since they do not require additional energy to operate and are simply activated by earthquake motion. These systems are designed to dissipate a

large portion of the earthquake energy in special devices or at specially designed connection details. They can be investigated in two categories:

2.1.1.1 Seismic Isolation Systems

These systems are used to decouple the ground motion and prevent the structure from absorbing the earthquake energy. The entire superstructure should lie on discrete isolators where the earthquake energy is dissipated through displacement of these isolators (together with damping for some special devices). The superstructures isolated with this system behave more like a rigid body. An example of a seismic isolation application is given in Fig. 2.2.



Fig. 2.2 Seismic isolation by mechanical devices

2.1.1.2 Passive Energy Dissipation Systems

It is aimed to provide additional damping to the structure in this type of systems by which the structural response to the earthquake motions is significantly reduced. This may be achieved through the use of viscous dampers like viscoelastic dampers, hydraulic dampers or lead extrusion systems or by hysteretic dampers like metallic yielding or shape-memory alloy devices. When this system is used, much of the earthquake energy will be damped by deformations concentrated in the energy dissipation devices. A structure isolated by hydraulic dampers is shown in Fig. 2.3.



Fig. 2.3 A structure isolated by hydraulic dampers

2.1.2 Active Control Systems

This type of systems protects the structure from the destructive effects of the earthquakes by imposing forces on the structure to counter-balance the earthquake induced forces. These systems are “active” systems since they require an energy source and computer-controlled actuators to operate special braces and/or tuned mass dampers. This technique is utilized in one of the highest buildings on earth, Taipei 101, constructed in Taiwan. A schematic explanation of the application is given in Fig. 2.4 with the picture of the used weight to counter-balance the earthquake induced forces in Fig. 2.5.

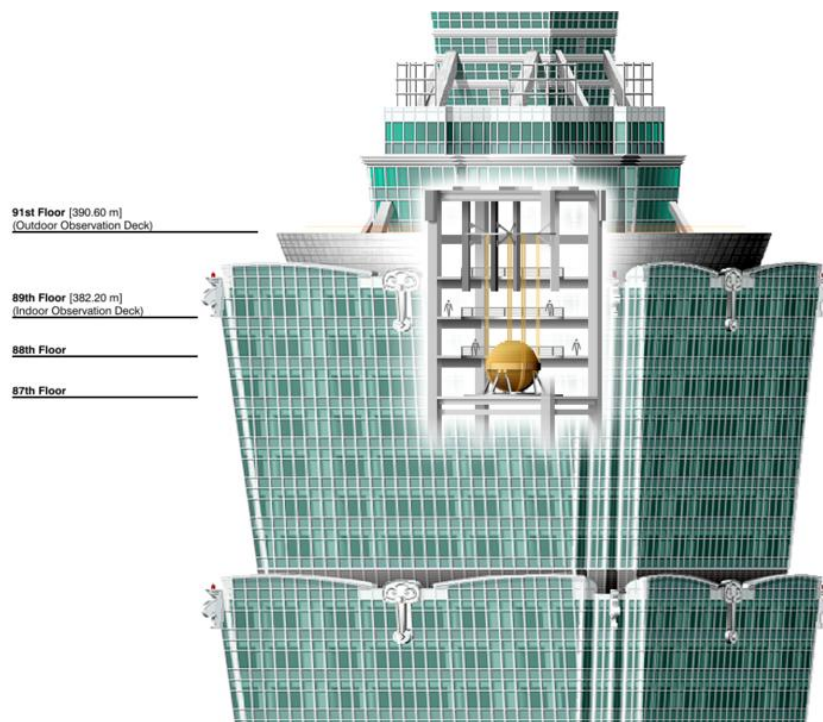


Fig. 2.4 Active system used in Taipei 101

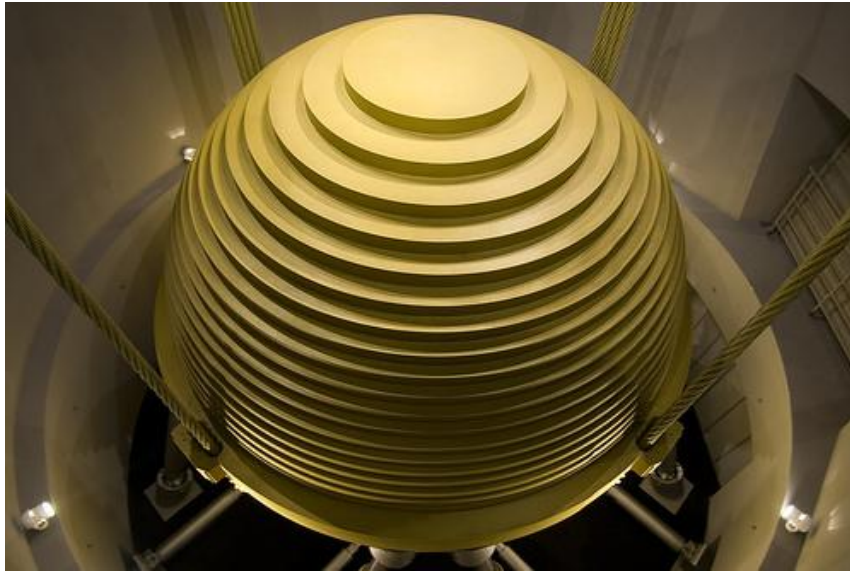


Fig. 2.5 “Golden Globe” of Taipei 101

2.1.3 Hybrid Control Systems

These systems are combined systems which uses passive and active systems together. They are, in general, more reliable and less expensive when compared to the active systems.

2.2 Seismic Isolators for Developing Countries

As mentioned in the previous part, the mechanical isolators are costly investments since they are special productions and require special staff and equipment for installation. Because of this fact, these systems are not being used in regular buildings especially in developing countries. However, such buildings compose most of the structures under collapse risk during an earthquake in such countries. So, many researchers have attempted to develop alternative, less costly and easily applicable seismic isolation systems. In this part some recent examples of these innovative seismic isolation systems will be described.

2.2.1 Tire Chips as Seismic Isolators

As the number of vehicles on earth has enormously increased during the past few decades, the tire consumption has also increased dramatically. Today, 2 billion scrap tires are stocked just in the United States with a growing rate of 200 – 250 million per year. Since the disposal of scrap tires has become a severe problem, there has grown a trend of searching for methods in which these scrap tires are used during the past decade. Due to the shape and size of the scrap tires it did not seem logical to the researchers to use it as a whole but rather they had chosen to shred the tires into smaller pieces which are called “tire chips” (Fig. 2.6). Today, tire chips are used in a wide range of engineering applications such as lightweight backfill material behind earth-retaining structures or as a noise absorber in motorways when being mixed with asphalt.



Fig. 2.6 Tire chips

The size of the tire chips usually ranges between 25mmx50mm to 100mmx450mm with the most common size 50mm*75mm. The index and engineering properties of the tire chips are studied by various researchers and still there are studies conducted in this area. However, among others the study of Edil and Bosscher (1994) gives a more detailed and fundamental knowledge about the engineering properties of the tire chips-soil mixtures for different mixing ratios. Among the data given in the cited study, the most important one is the compression behavior of the tire chips-soil mixtures under cyclic loading for the purpose of seismic isolation.

In Edil and Bosscher (1994) it was stated that, tire chips are highly compressive because of their high porosity and high rubber content. Under cyclic loading, most of the plastic deformation occurs in the first cycle and the rate of plastic strain accumulation decreases at each load cycle without a significant change in the ultimate strain corresponding to the ultimate stress (Fig. 2.7). On the other hand, it is important to note that mixing tire chips with sand does not improve the compression behavior of the mixture with respect to the pure tire chips case until the percent sand by volume in the mixture has reached about 50% (Fig. 2.8).

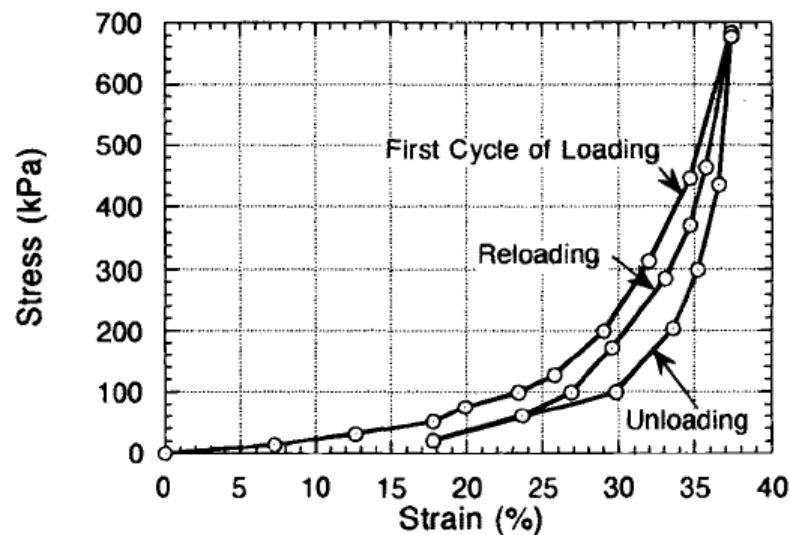


Fig. 2.7 Stress-strain behavior of pure tire chips under cyclic loading (Edil and Bosscher, 1994)

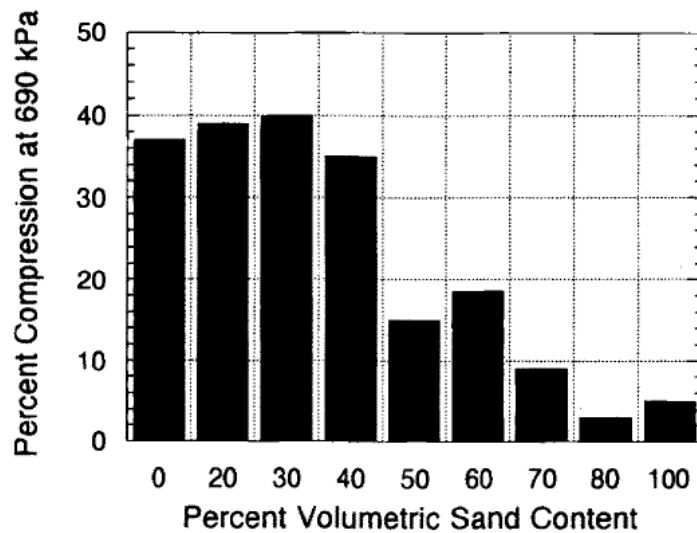


Fig. 2.8 Sand content vs. percent compression (Edil and Bosscher, 1994)

In a study by Tsang (2008) the usability of tire chips-soil mixtures for seismic isolation was investigated by performing numerical analyses. In the proposed scheme a 10-storey building having 40m. width was surrounded by a 10m. thick RSM (rubber-soil mixture) (Fig. 2.9).

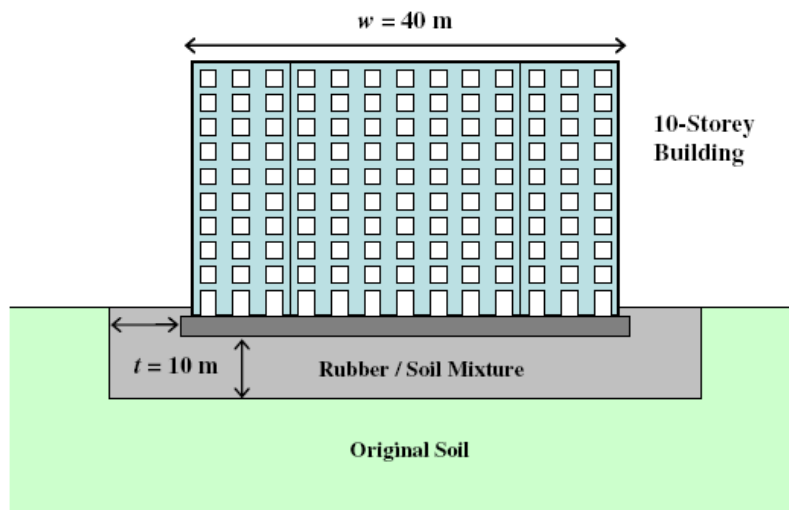


Fig. 2.9 The proposed scheme (Tsang, 2008)

The engineering properties of RSM75 (rubber-soil mixture containing 75% rubber by volume) were used in the analyses. In order to compare the results with the non-isolated case, the system was solved for the case that the building was founded on pure sand. The unit weight of the sand and RSM75 were taken as 17.4 kN/m^3 and 9.5 kN/m^3 , while the G_{\max} values were taken as 222 MPa and 7.5 MPa respectively. The degradation and increase in the damping of both pure sand and RSM75 were included in the analyses using the curves given in Fig. 2.10.a and Fig. 2.10.b respectively.

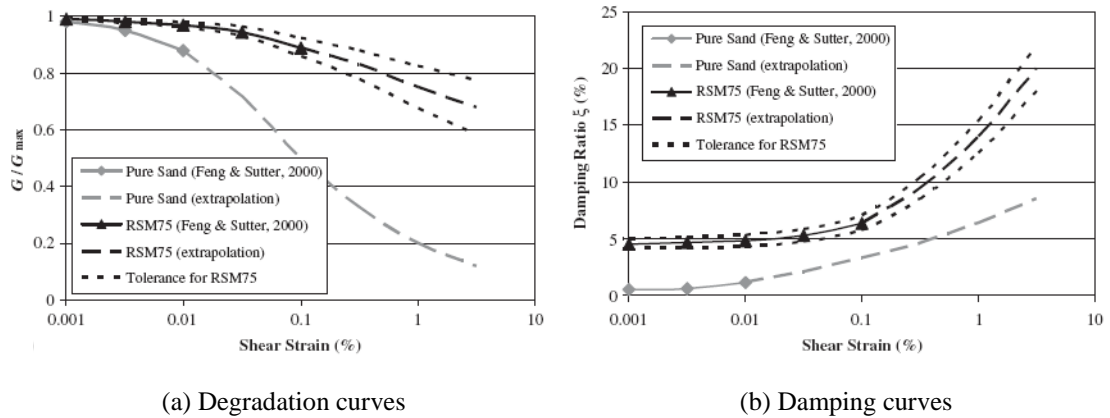


Fig. 2.10 Degradation and damping curves for tire-chips isolators (Tsang, 2008)

Then the system was analyzed by using the Northridge earthquake strong motion data as the input motion. The resulting horizontal and vertical accelerations for pure sand and RSM are given in Fig. 2.11.a and Fig. 2.11.b respectively. In the figures the accelerations were normalized with the absolute maximum ground acceleration of pure sand case. As it can be seen from the figures the horizontal and vertical accelerations were decreased by 80% and 90% on average respectively when a RSM layer is used for seismic isolation.

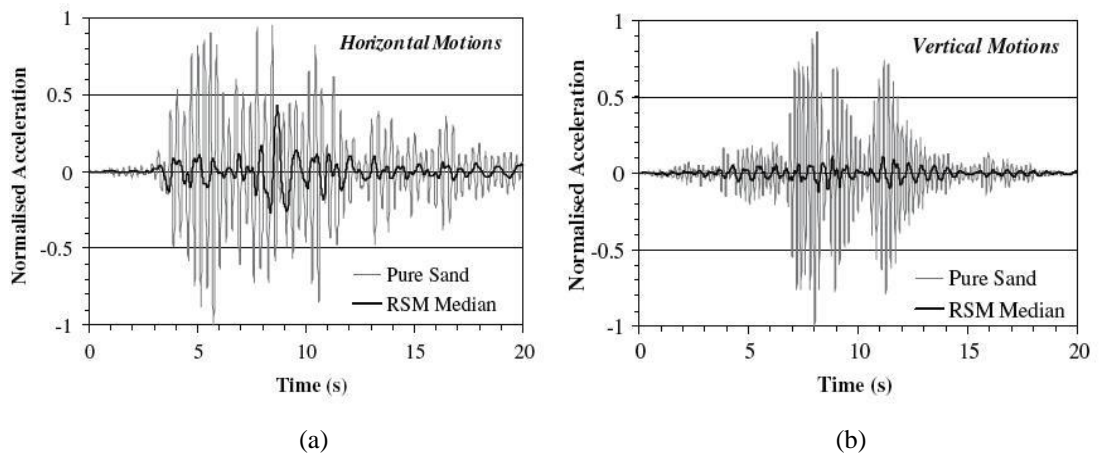


Fig. 2.11 Normalized (a) horizontal (b) vertical acceleration-time histories (Tsang, 2008)

2.2.2 Use of EPS Geofoam as Seismic Buffer

2.2.2.1 Basic Engineering Properties of EPS Geofoam

Expanded polystyrene (EPS) geofoam is a cellular plastic material that is strong but has very low density (1% of traditional earth materials). It is manufactured in block form in a range of densities and thicknesses. The main factor affecting the engineering properties of the geofoam is its density. As an example, Horvath (1995) had suggested the Eq. 2.1 to estimate the initial tangential modulus (ρ : density in kg/m^3 and E_{ti} : in MPa). The analysis and design methodologies for use of EPS geofoams as a compressible inclusion in order to reduce static forces was studied in detail in Horvath (1998). The alternatives studied in this study are revealed in Fig. 2.12.

$$E_{ti} = 0.45\rho^{-3} \quad (2.1)$$

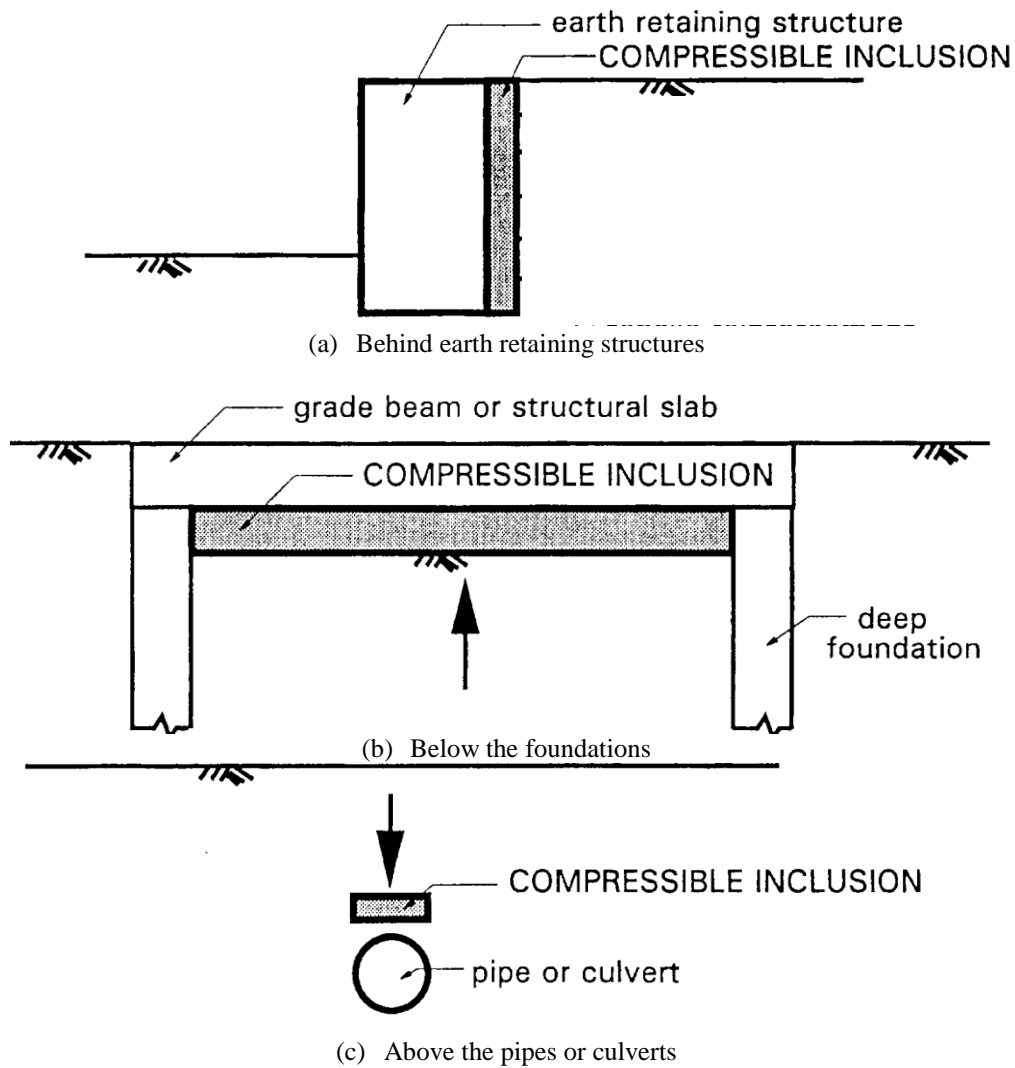


Fig. 2.12 Design alternatives for EPS Geofoam as compressible inclusion (Horvath, 1998)

The elastic modulus (E) of the geofoam decreases with increasing axial strain. Also, in Duškov (1997), it was found out that the axial strain rate did not significantly affect the strain dependency of elastic modulus (Fig. 2.13).

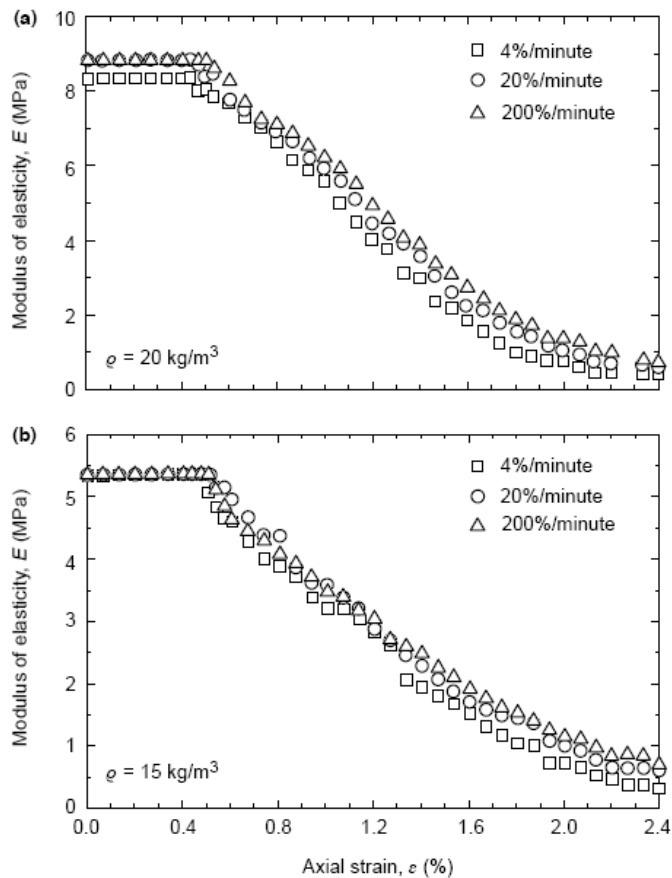


Fig. 2.13 Axial strain vs. E relationship for different axial strain rates and geofoam densities (Duškov, 1997)

2.2.2.2 Dynamic Properties of EPS Geofoam

The dynamic properties of EPS geofoam were studied in detail by Athanasopoulos et al. (1999). In their study, the researchers had performed resonant column and cyclic uni-axial tests for two different geofoam densities and obtained the degradation and damping curves for these geofoams.

According to the results of Athanasopoulos et al. (1999):

- The density of the geofoam has a considerable effect on the dynamic moduli (E_{dyn}) of the geofoam (moduli increase with increasing density). However, it has no appreciable effect on damping ratio.
- The loading frequency has practically no effect on the dynamic moduli values whereas the damping ratio increases significantly with decreasing loading frequency (Fig. 2.14).
- The amplitude of cyclic strain has a considerable effect on the elastic moduli and damping ratio values. The elastic moduli decreases with increasing strains (especially after 1% strain) while the damping ratio significantly increases (up to 15% for maximum strain level ($\approx 8\%$) applied).

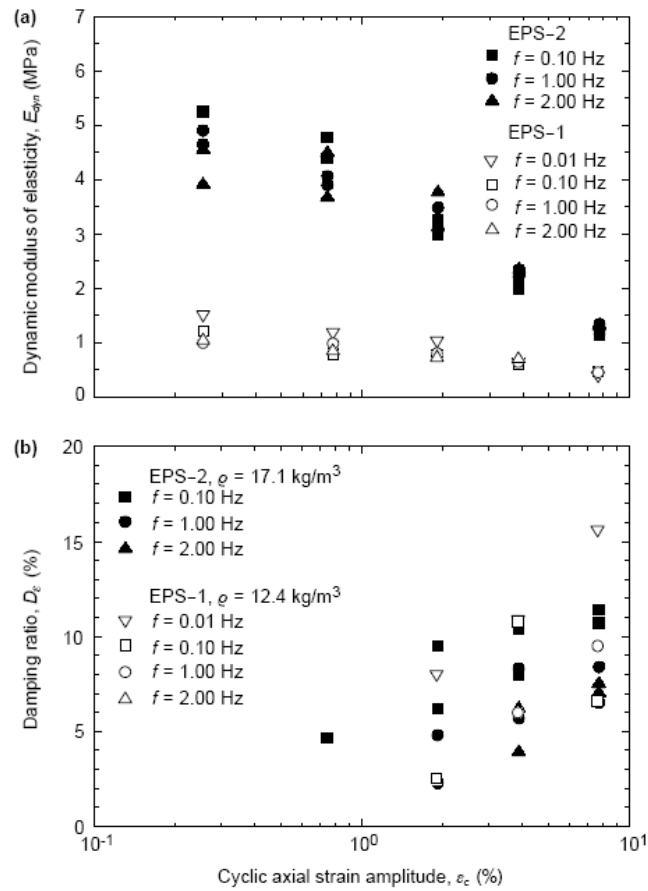


Fig. 2.14 ε_c vs. E_{dyn} and ε_c vs D_ε (Athanasopoulos et al., 1999)

2.2.2.3 EPS Geofoam as Seismic Buffer

The use of EPS geofoam blocks behind earth retaining structures in order to decrease the static earth pressures on the structure is a known method (Karpurapu and Bathurst, 1992) the application of which has increased over the past decade. However, the use of EPS geofoam for seismic load reduction is a relatively new topic which was studied by Bathurst et al. (2007) experimentally.

In the mentioned study, shaking table tests were performed for an earth retaining structure model, using geofoams of three different densities with the same thicknesses behind the wall. The experimental setup is demonstrated in Fig. 2.15.

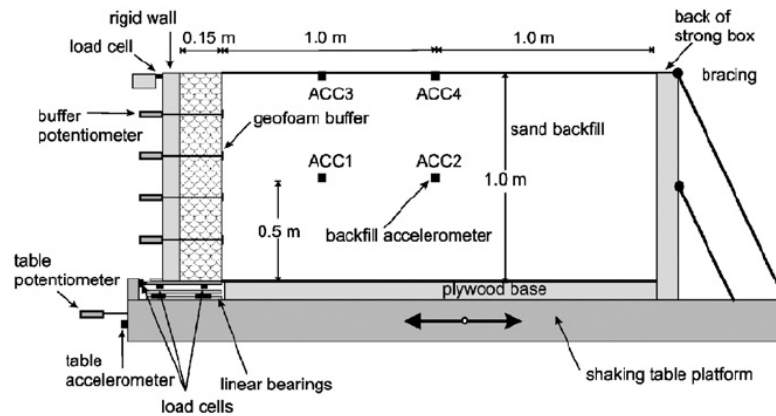


Fig. 2.15 Experimental Setup of Bathurst et al. (2007)

As a result, for a peak base acceleration of 0.7g, the seismic forces acting on the wall were reduced by 16, 20 and 31% for geofoam densities of 16, 14 and 6 kg/m³ respectively, with respect to the case without geofoam seismic buffer behind the wall (Fig. 2.16). Following this study, the response of EPS geofoam buffers under seismic effects were simulated by a simple displacement model by Bathurst et al. (2007).

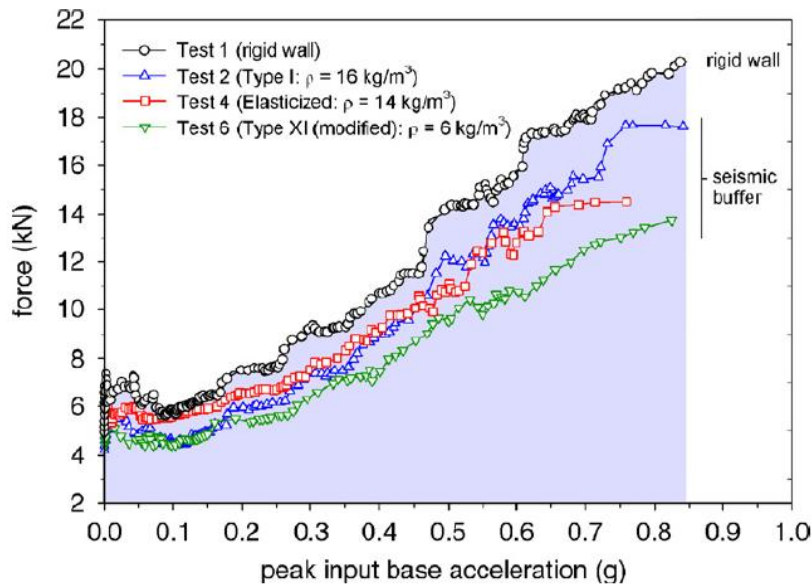


Fig. 2.16 Peak input base acc. vs. Force acting on the Wall (Bathurst et al., 2007)

2.2.3 Low-cost elastomers as Seismic Isolators

Fiber reinforced low-cost elastomers were used as seismic isolators in Kelly (2002). The behavior of low-cost elastomers was investigated both numerically and experimentally (Fig. 2.17). The elastomers were placed at the column-footing joints. According to the results of the study, significant improvements were achieved in the durability of the structures at the expense of increased lateral displacements concentrated at the installation point of the elastomers (Fig. 2.18).

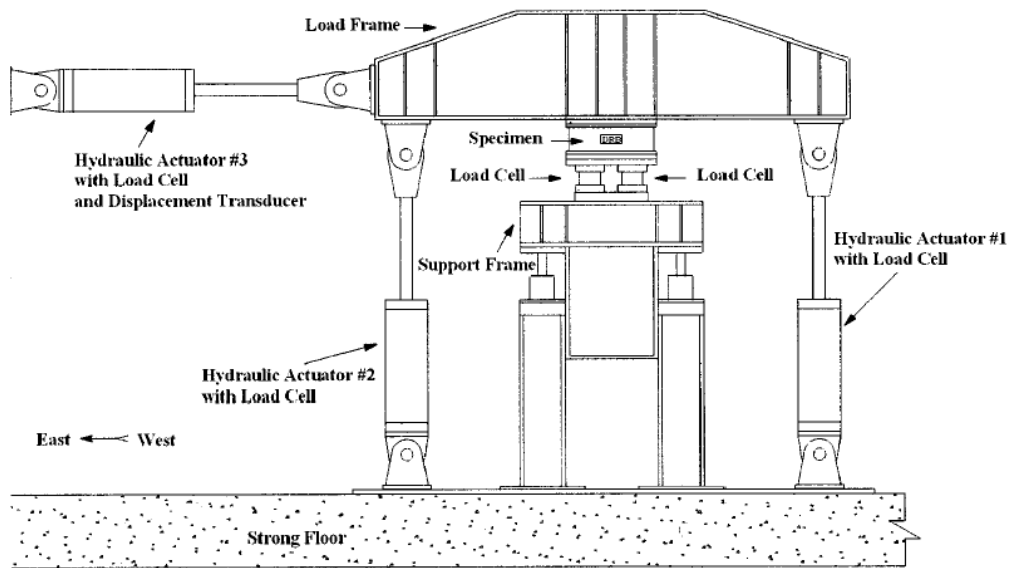


Fig. 2.17 The experimental setup in Kelly (2002)



Fig. 2.18 The elastomer seismic isolator at failure (Kelly, 2002)

2.2.4 Geosynthetics as Seismic Isolators

The idea in the use of geomembrane-geotextile layers as seismic isolators is to form a smooth layer beneath the structure by which some of the earthquake energy is dissipated through friction between these two materials while the rest is dissipated through allowed displacements.

For the use of this concept, at first the dynamic interface shear strength properties of geomembranes and geotextiles had to be studied which was investigated in detail through laboratory tests in Yegian and Lahlaf (1992) and Yegian et al. (1995). In these studies, shaking table tests were performed for different combinations of frequencies of table motion, table acceleration, normal stress and dry versus submerged conditions. In these tests, HDPE type

geomembrane and nonwoven, continuous filament, needlepunched geotextile were used. Eventually, the observed behavior was as follows:

- The liner transferred the applied acceleration directly to the structure until the induced force exceeded the shear strength of the liner interface. Upon that point the accelerations transferred to the structure slightly increased with increasing applied acceleration nearly independent of the frequency of the input motion. (see Fig. 2.19).
- The peak friction angle under dynamic loading was slightly larger than the one under static conditions. Moreover the residual friction angle of dynamic loading was nearly equal to peak angle of the static loading. Also, the friction angle of submerged condition was lower than the one measured for dry condition. The values can be compared through Table. 2.1 and Table. 2.2.

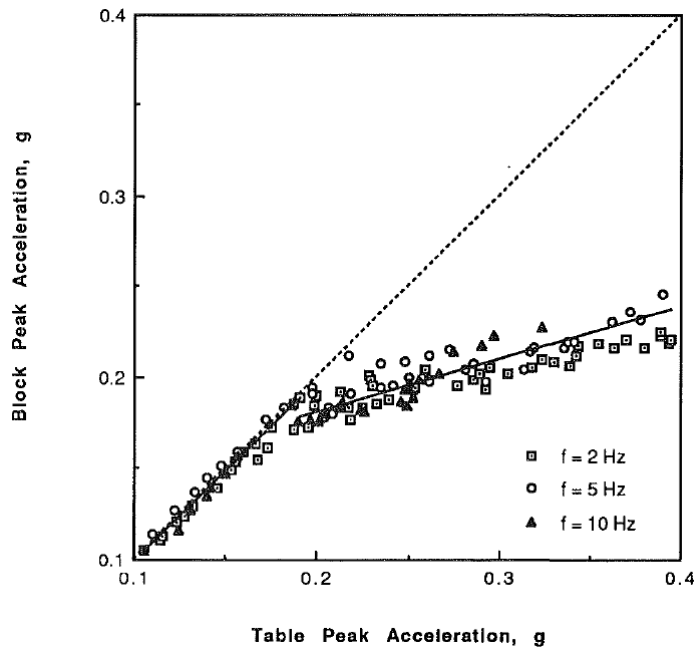


Fig. 2.19 Shaking table test results for geomembrane-geotextile interface, submerged condition, normal stress=8.5 kPa, $f=2,5,10$ Hz (Yegian and Lahlaf, 1992)

Table. 2.1 Dynamic friction angles (Yegian and Lahlaf, 1992)

Interface condition (1)	Acceleration transmitted to block at first observation of sliding (2)	Peak dynamic friction angle (3)	Acceleration transmitted to the block after sliding is initiated (4)	Residual dynamic friction angle (5)
Geomembrane ^a /geotextile ^b dry	0.2 g	11.3°	0.19 g ^c –.24 g ^d	10.7–13.5°
Geomembrane ^a /geotextile ^b submerged	0.19 g	10.7°	0.17 g ^c –.23 g ^d	9.6–13°

^aGundle HD60: hard, smooth HDPE.
^bPolyfelt TS700: Nonwoven, continuous filament, needlepunched geotextile.
^cAt first observation of sliding.
^dAt table acceleration of 0.4 g.

Table. 2.2 Static friction angles (Yegian and Lahlaf, 1992)

Interface condition (1)	Peak angle of friction ϕ (2)	$\tan \phi$ (3)	Residual angle of friction ϕ (4)	$\tan \phi$ (5)
Geomembrane ^a /geotextile ^b dry	10.7°	0.19	10.0°	0.18
Geomembrane ^a /geotextile ^b sub-merged	9.6°	0.17	8.5°	0.15

^aGundle HD60: hard, smooth HDPE.
^bPolyfelt TS700: Nonwoven, continuous filament, needlepunched geotextile.

After this research in which the fundamental dynamic characteristics of such systems were determined and their potential applicability for seismic isolation was verified, more detailed tests were needed on liners composed with different combinations of different types of geomembranes and geotextiles in order to determine the most suitable combination. Such an investigation was conducted by Yegian and Kadakal (2004). In this study, the structure was thought to be placed over a liner. (Fig. 2.20). At first the combination with minimum friction coefficient was determined since the minimum friction coefficient would provide the maximum reduction in the earthquake induced forces. The shaking table tests (Fig. 2.21) have revealed that the combination in which a nonwoven, high strength geotextile was placed over a ultra high molecular weight polyethylene (UHMWPE) led to the minimum friction coefficient (Table. 2.3).

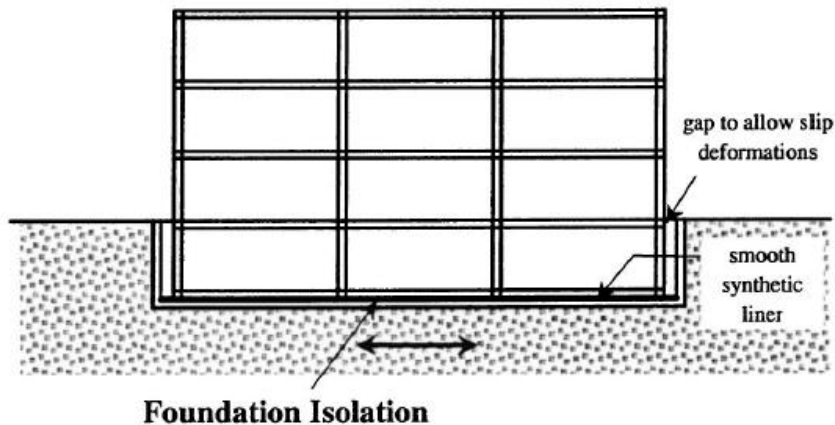


Fig. 2.20 Seismic isolation using smooth synthetic liner (Yegian and Kadakal, 2004)

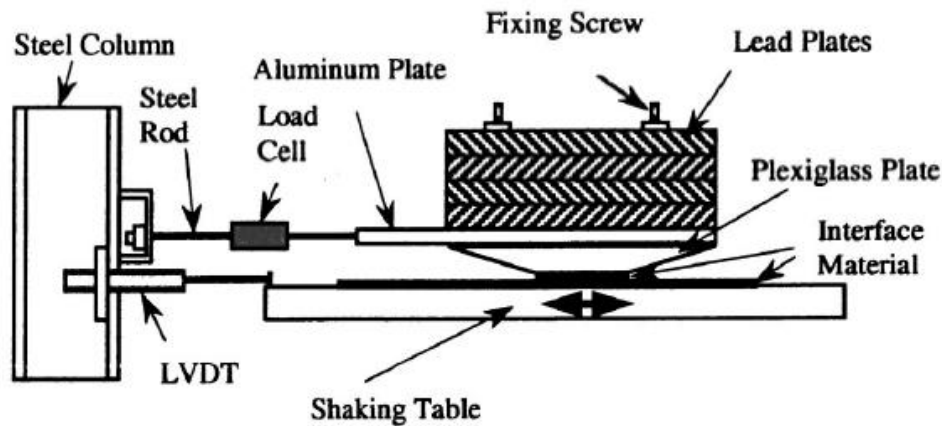


Fig. 2.21 Shaking table used in the experiments (Yegian and Kadakal, 2004)

Table 2.3 Friction coefficients for liner combinations (Yegian and Kadakal, 2004)

Interface	Description	Friction coefficient ^a
Geotextile/HDPE	A high-strength nonwoven geotextile, "Tyvar 3601" against 1.5 mm smooth HDPE (high density polyethylene)	0.15–0.3
PTFE/PTFE	Two sheets of 1.5 mm thickness PTFE (polypropylene)	0.08– 0.15
UHMWPE/UHMWPE	Two layers of 6.4 mm thick UHMWPE (ultrahigh molecular weight polyethylene) "TIVAR 88-2 AntiStatic"	0.09–0.25
Geotextile/UHMWPE	Tyvar 3601 geotextile against TIVAR 88-2, 6.4 mm thick UHMWPE	0.06–0.08

^aRange depends on number of cycles, normal stress, and sliding velocity.

Having a low friction coefficient was good but not enough for a liner to be applicable as a seismic isolation system. The liner had to reveal similar friction characteristics under different normal stresses, different number of cycles of loading and different sliding velocities to be reliable for use under different conditions. The results of the tests for each of the parameters listed above are given in Fig. 2.22, 2.23 and 2.24, respectively. As it can be seen from the figures, the only combination which was nearly independent of the all mentioned parameters together with the minimum friction coefficient was the one with nonwoven, high strength geotextile placed over a ultra high molecular weight polyethylene (UHMWPE). As a result, this combination was determined as the most suitable liner for seismic isolation.

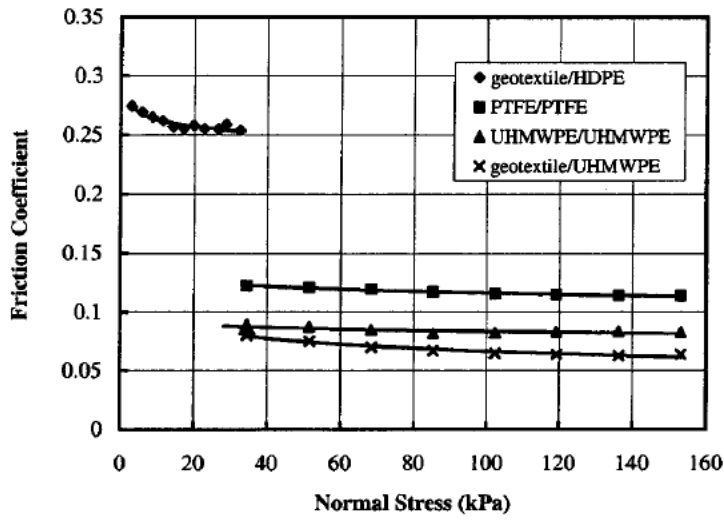


Fig. 2.22 Normal stress vs. friction coefficient (Yegian and Kadakal, 2004)

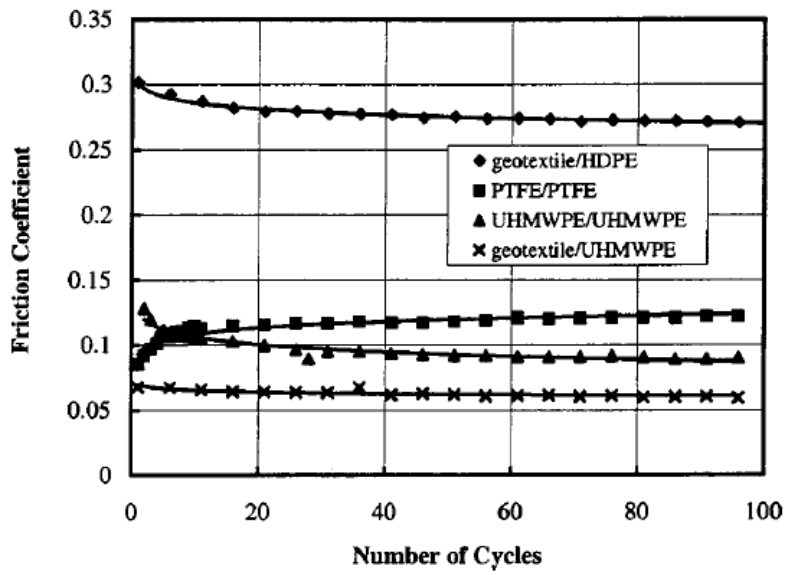


Fig. 2.23 Number of cycles vs. friction coefficient (Yegian and Kadakal, 2004)

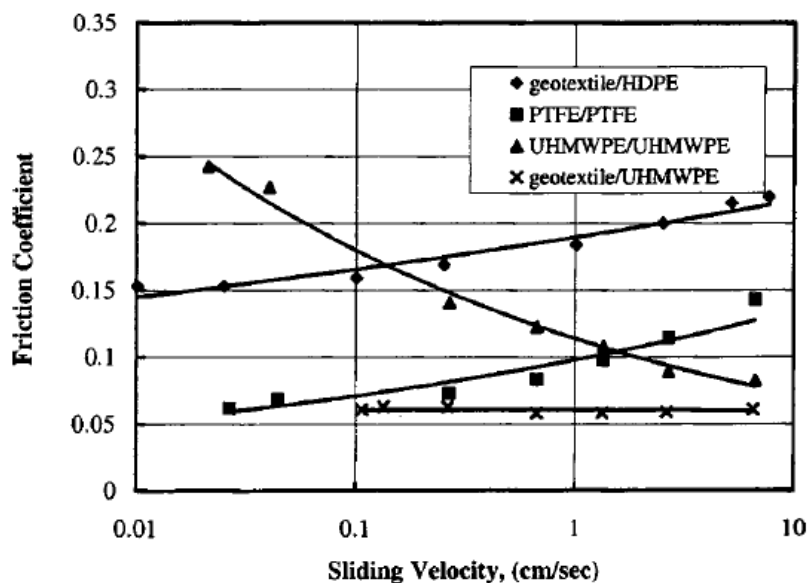


Fig. 2.24 Sliding velocity vs. friction coefficient (Yegian and Kadakal, 2004)

After determining the most suitable liner combination, the following experiments were performed only with this combination. The second step was to observe the acceleration and displacements of the system under different table accelerations applied at different frequencies. Similar to the one in Yegian and Lahlaf (1992), the liner transferred the accelerations directly up to a point at which the shear strength of the interface is exceeded by the induced dynamic forces. But this point was determined to be 0.08g which is nearly half of the one measured in Yegian and Lahlaf (1992). Moreover, in contrast to the observation in Yegian and Lahlaf (1992), the acceleration after the slip point (0.08g) did not increase with increasing table acceleration. Also the measured accelerations were nearly independent of the frequency of the applied loads (Fig. 2.25).

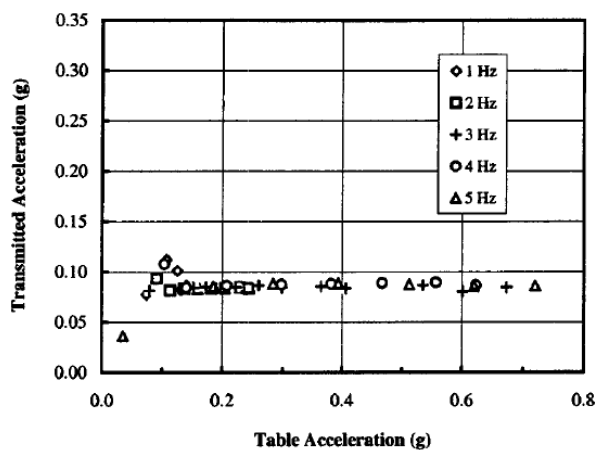


Fig. 2.25 Table acceleration vs. transmitted acceleration (Yegian and Kadakal, 2004)

Also, slip displacements were observed to increase with the increasing table acceleration and decrease with increasing frequency of loading, as expected (see Fig. 2.26).

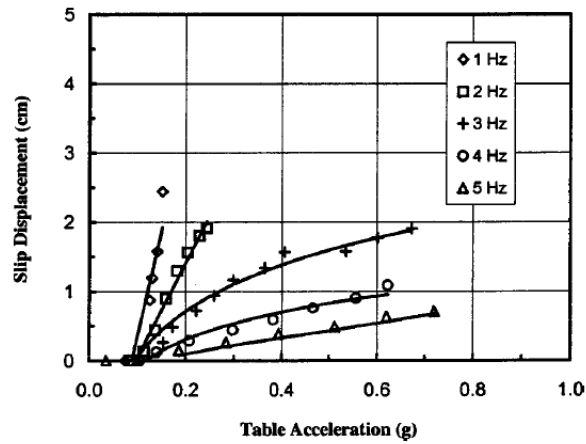


Fig. 2.26 Table acceleration vs. slip displacement (Yegian and Kadakal, 2004)

The third step was to observe the system under earthquake motions. For this purpose three earthquake records (Capitola, Corralitos and Santa Cruz) scaled to different maximum accelerations were used. The Capitola record contains frequencies in a wide intermediate band while Corralitos and Santa Cruz records contain narrow band low and high frequencies respectively (see Fig. 2.27). The difference in the frequency contents of the three ground motion records did not lead to a significant change in the transferred accelerations to the system (Fig. 2.28) however the permanent slip displacement changed significantly with the frequency content of the input motion (Fig. 2.29).

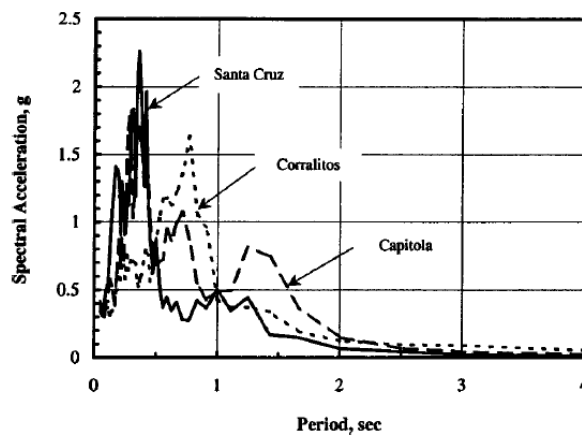


Fig. 2.27 Response spectra of the three earthquakes (Yegian and Kadakal, 2004)

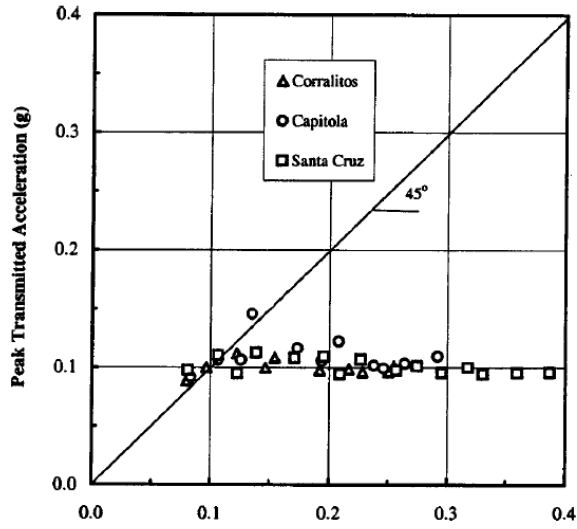


Fig. 2.28 Peak table acceleration vs. peak transmitted acceleration (Yegian and Kadakal, 2004)

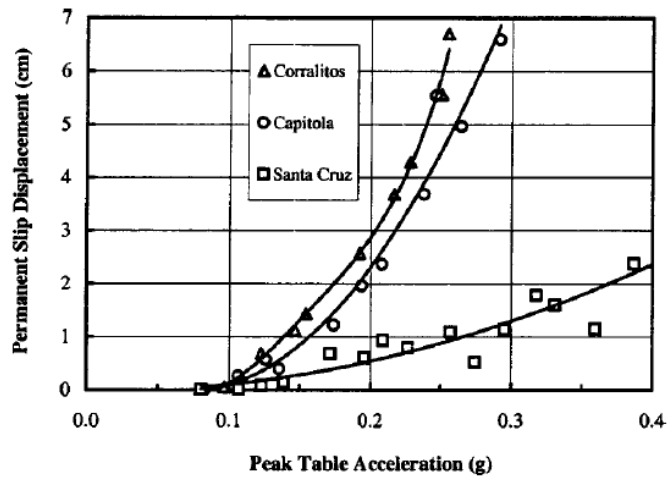


Fig. 2.29 Peak table acceleration vs. permanent slip displacement (Yegian and Kadakal, 2004)

Finally, the effect of the use of liner on the peak drifts of the structure was investigated by applying the same earthquake records to a one-storey model (Fig. 2.30). For all of the three tests the peak drifts observed in the isolated structure were almost the same independent of the earthquake record and were significantly reduced for all records with the largest reduction in Santa Cruz record (Fig. 2.31).

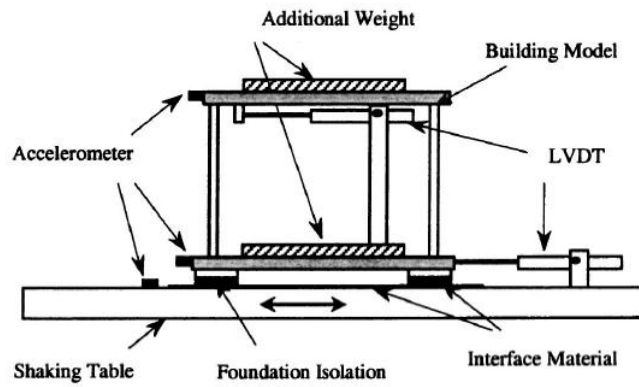


Fig. 2.30 Test setup of single-storey model (Yegian and Kadakal, 2004)

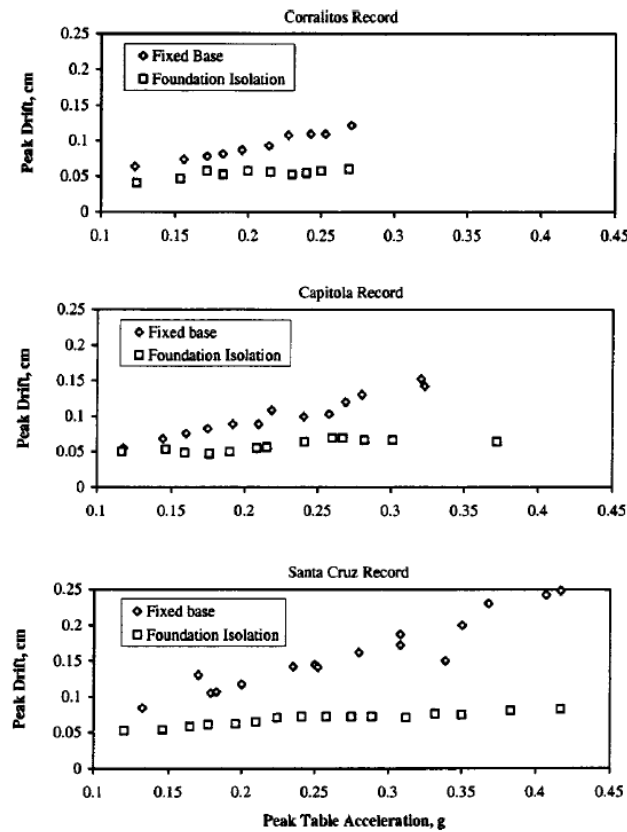


Fig. 2.31 Peak table acceleration vs. peak drift (Yegian and Kadakal, 2004)

Another study about the subject was Yegian and Catan (2004). In their study, they considered to place the isolation layer beneath the soil rather than just below the building and named this system as “soil isolation” (Fig. 2.32).

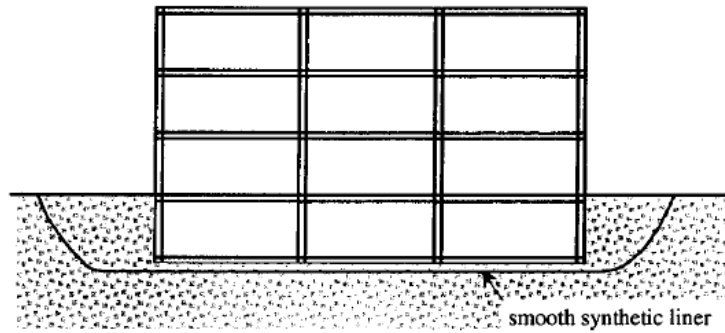


Fig. 2.32 Soil isolation for buildings (Yegian and Catan, 2004)

Two alternatives of soil isolation were evaluated by the researchers to be appropriate. The first alternative was the cylindrical-shaped soil isolation in which the liner was put in a cylindrical shape. For this alternative, a test setup was prepared in a 179cmx46cmx46cm tank with $H/D=6.6$ (Fig. 2.33) and table accelerations up to 1.0g was applied to the system at different frequencies. The slip has initiated at 0.18g table acceleration and opposite to the situation in the former study, the transmitted acceleration has continued to increase after slip has occurred (Fig. 2.34). Moreover, the model used in the tests was observed to go under rigid body rotation rather than translation.

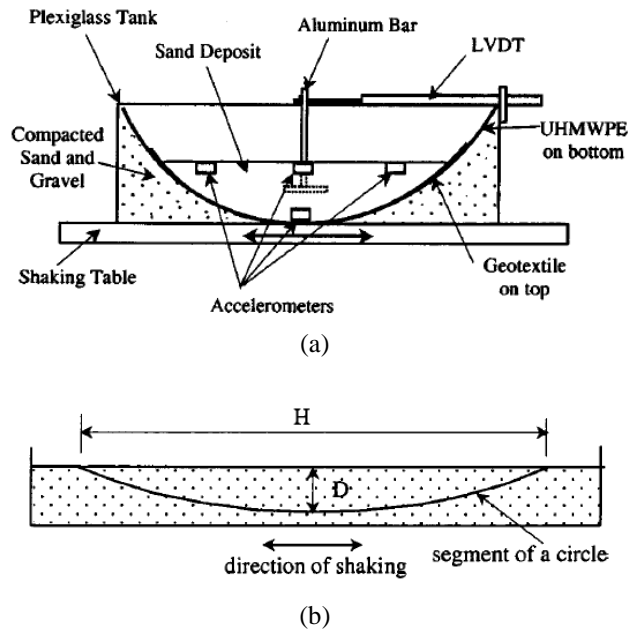


Fig. 2.33 Cylindrical-shaped isolation liner (a) test setup (b) application for $H/D = 6.6$ (Yegian and Catan, 2004)

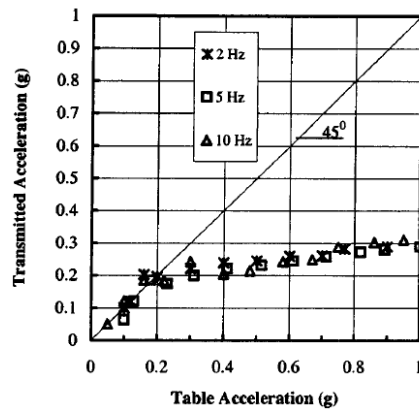


Fig. 2.34 Table acceleration vs. transmitted acceleration for cylindrical-shaped liner (Yegian and Catan, 2004)

Due to the possible difficulties in real life applications of the cylindrical-shaped liners, the other alternative, which was thought to be more applicable, was the tub-shaped liner. For this alternative, the same tank used in the previous case was used with $H/D=9$ (Fig. 2.35). The slip had initiated at 0.2g which indicates a slight increase with respect to the former case. Moreover, the movements of the model structure were mainly translational indicating a more reliable system than the former one.

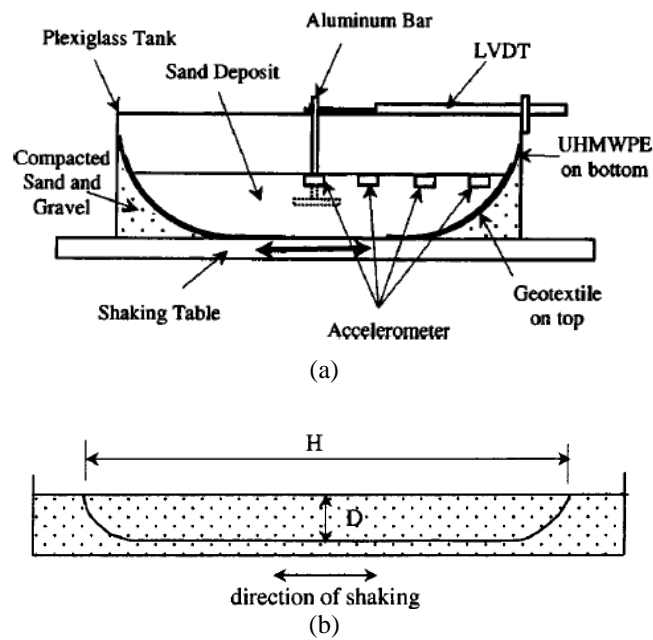


Fig. 2.35 Tub-shaped isolation liner (a) test setup (b) application for $H/D = 9$ (Yegian and Catan, 2004)

Also, numerical analyses were performed in order to assess the effectiveness of the tub-shaped liner system for field scale applications. In the analyses, systems with different H/D ratios for $D > 3\text{m}$ were analyzed under 2Hz cyclic shaking with 0.6g acceleration (Fig. 2.36). Eventually, it was concluded that the transmitted accelerations are minimized when $H/D > 10$. Also an additional

suggestion was that the curved portion of the liner to extend away from the edge of the building at a distance equal to the depth of the foundation.

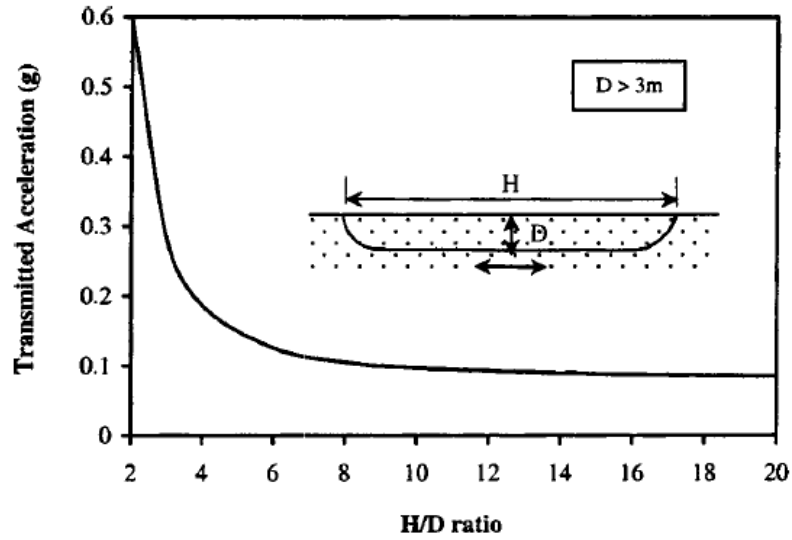


Fig. 2.36 Transmitted acceleration as a function of H/D ratio (Yegian and Catan, 2004)

As summarized above, the data presented in the literature for the behavior of composite liner systems were obtained from shaking table tests conducted on highly rigid models which have very high natural frequencies as compared to the input motion frequencies. As a consequence, the dynamic behavior of the composite liner system was found to be independent of the input motion since there is no interaction between the base motion and the superstructure. In this study, the experiments were conducted on models with representative natural frequencies of their prototypes in order to capture such an interaction. Also, test results are presented in the following chapters include the response analyses of the tested models.

CHAPTER 3

THE EXPERIMENTAL SETUP

The experimental setup was mainly composed of three parts which were the shaking table, the models and the measurement devices. The establishment of the setup is described in detail in this chapter.

3.1 The Shaking Table

The shaking table in the Soil Mechanics Laboratory of Civil Engineering Department of Middle East Technical University have been modified and improved for this research.

Previously, the shaking table was composed of 9 laminar boxes placed on top of each other and the system was activated by a simple mechanically controlled electric motor. The electric motor could excite the system only with harmonic motion with a maximum frequency of 5 Hz and an amplitude of ± 6 mm. (Fig. 3.1)

The system capabilities have been improved by replacing the old engine by a computer-controlled servo-motor which utilizes a fully changed excitation system (Fig. 3.2). This servo-motor (Fig. 3.3) is controlled by the touchscreen LCD panel (Fig. 3.4) which is placed on the control table. The motion data is uploaded to the system as a text file on this panel and transferred to the servo-motor after read by the PLC driver (Fig. 3.5). The rotational motion of the servo-motor is translated to axial displacement by the shaft which was located between the shaking table and the servo-motor (Fig. 3.6). A proximity switch to detect the start (reference) point of the motion (Fig. 3.7) and an emergency stop to control the motion in case of an emergency (Fig. 3.8) together with two limit switches to stop the motion (Fig. 3.9) when the safe displacement limits are exceeded, were also installed on the system

The main body of the machine was not stiff enough to resist the dynamic loading which will occur during experiments. So, it has been decided to change the main body of the shaking table. The whole body of the machine was changed with stiffer elements which moved on high-tech rails (Fig. 3.10) instead of old rubber bearings (Fig. 3.11).

As a result of these modifications the system has become able to perform uni-directional dynamic experiments with random motion excitation in a fully computer controlled manner with a maximum frequency of 5 – 7 Hz (depending on the payload, maximum 2 tonnes), an amplitude of ± 300 mm (Fig. 3.12) and at a maximum acceleration of $a_{\max} = 0.3g$. The dimensions and properties of the shaking table are summarized in Table 3.1.

The motion given to the system is generated based on the displacement – time history of the motion. The original displacement – time history is transferred to a data set (text file) which is composed of two columns. In the first column the position is given in “mm” and the velocity which will be applied while going to that position is given in the second column in terms of mm/s. A sample input motion data is given in Appendix A.



Fig. 3.1 The older shaking table, electric motor and gear system



Fig. 3.2 The new excitation system

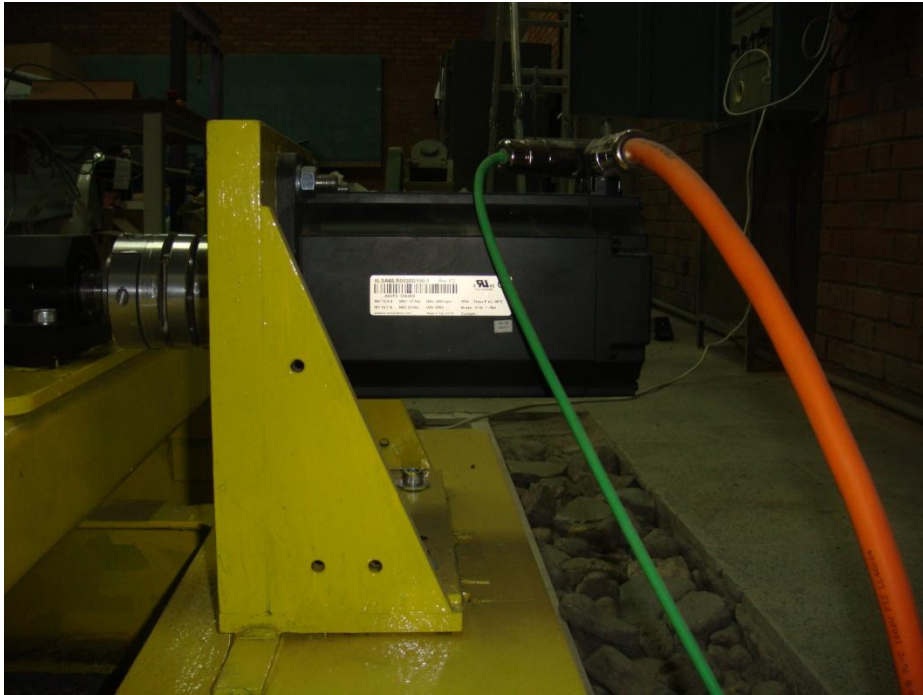


Fig. 3.3 The servo-motor



Fig. 3.4 The control panel



Fig. 3.5 The PLC driver

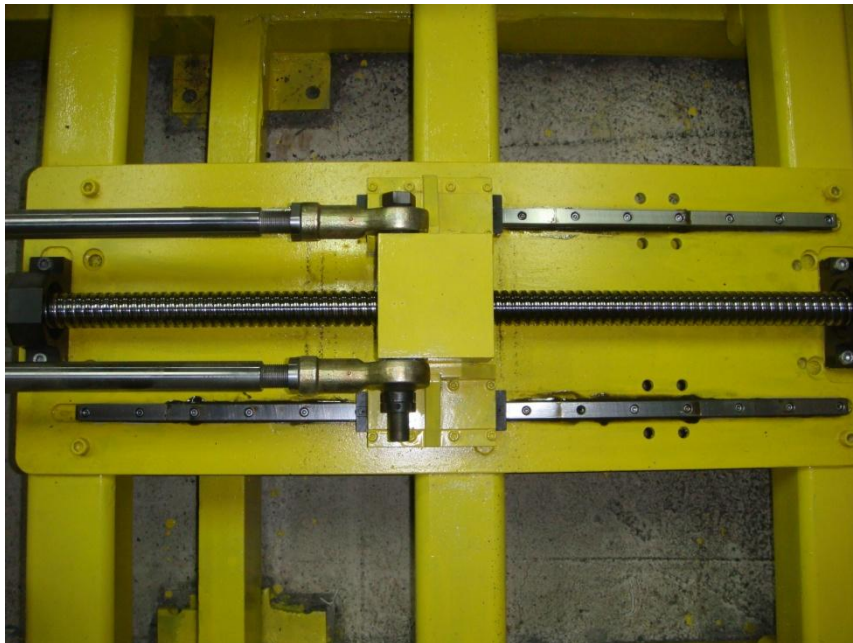


Fig. 3.6 The shaft of the new shaking table



Fig. 3.7 The proximity switch

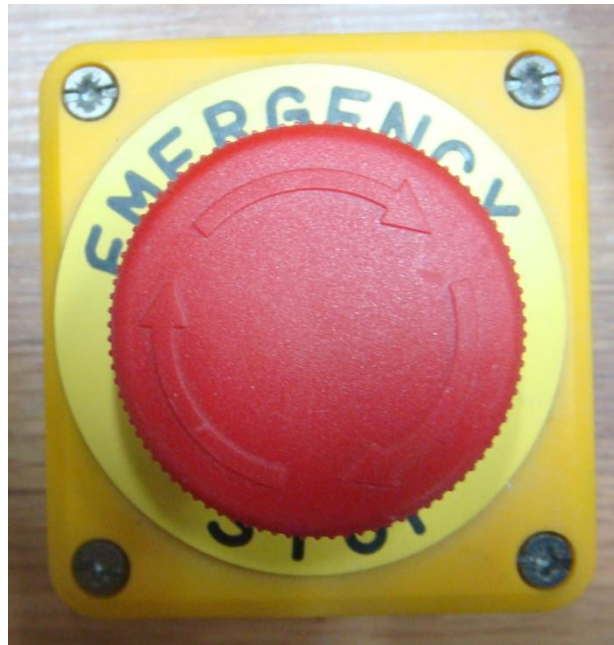


Fig. 3.8 The emergency stop



Fig. 3.9 The limit switch

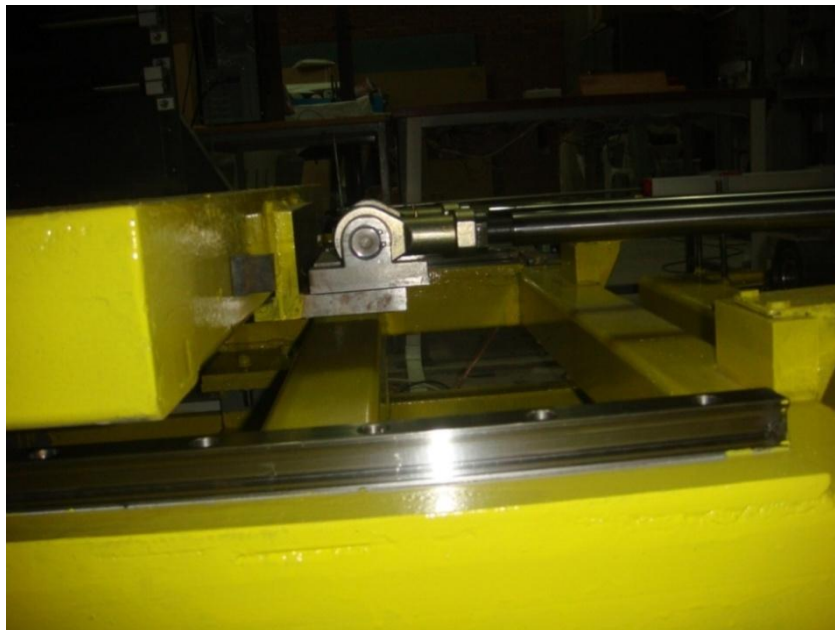


Fig. 3.10 A view of the rails of the new shaking table



Fig. 3.11 Rubber bearings supporting the base in the older system



Fig. 3.12 General view of the new shaking table

Table 3.1 Summary of the shaking table properties

Engine:	Rated Torque	Rated Power
	24 Nm	6600 W
Dimensions:	Externally	Laminar Tank
	2m x 4m	1m x 1.5m
Motion:	Maximum Stroke	Maximum Acceleration
	± 300mm	0.3 g

3.2 The Models

For this research, two models which were 3-storey and 5-storey structures were produced. The floors of the models were made of 10mm thick fiberglass plates which were 35 x 50cm in dimension and these floors were attached to the 1.5mm thick aluminum plates, which were 4.5cm wide, at 4 corners. The storey height was arranged to be 25cm (scale = 1:12) which makes a total height of $L = 1\text{m}$ for the 5 – storey and $L = 50\text{cm}$ for the 3 – storey model (Fig. 3.13 and 3.14). The utilization of shaking table for small scale models were similar to the ones presented in Chung et al. (1999) and Li et al. (2006). Also, the well-known Buckingham Pi-theorem and the general similitude rules given in Iai (1988) were concerned during the production of the models. The similitude calculations are provided in Appendix B.

In order to simulate the normal stress beneath the prototypes of the model structure, 4 fiberglass blocks were mounted under the basement floor of the models symmetrically 10cm away from the corners of the floor. The dimensions of these blocks were determined as 1.5cm x 3.5cm so that each storey caused an additional compressive load of 10kPa beneath these blocks (Fig. 3.15). Total weight of the 3 - storey model was measured as $W = 0.063\text{kN}$ and that of the 5 – storey model was $W = 0.105\text{kN}$. The models were mounted to the shaking table in a way that the long side of the models was parallel to the motion direction. Also the wider sides of the aluminum columns were attached to the floors, perpendicular to the direction of the motion. This provided the models to be more rigid in the transverse direction and against torsion as compared to that in motion direction. As a consequence, transverse and torsional movements of the models were avoided during experiments (Fig. 3.16).



Fig. 3.13 The 5-storey model

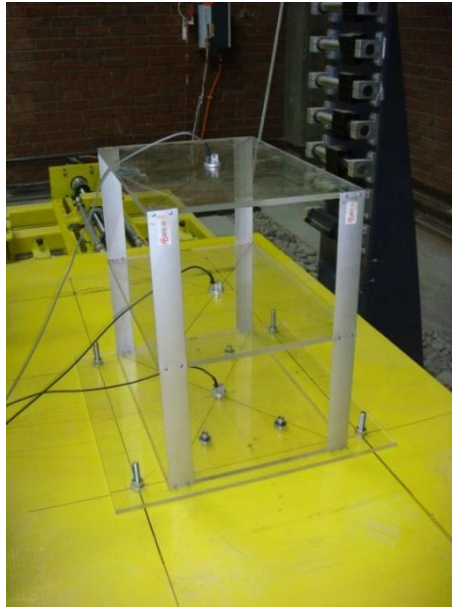


Fig. 3.14 The 3-storey model

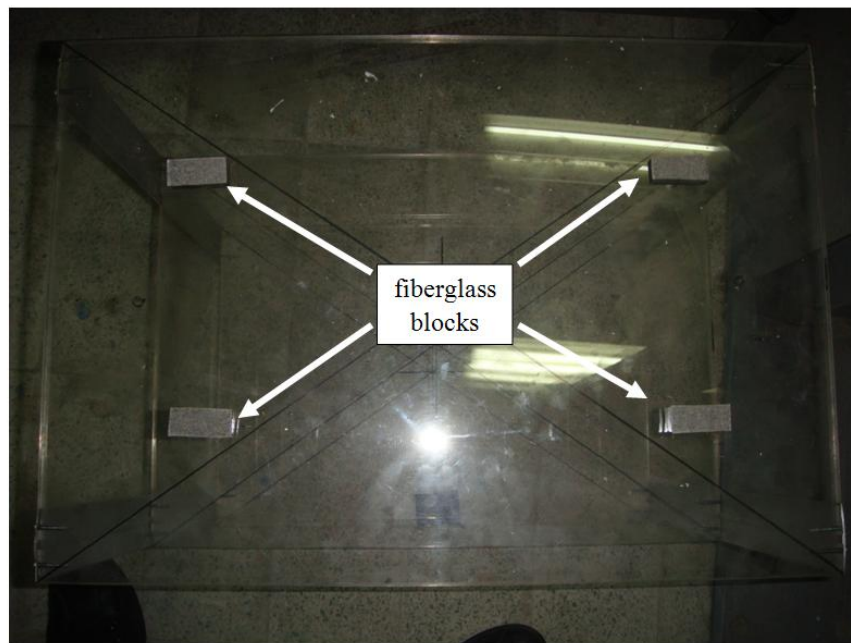


Fig. 3.15 Fiberglass blocks

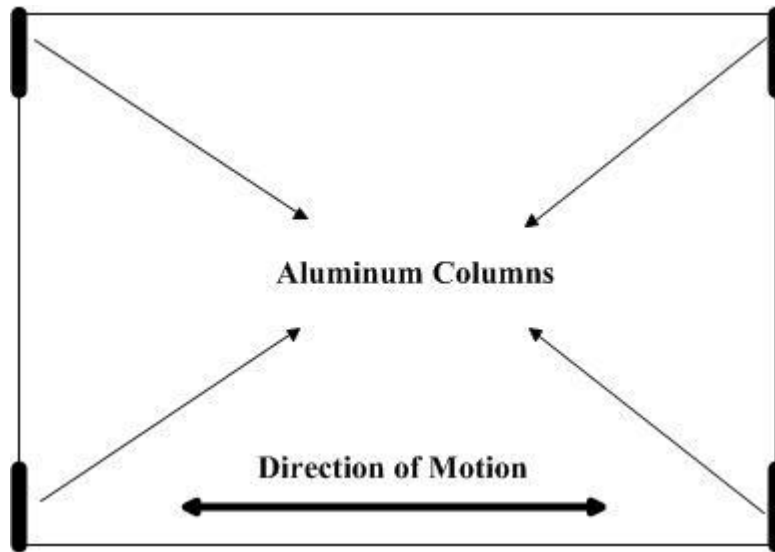


Fig. 3.16 Model floor plan view

3.3 The Measurement Devices

The experimental setup was composed of accelerometers and potentiometric rulers. There were two potentiometric displacement sensors (OPKON – LPT600) with 600 mm maximum stroke (Fig. 3.17). The displacements of the shaking table were measured by one of these rulers. The other one was fixed to the shaking table and attached to the basement of the models to measure the relative slip movements of the models for the isolated cases with respect to the shaking table.

5 strain-gauge based accelerometers with $\pm 1g$ capacity were available. Four of these accelerometers were KYOWA-AS-1GB (Fig. 3.18) and the other was KYOWA-ASW-1A (Fig. 3.19) type.

The “TDG TESTBOX 2010” dynamic data logger (Fig. 3.20) was used for data acquisition. The 16-channel data logger has 24-bit resolution and is directly connected to the computer by ethernet cable. Synchronized data can be collected from all channels independently at a maximum speed of 500 Hz. The technical specifications of the data logger are summarized in Table 3.2.

Table 3.2 Technical Specifications of Data Acquisition System

Device:	TESTBOX 2010
Type:	Data Logger
Producer:	TDG
Origin:	Turkey
Resolution:	24-bit
Connection:	Ethernet
Channel:	16
Sampling Speed:	500 Hz
Excitation Voltage:	5V - 12V
Measuring Voltage:	± 30 mV to ± 12 V
Safe Temperature Range:	10 to 35 $^{\circ}C$

The technical properties of the measurement devices are summarized below in Table 3.3.

Table 3.3 Technical Properties of Measurement Devices

Device:	AS1-GA	ASW-1A	LPT 600
Type:	Accelerometer	Accelerometer	Displacement Sensor
Producer:	KYOWA	KYOWA	OPKON
Origin:	Japan	Japan	Turkey
Rated Capacity:	$\pm 1g$	$\pm 1g$	600 mm
Nonlinearity:	$\leq \pm 1\%$ of RO	$\leq \pm 1\%$ of RO	$\leq \pm 0.05\%$
Hysteresis:	$\leq \pm 1\%$ of RO	$\leq \pm 1\%$ of RO	$\leq \pm 0.01\%$
Rated Output (RO):	0.5 mV/V	0.5 mV/V	-
Safe Overload Rating:	300%	300%	-
Safe Excitation Voltage:	6V AC / DC	6V AC / DC	12 - 30V DC
Safe Temperature Range:	-15 to 65 °C	-15 to 65 °C	-20 to 80 °C
Resonance Frequency:	70 Hz	40 Hz	-
Displacement Speed:	-	-	≤ 5 m/s

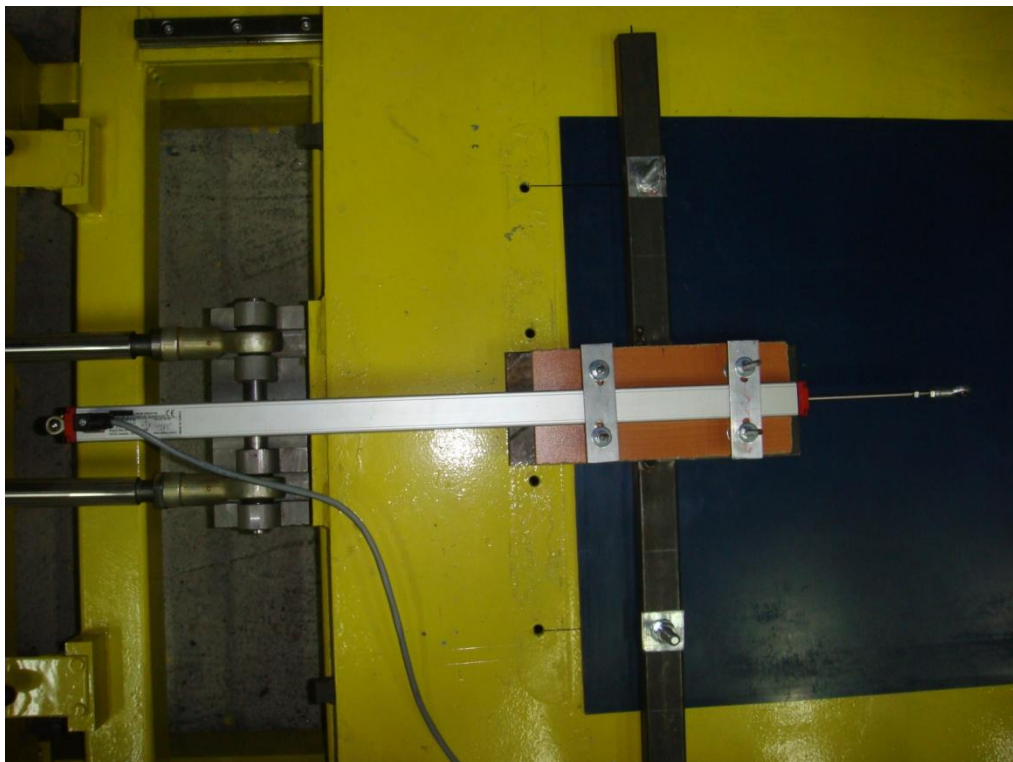


Fig. 3.17 LPT 600 Displacement Sensor



Fig. 3.18 AS-1GB accelerometer



Fig. 3.19 ASW-1A accelerometer



Fig. 3.20 The data logger

3.4 Test Setup

The parts of the test setup are described in this part. Accelerometers were installed at the middle of the each floor. The displacements of the shaking table were measured by one of the rulers. The other one was fixed to the shaking table and attached to the basement of the models to measure the relative slip movements of the models for the isolated cases with respect to the shaking table.

The models were directly fixed on the shaking table for the fixed base experiments. For the “IB” cases a 60 x 160 cm part of UHMWPE TIVAR 88-2 (6.4 mm thick) geomembrane was cut from the large sheet with 120 x 320 cm dimensions (Fig. 3.21) and fixed to the shaking table at four corners (Fig. 3.22), the fixing points of which were arranged formerly during the production of the shaking table. The fiberglass blocks beneath the models were covered with the nonwoven, high strength Typar- 3601 geotextile. Descriptive photographs of the test setup for the fixed base (FB) and the isolated base (IB) cases are given in Fig. 3.23 - 3.26 for both models.



Fig. 3.21 The UHMWPE geomembrane sheet



Fig. 3.22 The base used in the “IB” tests



Fig. 3.23 General view of test setup for the 3-storey model (FB)

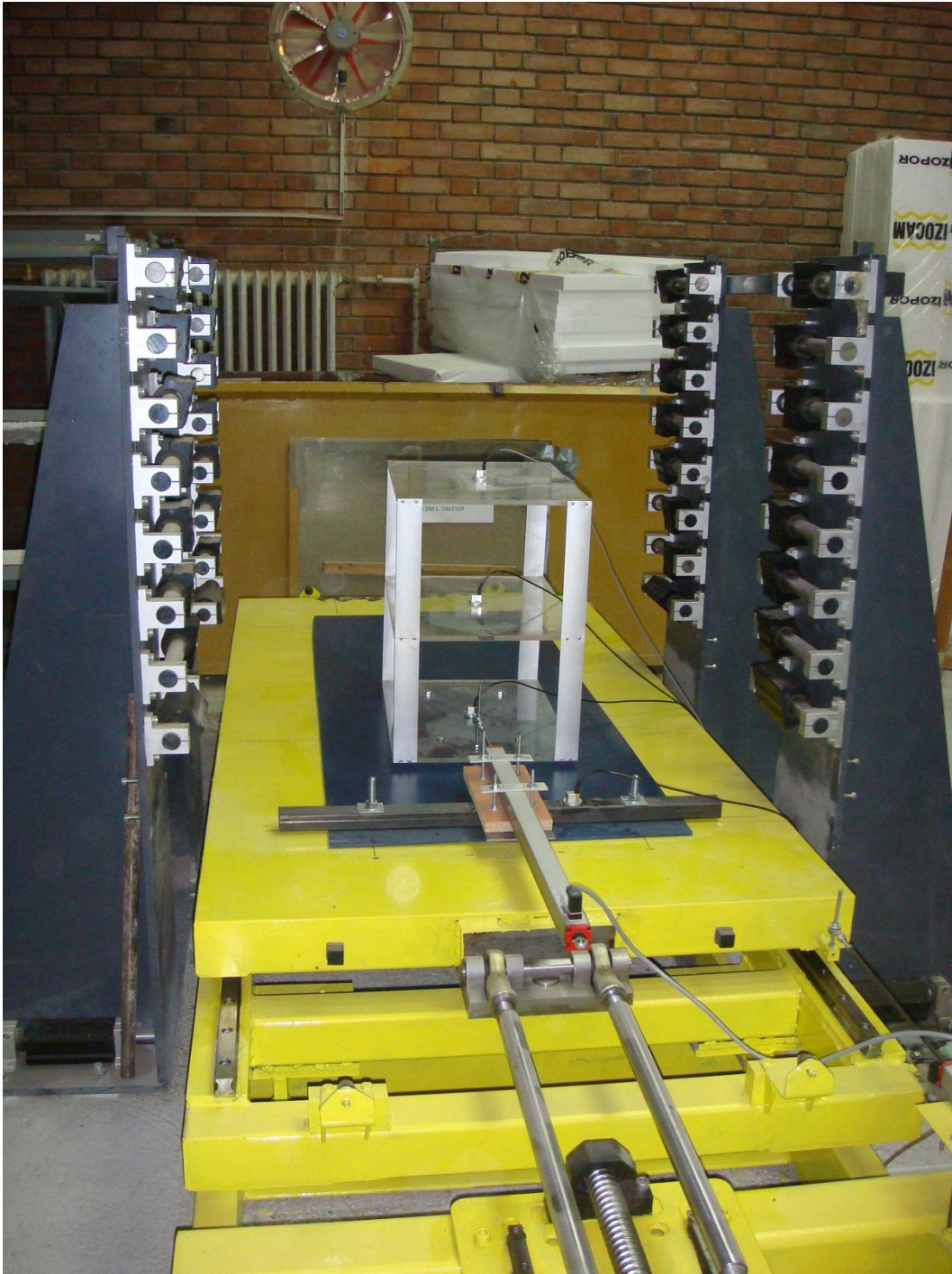


Fig. 3.24 A view of test setup for the 3-storey model (IB)



Fig. 3.25 A view of test setup for the 5-storey model (FB)

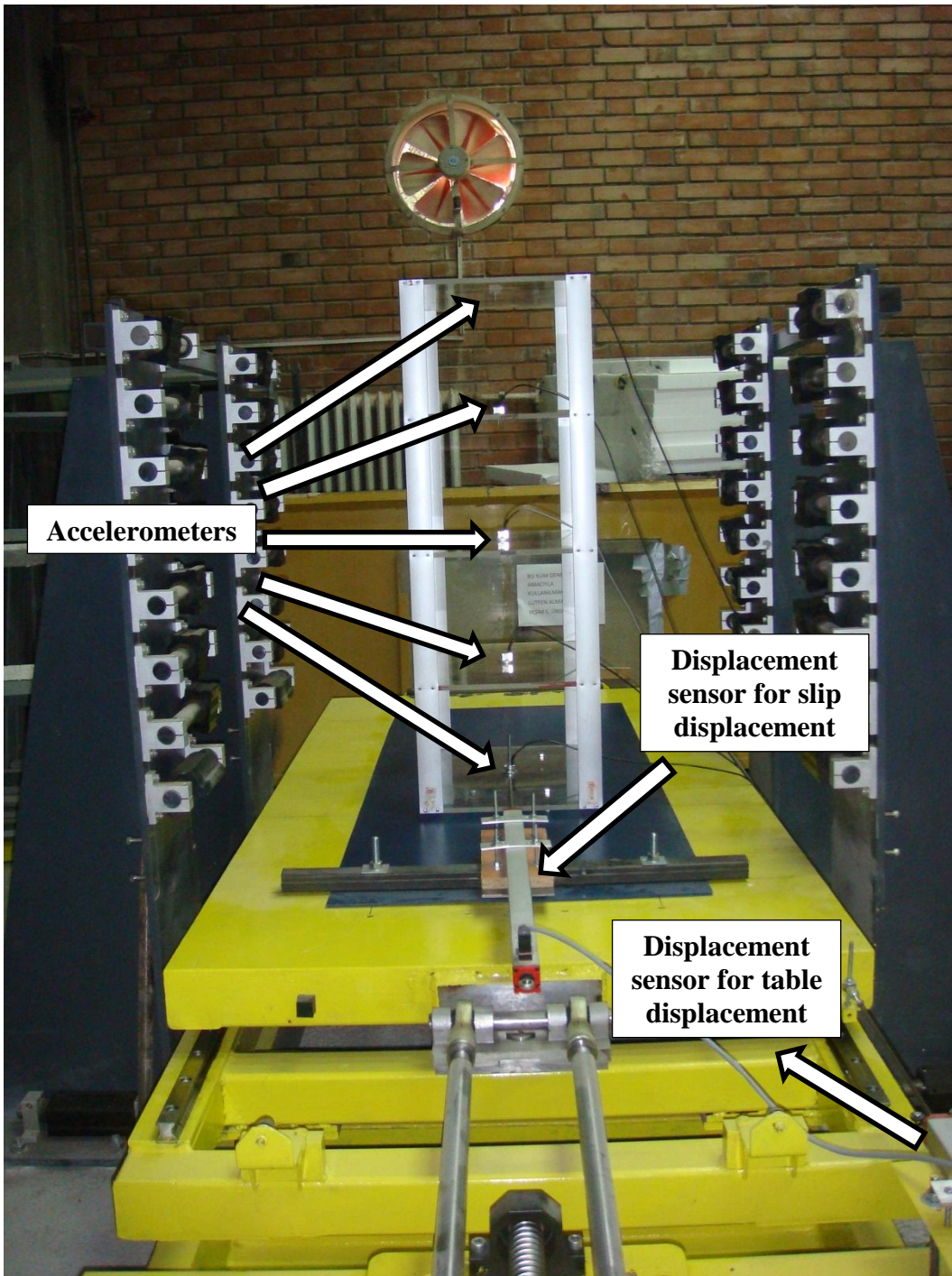


Fig. 3.26 Instrumentation of the test setup for the 5-storey model (IB)

CHAPTER 4

THE EXPERIMENTS AND RESULTS

A total of 138 dynamic experiments were performed throughout the research. In this chapter, firstly the results of free vibration tests will be presented. Then the results of the experiments in which the models were tested under variable harmonic and random excitations will be presented mainly focusing on the change in the measured parameters between the fixed base (FB) and the isolated base (IB) conditions for both models described in the previous chapter.

4.1 Free Vibration Tests

Free vibration tests were performed on the two models by applying a small displacement from the uppermost level to excite the model and measuring the accelerations at the same level under free vibration. As it can be observed from Fig. 4.1 and Fig. 4.2 the models have well-defined and stable damping and vibration characteristics. Based on the performed experiments the first-mode natural frequencies (f_n) of the structural models were determined to be $f_n = 4.35$ Hz ($T = 0.23$ s) and $f_n = 2.33$ Hz ($T = 0.43$ s) for the 3-storey (Base+2) and 5-storey (Base+4) models, respectively. These values are evaluated to be representative of the ones expected for the prototypes of these models.

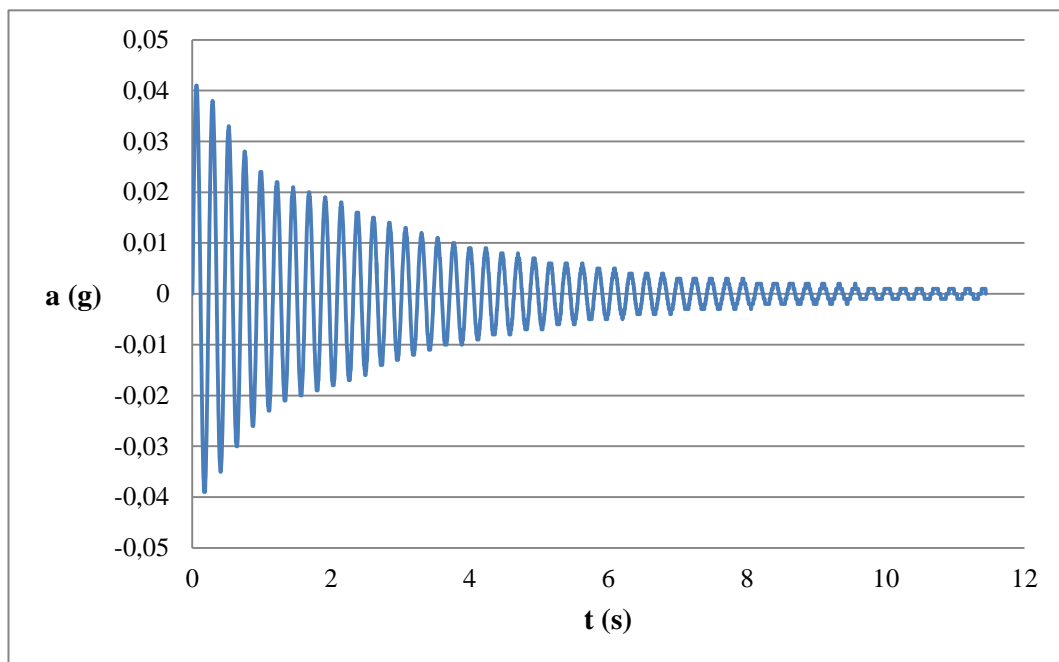


Fig. 4.1 The a-t plot for 3-storey model

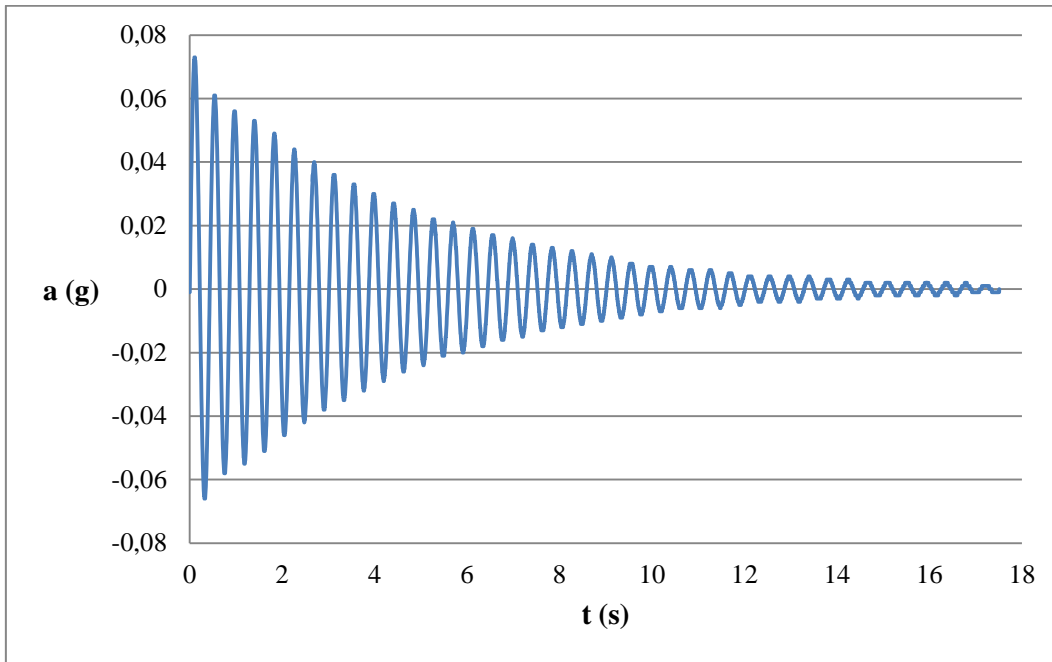


Fig. 4.2 The a-t plot for 5-storey model

The critical damping ratios of the models were calculated as given below according to Eq. (4.1).

$$\ln(z_i/z_{i+n}) = 2\pi nD \quad (4.1)$$

where,

z_i = amplitude at i^{th} cycle

z_{i+n} = amplitude at $(i+n)^{\text{th}}$ cycle

D = critical damping ratio

For the 3-storey model:

$z_4 = 0.024$ for $t = 0.98$ s and $z_{27} = 0.004$ for $t = 6.30$ s; $n = 27-4 = 23$

$$\ln(0.024/0.004) = 2 \times \pi \times 23 \times D \rightarrow D = 1.24 \%$$

For the 5-storey model:

$z_1 = 0.061$ for $t = 0.53$ s and $z_{28} = 0.004$ for $t = 12.08$ s; $n = 28-1 = 27$

$$\ln(0.061/0.004) = 2 \times \pi \times 27 \times D \rightarrow D = 1.60 \%$$

So, the critical damping ratios of the two models were calculated to be $D = 1.24\%$ and $D = 1.60\%$ for the 3-storey and 5-storey models respectively.

4.2 Tests with Harmonic Motions

64 experiments were conducted for this part of the study. The harmonic motions utilized in the experiments had a maximum acceleration range of $a_{\max} = 0.08 - 0.30g$. The frequencies of the applied motions were selected as $f = 1, 2, 3$ and 4Hz in order to investigate the behavior of the models both within a frequency range which covers low frequencies together with the natural frequencies of the models, since the natural frequencies of the models were determined to be close to $f = 4\text{Hz}$ and $f = 2\text{Hz}$ for the 3-storey ($f_n = 4.35\text{Hz}$) and 5-storey ($f_n = 2.33\text{Hz}$) models respectively. Each motion was applied for 30 cycles. The properties of the utilized harmonic motions are listed in Table 4.1. The experiments were performed both for the cases where the bases of the models were fixed to the table (fixed base condition, FB) and isolated with the described composite liner system (isolated base condition, IB). In the experiments, the data were collected at 250Hz sampling rate with the previously described equipments. In addition, the generated harmonic motions were named such that the first two digits described the frequency of the motion while the rest described the amplitude. To illustrate, “f2d5” means a motion with $f = 2\text{Hz}$ frequency and $d = 5\text{mm}$ amplitude.

Table 4.1 The harmonic input motion properties

Frequency (Hz)	a_{\max} (g)			
	0.08	0.16	0.24	0.30
	Peak amplitudes (mm)			
1	20	40	60	75
2	5	10	15	18.75
3	2.22	4.44	6.66	8.33
4	1.25	2.50	3.75	4.69

4.2.1 Harmonic Tests on 3-Storey Model

The results of the harmonic tests which were conducted on the 3-storey model are presented in this section. The accelerations at each floor level are given for the tested motions for both “FB” and “IB” cases in Fig. 4.3 - 4.6. In these figures; H/L is defined as the ratio of the height (H) to the total height (L) of the model and “a” stands for the measured acceleration in units of “g”.

As it can be seen from Fig. 4.3 – 4.6, for each motion frequency, the base accelerations were decreased to a certain level (defined as threshold acceleration, a_t) such that for that frequency if the maximum acceleration of the base motion (a_{\max}) was below this level the composite liner system did not provide any change in the measured floor accelerations (see “f1d20”, “f1d40” and “f2d5” motions in Fig. 4.3 and 4.4 respectively). The amount of decrease in the base acceleration was highly dependent on the input motion frequency. As the input motion frequency “f” gets closer to the natural frequency “ f_n ” of the model (as increases from 1Hz to 4Hz for this model) the magnitude of the threshold acceleration (a_t) for the “IB” becomes smaller. To illustrate, the threshold acceleration of the isolated model was measured around $a_t = 0.16g$ for the base motions with $f = 1\text{Hz}$ while $a_t = 0.13, 0.10$ and $0.07g$ for the base motions with frequencies $f = 2, 3$ and 4Hz respectively. Also, a slight increase (up to 10%) was observed in the base accelerations of the models for “IB” cases, as the “ a_{\max} ” of the applied motion was increased when motion frequency was kept constant for the experiments during which the composite liner system was triggered. The amount of this increase became smaller as the motion frequency got closer to the natural frequency of the model.

Another noteworthy point was the decrease in the interstorey drift ratios (Δ) defined below:

$$\Delta_i = (d_i - d_{i-1})/h \quad (4.2)$$

where,

d = horizontal displacement of the floor

h = floor height

As it can be followed from Fig. 4.7 to 4.10, significant decrease was observed in the “ Δ ” values for motions with “ a_{max} ” larger than the threshold acceleration “ a_t ” value to which the base accelerations were decreased by the composite liner system for that motion frequency. Similar to the case in the base accelerations the composite liner system provided the maximum drop in the “ Δ ” values for motions with frequencies close to the natural frequency of the model. In other words, the least improvement was observed in motions with $f = 1\text{Hz}$ and the effectiveness of the system increased as the motion frequency increased from $f = 1\text{Hz}$ to $f = 4\text{Hz}$ for this model with $f_n = 4.35\text{ Hz}$. Also, the “ Δ ” values of “IB” cases were almost constant when motion frequency was kept constant and independent of the “ a_{max} ” of the input motion for the motions for which the composite liner system had been triggered. The percent decrease in “ Δ ” values reached up to 80% for “f4d4.69” motion (see Fig. 4.10.d). On the other hand, as it can be seen from Fig. 4.7.a, 4.7.b and 4.8.a, there is no difference in the “ Δ ” values for “FB” and “IB” cases since the composite liner system was not triggered for these input motions.

It should be also stated that, based on the “ Δ ” values and the observed behavior in the models during tests it can be said that the mode of vibration and the displacement profile of the model was not altered by the composite liner system but the magnitudes were significantly reduced. This phenomenon is attributed to fact that the contact between the base and the structure is not broken. So, the base motions are transferred to the superstructure with the same motion frequency but with a smaller base acceleration. The slip displacements for harmonic motions were observed to be constant per cycle. In other words, the model slipped for a constant amount at each cycle of motion and these displacements accumulated at the end of the test. The slip displacements measured during experiments are summarized in Table 4.2. As it can be seen on the table the slip displacements tend to increase with increasing “ a_{max} ”, and decrease with increasing motion frequency “f” similar to the findings of Yegian and Kadakal (2004). Another noteworthy point was that the measured accelerations at each floor for both “FB” and “IB” cases were constant for all cycles of motions during an experiment after first a few (up to 4) cycles needed to reach to a steady state vibration.

Table 4.2 The slip for 3-storey model under harmonic motion

Frequency (Hz)	a_{max} (g)			
	0.08	0.16	0.24	0.30
	Slip per cycle (mm)			
1	0.00	0.00	0.91	1.89
2	0.00	0.68	0.89	0.94
3	0.25	0.26	0.32	0.72
4	0.23	0.25	0.30	0.68

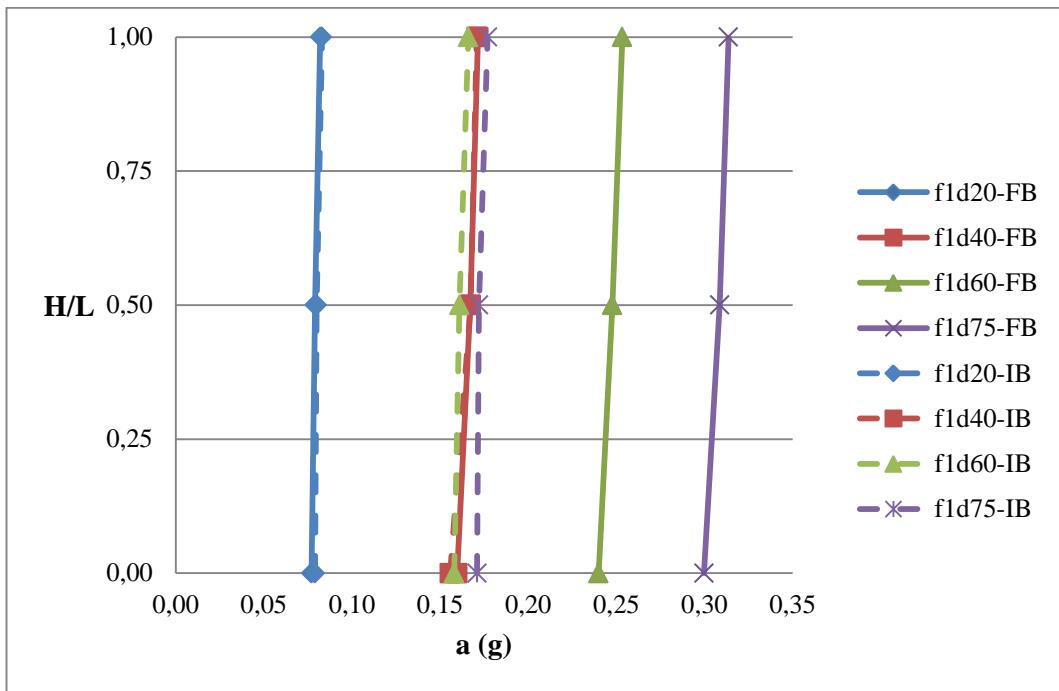


Fig. 4.3 a vs. H/L for $f = 1\text{Hz}$ (3-storey model)

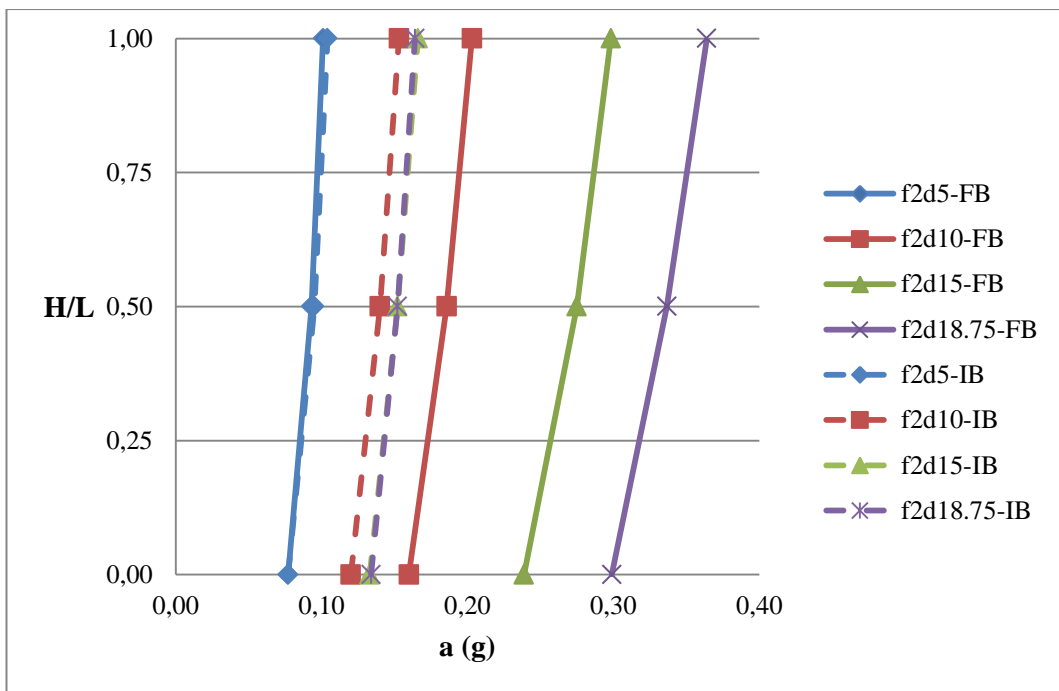


Fig. 4.4 a vs. H/L for $f = 2\text{Hz}$ (3-storey model)

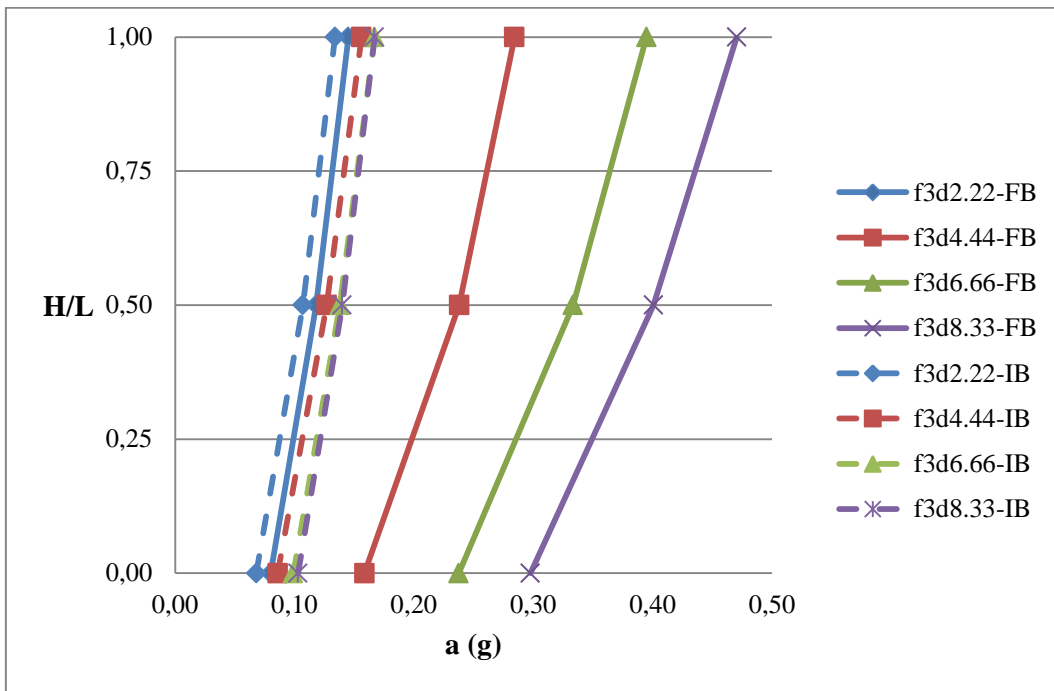


Fig. 4.5 a vs. H/L for $f = 3\text{Hz}$ (3-storey model)

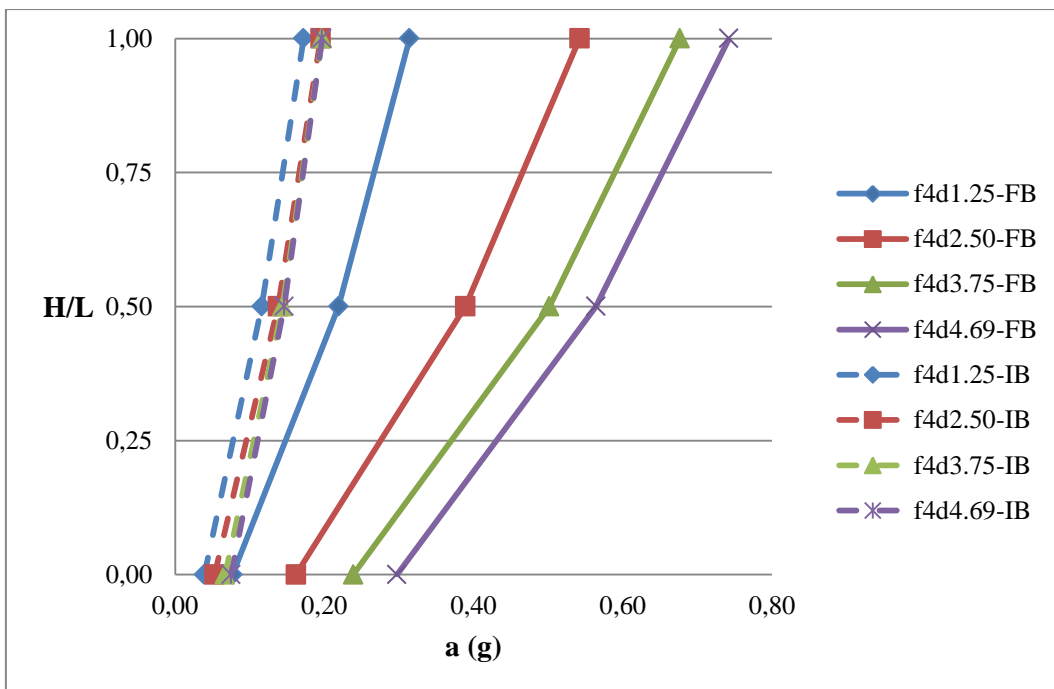
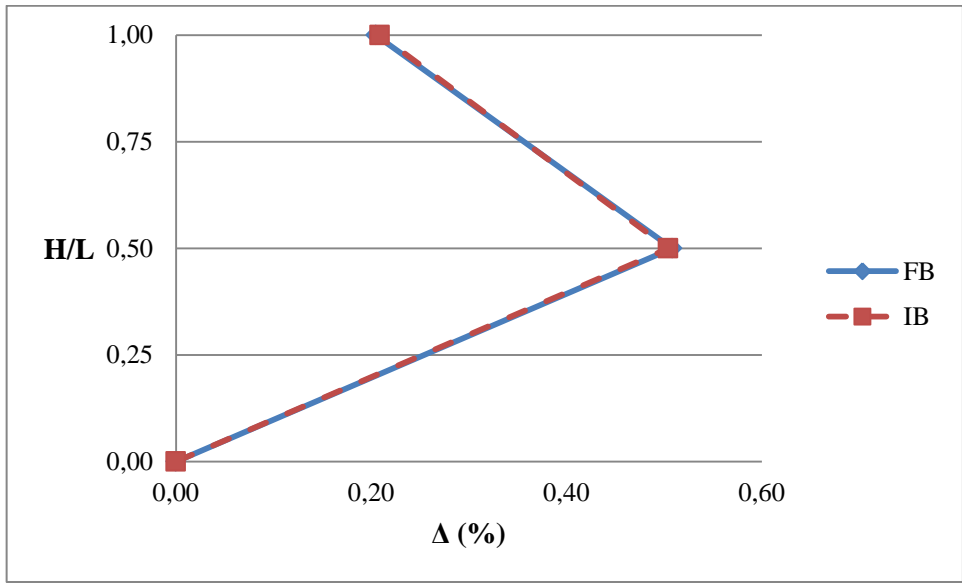
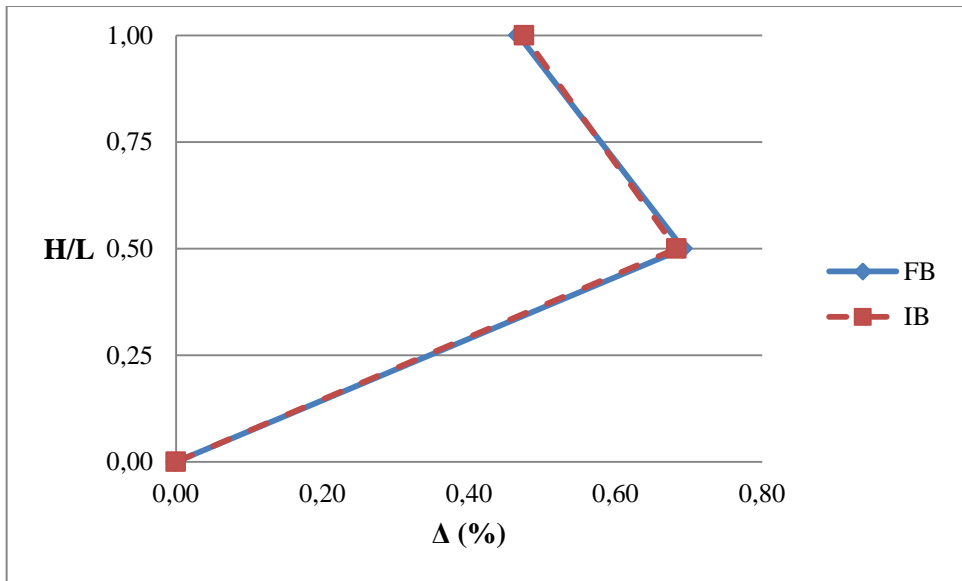


Fig. 4.6 a vs. H/L for $f = 4\text{Hz}$ (3-storey model)

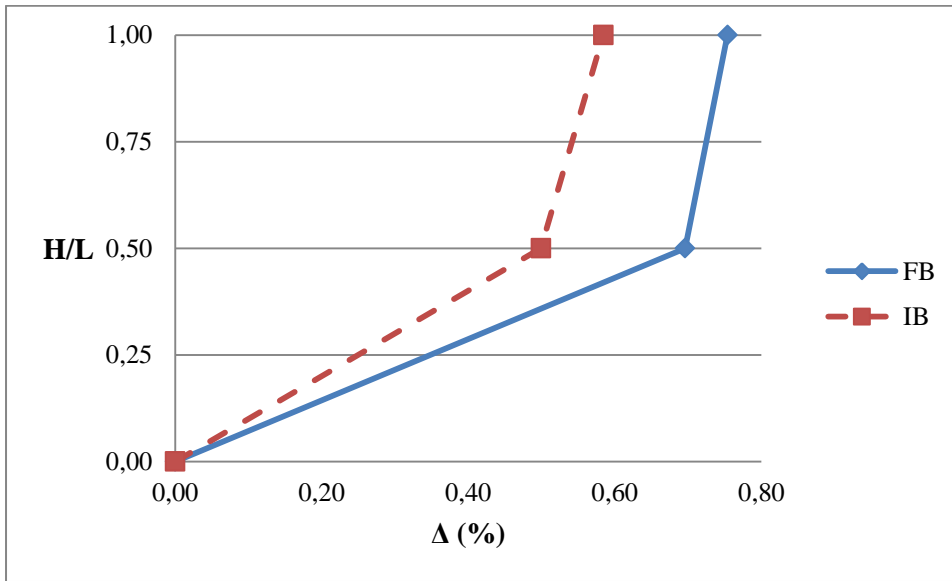


a. $f = 1\text{Hz}; d = 20\text{mm}$

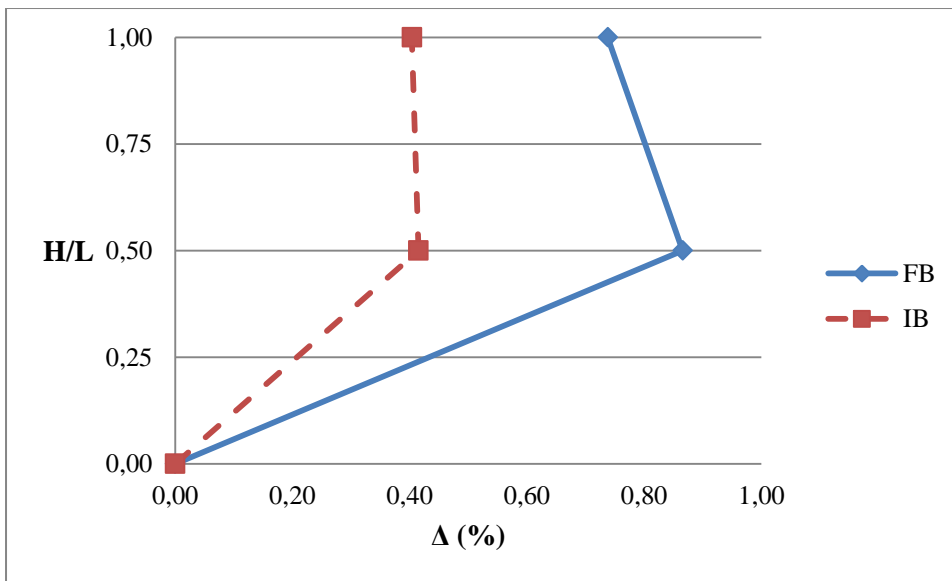


b. $f = 1\text{Hz}; d = 40\text{mm}$

Fig. 4.7 Δ vs. H/L for $f = 1\text{Hz}$ (3-storey model)

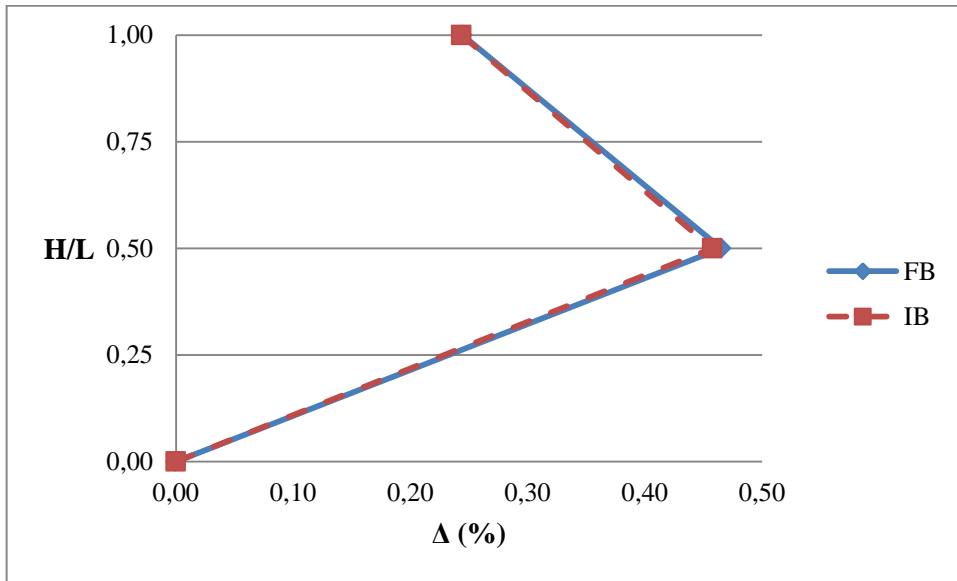


c. $f = 1\text{Hz}; d = 60\text{mm}$

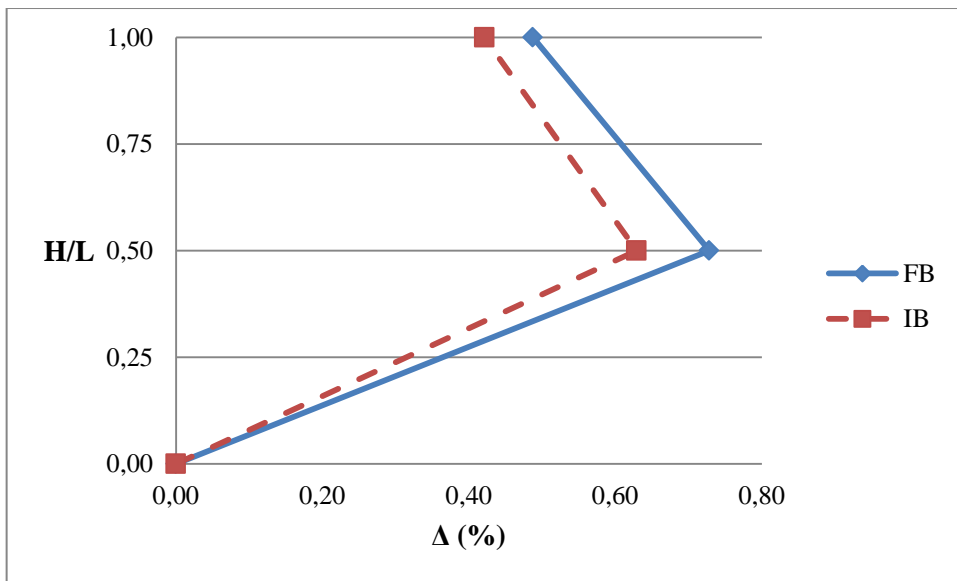


d. $f = 1\text{Hz}; d = 75\text{mm}$

Fig. 4.7 Δ vs. H/L for $f = 1\text{Hz}$ (3-storey model) (continued)

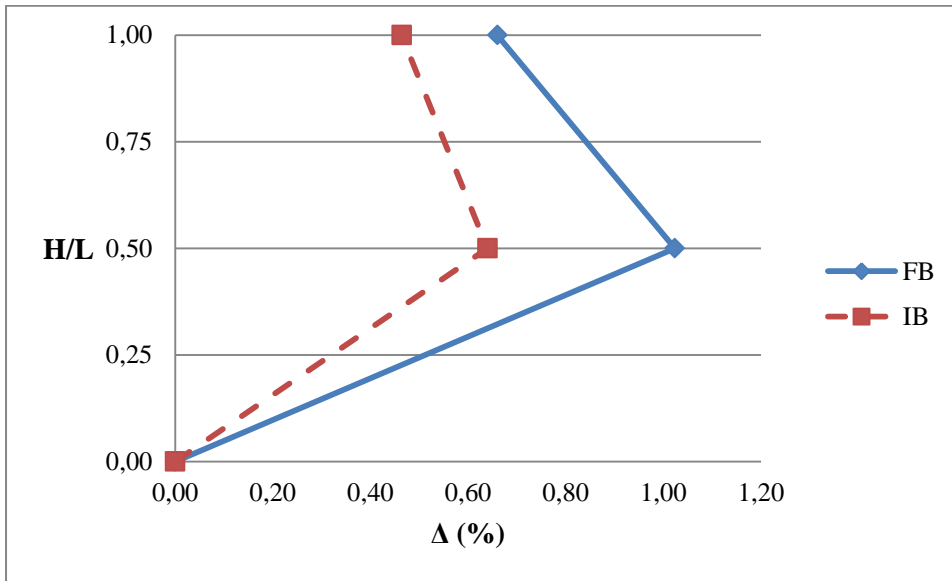


a. $f = 2\text{Hz}; d = 5\text{mm}$

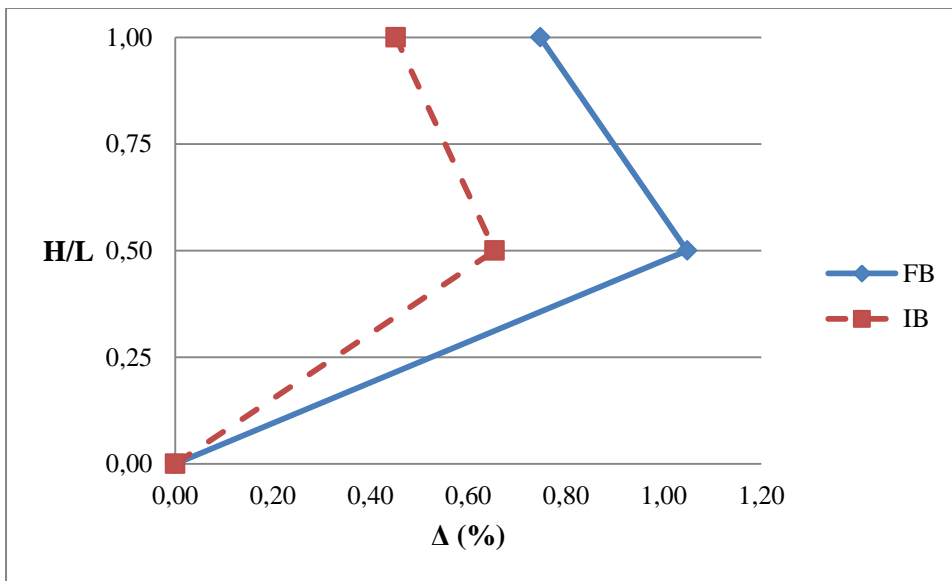


b. $f = 2\text{Hz}; d = 10\text{mm}$

Fig. 4.8 Δ vs. H/L for $f = 2\text{Hz}$ (3-storey model)

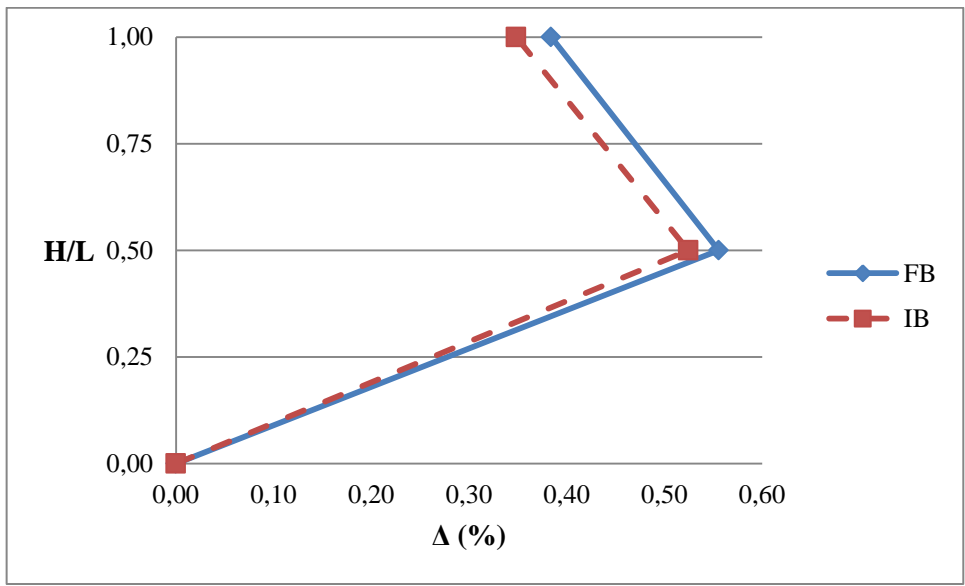


c. $f = 2\text{Hz}; d = 15\text{mm}$

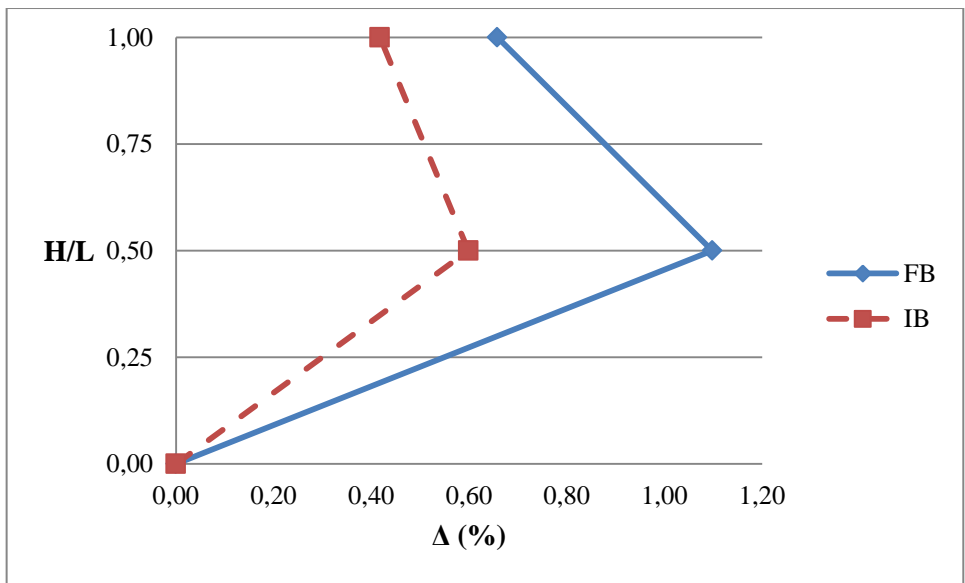


d. $f = 2\text{Hz}; d = 18.75\text{mm}$

Fig. 4.8 Δ vs. H/L for $f = 2\text{Hz}$ (3-storey model) (continued)

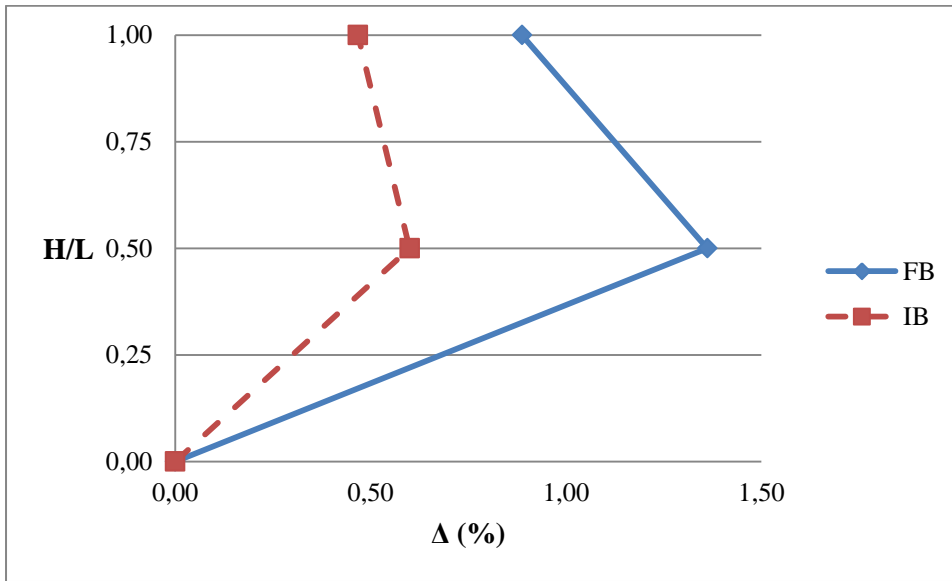


a. f = 3Hz; d = 2.22mm

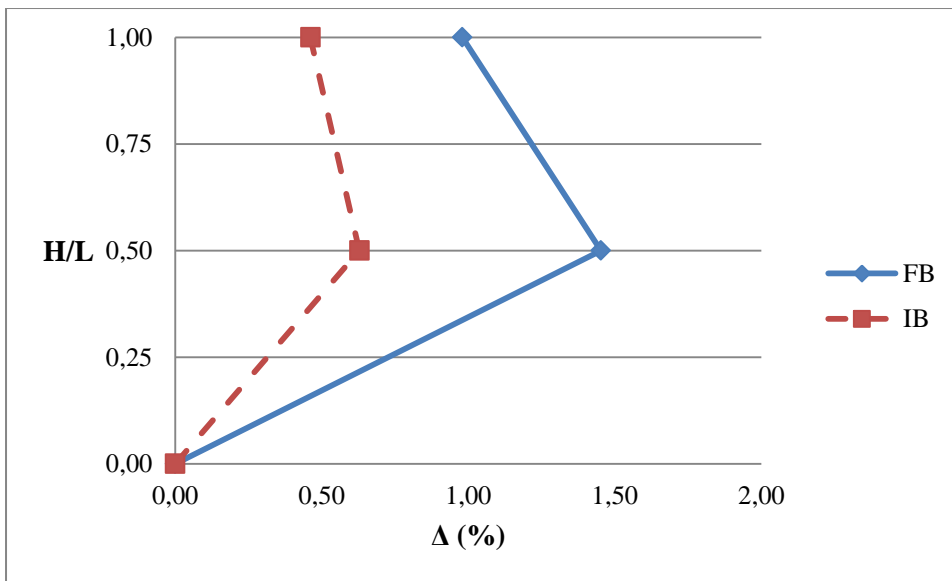


b. f = 3Hz; d = 4.44mm

Fig. 4.9 Δ vs. H/L for f = 3Hz (3-storey model)

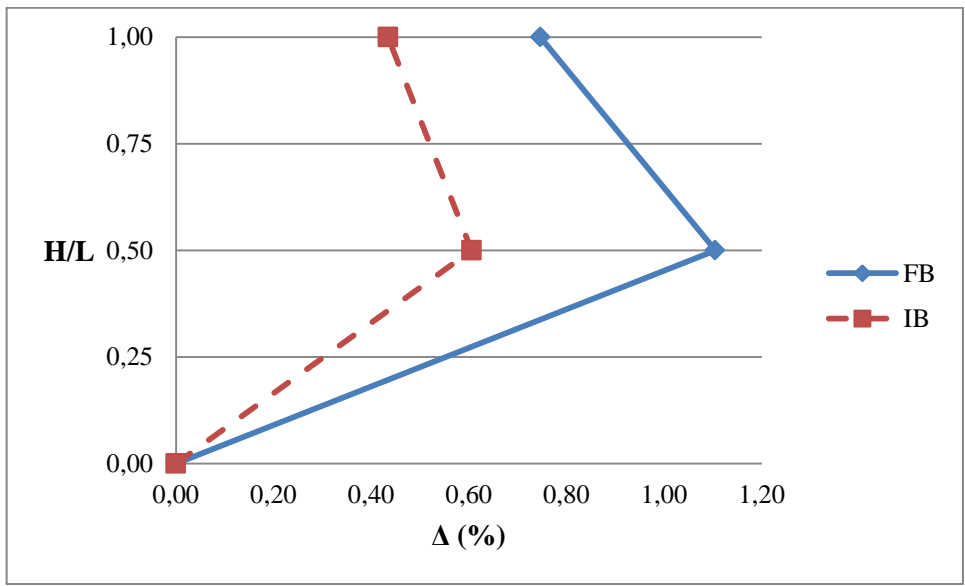


c. $f = 3\text{Hz}; d = 6.66\text{mm}$

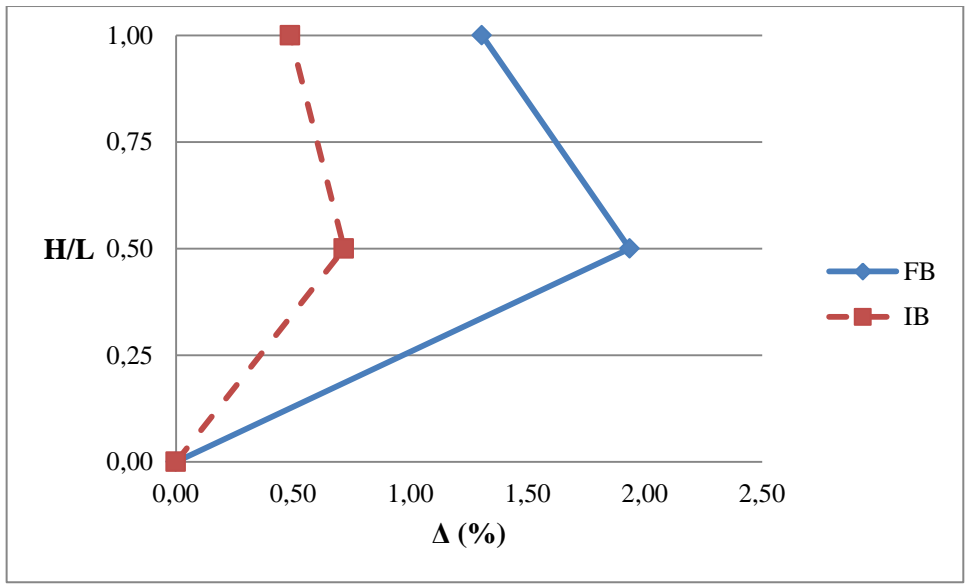


d. $f = 3\text{Hz}; d = 8.33\text{mm}$

Fig. 4.9 Δ vs. H/L for $f = 3\text{Hz}$ (3-storey model) (continued)

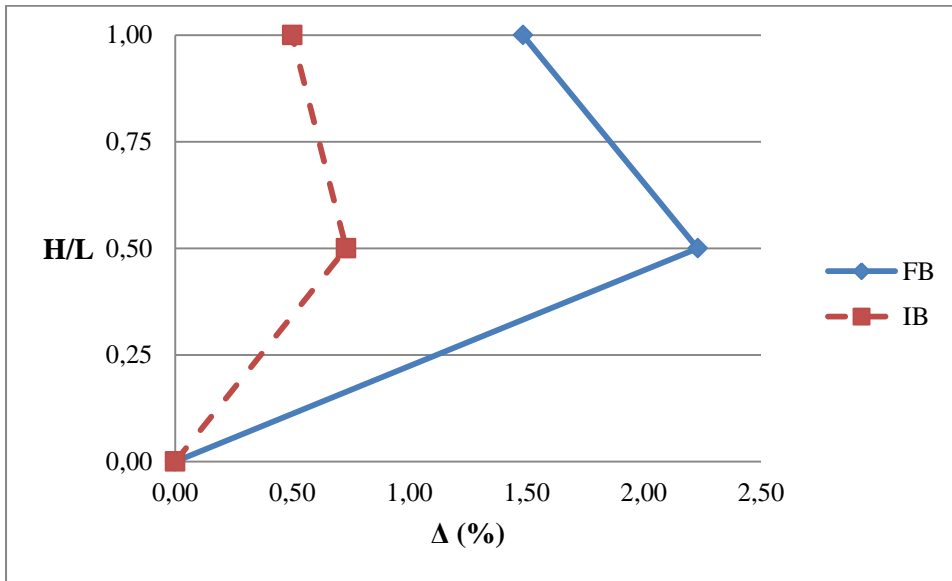


a. f = 4Hz; d = 1.25mm

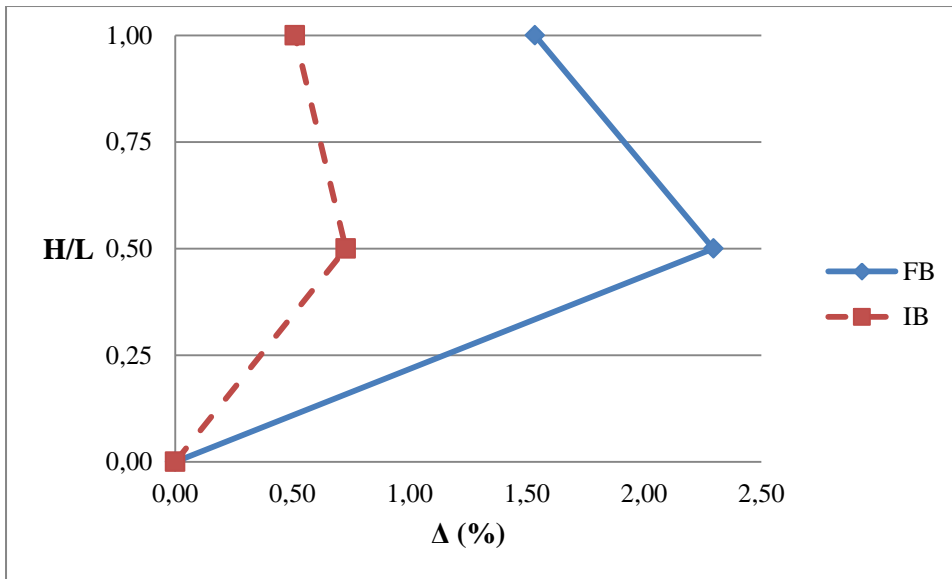


b. f = 4Hz; d = 2.50mm

Fig. 4.10 Δ vs. H/L for f = 4Hz (3-storey model)



c. $f = 4\text{Hz}$; $d = 3.75\text{mm}$



d. $f = 4\text{Hz}$; $d = 4.69\text{mm}$

Fig. 4.10 Δ vs. H/L for $f = 4\text{Hz}$ (3-storey model) (continued)

4.2.2 Harmonic Tests on 5-Storey Model

The results of the harmonic tests which were conducted on the 5-storey model are presented in this section. The accelerations at each floor level are given for the tested motions for both fixed base and isolated base cases in Fig. 4.11 - 4.14.

As it can be observed from Fig. 4.11 to 4.14, similar to that of the previous part, the composite liner system was most effective for motions with frequencies close to the natural frequency of the model namely, $f = 2\text{Hz}$ and $f = 3\text{Hz}$ recalling that the natural frequency of the model was $f_n = 2.33\text{Hz}$. The base accelerations were decreased to about $a_t = 0.13\text{g}$, 0.07g and 0.08g for $f = 1$, 2 and 3Hz motion frequencies respectively nearly independent of the “ a_{max} ” of the input motion. The composite liner system was not triggered for “f1d20” motion which has $f = 1\text{Hz}$ frequency and $a_{\text{max}} = 0.08\text{g}$ since the “ a_{max} ” value of the input motion was less than the threshold acceleration $a_t = 0.13\text{g}$ at this frequency level and consequently could not trigger the composite liner system. It is interesting that the composite liner system did not provide any improvement at $f = 4\text{Hz}$ frequency level. The base accelerations for the “FB” and “IB” cases were just the same for all “ a_{max} ” levels. Based on this data, it is concluded that the composite liner system is almost ineffective for motions with high frequencies as compared to the natural frequency of the superstructure. In addition, the measured accelerations at each floor did not differ for each cycle of motion during an experiment and the model reached to a steady state vibration after a few first cycles of motion (up to 5 cycles) similar to the case in the 3-storey model.

The “ Δ ” values are provided in Fig. 4.15 to 4.18. As it can be observed from these plots, the advantage of the utilized system became more visible as the “ a_{max} ” of the input motion increased. As expected, the system provided the maximum improvement when the input motion frequency was close to the first-mode natural frequency “ f_n ” of the superstructure similar to the case in the accelerations. As it was also observed for the 3-storey model, the “ Δ ” values for “IB” cases were almost independent of the “ a_{max} ” of the input motion and highly dependent on the input motion frequency provided that the “ a_{max} ” of the input motion was above the threshold acceleration “ a_t ” value for that specific motion frequency, in other words for cases where the composite liner system was triggered during the applied input motion. It is also noted that the amount of maximum decrease in “ Δ ” values was approximately 80% similar to that of the 3-storey model (see Fig. 4.17.d). The composite liner system did not alter the mode of vibration and the displacement profile of the tested model. The reason for this phenomenon was discussed in the section 4.2.1.

The slip displacements for harmonic motions were observed to be constant for each cycle of motion, similar to the case for the 3-storey model. The slip displacements measured during experiments are summarized in the Table 4.3. As it can be seen on the table the slip displacements tend to increase with increasing “ a_{max} ”, and decrease with increasing base motion frequency similar to the case for 3-storey model and in the study of Yegian and Kadakal (2004). It should also be noted that, the slip displacements measured for the 5-storey model was significantly higher than those of the 3-storey model. The difference is maximum for $f = 1\text{Hz}$ motion frequency since the largest slip displacements were measured at this frequency and the resultant differences are also largest consistently.

Table 4.3 The slip for 5-storey model under harmonic motion

Frequency (Hz)	a_{max} (g)			
	0.08	0.16	0.24	0.30
	Slip per cycle (mm)			
1	0.00	1.66	9.96	10.96
2	1.24	1.55	2.40	2.84
3	1.01	1.16	1.36	2.25
4	0.00	0.00	0.00	0.00

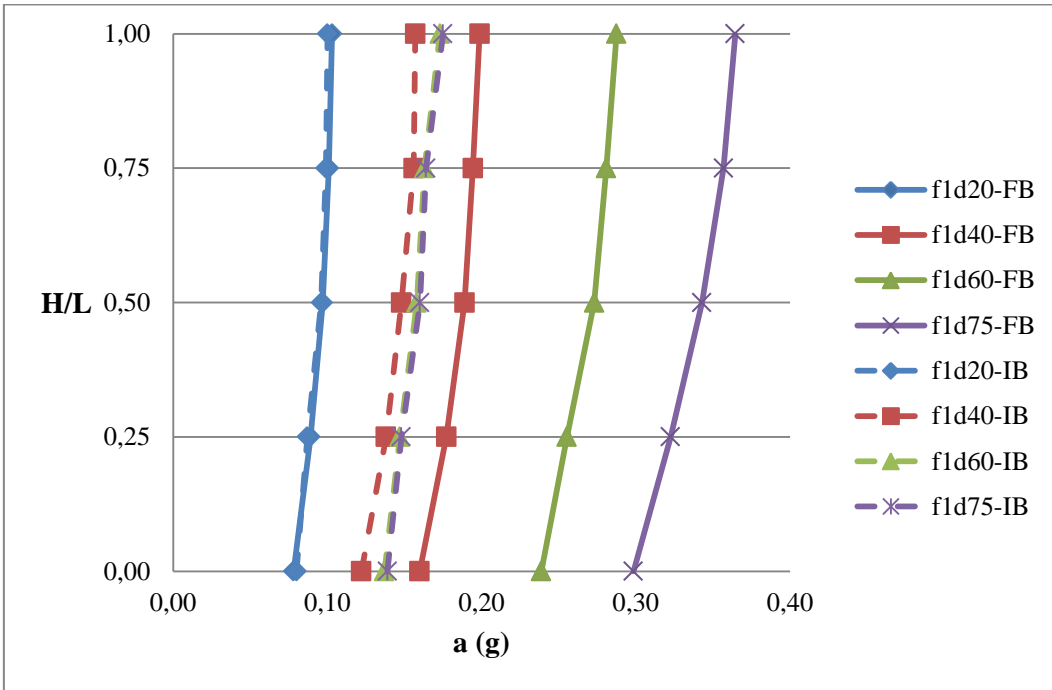


Fig. 4.11 a vs. H/L for $f = 1\text{Hz}$ (5-storey model)

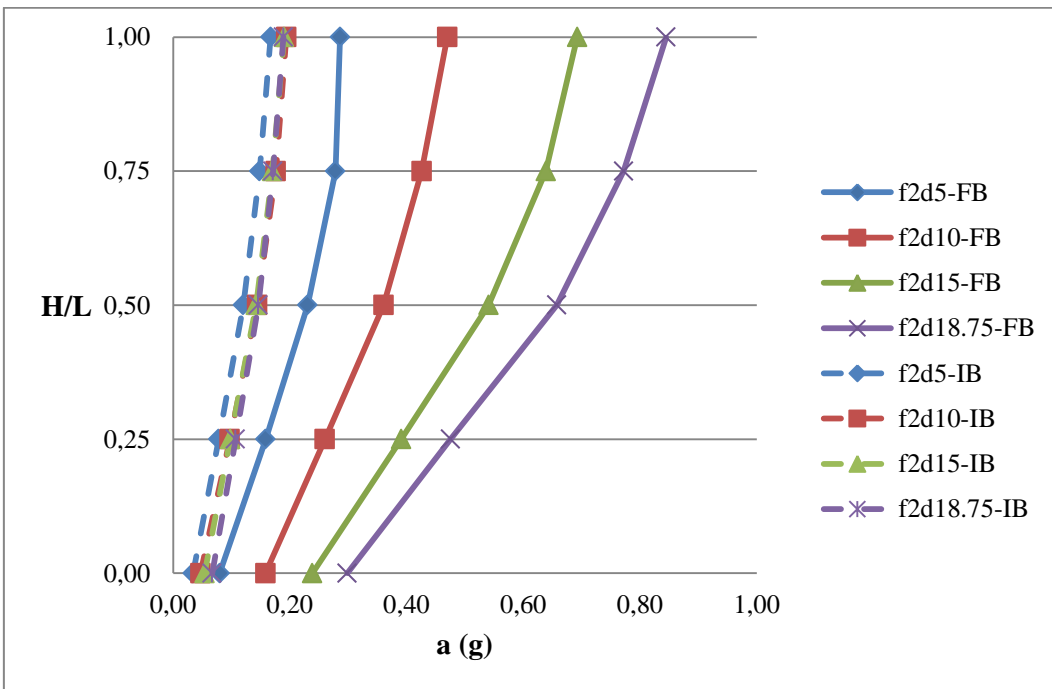


Fig. 4.12 a vs. H/L for $f = 2\text{Hz}$ (5-storey model)

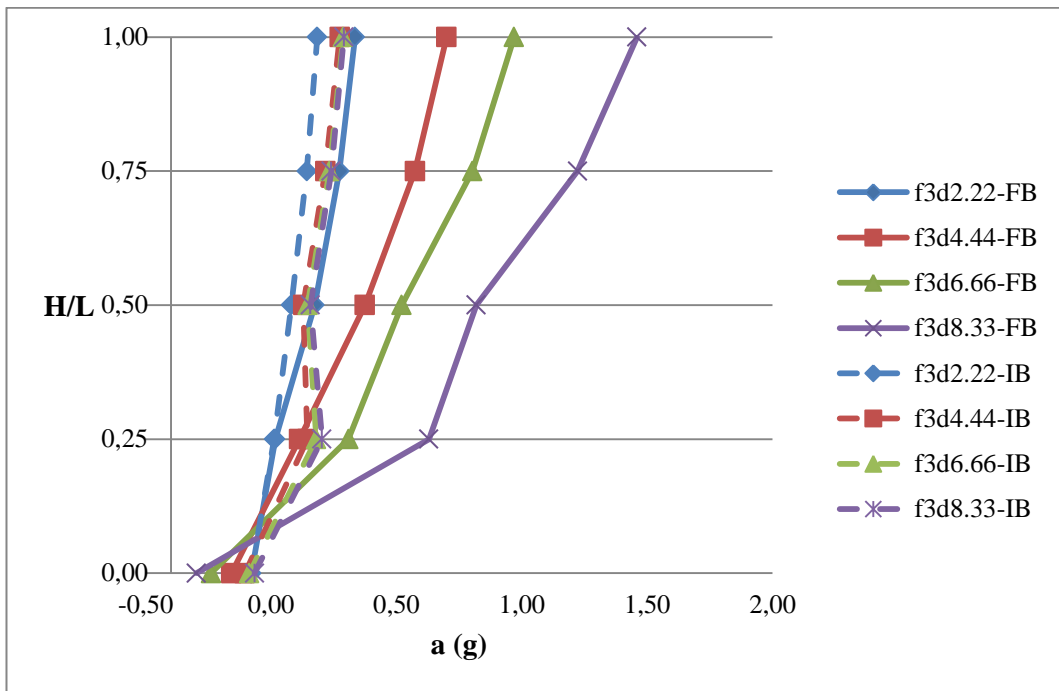


Fig. 4.13 a vs. H/L for $f = 3\text{Hz}$ (5-storey model)

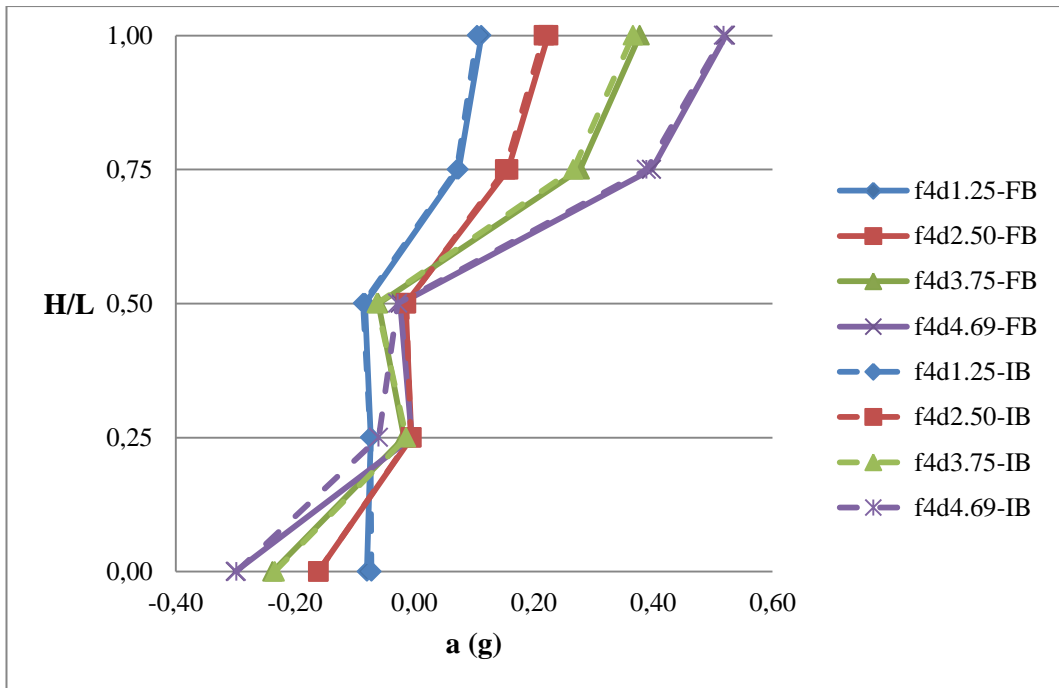
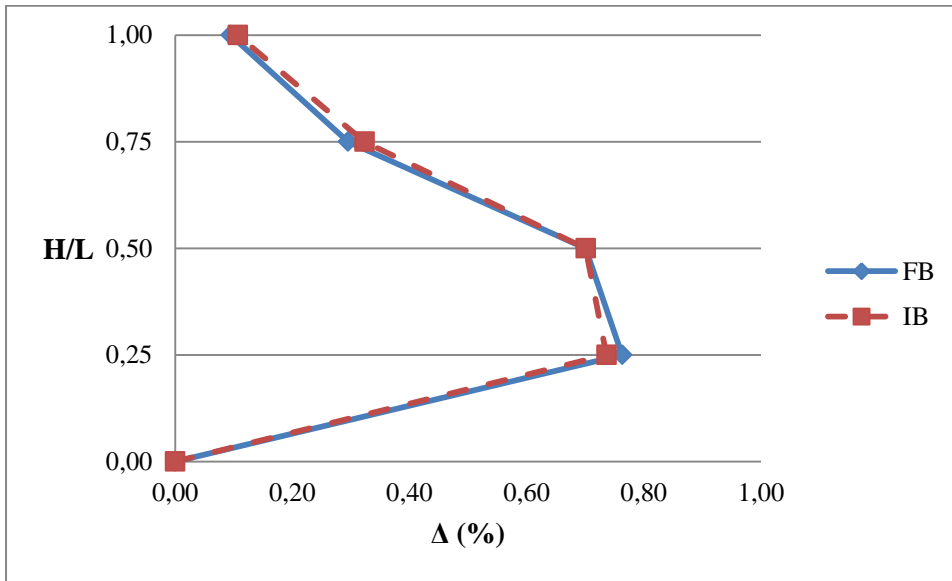
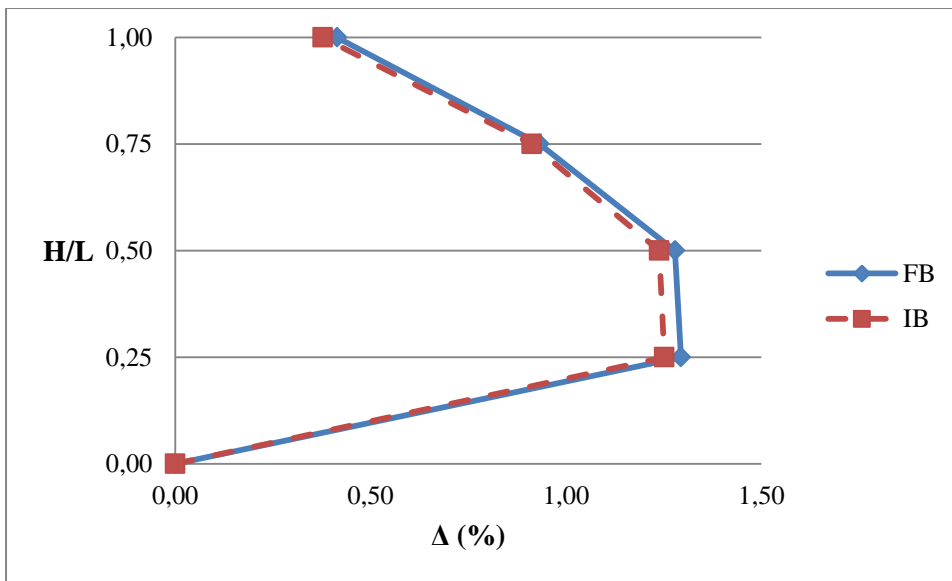


Fig. 4.14 a vs. H/L for $f = 4\text{Hz}$ (5-storey model)

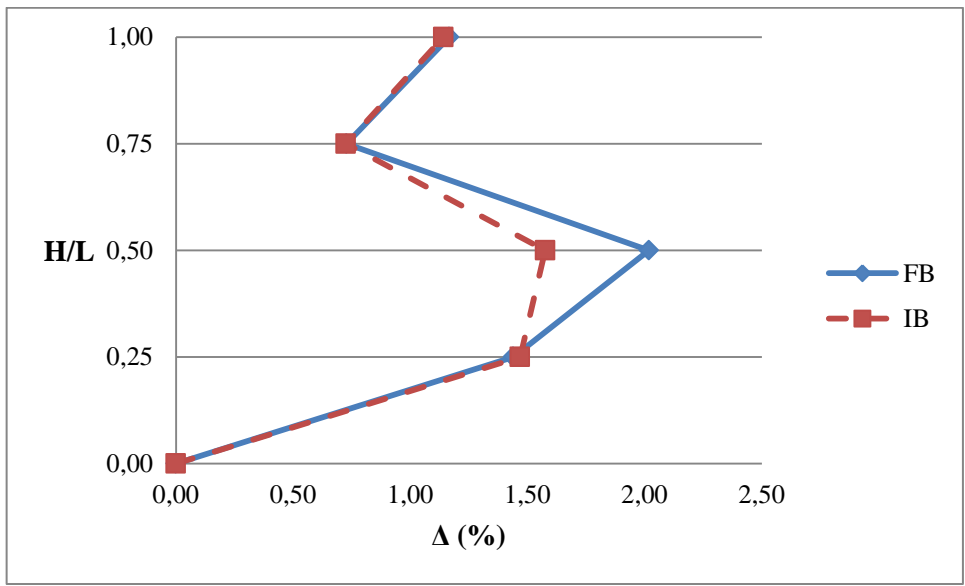


a. $f = 1\text{Hz}; d = 20\text{mm}$

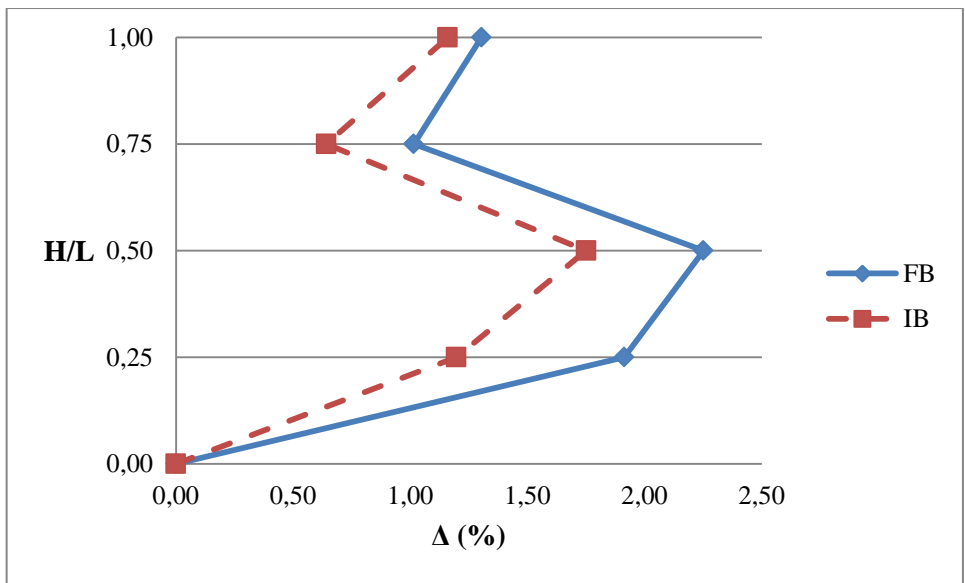


b. $f = 1\text{Hz}; d = 40\text{mm}$

Fig. 4.15 Δ vs. H/L for $f = 1\text{Hz}$ (5-storey model)

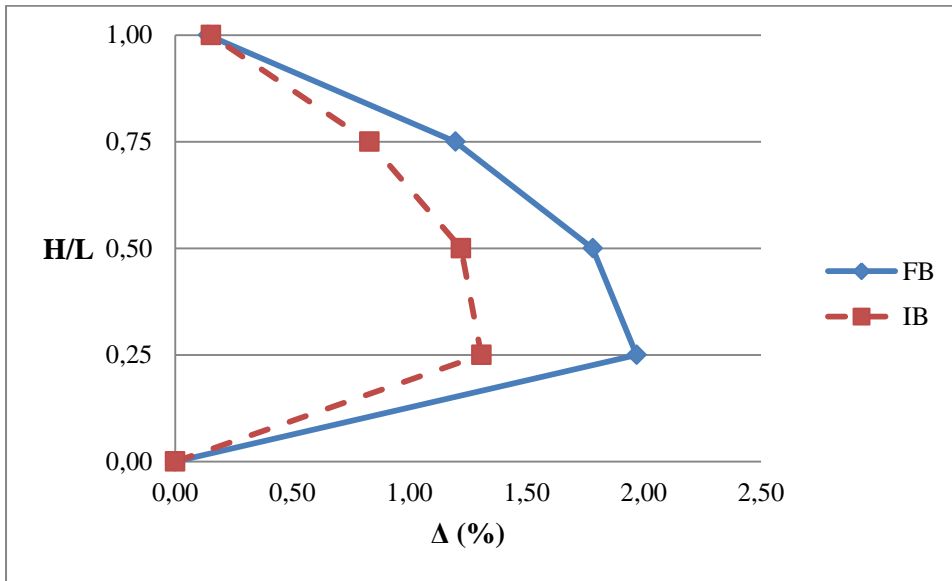


c. $f = 1\text{Hz}; d = 60\text{mm}$

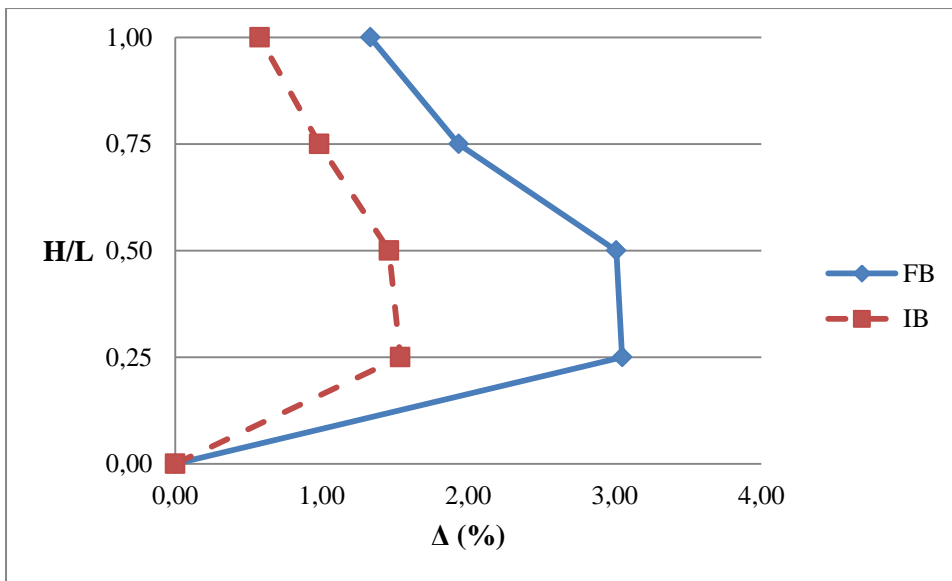


d. $f = 1\text{Hz}; d = 75\text{mm}$

Fig. 4.15 Δ vs. H/L for $f = 1\text{Hz}$ (5-storey model) (continued)

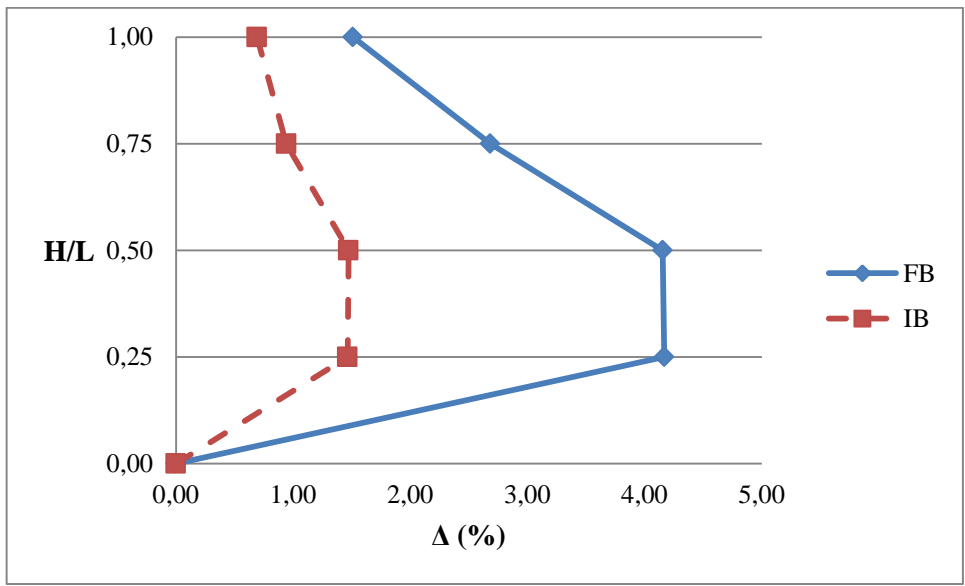


a. $f = 2\text{Hz}; d = 5\text{mm}$

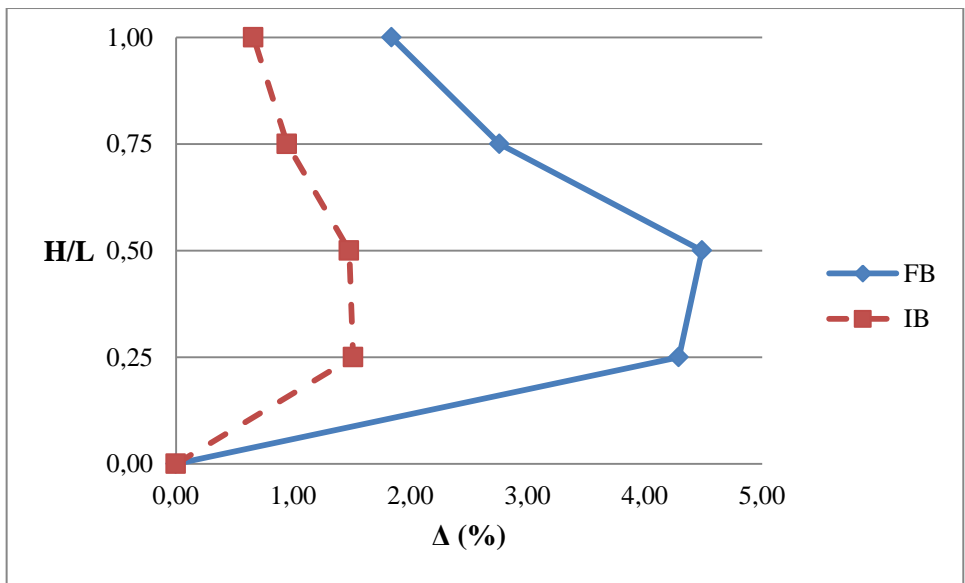


b. $f = 2\text{Hz}; d = 10\text{mm}$

Fig. 4.16 Δ vs. H/L for $f = 2\text{Hz}$ (5-storey model)

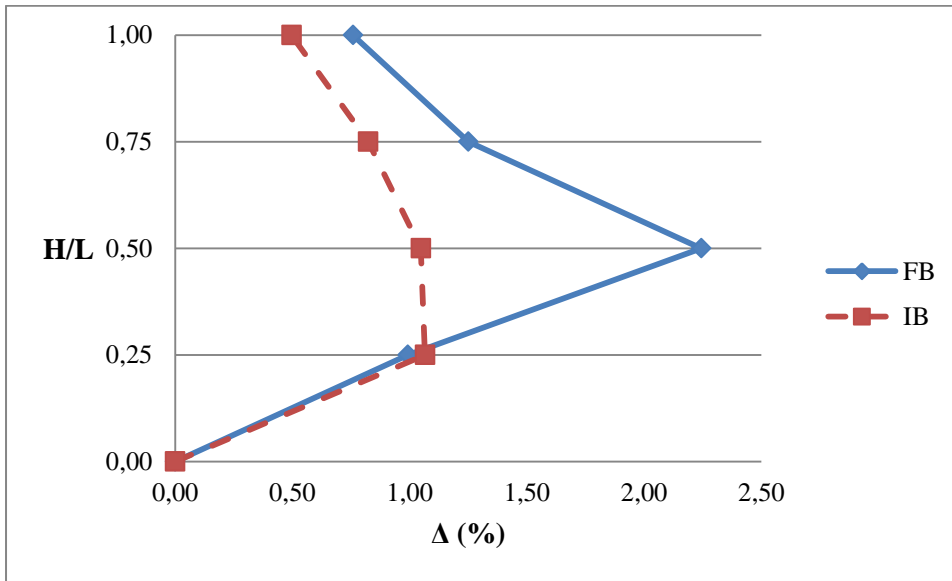


c. $f = 2\text{Hz}; d = 15\text{mm}$

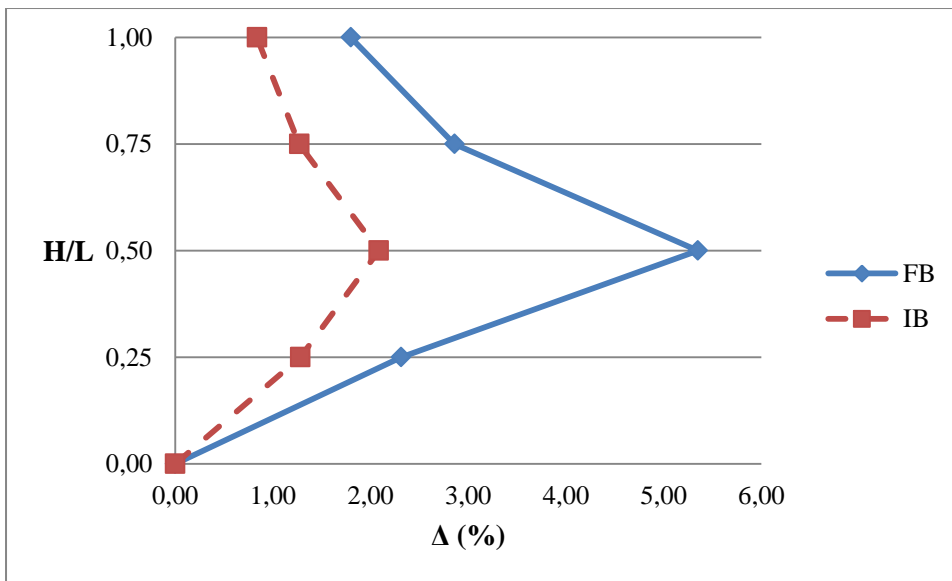


d. $f = 2\text{Hz}; d = 18.75\text{mm}$

Fig. 4.16 Δ vs. H/L for $f = 2\text{Hz}$ (5-storey model) (continued)

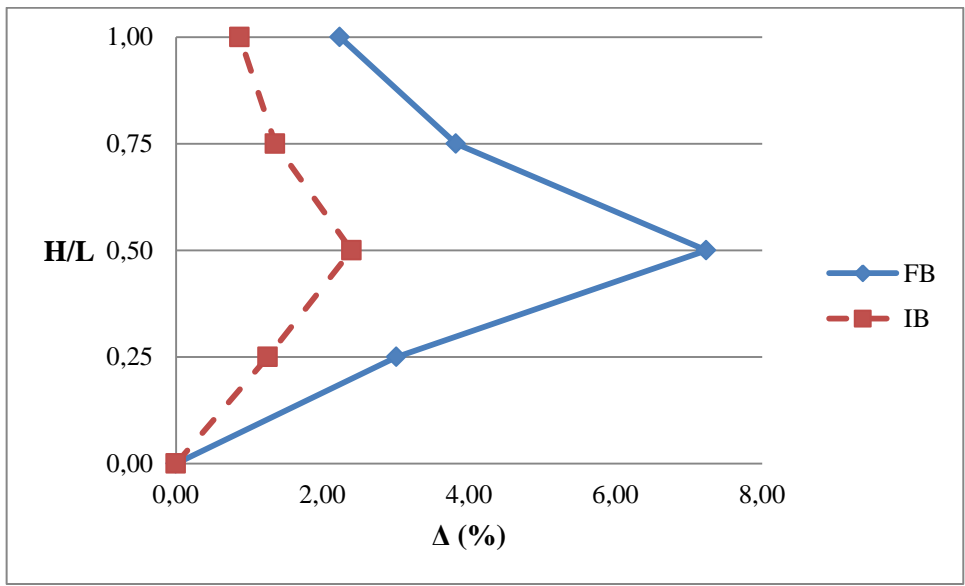


a. $f = 3\text{Hz}; d = 2.22\text{mm}$

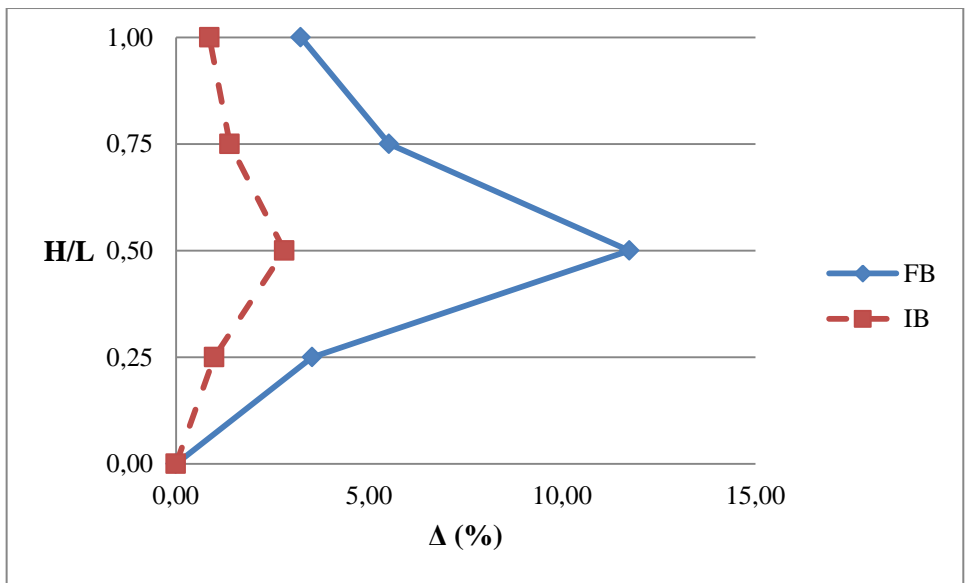


b. $f = 3\text{Hz}; d = 4.44\text{mm}$

Fig. 4.17 Δ vs. H/L for $f = 3\text{Hz}$ (5-storey model)

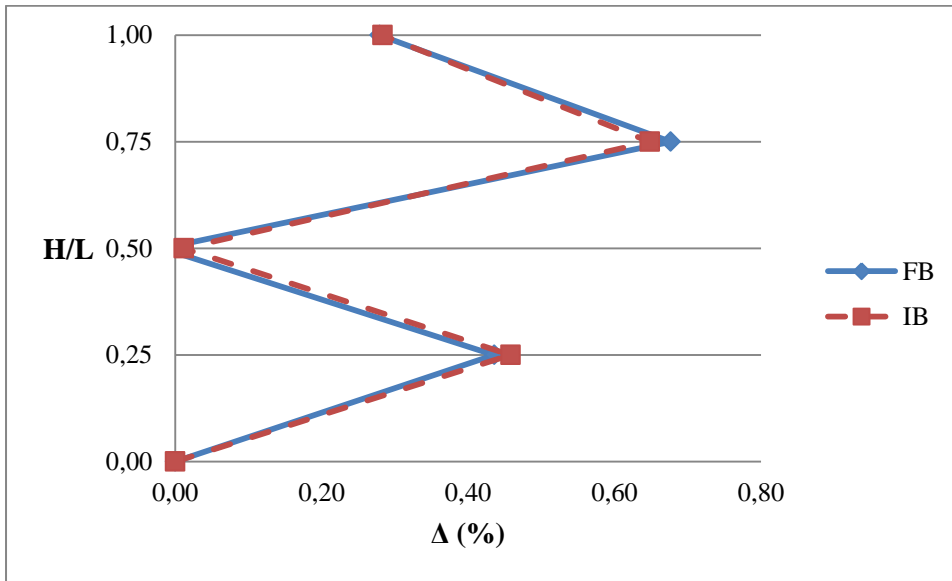


c. $f = 3\text{Hz}; d = 6.66\text{mm}$

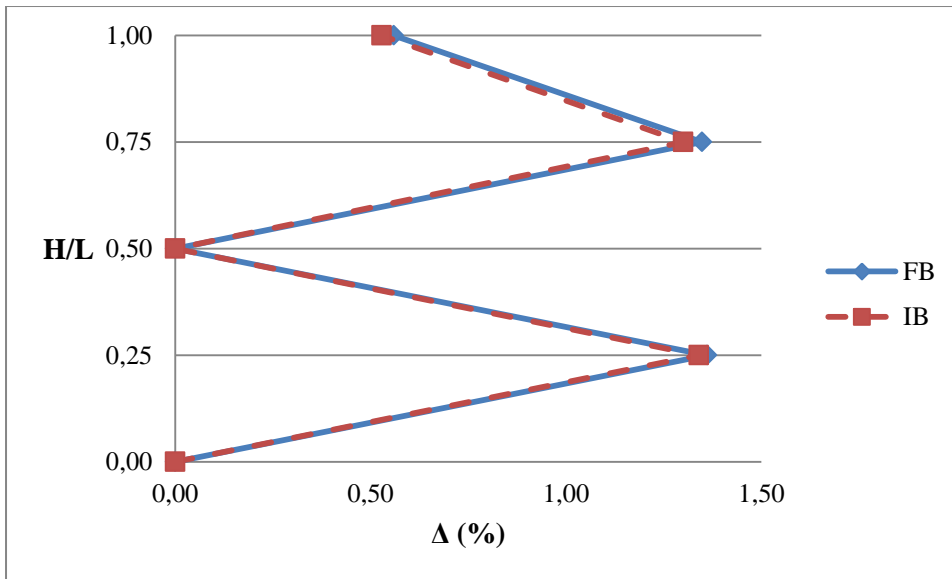


d. $f = 3\text{Hz}; d = 8.33\text{mm}$

Fig. 4.17 Δ vs. H/L for $f = 3\text{Hz}$ (5-storey model) (continued)

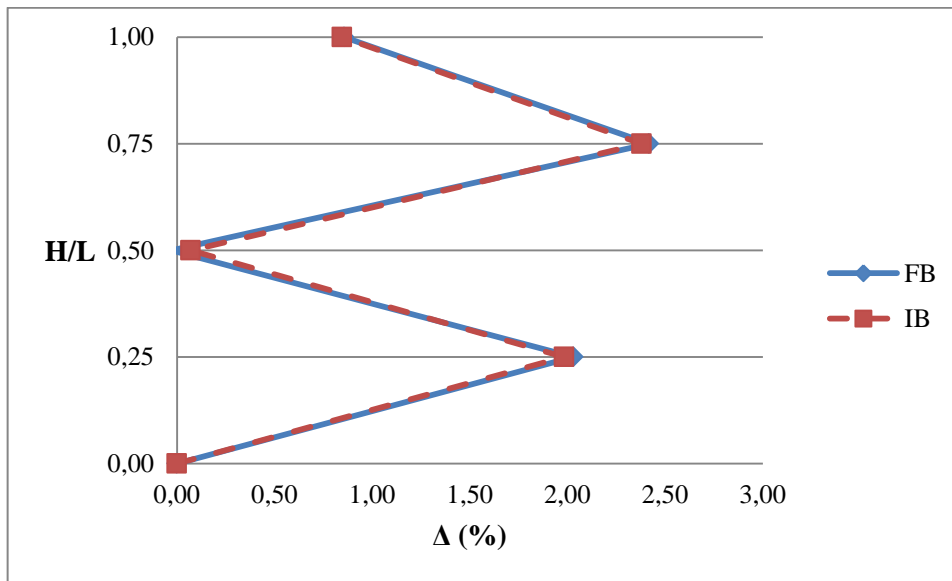


a. $f = 4\text{Hz}$; $d = 1.25\text{mm}$

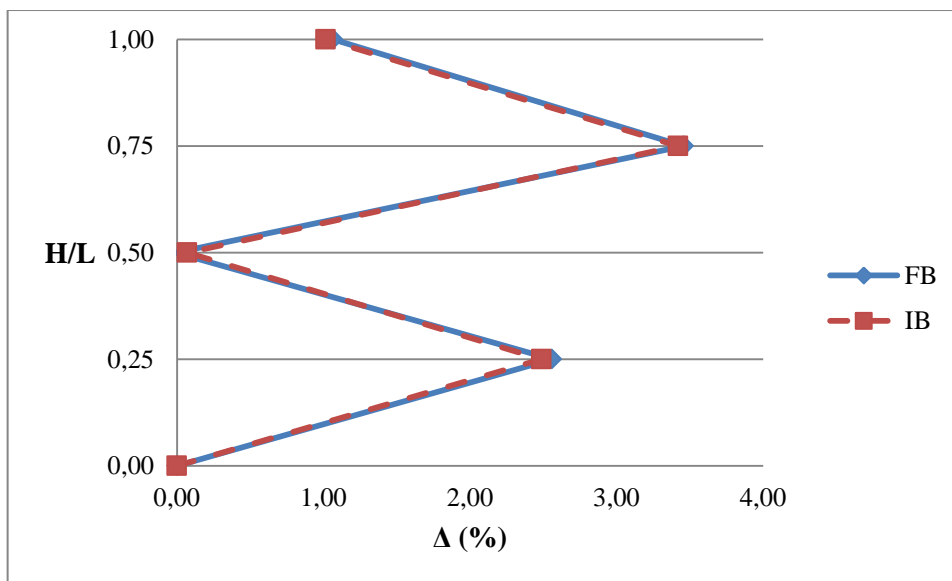


b. $f = 4\text{Hz}$; $d = 2.50\text{mm}$

Fig. 4.18 Δ vs. H/L for $f = 4\text{Hz}$ (5-storey model)



c. $f = 4\text{Hz}; d = 3.75\text{mm}$



d. $f = 4\text{Hz}; d = 4.69\text{mm}$

Fig. 4.18 Δ vs. H/L for $f = 4\text{Hz}$ (5-storey model) (continued)

4.3 Tests with Modified Ground Motion Data

In this part of the study, a total of 72 experiments were performed. The experiments were conducted by 6 different ground motion records scaled to three different maximum accelerations; $a_{\max} = 0.1, 0.2$ or $0.3g$. Three of these records were selected among the earthquake records associated with strike-slip fault mechanisms while the others were obtained during reverse fault mechanisms. For both fault mechanisms the records were selected in a way that the predominant frequency of the applied motion was approximately $f = 1, 2$ or 4Hz . The ground motion records of Landers and Coalinga earthquakes were time scaled to make the $f = 1\text{Hz}$ by time scales of $t_s = 0.75$ and $t_s = 0.95$ respectively. The motion data were acquired from the ground motion database of the

“Pacific Earthquake Engineering Research Center, PEER”. These data were originally filtered and baseline corrected. However in order to ensure that the high frequencies which are out of the scope of the machine was completely removed from the records, they were filtered by a fourth degree Butterworth bandpass filter having $f_{\text{low-cut}} = 0.2\text{Hz}$ and $f_{\text{high-cut}} = 5\text{Hz}$ upper and lower corner frequencies respectively. These boundaries were selected based on the concerned issues in Douglas and Boore (2011) and Akkar et al. (2011) about the possible boundaries for high-frequency filtering. In these studies it is indicated that the upper-bound frequency for filtering may be selected based on the Fourier amplitude spectra of the motion such that the peak spectral accelerations will not decrease more than 15%. This criterion is satisfied for all utilized records. The response and Fourier amplitude spectra of original and filtered motions are given in Appendix C. The list of the utilized ground motion records are given in Table 4.4. The modified ground motions are renamed to facilitate the presentation of the results. These names are given in Table 4.5 and Table 4.6 and will be referred throughout the thesis. The time histories of the utilized base motions are provided in Appendix D. Sampling rate was 250Hz during experiments.

Table 4.4 The utilized earthquake records

Earthquake	Date	Station	Mechanism	f (Hz)
Landers	28.06.1992	Arcadia Av	Strike-Slip	1
Chalfant Valley	21.07.1986	Tinemaha Res	Strike-Slip	2
Loma Prieta	18.10.1989	Capitola	Strike-Slip	4
Coalinga	02.05.1983	Park Field	Reverse	1
Northridge	17.01.1994	Sylmar-County Hospital	Reverse	2
San Fernando	09.02.1971	Carbon Canyon Dam	Reverse	4

Table 4.5 Base motions derived from ground motion data (strike-slip fault)

Earthquake	a_{max} (g)		
	0.10	0.20	0.30
Landers	S1_0.1	S1_0.2	S1_0.3
Chalfant Valley	S2_0.1	S2_0.2	S2_0.3
Loma Prieta	S3_0.1	S3_0.2	S3_0.3

Table 4.6 Base motions derived from ground motion data (reverse fault)

Earthquake	a_{max} (g)		
	0.10	0.20	0.30
Coalinga	R1_0.1	R1_0.2	R1_0.3
Northridge	R2_0.1	R2_0.2	R2_0.3
San Fernando	R3_0.1	R3_0.2	R3_0.3

4.3.1 Tests on 3-Storey Model with Modified Base Motions

The results of the tests with modified base motions (discussed in the previous part) which were conducted on the 3-storey model are presented in this section. Similar to the behavior under harmonic motions, the results were strongly dependent on the predominant frequency of the applied base motion.

Results of the tests are interpreted in terms of a constant “ η ” defined in Eq. (4.3) below, to determine the efficiency of the composite liner system. The term “ η ” reveals the percent change in the maximum difference of base and top floor accelerations in case of isolation (IB), with respect to the fixed base (FB). The maximum floor accelerations act on the models at the same instance for all floors. Figures which reveal the changes in floor accelerations are also given in Appendix E. In these figures “R” term stands for the percent reduction in the mid-floor accelerations in case of “IB” with respect to the “FB” case.

$$\eta = (\Delta a_1 - \Delta a_2) / \Delta a_1 \quad (4.3)$$

where,

Δa_1 = the difference in top and base floor accelerations for fixed base (FB)

Δa_2 = the difference in top and base floor accelerations for isolated base (IB)

As it can be observed in Fig. 4.19, for base motions derived from earthquake data associated with strike-slip fault mechanisms (S1, S2 and S3 motions), the predominant frequency of the input motion does not have a significant effect on the efficiency of the system unless it is in the close vicinity of “ f_n ” of the super structure. The predominant frequency of the input motion becomes more important for low a_{max} values (0.1g in this study) since the efficiency levels become highly dependent on the predominant frequency of the input motion and for higher values of a_{max} , the efficiency of the composite liner system varies in a very narrow band (0.75 – 0.85), almost independent of the predominant frequency of the input motion, for which 0.8 may be taken as the average value, meaning that the acceleration difference between the top and base floors of the model was decreased by 80% when the composite liner system was utilized.

According to the results presented in Fig. 4.20, the predominant frequency of the input motion has a much more important role in the efficiency of the isolation system when subjected to base motions stemming from reverse fault mechanisms (R1, R2 and R3 motions) as compared to those associated with strike-slip fault mechanisms (S1, S2 and S3 motions) for the tested motions. The efficiency “ η ” obtained for $f = 4\text{Hz}$ motion is much higher than those of motions with $f = 1\text{Hz}$ and $f = 2\text{Hz}$ for all “ a_{max} ” values and close to that of the ones obtained for base motions associated with strike-slip fault mechanism at the same predominant frequency. Based on this finding it can be stated that the importance of fault mechanism becomes negligible when the “ f ” of the motion is in the close vicinity of the “ f_n ” of the superstructure. Also it should be added that, the percent decreases in floor accelerations gained by the utilization of the composite liner system with respect to the unisolated case (R, see Appendix E) were proportional with the presented “ η ” values. It should also be noted that, the efficiency levels for motions with $f = 1\text{Hz}$ and $f = 2\text{Hz}$ are very close to each other but lower than those obtained for motions with strike-slip fault mechanisms for $a_{max} = 0.2\text{g}$ and $a_{max} = 0.3\text{g}$, while the η values are very close for $a_{max} = 0.1\text{g}$ for both fault mechanisms.

The acceleration-time histories for base accelerations of “FB” and “IB” cases are given in Appendix F. As it can be seen in these figures, the maximum accelerations were generally deamplified. Also it can be observed that the maximum accelerations developed in the model for “IB” cases were measured usually at the same time as the a_{max} of the input motion or so close to that instance. The filtering in accelerations was more visible for input motions with predominant frequencies close to the natural frequency of the model and for experiments with higher “ a_{max} ” values, as expected (see Fig. F.6.c). However, evaluating the behavior of the composite liner system in the time domain may be misleading since the system provided main benefits by altering the frequency content of the motion and the corresponding spectral accelerations rather than

directly decreasing the accelerations. For this reason the following evaluations were done based on the response and Fourier amplitude spectra, in other words in the frequency domain.

The response spectra ($D=1.24\%$) for the “FB” and “IB” cases are given in Fig. 4.21 – 4.38 for the performed experiments. As it can be observed in these figures, the base accelerations were generally decreased when the composite liner system was utilized. But more interestingly, the spectral accelerations significantly dropped at the first mode natural period of the tested model ($T_n = 0.23s$). This fact provides the decrease in the difference between top and base floor accelerations (the η discussed previously). It should be also noted that, very slight amplifications ($\leq 10\%$) occurred in the base accelerations for motions with low frequency and/or low “ a_{max} ” levels but even for these cases improvement was observed in the model behavior. To illustrate; for “S1_0.1” motion, the base acceleration was increased to 0.11g for “IB” case but nevertheless the efficiency of the system was determined as $\eta = 20\%$ for this motion. The response spectra for $D = 5\%$ damping are also given in Appendix G.

The Fourier amplitude (F.A.) spectra for “FB” and “IB” are given in Fig. 4.39 – 4.56. In these figures it can be observed that, the frequency contents of the base motions were altered when the composite liner system was utilized. The Fourier amplitudes were deamplified in the close vicinity of the “ f_n ” of the superstructure at the expense of amplifications at higher frequencies. This effect was more clearly observed as predominant frequency of the base motion got closer to the “ f_n ” of the superstructure (see Fig. 4.56). The general behavior of the composite liner system was similar for motions corresponding to both fault mechanisms.

In contrast to the situation in the harmonic motions, the composite liner system was triggered in all experiments regardless of the input motion frequency “ f ” and maximum base acceleration “ a_{max} ”. The magnitudes of slip displacements for each base motion are listed below in Table 4.7 and Table 4.8. The maximum displacement of the model during the experiment with respect to the initial position is given as the slip displacement in the tables below. It is observed from these tables that the magnitude of the slip displacement increases with increasing “ a_{max} ”. The recorded slip displacements were higher for motions with low predominant frequency ($f = 1Hz$). Another noteworthy point is that the amount of slip displacements increased noticeably when the predominant frequency “ f ” of the base motion is in the close vicinity of the first-mode natural frequency “ f_n ” of the superstructure which results in significant reduction in acceleration values and an increase in the composite liner system efficiency, “ η ”. It is also observed that the slip displacements recorded during experiments for the base motions obtained by modifying the earthquake records associated with reverse fault mechanisms were slightly less than those recorded for base motions associated with strike-slip fault mechanisms for the same predominant motion frequency “ f ” and maximum acceleration “ a_{max} ”.

Table 4.7 The slip for 3-storey model (strike-slip fault mechanism)

Base Motion	Slip (mm)
S1_0.1	1.62
S1_0.2	16.82
S1_0.3	28.19
S2_0.1	1.43
S2_0.2	9.49
S2_0.3	11.23
S3_0.1	2.11
S3_0.2	10.18
S3_0.3	15.27

Table 4.8 The slip for 3-storey model (reverse fault mechanism)

Base Motion	Slip (mm)
R1_0.1	1.36
R1_0.2	7.67
R1_0.3	24.57
R2_0.1	0.76
R2_0.2	5.96
R2_0.3	9.06
R3_0.1	1.20
R3_0.2	6.41
R3_0.3	14.70

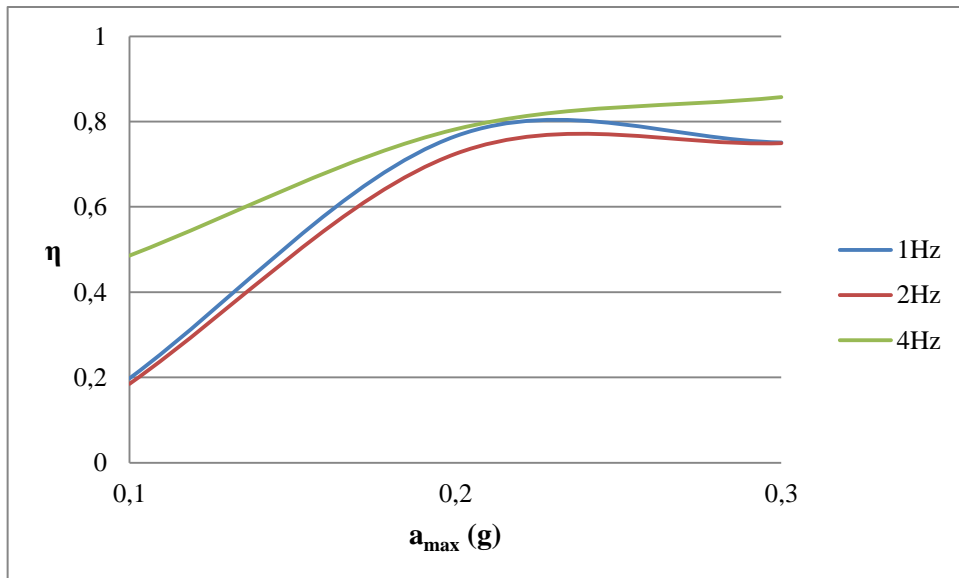


Fig. 4.19 a_{max} vs. η for strike-slip fault mechanism ($f_n = 4.35$ Hz)

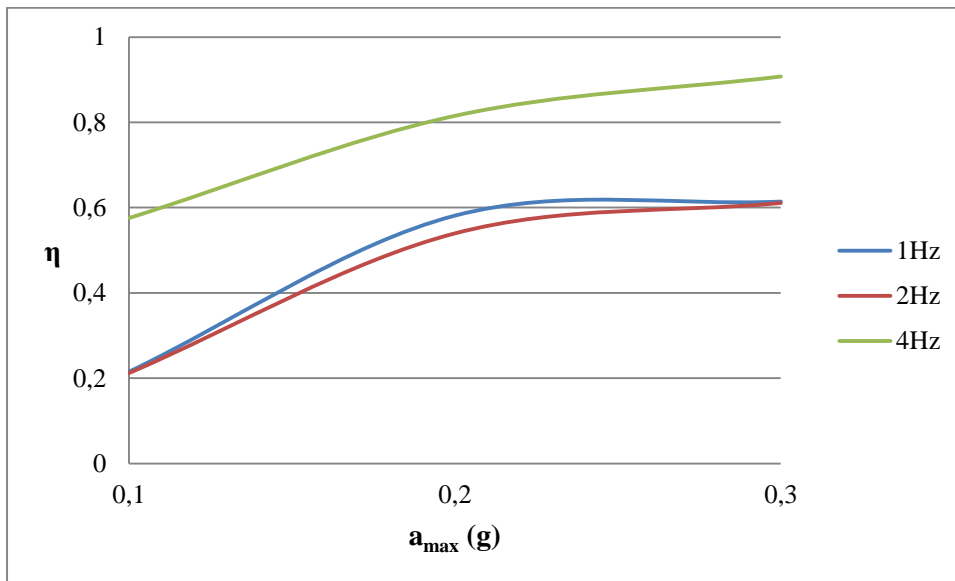


Fig. 4.20 a_{max} vs. η for reverse fault mechanism ($f_n = 4.35$ Hz)

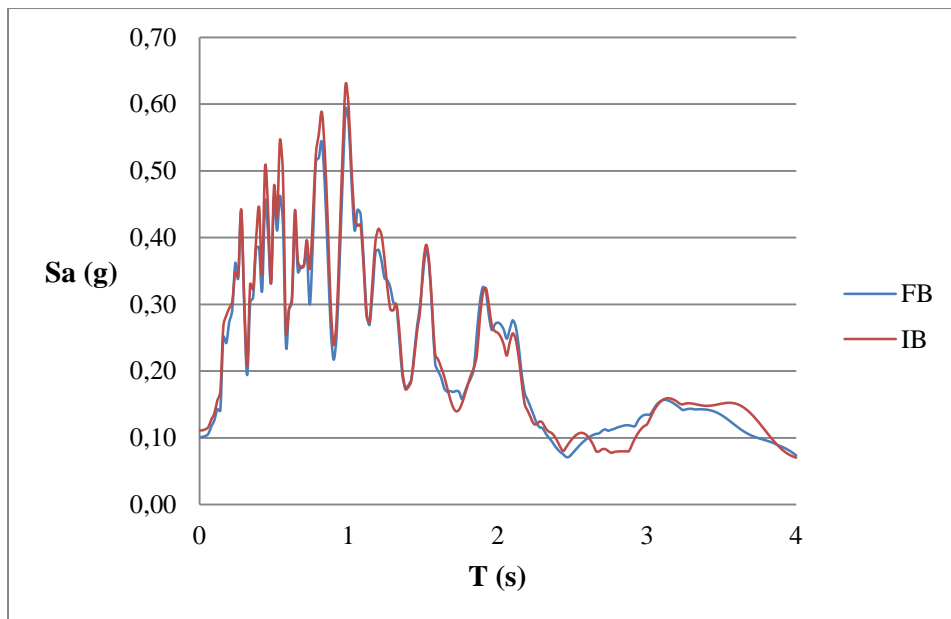


Fig. 4.21 Response spectra for S1_0.1 motion ($D = 1.24\%$)

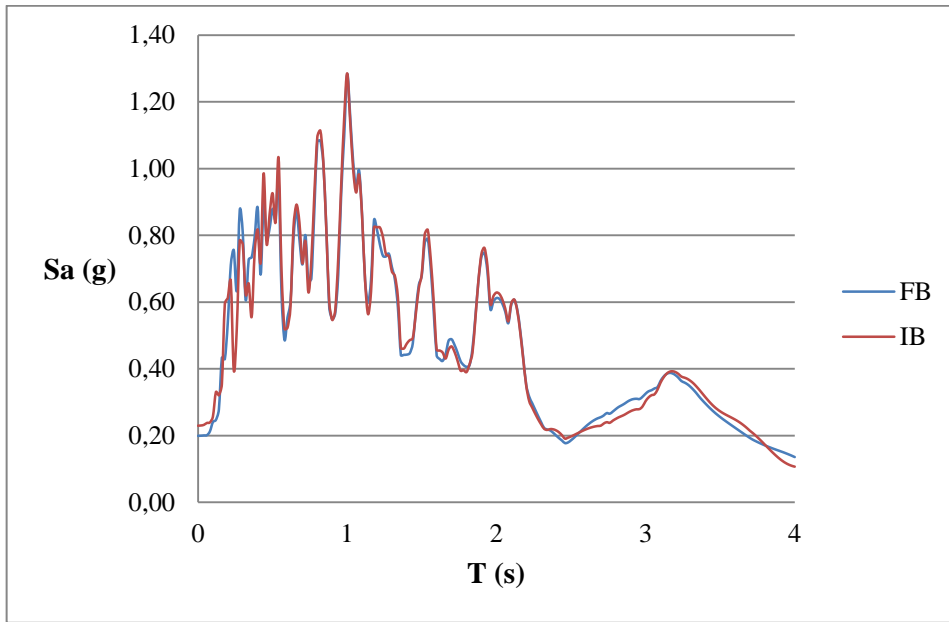


Fig. 4.22 Response spectra for S1_0.2 motion (D = 1.24%)

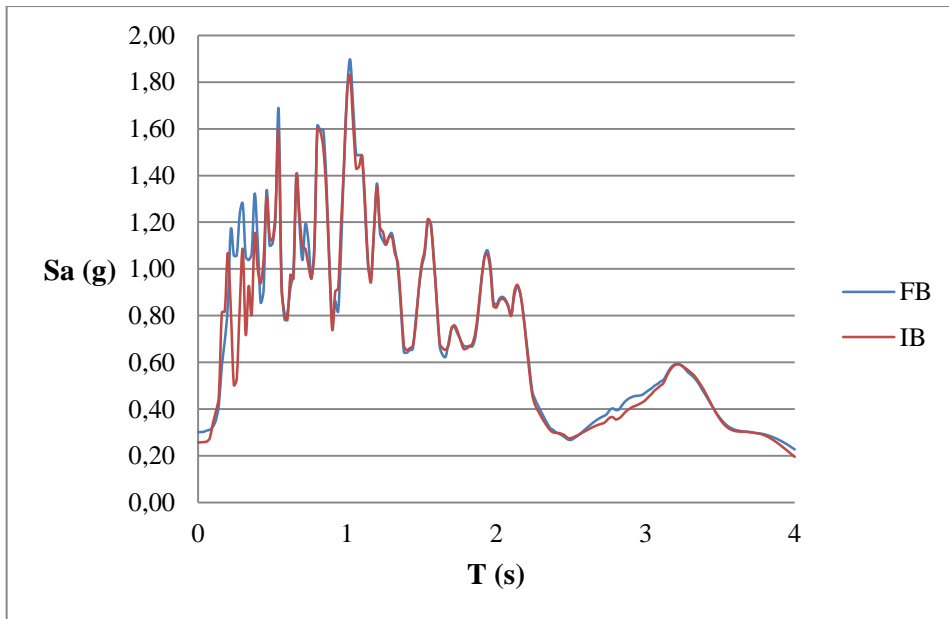


Fig. 4.23 Response spectra for S1_0.3 motion (D = 1.24%)

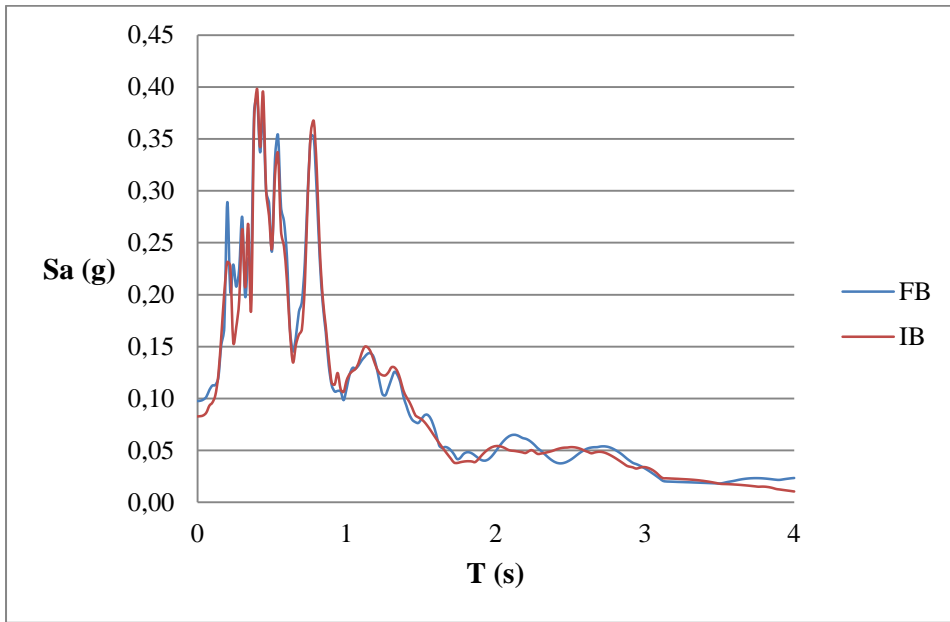


Fig. 4.24 Response spectra for S2_0.1 motion (D = 1.24%)

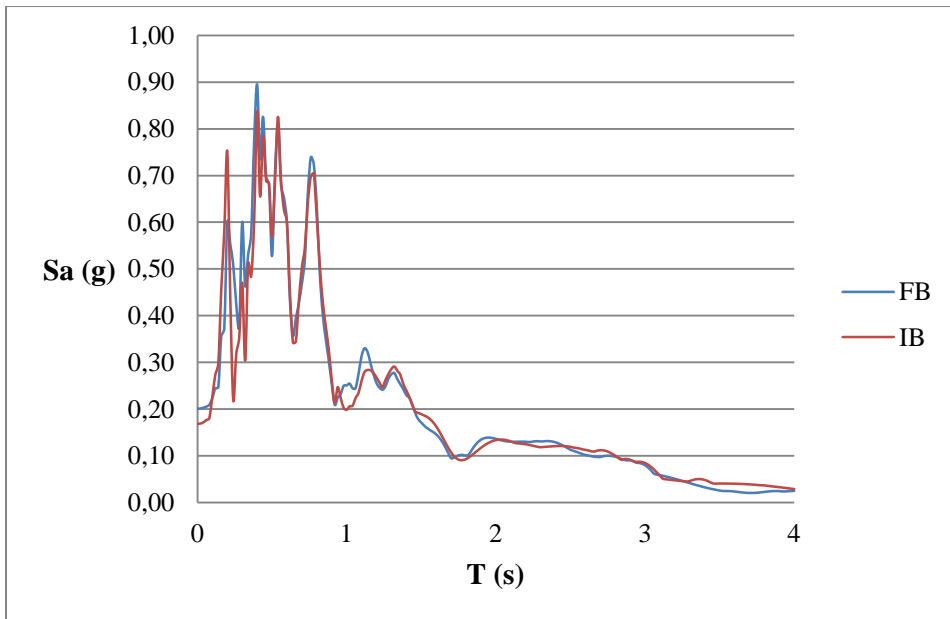


Fig. 4.25 Response spectra for S2_0.2 motion (D = 1.24%)

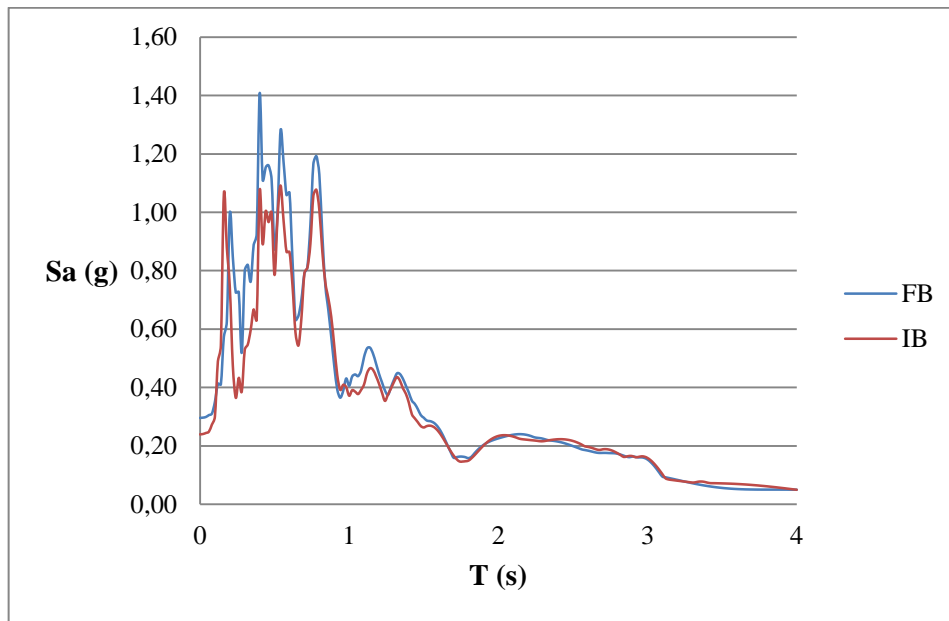


Fig. 4.26 Response spectra for S2_0.3 motion (D = 1.24%)

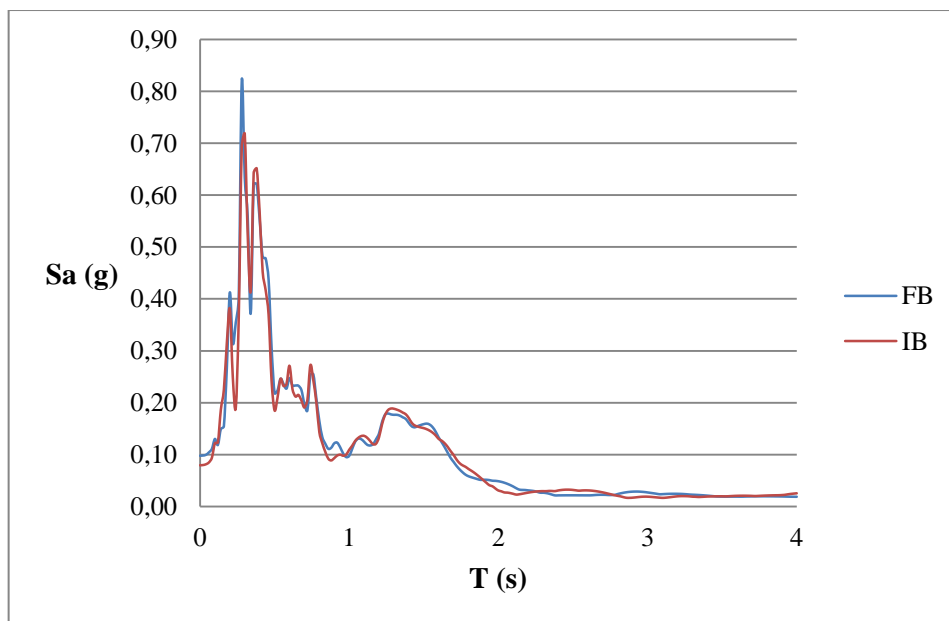


Fig. 4.27 Response spectra for S3_0.1 motion (D = 1.24%)

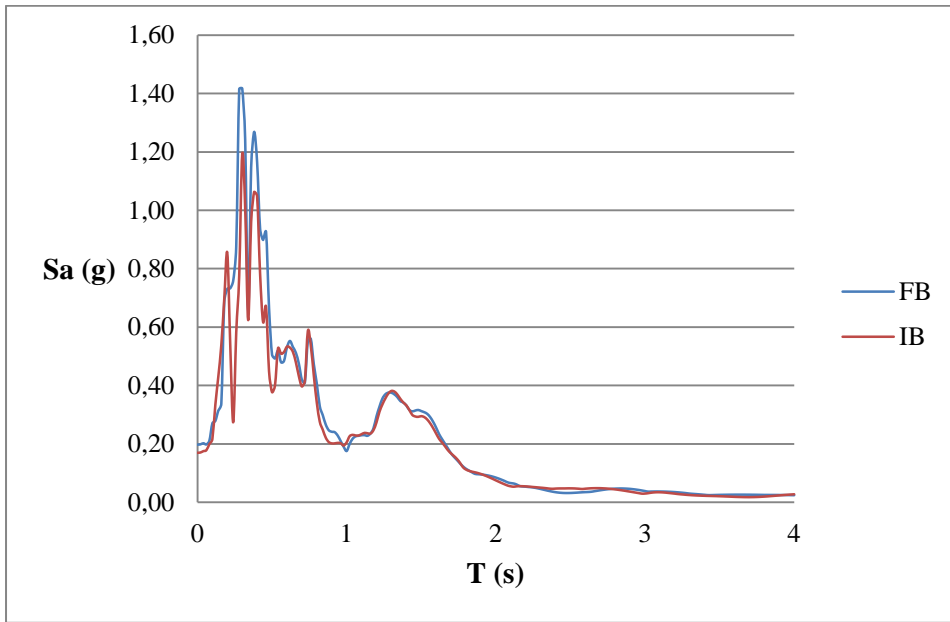


Fig. 4.28 Response spectra for S3_0.2 motion (D = 1.24%)

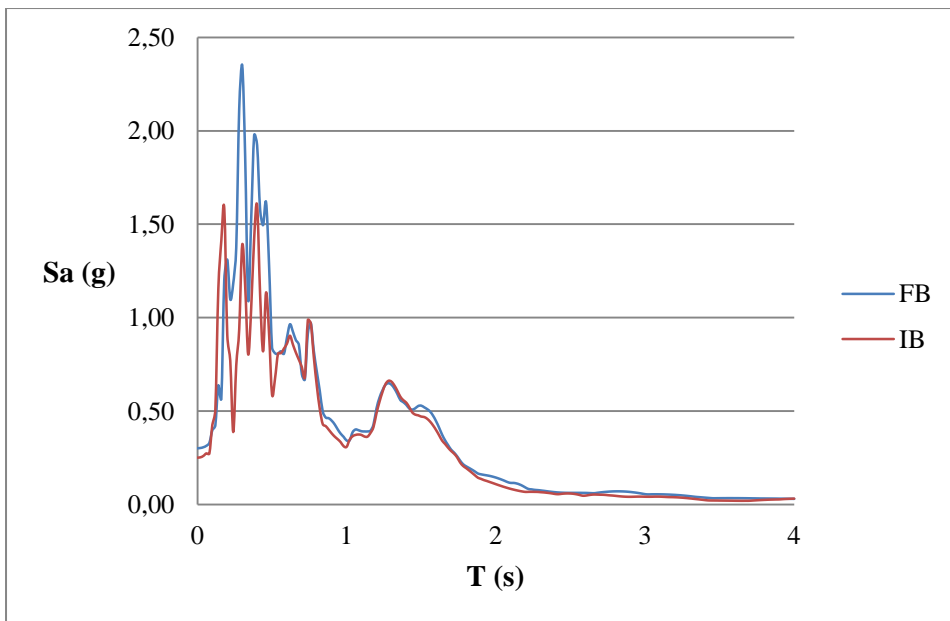


Fig. 4.29 Response spectra for S3_0.3 motion (D = 1.24%)

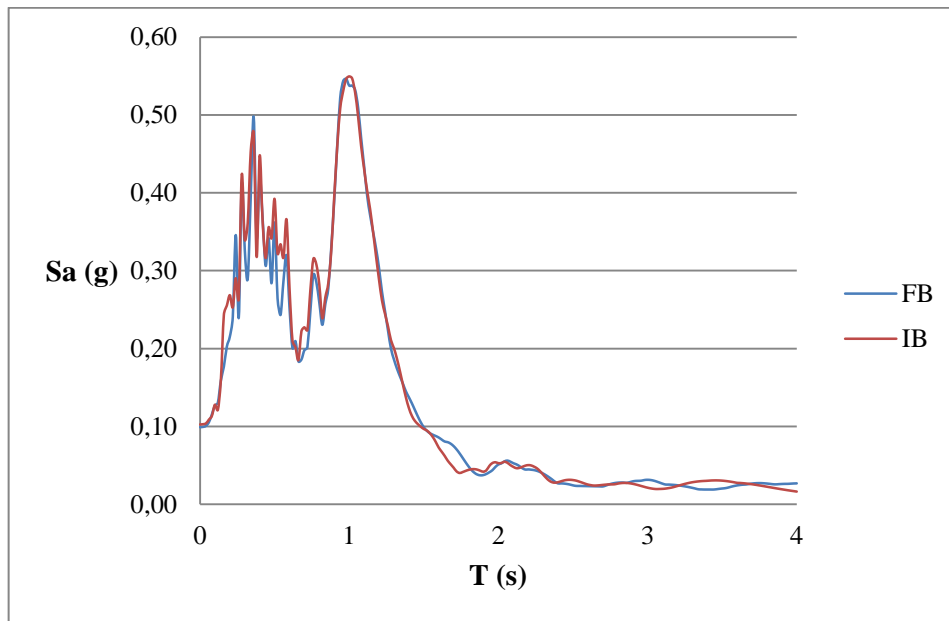


Fig. 4.30 Response spectra for R1_0.1 motion (D = 1.24%)

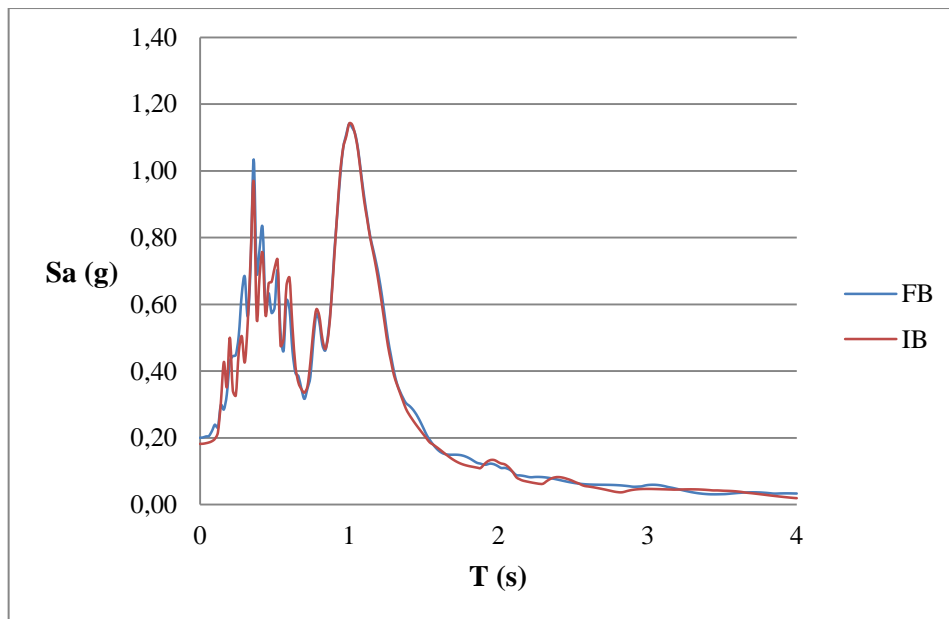


Fig. 4.31 Response spectra for R1_0.2 motion (D = 1.24%)

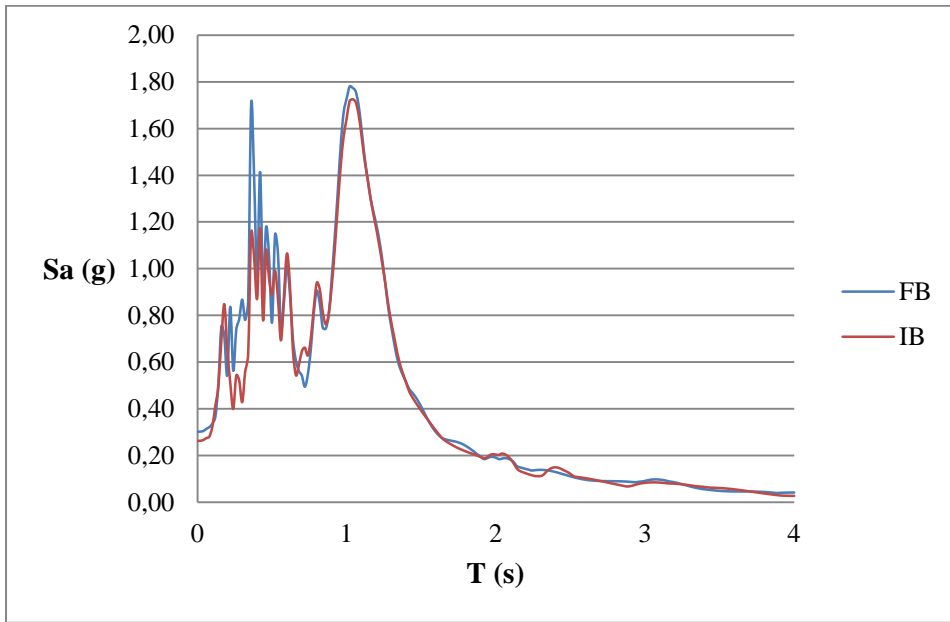


Fig. 4.32 Response spectra for R1_0.3 motion (D = 1.24%)

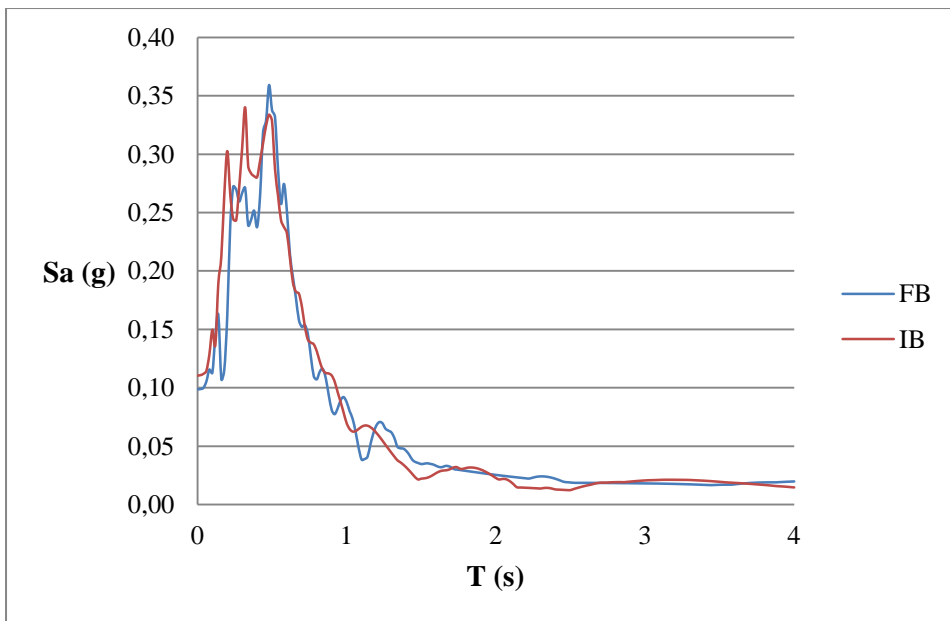


Fig. 4.33 Response spectra for R2_0.1 motion (D = 1.24%)

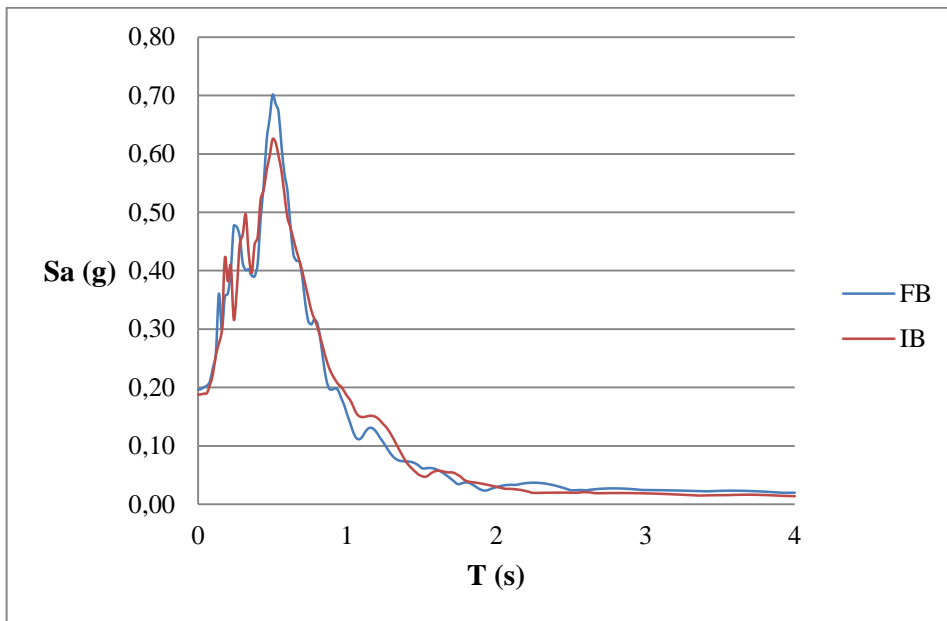


Fig. 4.34 Response spectra for R2_0.2 motion (D = 1.24%)

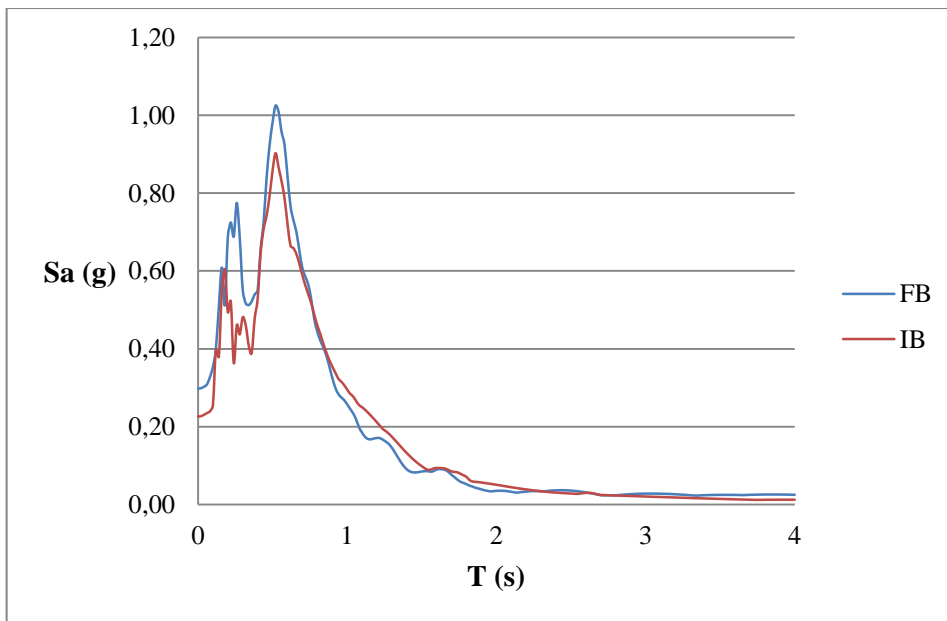


Fig. 4.35 Response spectra for R2_0.3 motion (D = 1.24%)

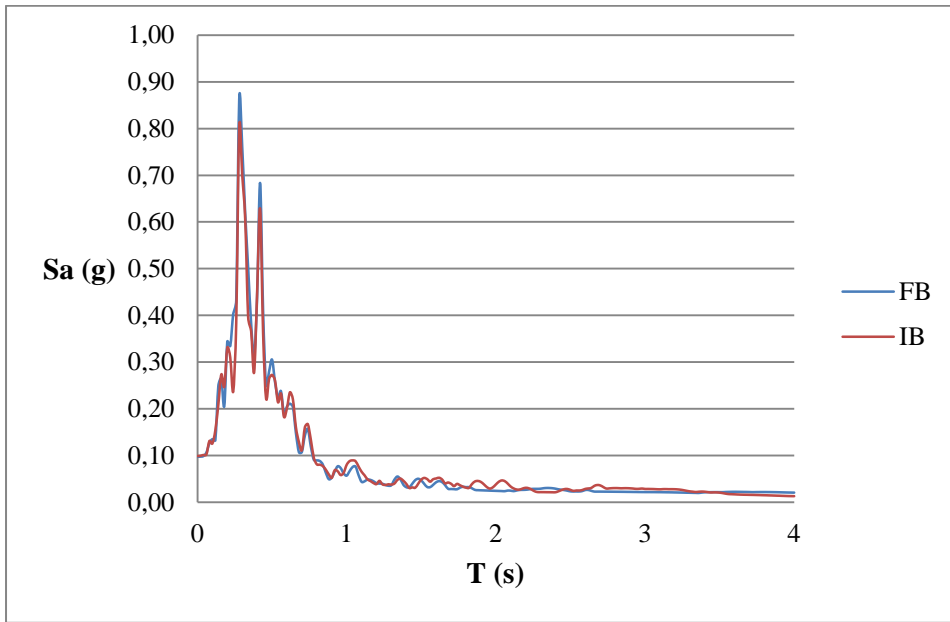


Fig. 4.36 Response spectra for R3_0.1 motion (D = 1.24%)

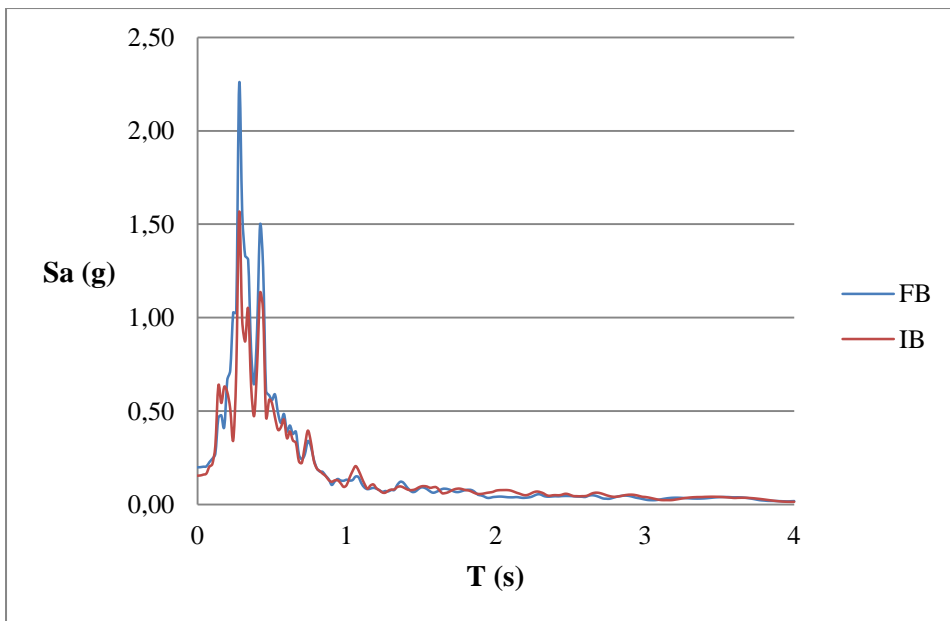


Fig. 4.37 Response spectra for R3_0.2 motion (D = 1.24%)

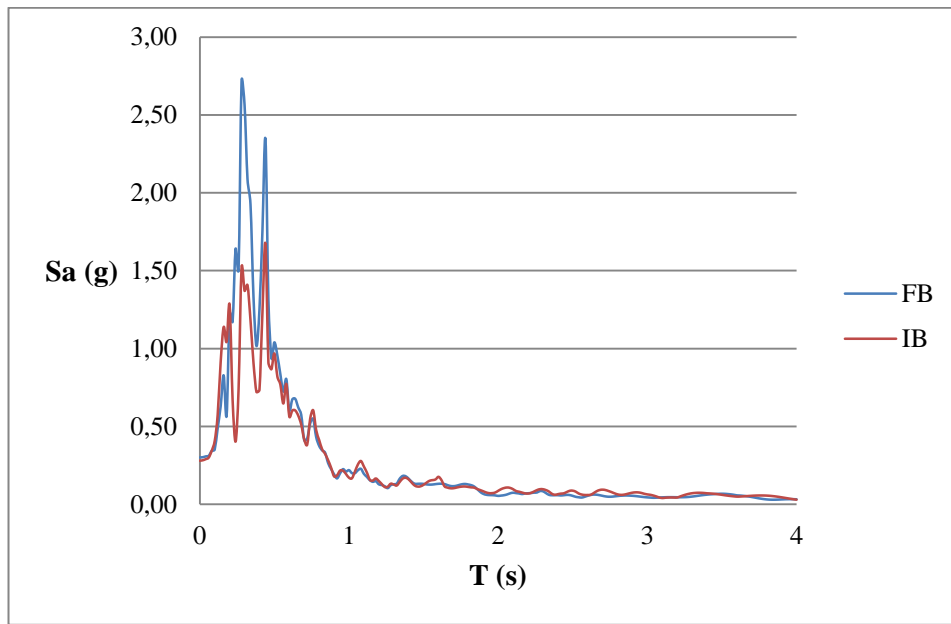


Fig. 4.38 Response spectra for R3_0.3 motion (D = 1.24%)

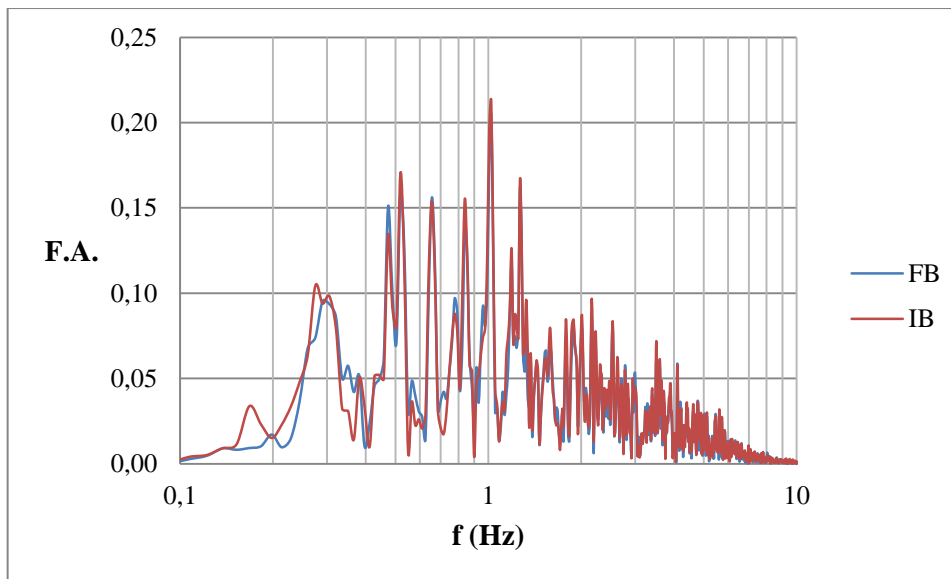


Fig. 4.39 Fourier amplitude spectra for S1_0.1 motion (3-storey model)

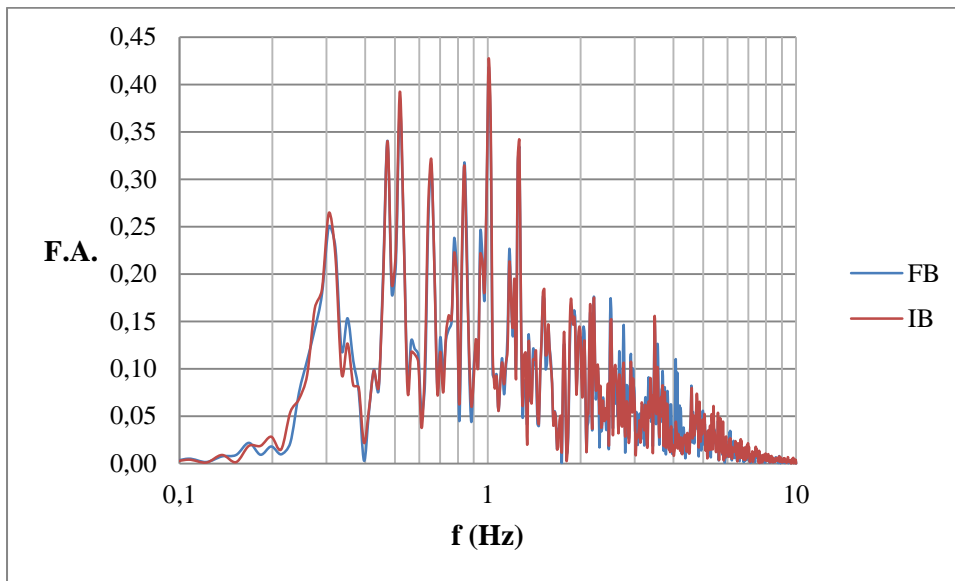


Fig. 4.40 Fourier amplitude spectra for S1_0.2 motion (3-storey model)

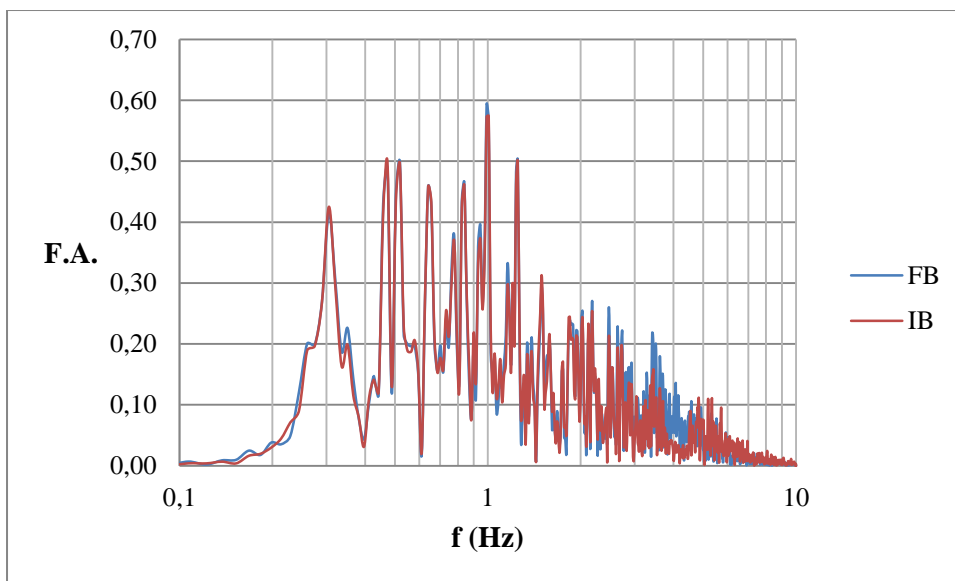


Fig. 4.41 Fourier amplitude spectra for S1_0.3 motion (3-storey model)

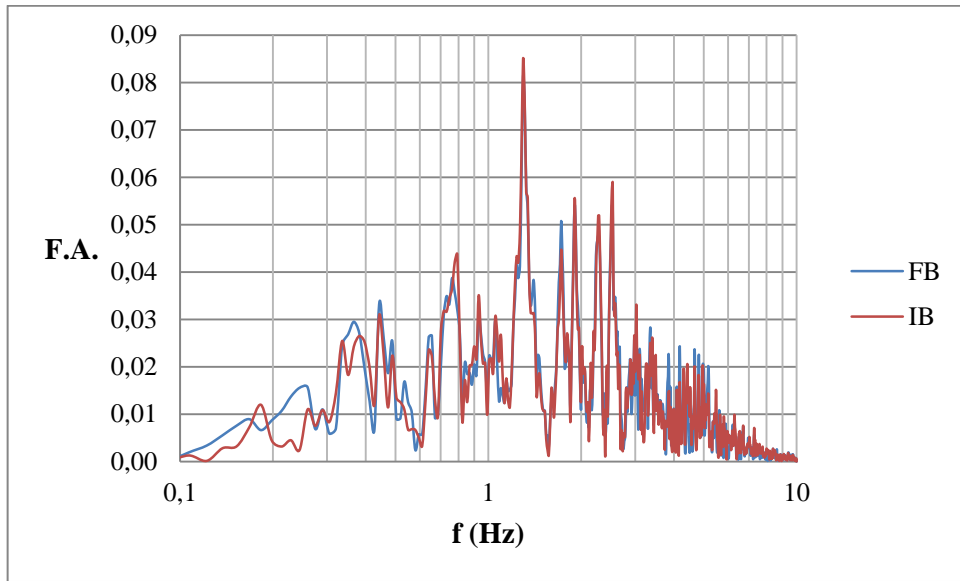


Fig. 4.42 Fourier amplitude spectra for S2_0.1 motion (3-storey model)

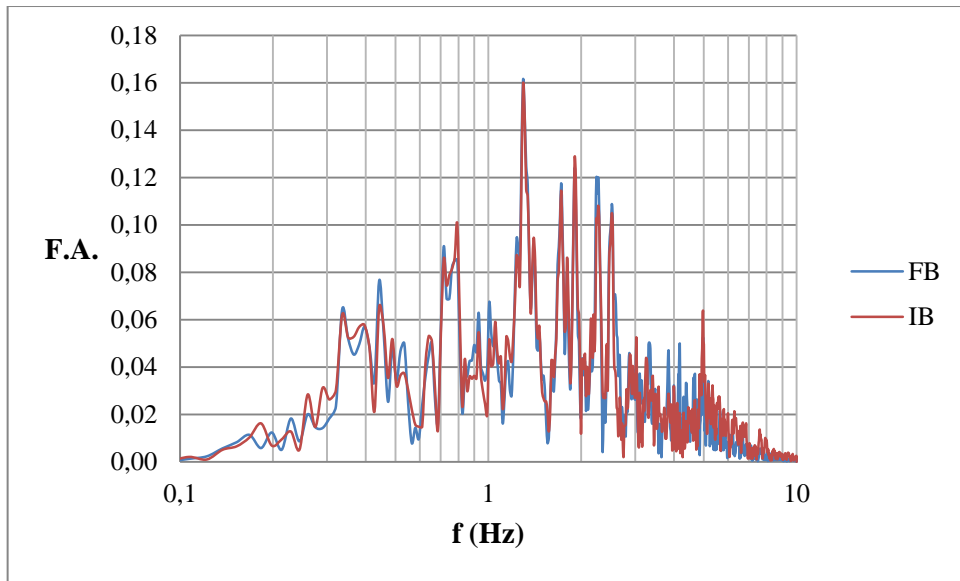


Fig. 4.43 Fourier amplitude spectra for S2_0.2 motion (3-storey model)

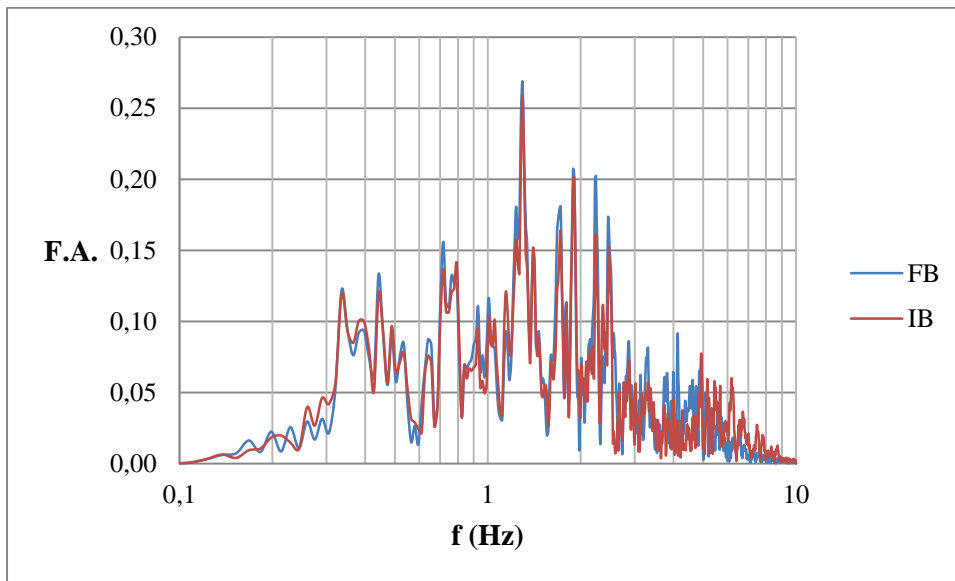


Fig. 4.44 Fourier amplitude spectra for S2_0.3 motion (3-storey model)

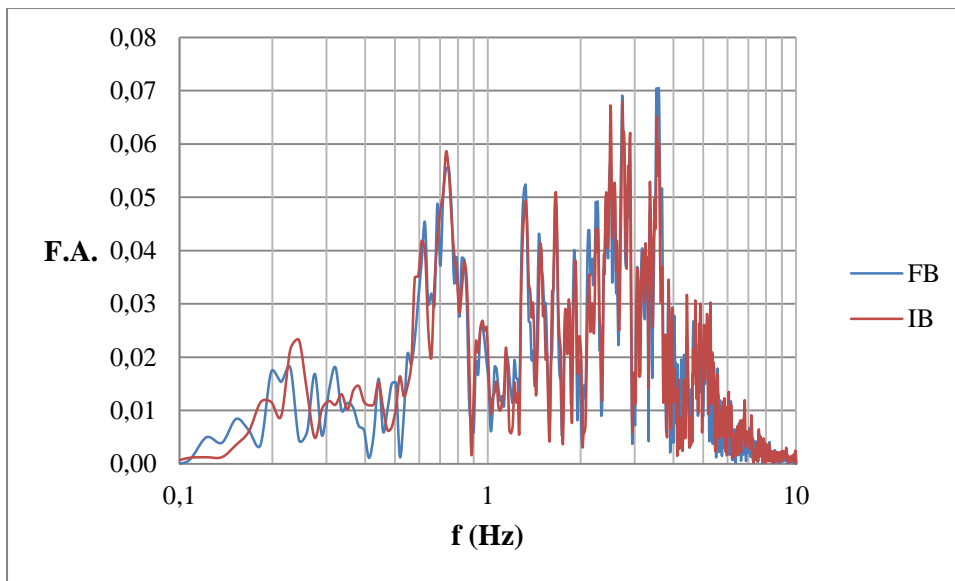


Fig. 4.45 Fourier amplitude spectra for S3_0.1 motion (3-storey model)

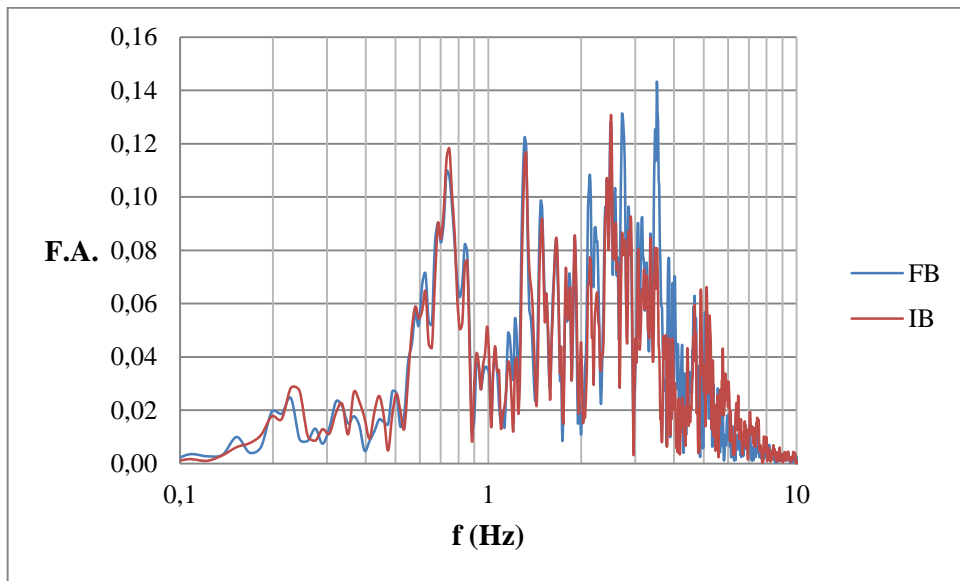


Fig. 4.46 Fourier amplitude spectra for S3_0.2 motion (3-storey model)

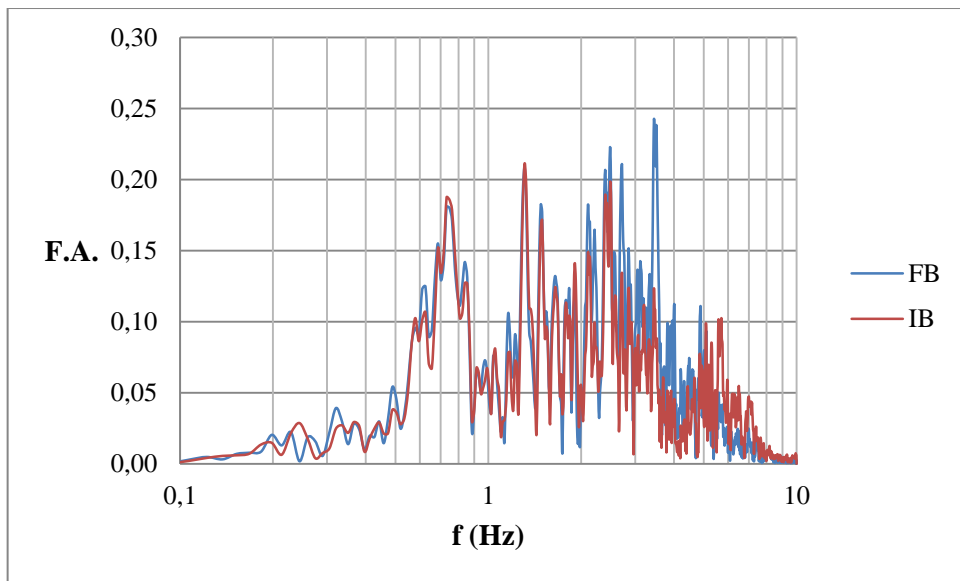


Fig. 4.47 Fourier amplitude spectra for S3_0.3 motion (3-storey model)

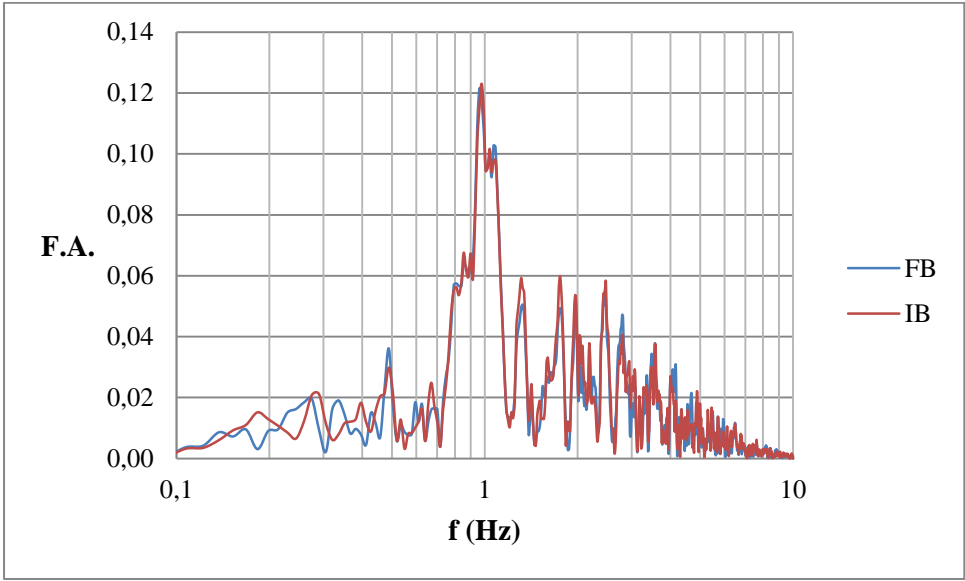


Fig. 4.48 Fourier amplitude spectra for R1_0.1 motion (3-storey model)

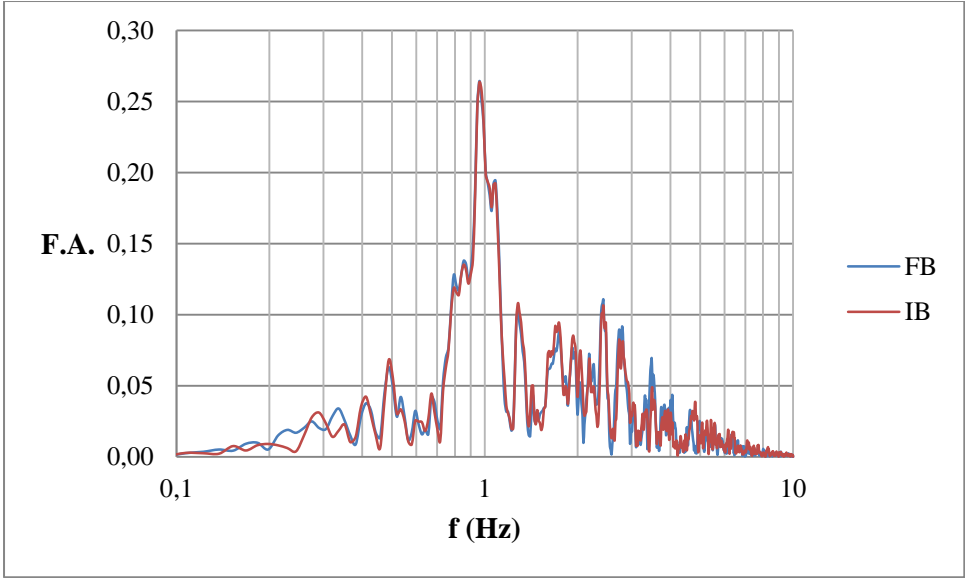


Fig. 4.49 Fourier amplitude spectra for R1_0.2 motion (3-storey model)

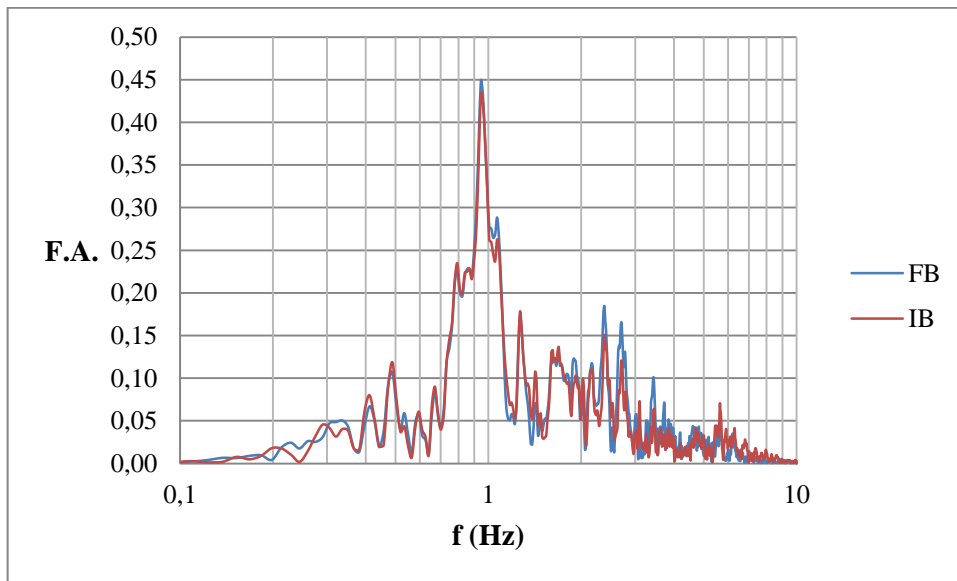


Fig. 4.50 Fourier amplitude spectra for R1_0.3 motion (3-storey model)

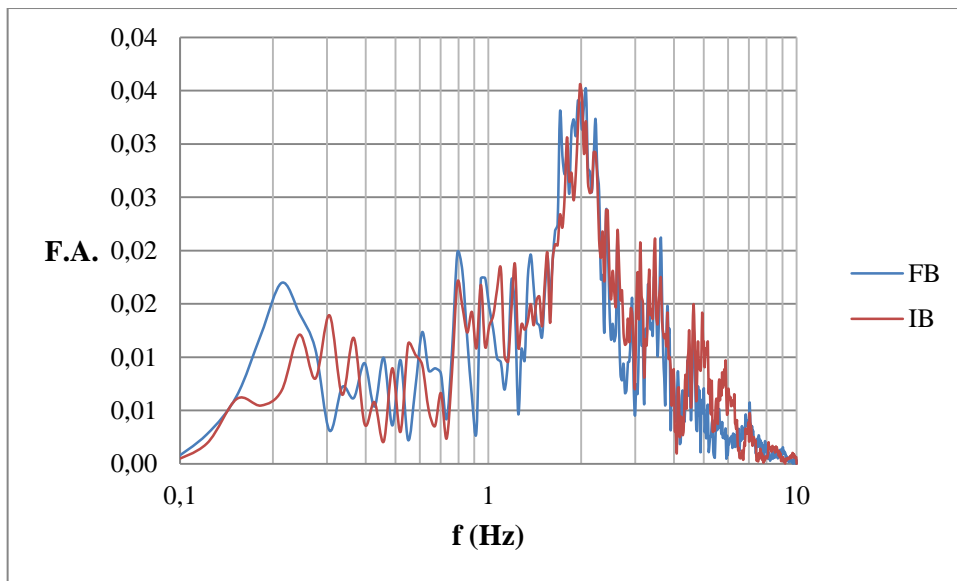


Fig. 4.51 Fourier amplitude spectra for R2_0.1 motion (3-storey model)

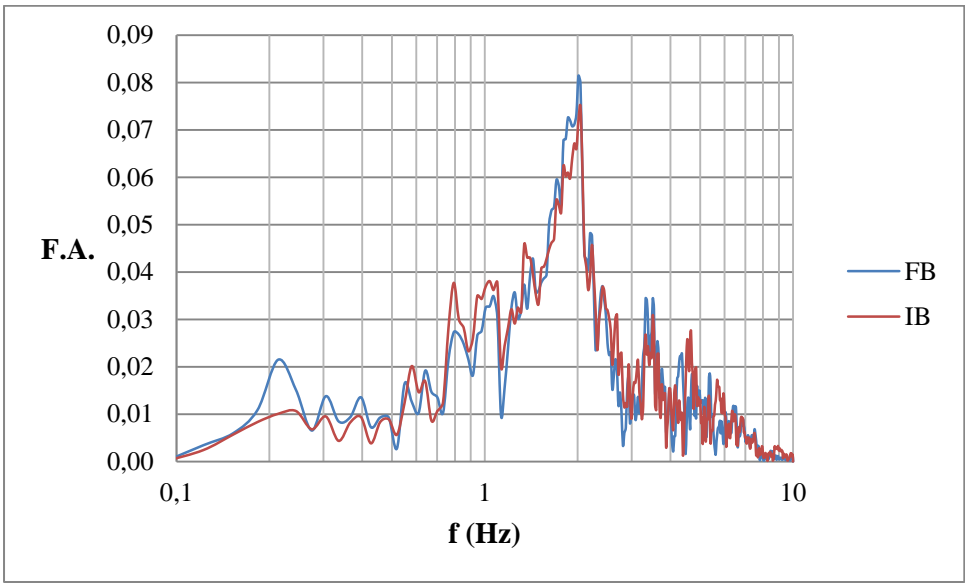


Fig. 4.52 Fourier amplitude spectra for R2_0.2 motion (3-storey model)

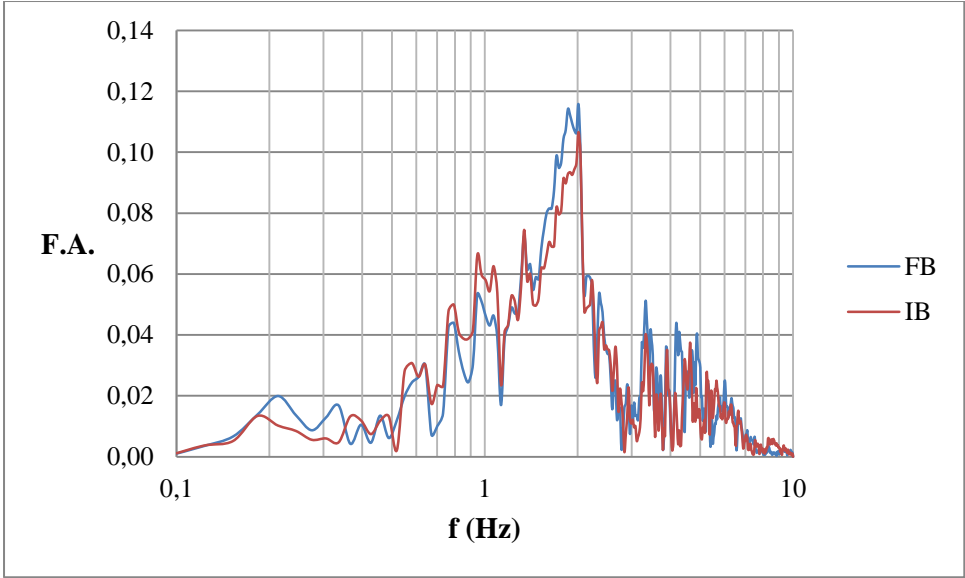


Fig. 4.53 Fourier amplitude spectra for R2_0.3 motion (3-storey model)

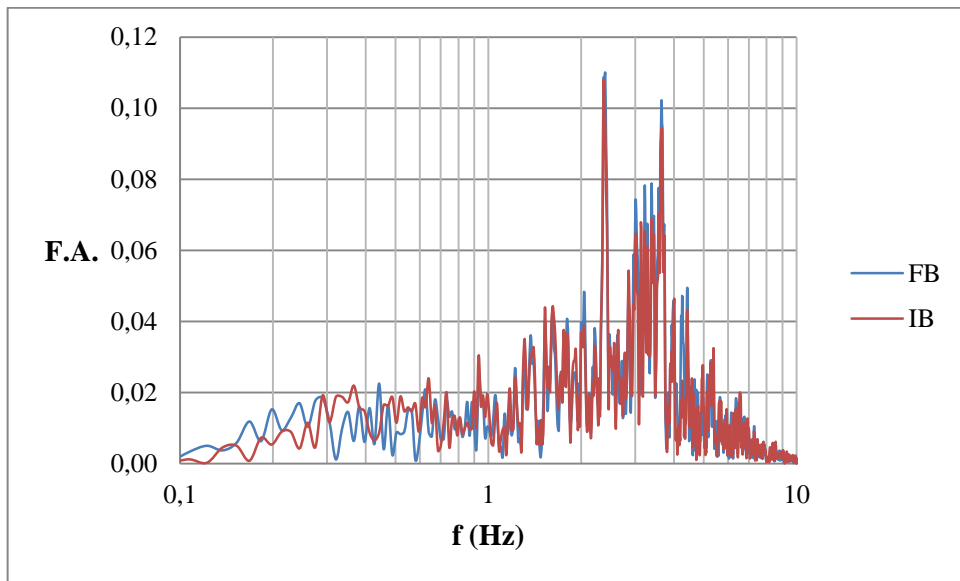


Fig. 4.54 Fourier amplitude spectra for R3_0.1 motion (3-storey model)

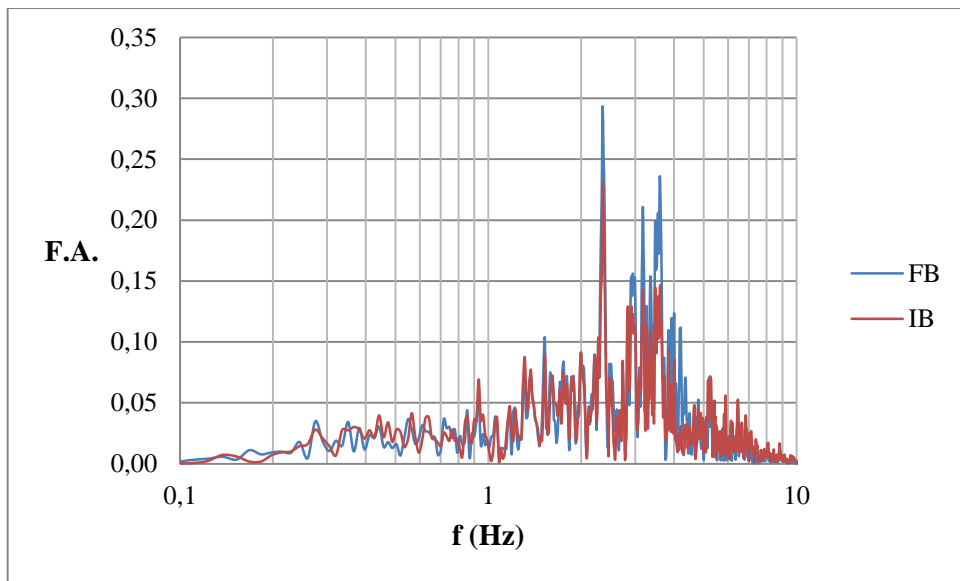


Fig. 4.55 Fourier amplitude spectra for R3_0.2 motion (3-storey model)

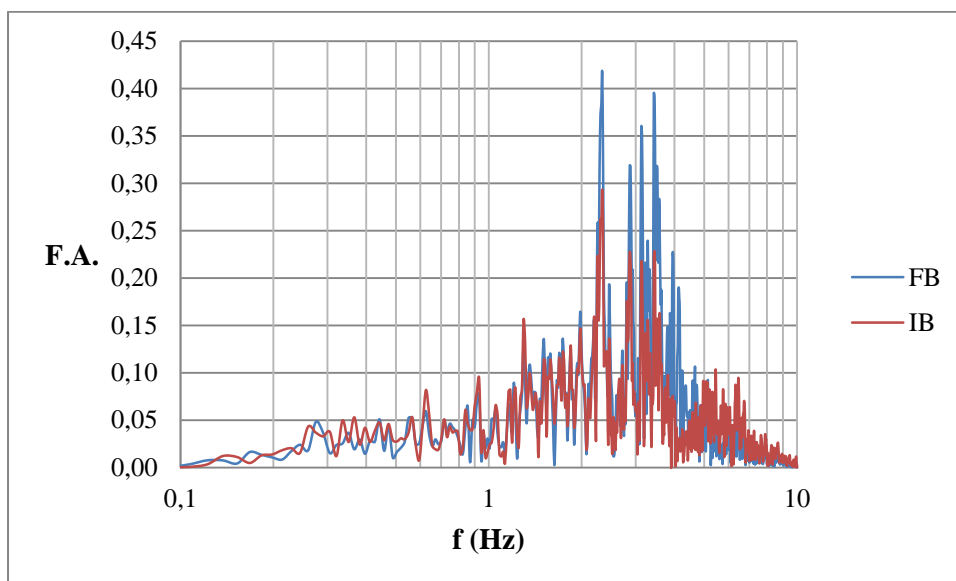


Fig. 4.56 Fourier amplitude spectra for R3_0.3 motion (3-storey model)

4.3.2 Tests on 5-Storey Model with Modified Base Motions

The results of the tests obtained by using base motions derived from the actual earthquake data and conducted on the 5-storey model are presented in this section. Although the change in the base accelerations were dependent on the predominant frequency of the input motion, the efficiency of the composite liner system was found to be almost independent of this parameter for both fault mechanisms.

As revealed in Fig. 4.57, the efficiency of the composite liner system was almost independent of the predominant frequency of the input motion for base motions S1, S2 and S3. The efficiency increased with increasing maximum base motion acceleration " a_{max} ". To illustrate, on average the $\eta \approx 55\%$ for $a_{max} = 0.1g$ while it was $\eta = 80\%$ and $\eta = 90\%$ for $a_{max} = 0.2g$ and $a_{max} = 0.3g$ respectively for base motions S1, S2 and S3.

As it can be seen in Fig. 4.58, the efficiency of the system was again almost independent of the predominant frequency of the input motion for base motions derived from actual earthquake data associated with reverse fault mechanisms, similar to the situation for strike-slip fault mechanism. Also, the effect of the " a_{max} " of the input motion on " η " was more significant as compared to that in motions associated with strike-slip fault mechanism. The efficiency levels obtained for R1_0.1, R2_0.1 and R3_0.1 motions was lower than those obtained for S1_0.1, S2_0.1 and S3_0.1 motions but almost equals at higher " a_{max} " levels. Figures which reveal the changes in floor accelerations are also given in Appendix H. In these figures "R" term stands for the percent reduction in the mid-floor accelerations in case of "IB" with respect to the "FB" case and the reductions obtained were proportional to the " η " values presented in Fig. 4.57 and Fig. 4.58.

The acceleration-time histories for base accelerations in "FB" and "IB" cases are given in Appendix I. Similar to those of the previous section, the decreases in the accelerations can be observed in base-isolated tests for most of the records. Also, the changes in acceleration-time histories become more visible as the predominant frequency of the motion gets closer to the natural frequency of the superstructure and same observation can be made for increasing maximum base acceleration " a_{max} ". However evaluations based on time-histories may not be readily seen since the real improvement provided by the utilized system was based on altering frequency contents. For this reason, evaluations were made based on the response and Fourier amplitude spectra of the experiments and presented in the following part.

The response spectra for the 5-storey model ($D=1.60\%$) are given in Fig. 4.59 to 4.76. Similar to the case in the previous section, the spectral accelerations were significantly reduced in the close vicinity of the first-mode natural period of the model ($T_n = 0.43s$) which provides the improvement under simulated base excitations. However, it should be emphasized that the amplifications in spectral accelerations were shifted to the low period (high frequency) range especially for low frequency motions regardless of the fault mechanism (see Fig. 4.59 – 4.61 and Fig. 4.68 – 4.70). Another point is that the base accelerations were more noticeably amplified in this model as compared to the 3-storey model and not only for low but for all “ a_{max} ” values for motions with $f = 1Hz$ regardless of the fault mechanism (for motions A1 and S1). Nevertheless, the composite liner system decreased the differential accelerations at least by $\eta = 56\%$ and $\eta = 31\%$ for S1_0.1 and R1_0.1 base motions respectively. In addition, the response spectra for $D = 5\%$ damping are also given in Appendix J.

The Fourier amplitude spectra for the 5-storey model are given in Fig. 4.77 – 4.94. In these figures, it can be observed that the frequency contents of the base motions were more noticeably altered by the composite liner system. The Fourier amplitudes in the close vicinity of the “ f_n ” of the superstructure were deamplified for all motions while those of the higher frequencies were amplified. This phenomenon is more clearly observed for motions the predominant frequencies of which coincide with the “ f_n ” of the superstructure (see Fig. 4.80 – 4.82 and Fig. 4.89 – 4.91). Another interesting point was that, as it can be seen in Fig. 4.83 – 4.85 and Fig. 4.92 – Fig. 4.94 for base motions (S3, R3) with respectively high predominant frequencies ($f = 4Hz$ for this study) as compared to the first-mode natural frequency of the superstructure ($f_n = 2.33 Hz$), the amplifications in Fourier amplitudes at high frequencies were much less as compared to other base motions.

The slip displacements recorded for the 5-storey model were significantly larger than those of the 3-storey model. The largest displacements were recorded for base motions with $f = 1Hz$ (S1 and R1). The magnitude of the slip displacements were very close between motions with $f = 2Hz$ and $f = 4Hz$ (S2-S3 and R2-R3) for the same maximum base acceleration “ a_{max} ”, but larger for excitations having a predominant frequency of $f = 2Hz$ since it coincides with the first-mode natural frequency “ f_n ” of the tested model. Similar to the case in the 3-storey model, the slip displacements recorded during base motions derived from earthquakes with reverse fault mechanisms (R1, R2 and R3) were slightly less than the ones recorded for base motions derived from strike-slip earthquakes (S1, S2 and S3) for the same predominant motion frequency “ f ” and maximum acceleration “ a_{max} ”.

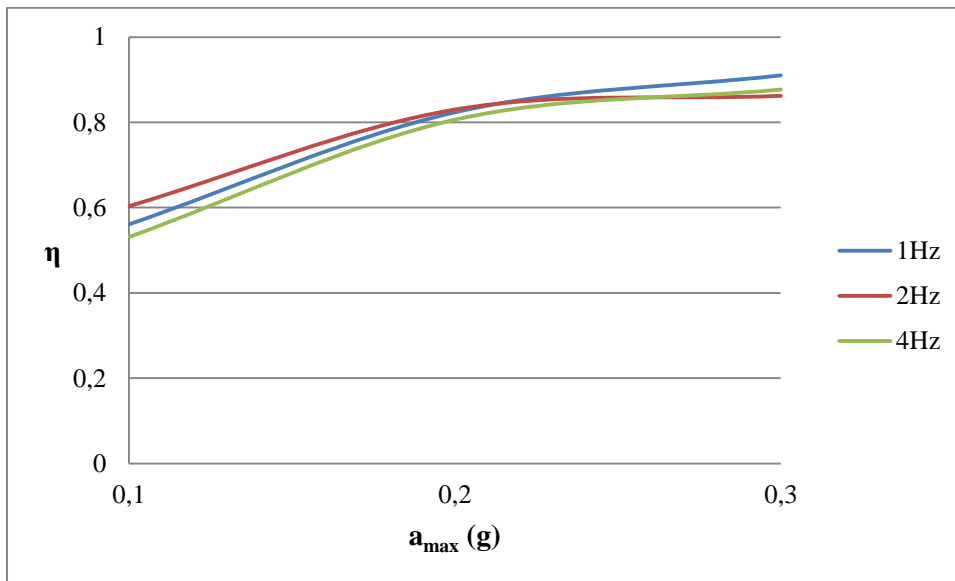


Fig. 4.57 a_{\max} vs. η for strike-slip fault mechanism ($f_n = 2.33$ Hz)

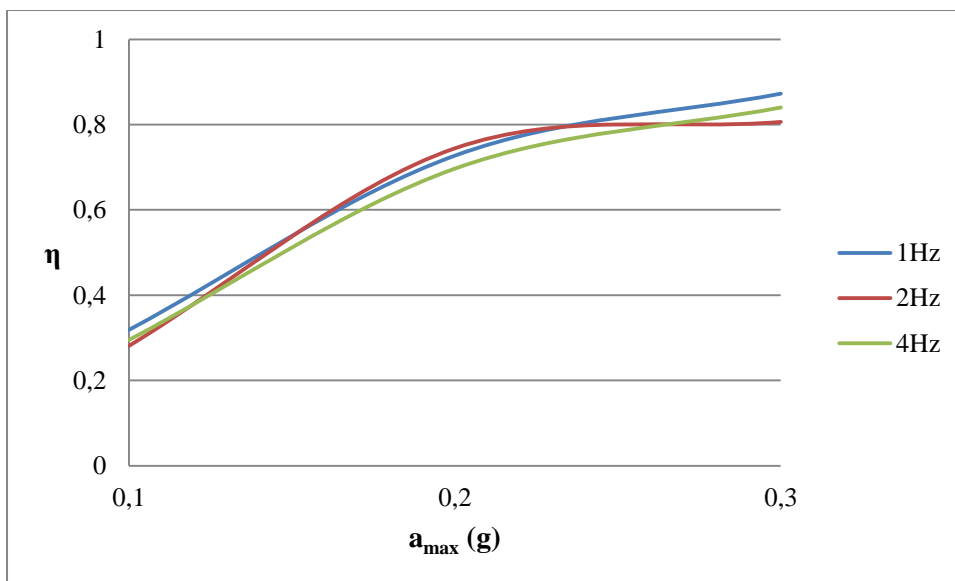


Fig. 4.58 a_{\max} vs. η for reverse fault mechanism ($f_n = 2.33$ Hz)

Table 4.9 The slip for 5-storey model (strike-slip fault mechanism)

Base Motion	Slip (mm)
S1_0.1	21.06
S1_0.2	131.25
S1_0.3	182.10
S2_0.1	11.64
S2_0.2	39.06
S2_0.3	44.96
S3_0.1	10.77
S3_0.2	32.35
S3_0.3	40.49

Table 4.10 The slip for 5-storey model (reverse fault mechanism)

Base Motion	Slip (mm)
R1_0.1	12.55
R1_0.2	66.07
R1_0.3	92.13
R2_0.1	6.29
R2_0.2	32.14
R2_0.3	42.29
R3_0.1	5.07
R3_0.2	30.29
R3_0.3	38.86

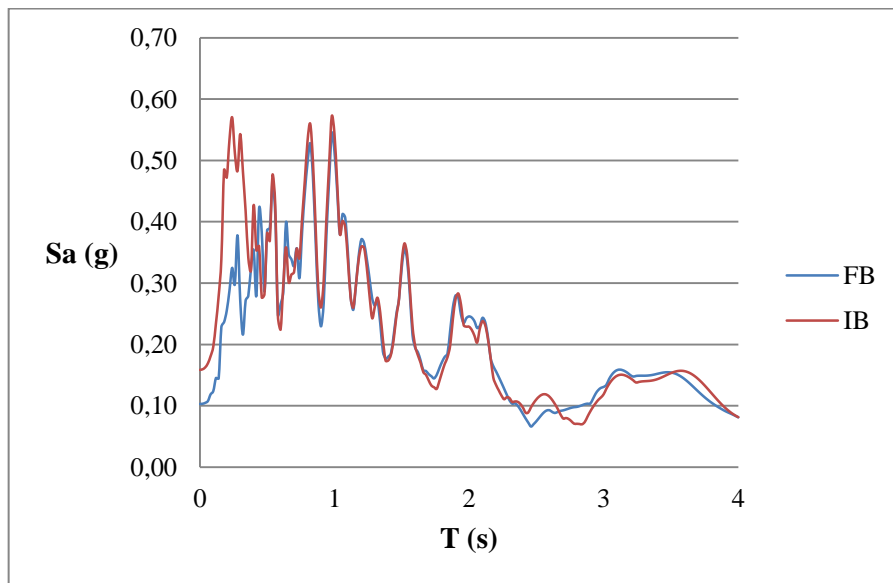


Fig. 4.59 Response spectra for S1_0.1 motion (D = 1.60%)

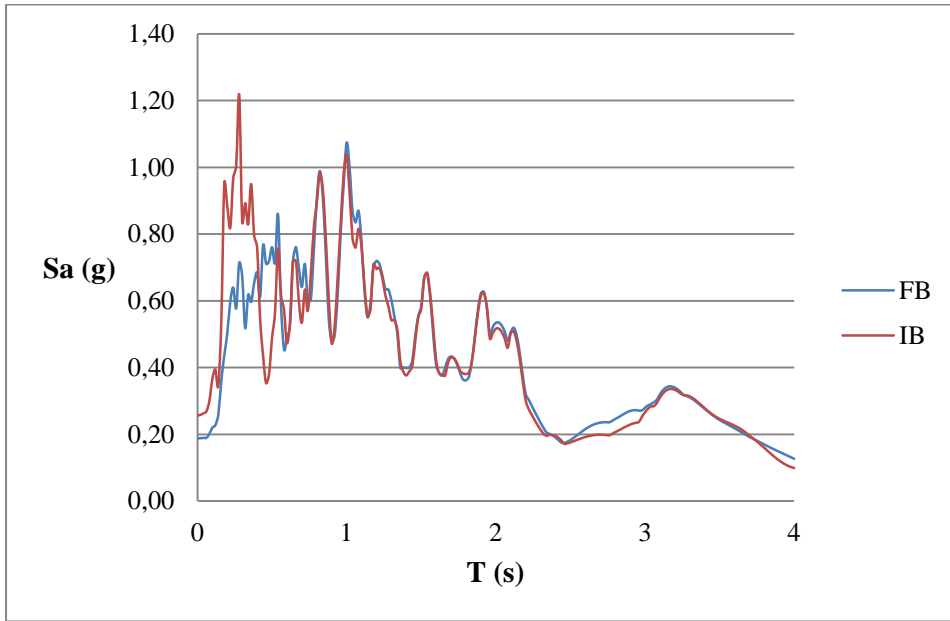


Fig. 4.60 Response spectra for S1_0.2 motion (D = 1.60%)

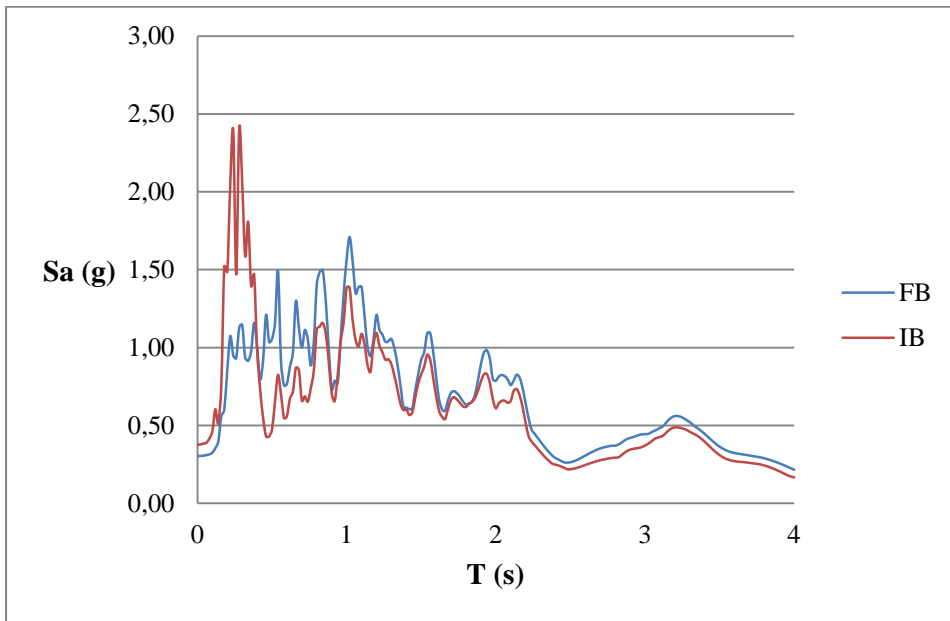


Fig. 4.61 Response spectra for S1_0.3 motion (D = 1.60%)

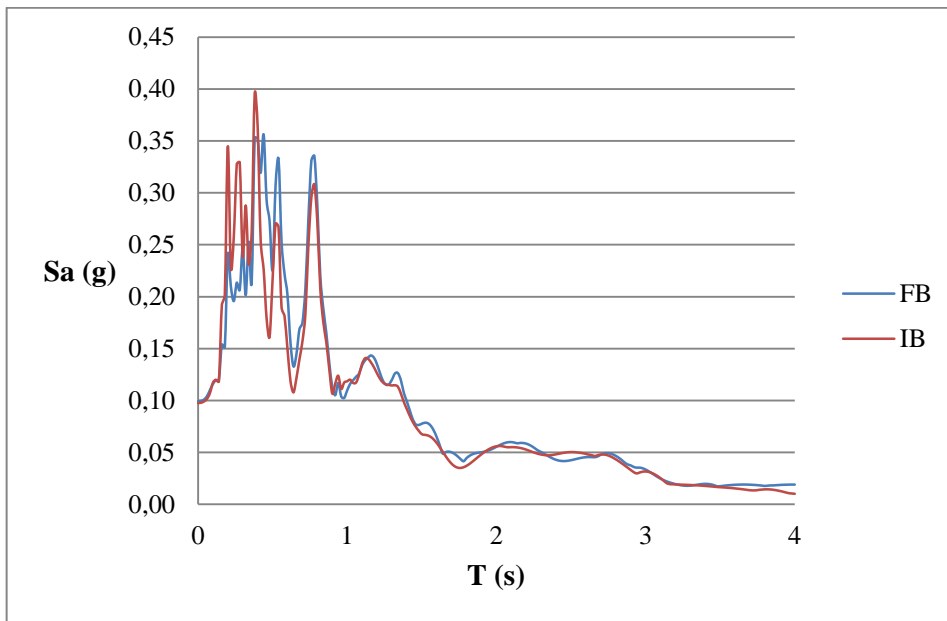


Fig. 4.62 Response spectra for S2_0.1 motion (D = 1.60%)

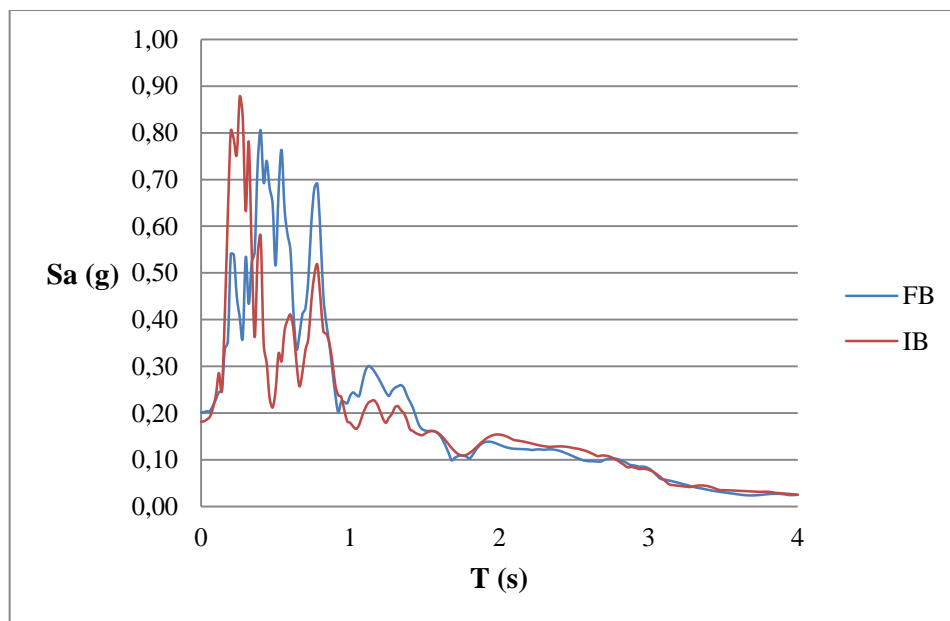


Fig. 4.63 Response spectra for S2_0.2 motion (D = 1.60%)

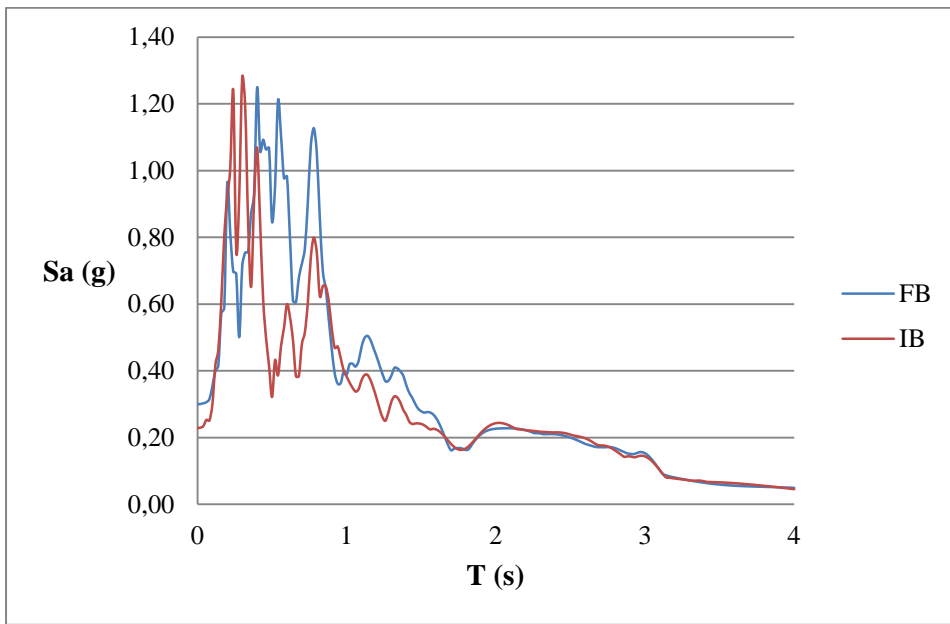


Fig. 4.64 Response spectra for S2_0.3 motion (D = 1.60%)

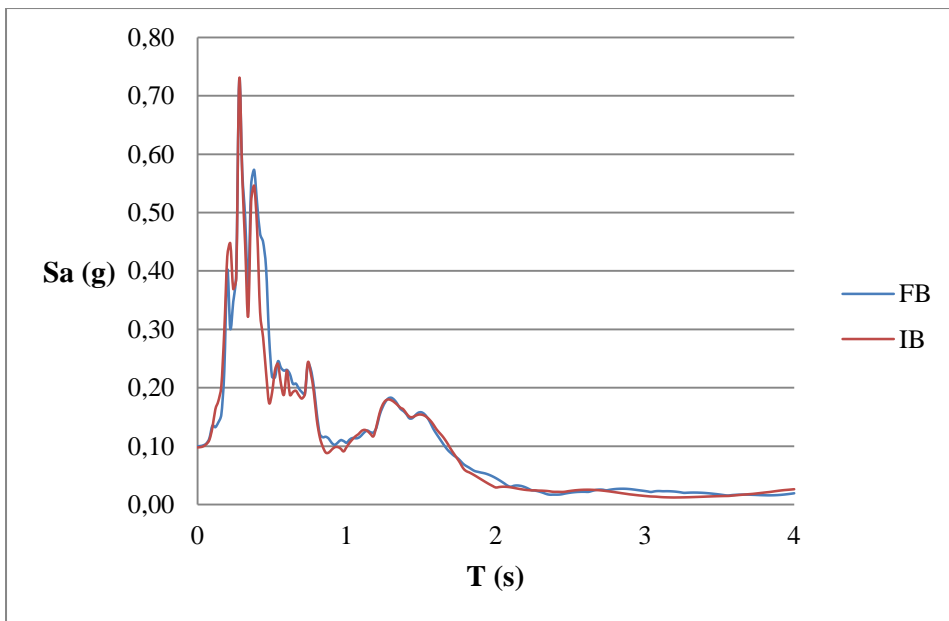


Fig. 4.65 Response spectra for S3_0.1 motion (D = 1.60%)

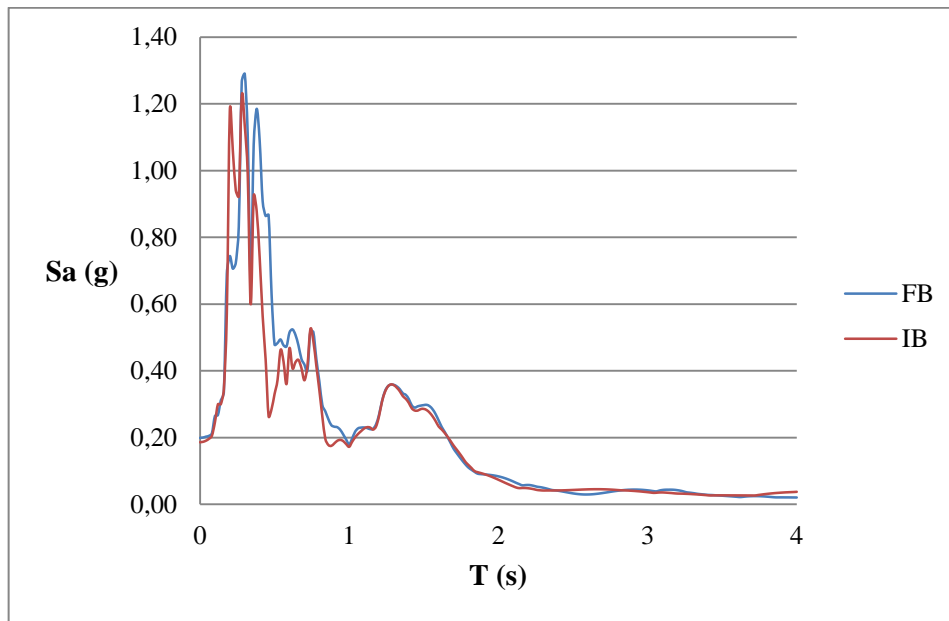


Fig. 4.66 Response spectra for S3_0.2 motion (D = 1.60%)

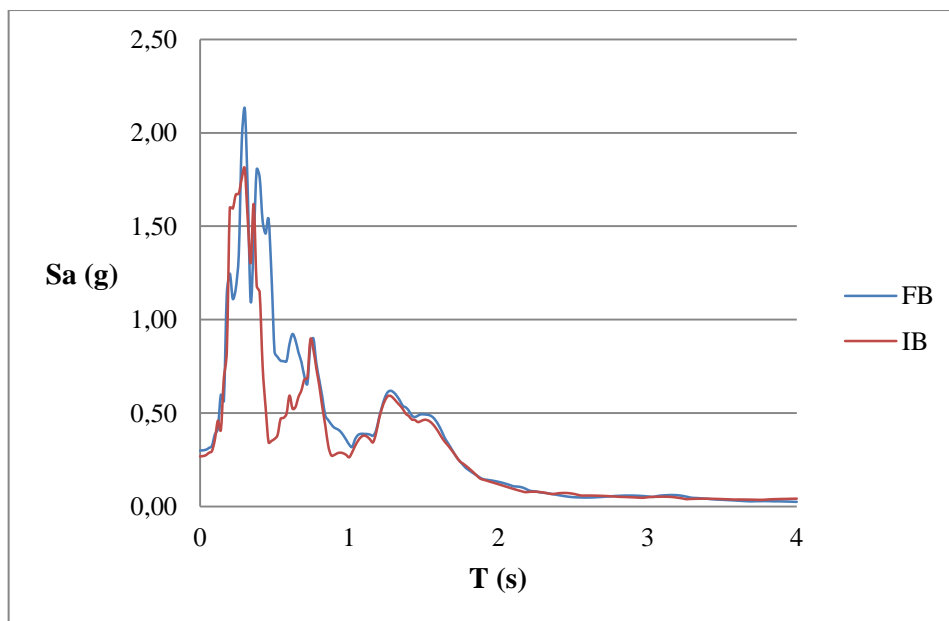


Fig. 4.67 Response spectra for S3_0.3 motion (D = 1.60%)

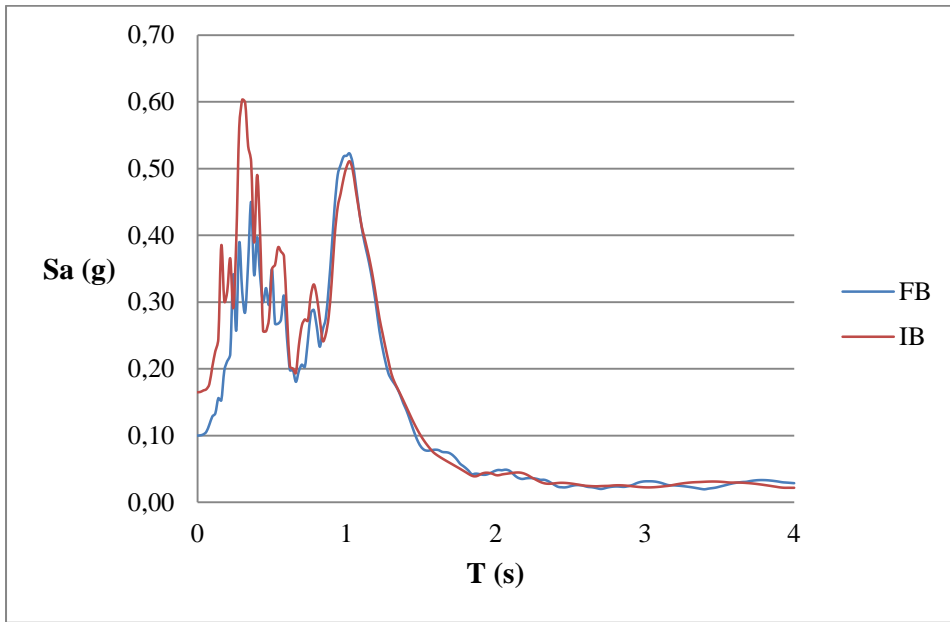


Fig. 4.68 Response spectra for R1_0.1 motion (D = 1.60%)

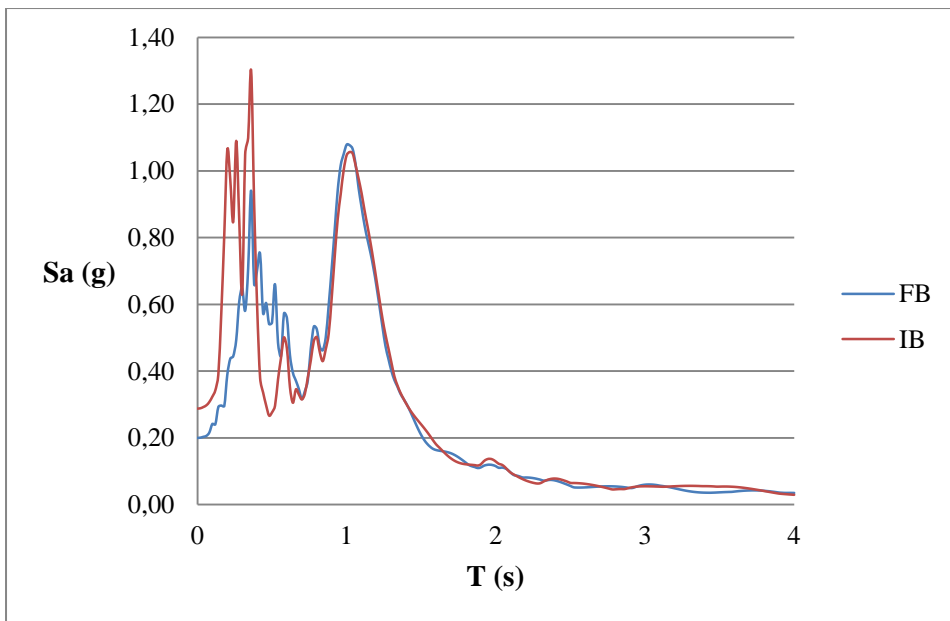


Fig. 4.69 Response spectra for R1_0.2 motion (D = 1.60%)

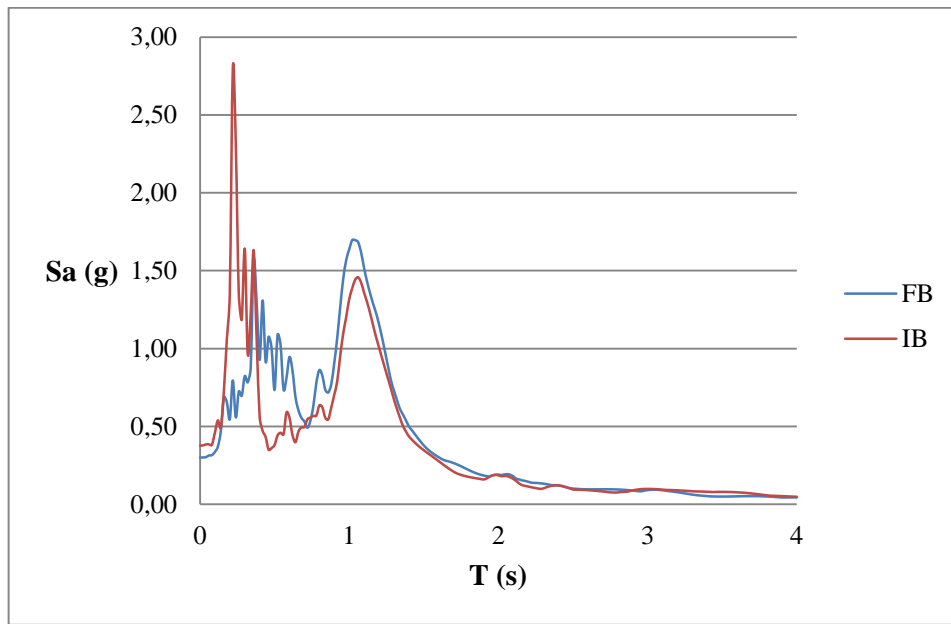


Fig. 4.70 Response spectra for R1_0.3 motion (D = 1.60%)

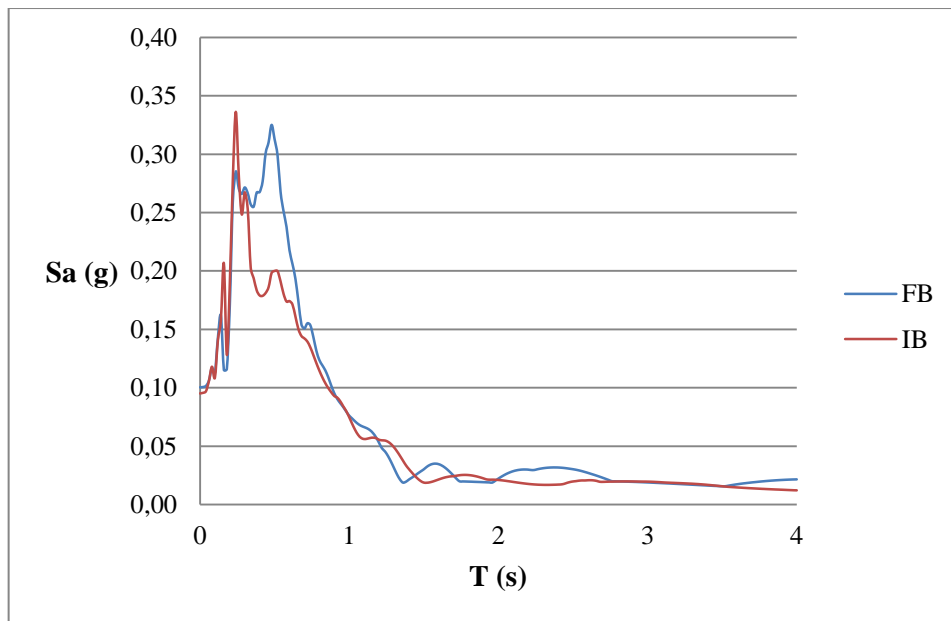


Fig. 4.71 Response spectra for R2_0.1 motion (D = 1.60%)

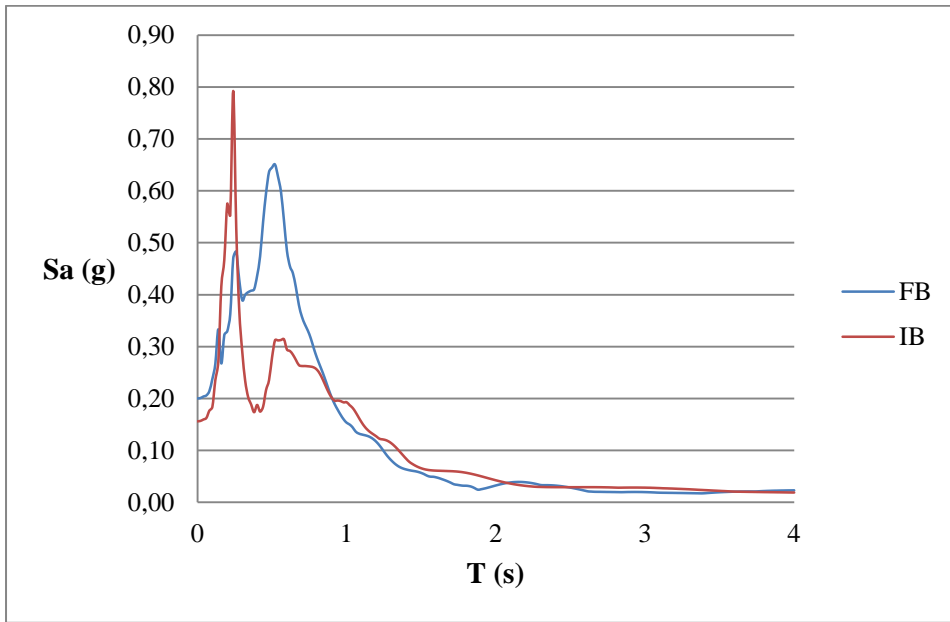


Fig. 4.72 Response spectra for R2_0.2 motion (D = 1.60%)

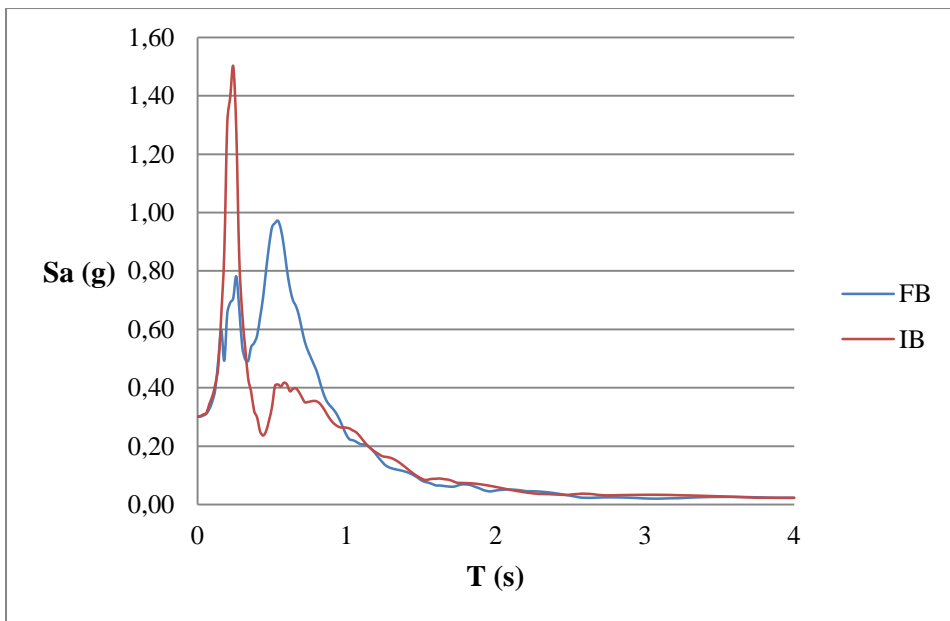


Fig. 4.73 Response spectra for R2_0.3 motion (D = 1.60%)

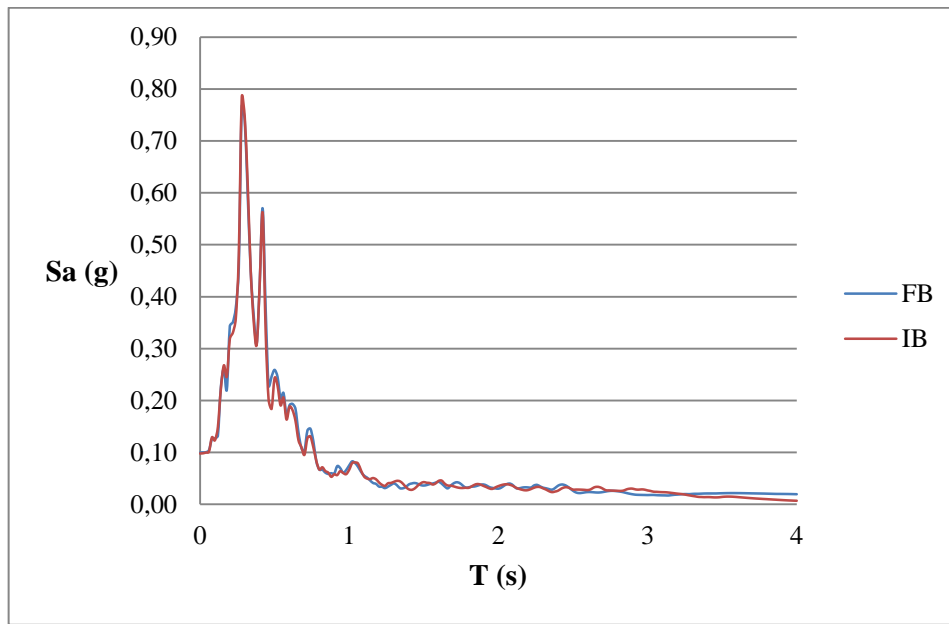


Fig. 4.74 Response spectra for R3_0.1 motion (D = 1.60%)

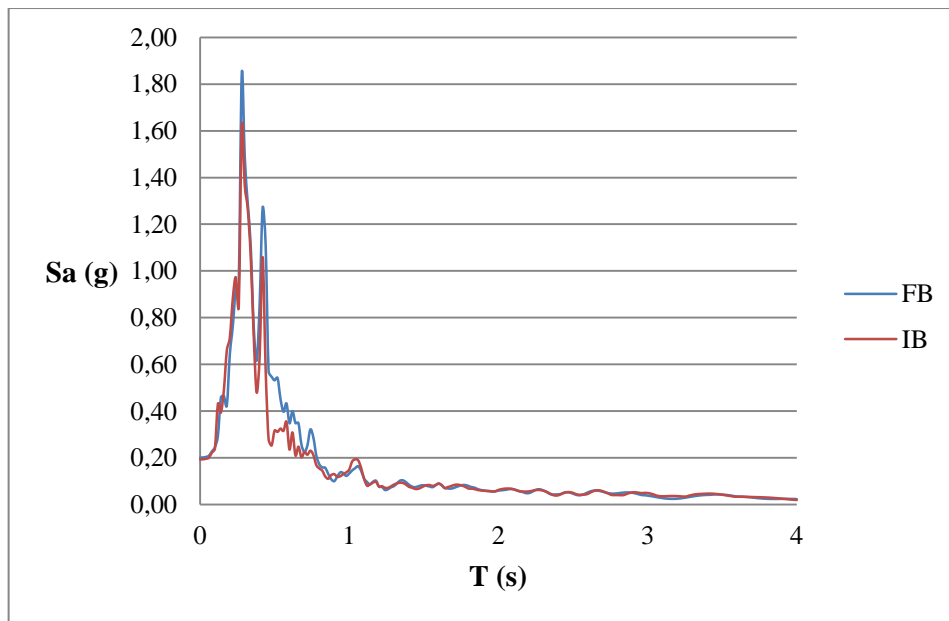


Fig. 4.75 Response spectra for R3_0.2 motion (D = 1.60%)

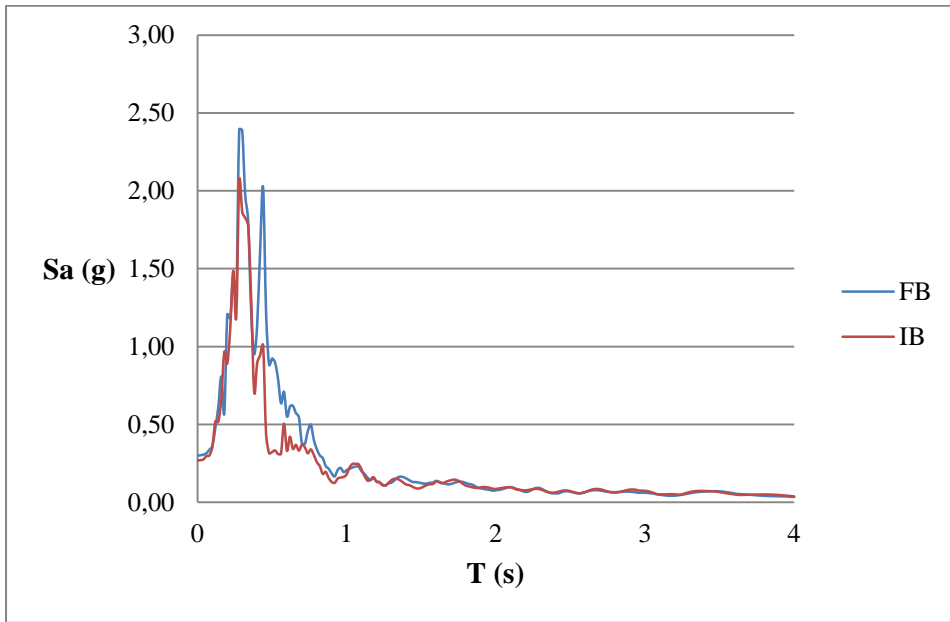


Fig. 4.76 Response spectra for R3_0.3 motion (D = 1.60%)

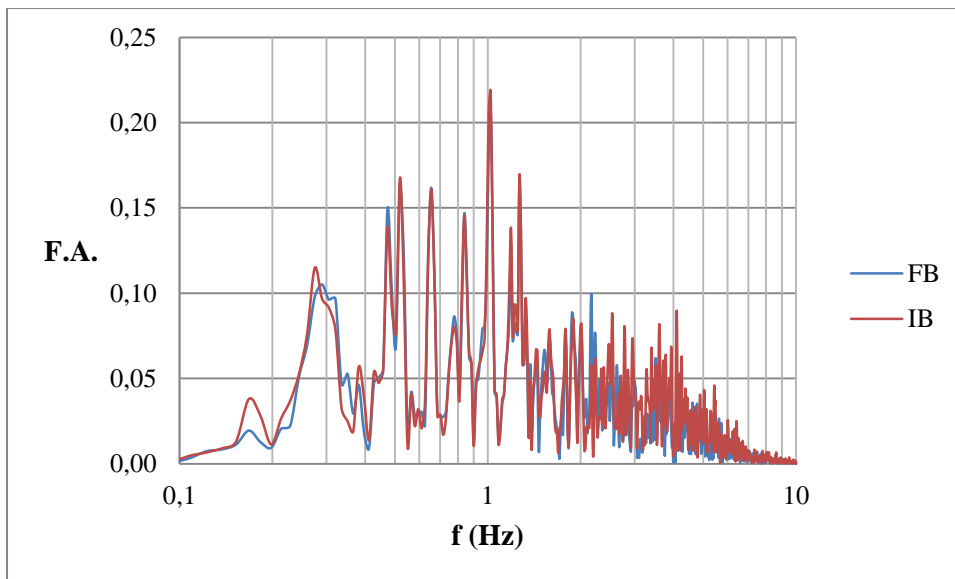


Fig. 4.77 Fourier amplitude spectra for S1_0.1 motion (5-storey model)

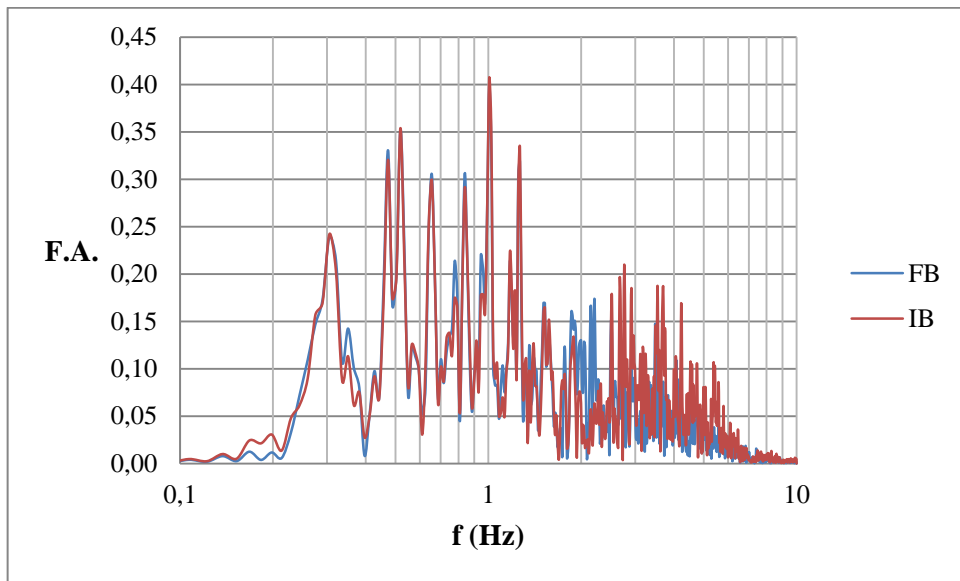


Fig. 4.78 Fourier amplitude spectra for S1_0.2 motion (5-storey model)

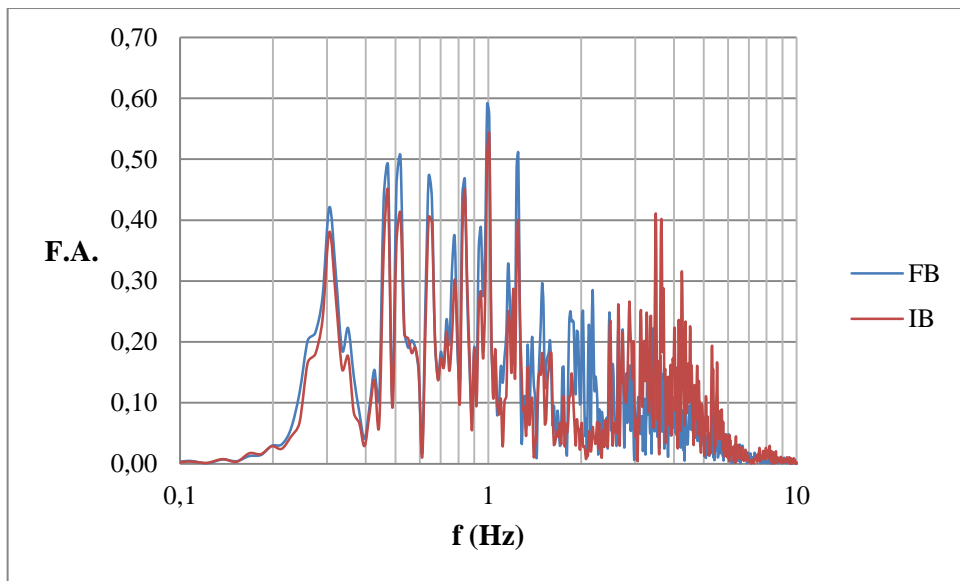


Fig. 4.79 Fourier amplitude spectra for S1_0.3 motion (5-storey model)

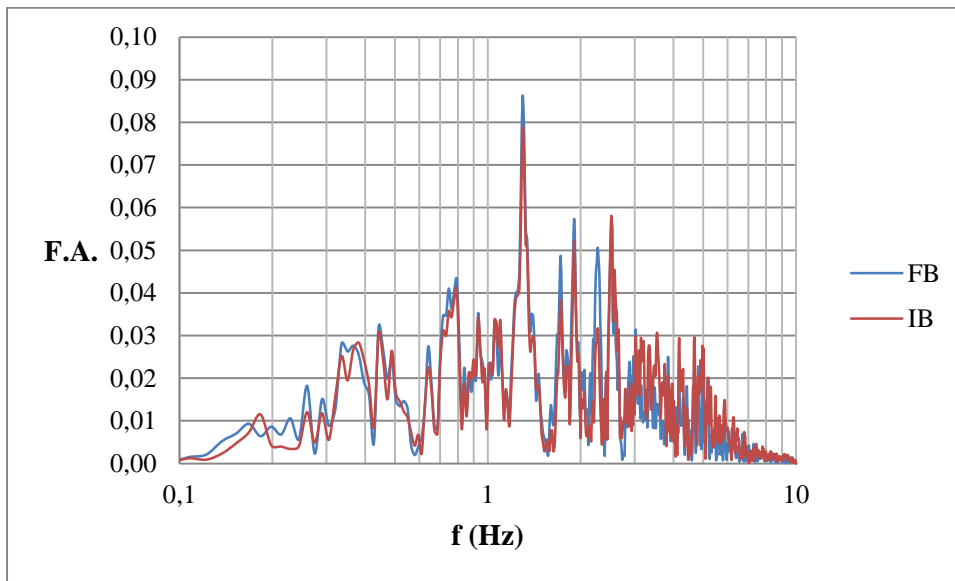


Fig. 4.80 Fourier amplitude spectra for S2_0.1 motion (5-storey model)

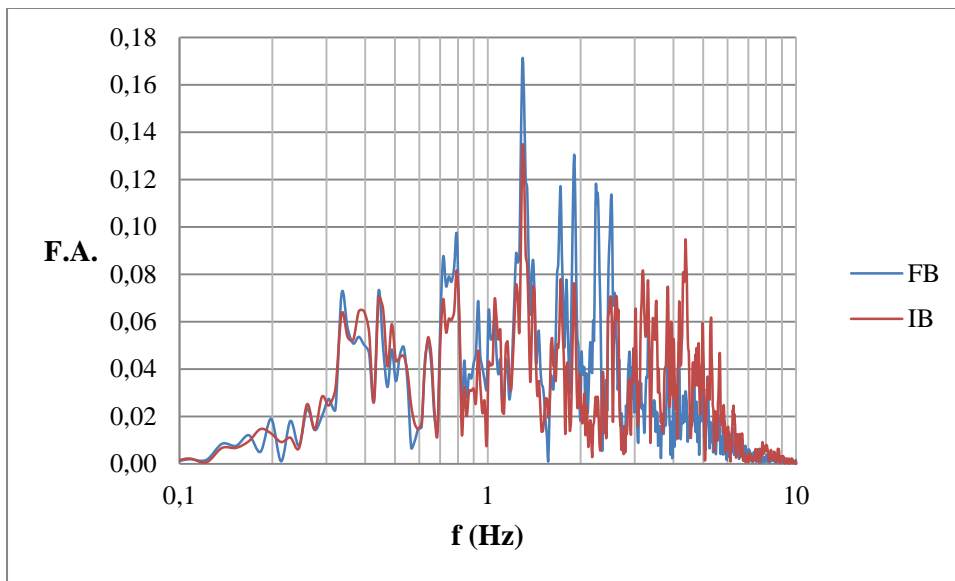


Fig. 4.81 Fourier amplitude spectra for S2_0.2 motion (5-storey model)

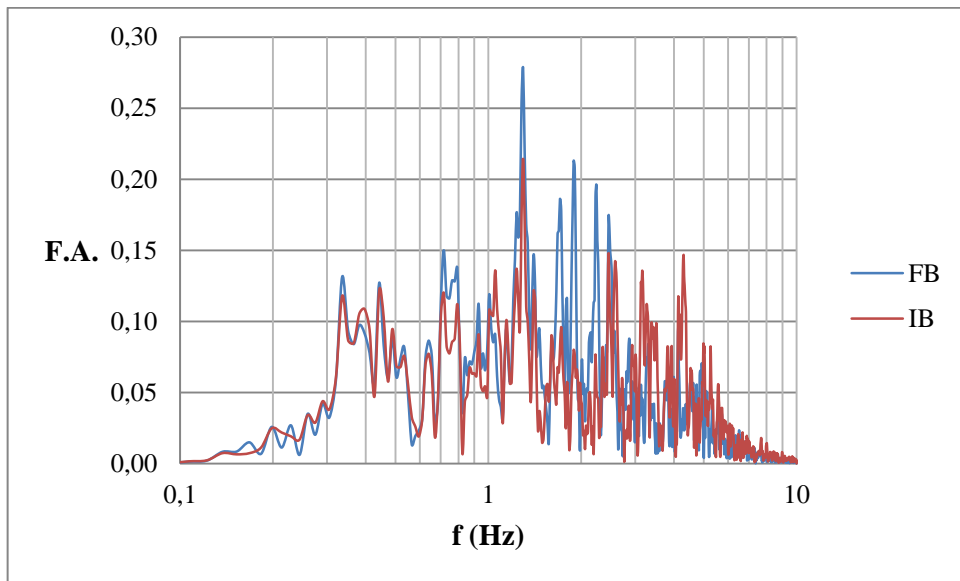


Fig. 4.82 Fourier amplitude spectra for S2_0.3 motion (5-storey model)

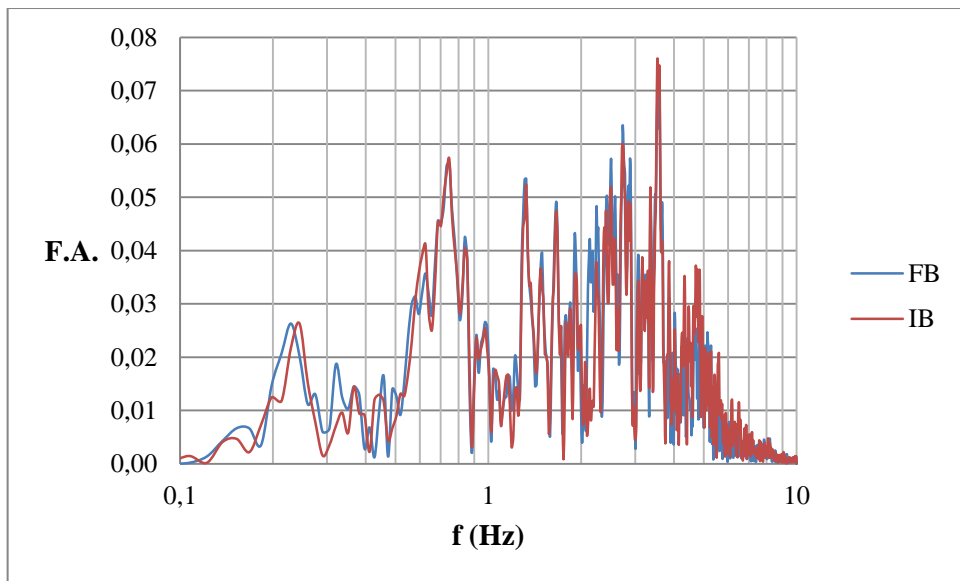


Fig. 4.83 Fourier amplitude spectra for S3_0.1 motion (5-storey model)

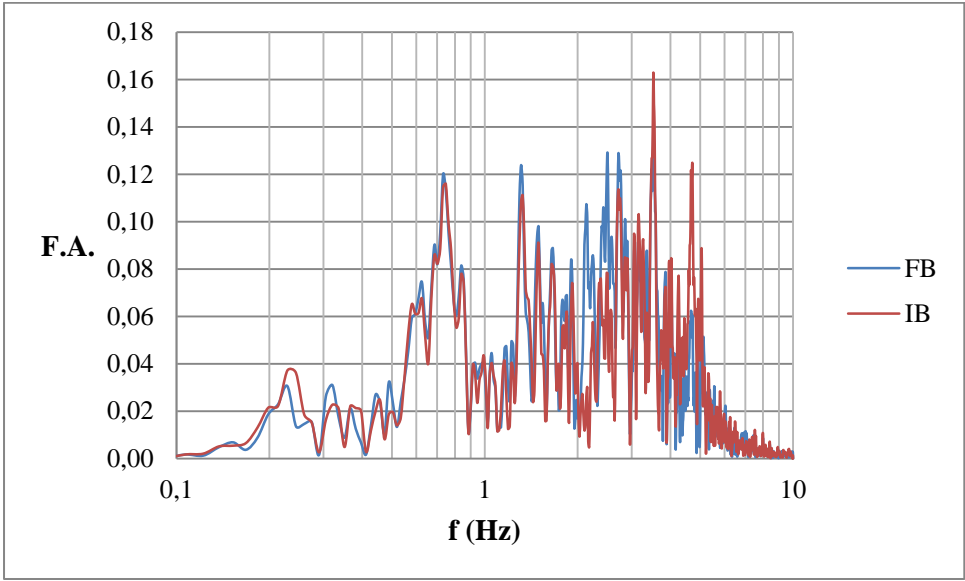


Fig. 4.84 Fourier amplitude spectra for S3_0.2 motion (5-storey model)

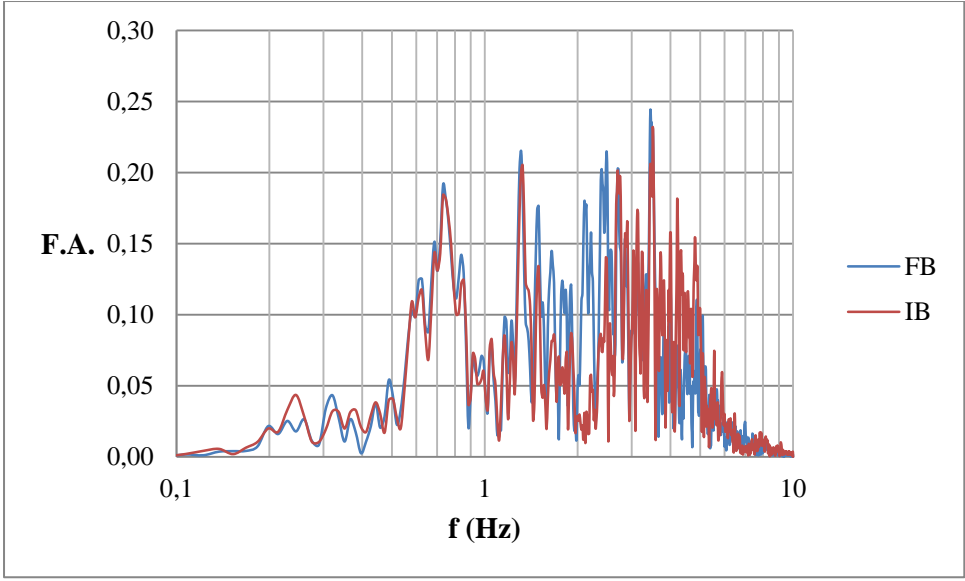


Fig. 4.85 Fourier amplitude spectra for S3_0.3 motion (5-storey model)

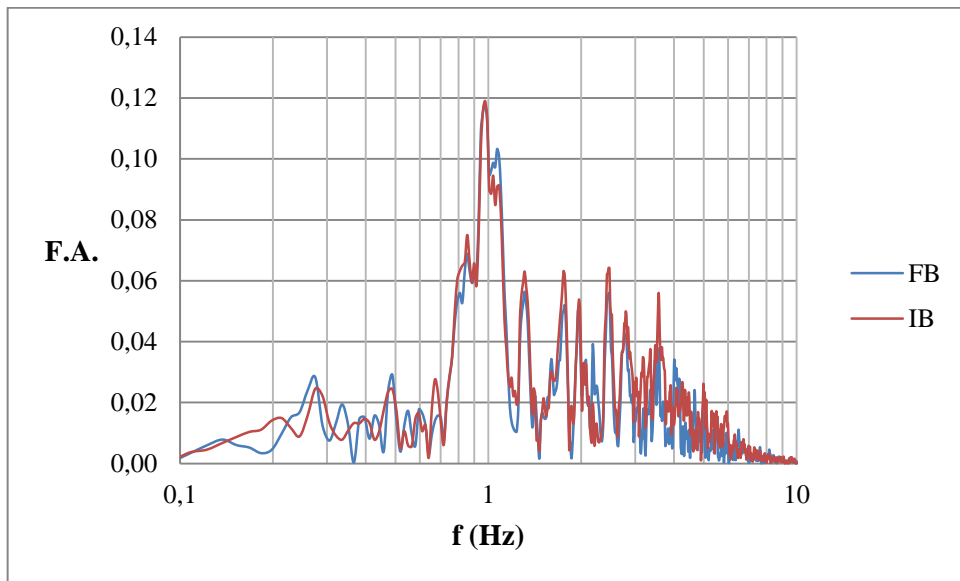


Fig. 4.86 Fourier amplitude spectra for R1_0.1 motion (5-storey model)

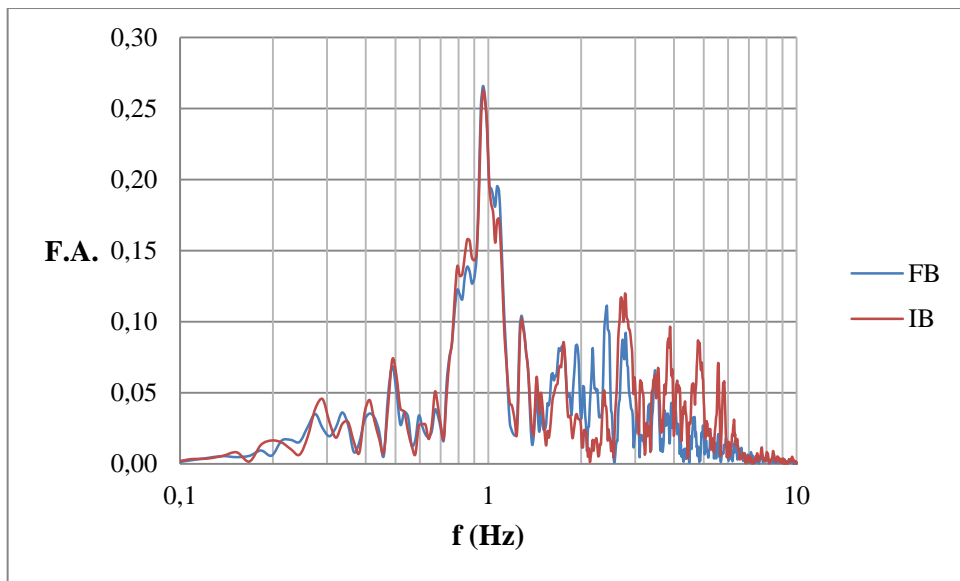


Fig. 4.87 Fourier amplitude spectra for R1_0.2 motion (5-storey model)

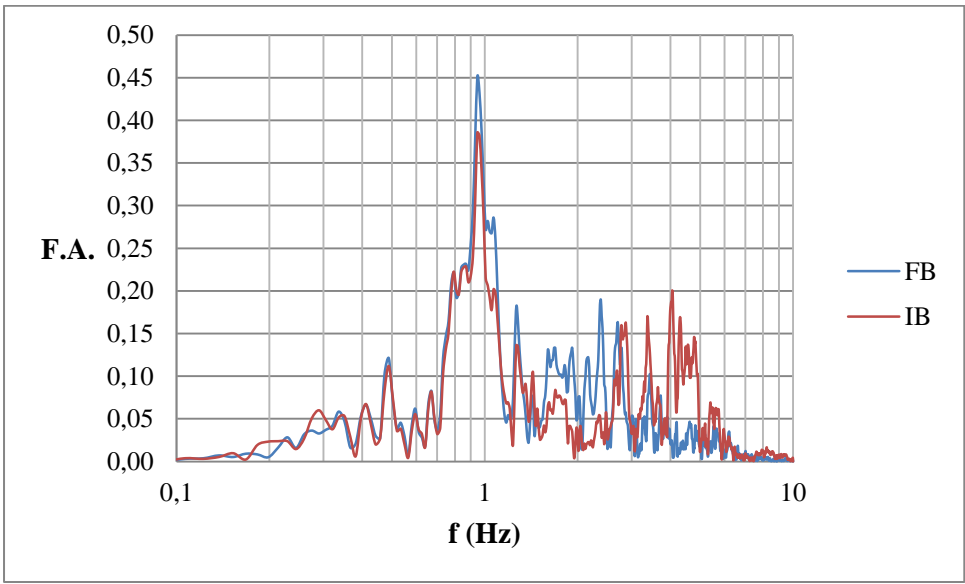


Fig. 4.88 Fourier amplitude spectra for R1_0.3 motion (5-storey model)

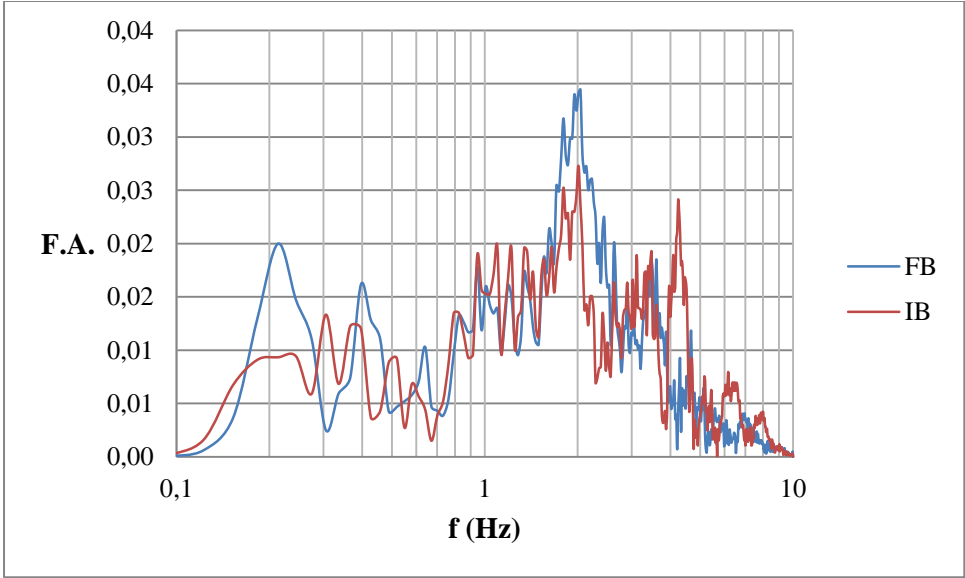


Fig. 4.89 Fourier amplitude spectra for R2_0.1 motion (5-storey model)

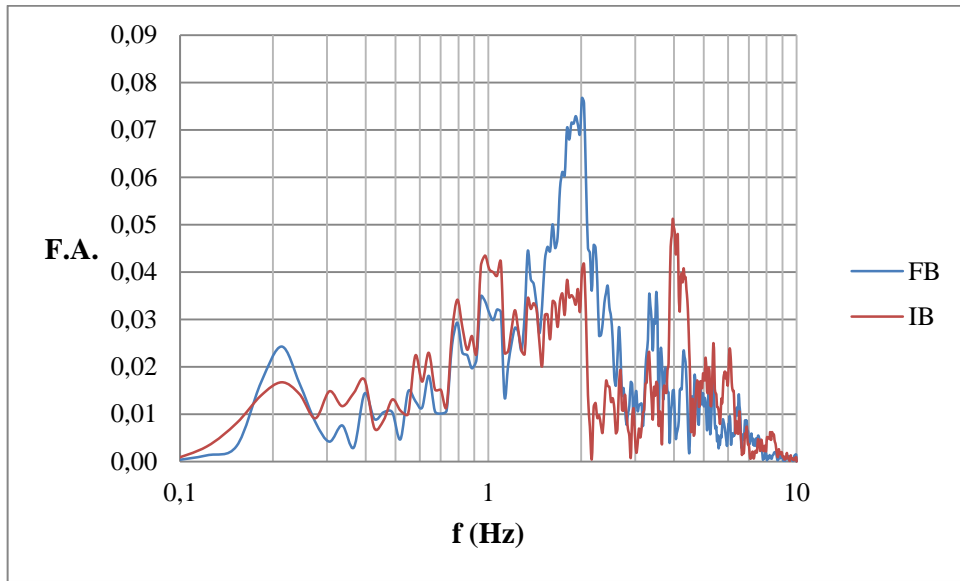


Fig. 4.90 Fourier amplitude spectra for R2_0.2 motion (5-storey model)

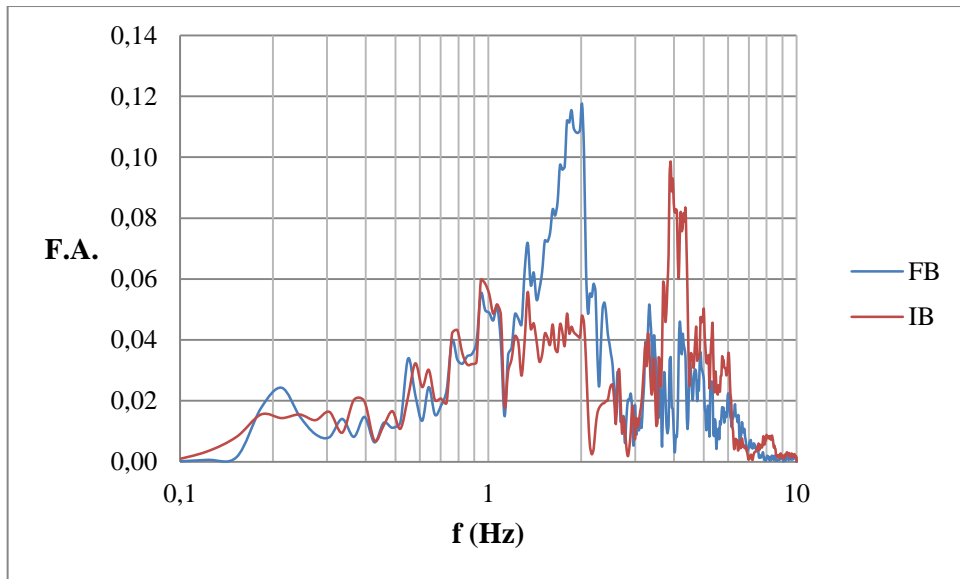


Fig. 4.91 Fourier amplitude spectra for R2_0.3 motion (5-storey model)

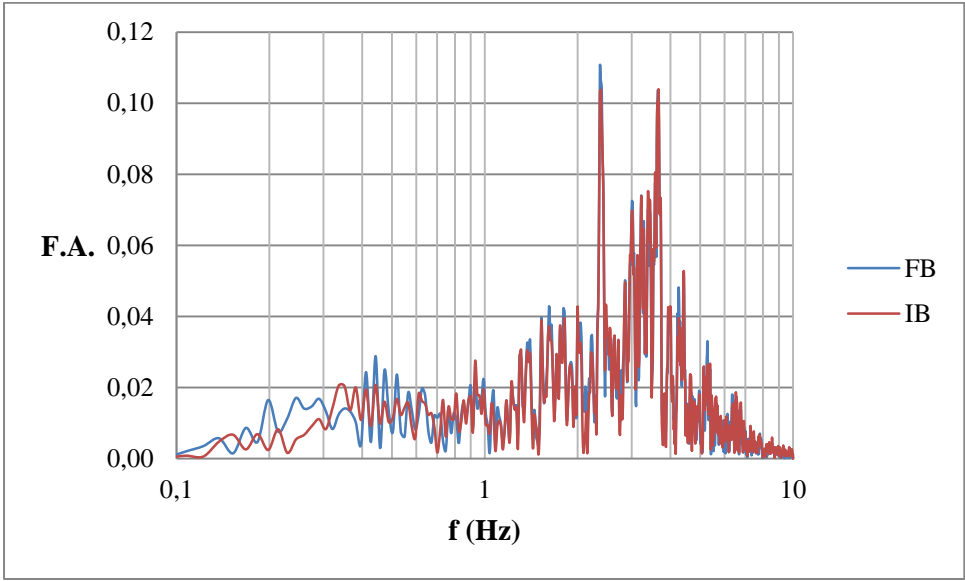


Fig. 4.92 Fourier amplitude spectra for R3_0.1 motion (5-storey model)

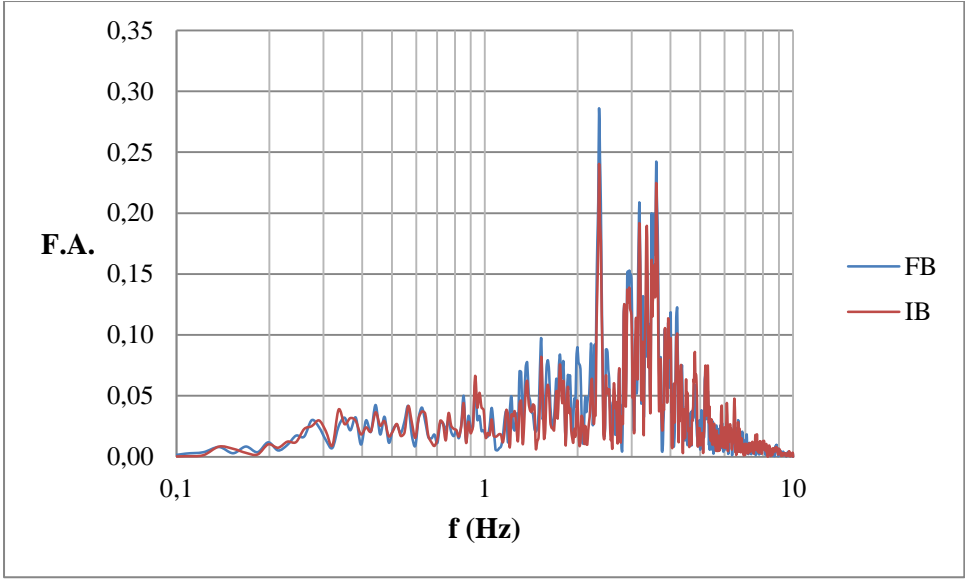


Fig. 4.93 Fourier amplitude spectra for R3_0.2 motion (5-storey model)

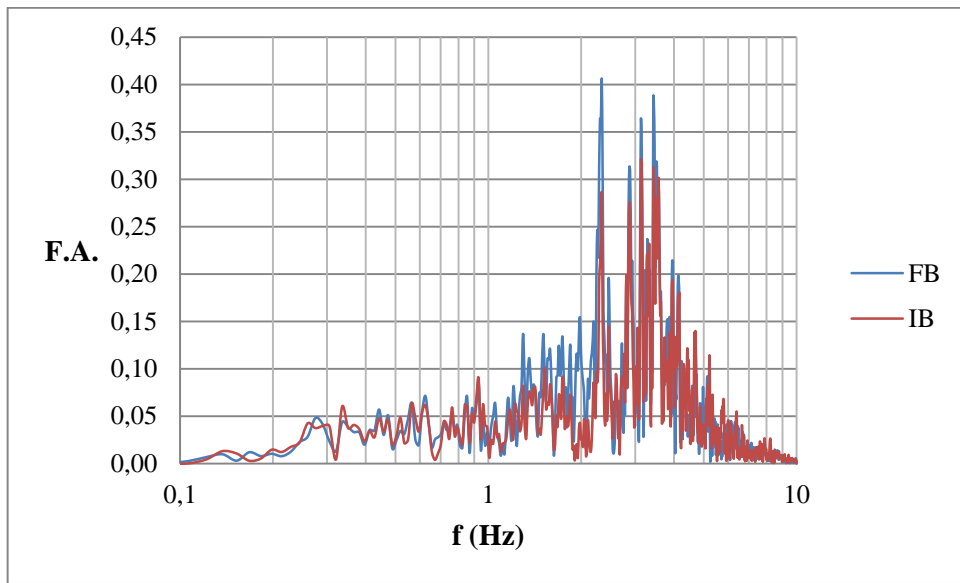


Fig. 4.94 Fourier amplitude spectra for R3_0.3 motion (5-storey model)

CHAPTER 5

EVALUATIONS AND CONCLUSIONS

In this study, it was aimed to evaluate the behavior and efficiency of an easily applicable, low cost seismic isolation system which is composed of a high strength non-woven geotextile laid over an ultra-high molecular weight polyethylene (UHMWPE) geomembrane which was placed just beneath the structure together called as “composite liner system”. The effect of this seismic isolation system on model structures was investigated through shaking table tests both under harmonic and random motions. For this purpose, the older shaking table of Soil Mechanics Laboratory was modified and changed to a shaking table which is capable of applying both harmonic and earthquake motions in a fully computer controlled system. Then, two models representing 3-storey and 5-storey structures were produced and accelerations at each storey level together with the base slip (for the isolated cases) were measured during the experiments. A total of 138 experiments were performed during the study. Firstly the first-mode natural frequencies (f_n) of the models were determined by free vibration tests and evaluated to be representative of the “ f_n ” of their prototypes.

In the next stage of the study, the tests with harmonic motions were performed for both 3-storey and 5-storey models and for fixed base “FB” and isolated base “IB” conditions. For this purpose, motions with $f = 1, 2, 3$ and 4 Hz frequencies and a maximum base acceleration range of $a_{max} = 0.08 - 0.30g$ were utilized during the experiments.

The last part of the study was the tests under base motions obtained by modifying the actual earthquake data. The experiments were conducted by 6 different base motion records scaled to three different maximum accelerations; $a_{max} = 0.1, 0.2$ or $0.3g$. Three of these records were selected among the earthquake records associated with strike-slip fault mechanisms while the others were recorded for reverse fault mechanisms. For both fault mechanisms the records were selected in a way that the predominant frequency of the applied motion was approximately $f = 1, 2$ or 4 Hz. The evaluations based on the results of these experiments are presented in the following part of this section.

5.1 Evaluations Based on Harmonic Motion Tests

- The decrease in the magnitude of base accelerations for “IB” case with respect to the “FB” case is highly dependent on the input motion frequency “ f ” and the natural frequency “ f_n ” of the superstructure.
- For each motion frequency, for base-isolated cases the base acceleration is decreased to a certain level (defined as threshold acceleration, a_t) almost independent of the maximum base motion acceleration “ a_{max} ” of the input motion and if the “ a_{max} ” of the input motion is below this certain level, the composite liner system is not triggered. Slight increases (on the order of 10% at maximum) occur in the base accelerations for “IB” cases as the “ a_{max} ” of the input motion increases when the motion frequency “ f ” is kept constant.
- For the 3-storey model, the threshold acceleration of the isolated model was measured around $a_t = 0.16g$ for the base motions with $f = 1$ Hz while $a_t = 0.13, 0.10$ and $0.07g$ for base motion frequencies $f = 2, 3$ and 4 Hz, respectively. The composite liner system did not provide any improvement for motions “f1d20”, “f1d40” and “f2d5” since the applied maximum base acceleration “ a_{max} ” was less than the threshold acceleration “ a_t ” which is the minimum acceleration value to trigger the composite liner system for that specific motion frequency.

- For the 5-storey model, the base accelerations were decreased to around $a_t = 0.13g$, $0.07g$ and $0.08g$ for $f = 1, 2$ and 3Hz base motion frequencies respectively nearly independent of the “ a_{max} ” of the input motion. The composite liner system was not triggered for “fld20” motion which has $f = 1\text{Hz}$ frequency and $a_{\text{max}} = 0.08g$ since the “ a_{max} ” value of the input motion was less than “ a_t ” of this frequency level. Interestingly, the composite liner system did not provide any improvement for harmonic motions with $f = 4\text{Hz}$ frequency.
- As it can be seen from the values given above, the composite liner system is most efficient under harmonic motions with frequencies close to the first-mode natural frequency “ f_n ” of the superstructure. The minimum accelerations are measured when the input motion frequency is in the close vicinity of the “ f_n ” of the superstructure. The threshold accelerations measured for this condition are similar to the ones given in Yegian and Kadakal (2004).
- The measured accelerations at each floor did not differ for each cycle of motion during an experiment and the model reached to a steady state condition after a few first cycles of motion (up to 4 cycles for 3-storey and 5 cycles for 5-storey model).
- The interstorey drift ratios can be significantly lowered by using the composite liner system. Reductions up to 80% were provided for the tested models with most reduction when the input motion frequency coincided with the “ f_n ” of the superstructure similar to the case for accelerations.
- The use of the composite liner system does not alter the mode of vibration or the displacement profile of the superstructure but deamplifies the magnitudes.
- The composite liner system does not provide any improvement when the input motion frequency is more than approximately twice that of the “ f_n ” of the superstructure for the performed experiments with 5-storey model.

5.2 Evaluations Based on Random Motion Tests

In this part, the observed behavior is slightly different for 3-storey and 5-storey structures and consequently the results will be evaluated separately.

5.2.1 Evaluations for 3-Storey Model

- In contrast to the situation in the harmonic motions, the composite liner system was triggered in all experiments regardless of the input motion frequency “ f ” and maximum base acceleration “ a_{max} ”.
- For base motions derived from earthquakes associated with strike-slip fault mechanisms (S1, S2, S3), the predominant frequency of the input motion did not have a significant effect on the efficiency (η) of the system unless it coincides with “ f_n ” of the super structure. The predominant frequency of the input motion becomes more important for low “ a_{max} ” values ($0.1g$ in this study) and for higher values of “ a_{max} ”, the efficiency of the composite liner system varies in a very narrow band ($75 - 85\%$). The improvement gained by the utilization of the composite liner system reached up to $\eta = 85\%$.
- In case of base motions derived from actual earthquake data associated with reverse fault mechanisms (R1, R2, R3), the test results revealed that the predominant frequency of the input motion “ f ” has a much more important role in the efficiency of the isolation system as compared to those stemming from strike-slip fault mechanisms (S1, S2 and S3 motions). The efficiency “ η ” obtained for $f = 4\text{Hz}$ (R3 motion) motion was much higher than those of motions with $f = 1\text{Hz}$ (R1 motion) and $f = 2\text{Hz}$ (R2 motion) for all “ a_{max} ” values and close to

that of the ones obtained for base motions derived from earthquakes with strike-slip fault mechanisms with the same predominant frequency (S3 motion). It should also be noted that, the efficiency levels for motions with $f = 1\text{Hz}$ and $f = 2\text{Hz}$ were very close to each other but lower than those obtained for motions with strike-slip fault mechanisms for $a_{\max} = 0.2\text{g}$ and $a_{\max} = 0.3\text{g}$, while the η values were very close for $a_{\max} = 0.1\text{g}$ for both fault mechanisms. The improvement gained by the utilization of the composite liner system reached up to $\eta = 90\%$.

- As it can be seen from the acceleration-time histories for base accelerations of “FB” and “IB” cases given in Appendix F, the maximum accelerations were generally deamplified. Also it can be observed that the maximum accelerations for “IB” cases were measured usually at the same time with the “ a_{\max} ” of the input motion or so close to that instance. The decreases in accelerations were more visible for input motions with predominant frequencies close to the natural frequency of the model and for experiments with higher “ a_{\max} ” values, as expected. However, evaluating the behavior of the composite liner system in the time domain may be misleading since the system provides main benefits by altering the frequency content of the motion and the corresponding spectral accelerations rather than directly decreasing the accelerations. For this reason the following evaluations were done based on the response and Fourier amplitude spectra, in other words in the frequency domain.
- Based on the response spectra given in section 4.3.1, it can be concluded that the base accelerations are generally decreased when the composite liner system is utilized. But a much more interesting point is that, the spectral accelerations significantly drops at the first-mode natural period of the tested model ($T_n = 0.23\text{s}$). This fact provides the decrease in the difference between top and base floor accelerations (the η discussed previously). It should be also noted that, very slight amplifications ($\leq 10\%$) occurred in the base accelerations for motions with low frequency and/or low “ a_{\max} ” levels but nevertheless minimum $\eta = 20\%$ improvement was obtained for the S1_0.1 motion with $f = 1\text{Hz}$ predominant frequency and $a_{\max} = 0.10\text{g}$ maximum base acceleration.
- The frequency contents of the base motions were altered when the composite liner system was utilized. The Fourier amplitudes were deamplified for the “ f_n ” of the superstructure at the expense of amplifications at higher frequencies. This effect is more clearly observed as predominant motion frequency gets closer to the “ f_n ” of the superstructure and the “ a_{\max} ” of the input motion increases. The behavior of the composite liner system was similar for both fault mechanisms.

5.2.2 Evaluations for 5-Storey Model

- Similar to the case in the 3-storey model, the composite liner system was triggered in all experiments regardless of the input motion frequency “ f ” and maximum base acceleration “ a_{\max} ”.
- For tested motions derived from earthquake data associated with strike-slip fault mechanisms (S1, S2 and S3 motions), the efficiency of the composite liner system was almost independent of the predominant frequency of the input motion. The efficiency increased with increasing “ a_{\max} ”.
- The efficiency of the system was almost independent of the predominant frequency of the input motion for tested base motions obtained from earthquakes associated with reverse fault mechanisms (R1, R2 and R3 motions), as in the case of motions derived from earthquakes with strike-slip fault mechanisms. Also, the effect of the “ a_{\max} ” of the input motion on “ η ” was more significant as compared to that under S1, S2 and S3 motions. The efficiency levels obtained for R1, R2 and R3 motions were lower than those obtained for the strike-slip fault mechanism for lower “ a_{\max} ” values but almost equals at higher “ a_{\max} ” levels. The

improvement gained by the utilization of the composite liner system reached up to $\eta = 90\%$ for both fault mechanisms.

- The acceleration-time histories for base accelerations in “FB” and “IB” cases are given in Appendix I. Similar to those of the 3-storey model, the decreases in the base accelerations can be observed for most of the records. Also, the changes in acceleration-time histories become more visible as the predominant frequency of the motion gets closer to the natural frequency of the superstructure and as the “ a_{\max} ” increased. However evaluations based on time-histories may be misleading since the real improvement provided by the utilized system was based on altering frequency contents. For this reason, the main evaluations were done based on the response and Fourier amplitude spectra of the experiments.
- Similar to the case in the 3-storey model, the spectral accelerations were significantly reduced at the first-mode natural period of the model ($T_n = 0.43\text{s}$) which provides the improvement. However, it should be emphasized that the amplifications in the spectral accelerations were shifted to the low period (high frequency) range especially for low frequency motions regardless of the fault mechanism. Another thing that should be emphasized is that the base accelerations were more noticeably amplified in this model as compared to the previous one and not only for low but for all “ a_{\max} ” values for motions with $f = 1\text{Hz}$ (S1 and R1 motions) regardless of the fault mechanism. Nevertheless, the composite liner system was triggered and minimum efficiencies were obtained as $\eta = 56\%$ and $\eta = 31\%$ for S1_0.1 and R1_0.1 base motions respectively.
- The frequency contents of the base motions were more noticeably altered by the composite liner system in the 5-storey model as compared to the 3-storey model. The Fourier amplitudes in the close vicinity of the “ f_n ” of the superstructure were deamplified for all motions while those of the higher frequencies were amplified. This phenomenon is more clearly observed for motions the predominant frequencies of which coincide with the “ f_n ” of the superstructure. Another interesting point was that, for base motions with respectively high predominant frequencies ($f = 4\text{Hz}$ for this study) as compared to the first-mode natural frequency of the superstructure ($f_n = 2.33\text{ Hz}$), the amplifications in Fourier amplitudes at high frequencies were much less as compared to other motions.

5.2.3 Evaluations for Slip Displacements

- In case of harmonic motions, the slip displacements are constant for a motion at each cycle of motion and accumulate at the end of the test. The slip displacements are generally increasing with increasing input motion acceleration “ a_{\max} ” and decreasing input motion frequency “ f ”. This behavior is in accordance with the results presented in Yegian and Kadakal (2004). As expected, since the activated mass is bigger, the magnitudes of the slip displacements were higher for the 5-storey model as compared to those of the 3-storey model for the motions during which the composite liner system was triggered for both models.
- For random base motions derived from actual earthquake data, the highest magnitude of slip displacements were observed for motions with low predominant frequency ($f = 1\text{Hz}$). The measured slip displacements did not significantly differ for motions with $f = 2\text{Hz}$ and $f = 4\text{Hz}$. But it should be noted that, the displacements become slightly larger when the predominant frequency “ f ” of the input motion is in the close vicinity of the natural frequency “ f_n ” of the model. The slip displacements had a tendency to increase with increasing “ a_{\max} ”. Another noteworthy point was that the recorded displacements were slightly larger in case of base motions associated with strike-slip fault mechanisms (S1, S2 and S3 motions) as compared to those recorded during experiments with base motions derived from earthquakes with reverse fault mechanisms (R1, R2 and R3 motions).

- According to the similitude calculations given in Appendix B, the slip displacements of the models measured during experiments are expected to be comparable with the values that will be obtained for the corresponding prototypes under the same base motions since the scale used for the forces causing the slip displacements are proportional in model and prototype when the mass participations are assumed as ideal in both. However, there are various factors which may affect the amount of slip displacements such as the three-dimensional characteristics of the earthquake motions, higher mode of vibrations of the superstructure, differences in mass participations, differences in time-histories of various earthquakes and earthquake mechanisms, scale effects and etc... As a consequence, the slip displacements given in this study and the evaluations about these values should be regarded as a preliminary data. In order to have a more definite idea on the possible slip displacements, large scale 1-g tests and/or small scale centrifuge tests with several earthquake motions should be performed.

5.3 Conclusions

Based on the performed experiments following conclusions are arrived at:

5.3.1 Experiments with Harmonic Motions

- The magnitudes of the accelerations acting on the superstructure in isolated models are highly dependent on the input motion frequency “ f ” and natural frequency “ f_n ” of the superstructure and almost independent of the “ a_{max} ” of the input motion unless it is not less than the threshold acceleration “ a_t ” for that motion frequency below which the composite liner system is not triggered. In that case simply the composite liner system does not provide any improvement.
- The maximum reductions in the accelerations are obtained for the cases where the input motion frequency is in the close vicinity of the natural frequency of the superstructure and the improvement obtained by the utilization of the composite liner system is reduced as these two parameters deviate from each other.
- The composite liner system does not alter the mode of vibration and the displacement profile of the superstructure. For the tested motions, the composite liner system is not triggered if the input motion frequencies are at least two times higher than the “ f_n ” of the superstructure.
- The accelerations recorded for both 3-storey and 5-storey models are independent of number of cycles of motion upon reaching a steady state condition. The models reached a steady state vibration after first a few (up to 4 cycles for 3-storey model and 5 cycles for 5-storey model) cycles of harmonic motion.

5.3.2 Experiments with Random Motions

- The effect of the predominant frequency of the random motion becomes more significant as the superstructure becomes more rigid. This fact is more clearly observed for base motions derived from earthquakes associated with reverse fault mechanism as compared to the ones associated with strike-slip fault mechanism.
- The efficiency of the composite liner system increases as the “ a_{max} ” of the input motion increases. For both fault mechanisms the efficiency of the system reaches up to 90%, in other words, the difference between the base and top accelerations acting on the structures can be reduced up to 90%. Additionally, the minimum improvement observed during the performed experiments was on the order of 20%. These improvements are obtained at the expense of lateral displacements of the superstructure.

- The composite liner system is triggered even the predominant frequency of the input motion is not close enough to the “ f_n ” of the superstructure. This result is thought to be due to the fact that the utilized base motions derived from actual earthquake data are generally composed of a frequency range which covers the frequency ranges for which the structure model resting on the composite liner system can start to slide; in contrast to the case in harmonic motions.
- For base motions with low predominant frequencies ($f \leq 1\text{Hz}$), the composite liner system may amplify the base accelerations which may probably be the case for sites composed of deep soft soils.
- The composite liner system alters the frequency contents of the base motions in a way that the Fourier amplitudes for frequencies close to the first-mode natural frequency (f_n) of the superstructure are deamplified while those at higher frequencies are amplified. This effect is more clearly observed for 5-storey model (as the superstructure becomes more flexible). Also, the deamplifications in Fourier amplitudes are maximum when the predominant frequency of the input motion “ f ” is in the close vicinity of the “ f_n ” of the superstructure.
- It may be said that the type of the fault mechanism has a secondary effect on the accelerations recorded in base-isolated models, as compared to the effect of the predominant frequency “ f ” and maximum acceleration “ a_{\max} ” of the input motion and the natural frequency “ f_n ” of the superstructure.
- The composite liner system provides the main improvement by filtering the motion at frequencies close to the “ f_n ” of the superstructure and reducing the corresponding spectral accelerations rather than directly decreasing the accelerations for most of the experiments. As a consequence, evaluating the system in time domain may be misleading, since some amplifications in the base accelerations may be observed in some cases described in the main text. But even for these cases improvements are achieved in the general behavior and they can be best observed in the frequency domain.

It is suggested that, future studies on composite liner systems may be carried out by large scale 1-g tests and/or small scale centrifuge tests for further evaluations. Studies directed to limit the slip displacements of the structure may be another interesting topic for future researches.

Tests carried out in this study are based upon the rigid base assumption. Further studies may be conducted by using models which simulate the stiffness of foundation soil in order to incorporate the soil-structure interaction.

REFERENCES

- Akkar, S., Kale, Ö., Yenier, E., Bommer, J.J. (2011). The high-frequency limit of usable response spectral ordinates from filtered analogue and digital strong-motion accelerograms. *Earthquake Engng Struct. Dyn.*, 40, 1387-1401.
- Athanasopoulos, G.A., Pelekis, P.C., Xenaki, V.C. (1999). Dynamic Properties of EPS Geofoam: An Experimental Investigation. *Geosynthetics International*, 6 (3), 171-194.
- Bathurst, R.J., Zarnani S., Gaskin, A. (2007). Shaking table testing of geofoam seismic buffers. *Soil Dynamics and Earthquake Engineering*, 27, 324-332.
- Bathurst, R.J., Keshavarz, A., Zarnani, S., Take, W.A. (2007). A simple displacement model for response analysis of EPS geofoam seismic buffers. *Soil Dynamics and Earthquake Engineering*, 27, 324-332.
- Bechtold, J. (1907). Earthquake Proof Building. *The United States Patent and Trademark Office*, US Patent No: 845046.
- Besa, J., Liera, J.C., Jünemann, R. (2010). Experimental behavior and design of a new kinematic isolator. *Engineering Structures*, 32, 508-522.
- Bucher, C. (2009). Probability-based optimal design of friction-based seismic isolation devices. *Structural Safety*, 31, 500-507.
- Chung, W.J., Yun, C.B., Kim, N.S., Seo, J.W. (1999). "Shaking table and pseudodynamic tests for the evaluation of the seismic performance of base-isolated structures". *Engineering Structures*, 21, 365-379.
- Douglas, J., Boore, D.M. (2011). High-frequency filtering of strong-motion records. *Bull Earthquake Eng*, 9, 395-409.
- Duškov, M. (1997). Materials Research on EPS-20 and EPS-15 Under Representative Conditions in Pavement Structures. *Geotextiles and Geomembranes*, 15, 147-181.
- Edil, T.B., Bosscher, P.J. (1994). Engineering Properties of Tire Chips and Soil Mixtures. *Geotechnical Testing Journal*, 17 (4), 453-464.
- Glicksberg, R.C. (1973). Earthquake-Insulation Foundations. *The United States Patent and Trademark Office*, US Patent No: 3748800.
- Horvath, J.S. (1995). Geofoam Geosynthetic. *Horvath Engineering*, P.C. Scarsdale, New York, USA, 217p.
- Horvath, J.S. (1998). The Compressible-Inclusion Function of EPS Geofoam: Analysis and Design Methodologies. *Manhattan College Research Report*, New York, USA. Report No: CE/GE-98-2.
- Iai, S. (1988). Similitude for Shaking Table Tests on Soil-Structure-Fluid Model in 1g Gravitational Field. *Report of the Port and Harbour Research Institute, Japan*, 27 (3), 3-24.
- Jangid, R.S. (2010). Stochastic response of building frames isolated by lead-rubber bearings. *Struct. Control Health Monit.*, 17, 1-22.

- Karpurapu, R., Bathurst, R.J. (1992). Numerical Investigation of Controlled Yielding of Soil-Retaining Wall Structures. *Geotextiles and Geomembranes*, 11, 115-131.
- Kelly, J.M. (2002). Seismic Isolation systems for Developing Countries. *Earthquake Spectra*, 18 (3), 385-406.
- Li, C.S., Lam, S.S.E., Zhang, M.Z., Wong Y.L. (2006). Shaking Table Test of a 1:20 Scale High-Rise Building with a Transfer Plate System. *Journal of Structural Engineering*, 132 (11), 1732-1744.
- Mizuno, T. (2000). Device for Minimizing Earthquake Shocks to a Small Building. *The United States Patent and Trademark Office*, US Patent No: 6085474.
- Prasad, S.K., Towhata, I, Chandradhara, G.P., Nanjundaswamy, P. (2004). Shaking table tests in earthquake geotechnical engineering. *Current Science*, 87 (10), 1398-1404.
- Sharma, A., Jangid, R.S. (2009). Behaviour of Base-Isolated Structures with High Initial Isolator Stiffness. *International Journal of Applied Science, Engineering and Technology*, 5 (3), 199-204.
- Spyrakos, C.C., Koutromanos, I.A., Maniatakis, Ch.A. (2009). Seismic response of base-isolated buildings including soil-structure interaction. *Soil Dynamics and Earthquake Engineering*, 29, 658-668.
- Stewart, J.P., Fenves, G.L., Seed, R.B. (1999). Seismic Soil-Structure Interaction in Buildings I: Analytical Methods. *J. Geotech. Geoenviron. Eng.*, 125 (1), 26-37.
- Stewart, J.P., Fenves, G.L., Seed, R.B. (1999). Seismic Soil-Structure Interaction in Buildings II: Empirical Findings. *J. Geotech. Geoenviron. Eng.*, 125 (1), 38-48.
- Tsang, H.H. (2008). Seismic isolation by rubber-soil mixtures for developing countries. *Earthquake Engng Struct. Dyn.*, 37, 283-303.
- USACE, (2005). Seismic Isolation and Energy Dissipation Systems. *Seismic Design for Buildings*, 8, 1-42.
- Wu, C., Li, Y., Li, H., Zhang, K. (2008). Parametric Study on Seismic Energy Response of Base-Isolated Structures. *Proceedings of International Workshop on Modelling, Simulation and Optimization*, 27-28 December 2008, Hong Kong, China, 375-378.
- Yegian, M.K., Lahlaf, A. M. (1992). Dynamic interface shear strength properties of geomembranes and geotextiles. *J. Geotech. Eng.*, 118 (5), 760-779.
- Yegian, M.K., Yee, Z.Y., Harb, J.N. (1995). Response of geosynthetics under earthquake excitations. *Geosynthetics*, 677-689.
- Yegian, M.K., Kadakal, U. (2004). Foundation isolation for seismic protection using a smooth synthetic liner. *J. Geotech. Geoenviron. Eng.*, 130 (11), 1121-1130.
- Yegian, M.K., Catan, M. (2004). Soil isolation for seismic protection using a smooth synthetic liner. *J. Geotech. Geoenviron. Eng.*, 130 (11), 1131-1139.
- Yuan, Z. (2009). Numerical Simulation of Base-isolated Methods of Multiple Building Structures." *Sci-tech Research Projects of Guangdong Province, China*, Report No: 20055190030.

APPENDIX A
SAMPLE INPUT MOTION

A part of the code for Landers earthquake scaled to $a_{\max} = 0.2g$ is given below:
("X" stands for position in "mm" and "F" is velocity in "mm/s")

G90 (Routine code)	X 0.4325 F 82.4800
G01 (Start code)	X 0.4536 F 84.4400
X 0.0000 F 0.0400	X 0.4759 F 89.2400
X 0.0000 F 0.1200	X 0.5003 F 97.2800
X 0.0001 F 0.2800	X 0.5273 F 108.1600
X 0.0002 F 0.5600	X 0.5577 F 121.7600
X 0.0005 F 1.0400	X 0.5921 F 137.3200
X 0.0009 F 1.6800	X 0.6307 F 154.4000
X 0.0015 F 2.4800	X 0.6738 F 172.4400
X 0.0024 F 3.2400	X 0.7215 F 190.9200
X 0.0034 F 4.1200	X 0.7739 F 209.6400
X 0.0046 F 4.8800	X 0.8310 F 228.4000
X 0.0060 F 5.6800	X 0.8928 F 247.0800
X 0.0077 F 6.5600	X 0.9591 F 265.4400
X 0.0096 F 7.8800	X 1.0298 F 282.6000
X 0.0121 F 9.8400	X 1.1038 F 295.8800
X 0.0153 F 12.8400	X 1.1790 F 301.0400
X 0.0196 F 17.0400	X 1.2522 F 292.5600
X 0.0252 F 22.4800	X 1.3187 F 265.9600
X 0.0325 F 29.1600	X 1.3737 F 220.1600
X 0.0417 F 37.0400	X 1.4135 F 159.2000
X 0.0532 F 45.7600	X 1.4364 F 91.6400
X 0.0670 F 55.2800	X 1.4433 F 27.5200
X 0.0833 F 65.2000	X 1.4369 F 25.6800
X 0.1021 F 75.0800	X 1.4205 F 65.4800
X 0.1232 F 84.4400	X 1.3966 F 95.6800
X 0.1463 F 92.6000	X 1.3655 F 124.3600
X 0.1711 F 98.9600	X 1.3251 F 161.7200
X 0.1968 F 103.0400	X 1.2709 F 216.6000
X 0.2230 F 104.8400	X 1.1972 F 294.8400
X 0.2492 F 104.6400	X 1.0978 F 397.4000
X 0.2750 F 103.0000	X 0.9677 F 520.5200
X 0.3000 F 100.2800	X 0.8040 F 655.0800
X 0.3242 F 96.8400	X 0.6073 F 786.4000
X 0.3475 F 92.9600	X 0.3837 F 894.7600
X 0.3697 F 89.0400	X 0.1441 F 958.2800
X 0.3911 F 85.5600	X -0.0952 F 957.3600
X 0.4119 F 83.1200	X -0.3153 F 880.2400

APPENDIX B

SIMILITUDE CALCULATIONS

B.1 Base Pressures

The prototypes were taken as 3-storey (Base + 2) and 5-storey (Base + 4) structures which applied 30 kPa and 50 kPa base pressures to the foundation. The models were built with $\lambda_1 = 1:12$ dimensional scale in all dimensions and fiberglass plates were used as floors. As a consequence, both models had a 30 cm x 55 cm plan dimensions and 25cm storey height. However, since the materials used in the models were different from the prototypes the base pressures were lower as compared to those of the prototypes. The 3-storey and 5-storey models were weighed as 0.063 kN and 0.105 kN respectively. In order to model the base pressures 4 fiberglass blocks were attached to the base of the models which increases the base pressures by decreasing the contact area. The dimensions of these blocks were determined as follows:

For $P_p = P_m$;

$$P_m = W_m / A_b$$

For 3-storey model:

$$P_m = W_m / A_b = 0.063 / A_b = 30 \text{ kPa}$$

$$A_b = 0.063 / 30 = 2.1E-03 \text{ m}^2 = 2100 \text{ mm}^2$$

There were 4 blocks. So area of one block is: $A_{\text{block}} = A_b / 4 = 2100 / 4 = 525 \text{ mm}^2$

The dimensions of one block were determined as 15 mm x 35 mm

For 5-storey model:

$$P_m = W_m / A_b = 0.105 / A_b = 50 \text{ kPa}$$

$$A_b = 0.105 / 50 = 2.1E-03 \text{ m}^2 = 2100 \text{ mm}^2$$

There were 4 blocks. So area of one block is: $A_{\text{block}} = A_b / 4 = 2100 / 4 = 525 \text{ mm}^2$

The dimensions of one block were determined as 15 mm x 35 mm

The blocks were attached to the base of the models, 10cm away from the four corners of each model symmetrically.

where,

P_p : base pressure of prototype

P_m : base pressure of model

W_m : weight of model

A_b : base area

A_{block} : area of one block

B.2 Slip Displacements

The slip displacements occur due to the force difference at the contact area of the composite liner system. The structure is forced to move with the a_{max} of the input motion and a force acts in the opposite direction due to the friction in the composite liner system. The resultant slip displacement is related with the difference of these forces. So the similitude can be established as:

For prototype:

$$F_p = m_p^1 \times a_p$$

$$F_{f,p} = \mu_p \times A_p \times P_p = \mu_p \times m_p \times g_p$$

$$\Delta F_p = F_p - F_{f,p} = (m_p^1 \times a_p) - (\mu_p \times m_p \times g_p)$$

where,

- F_p : force due to base acceleration in prototype
- m_p^1 : participated mass of the prototype
- a_p : base acceleration in prototype
- $F_{f,p}$: force due to friction in the composite liner system in prototype
- μ_p : friction coefficient of the composite liner system in prototype
- A_p : base contact area of prototype
- P_p : base pressure of prototype
- m_p : mass of prototype
- g_p : acceleration of gravity in prototype
- ΔF_p : the differential force in prototype

For model:

$$F_m = m_m^1 \times a_m$$

$$F_{f,m} = \mu_m \times A_m \times P_m = \mu_m \times m_m \times g_m$$

$$\Delta F_m = F_m - F_{f,m} = (m_m^1 \times a_m) - (\mu_m \times m_m \times g_m)$$

where,

- F_m : force due to base acceleration in model
- m_m^1 : participated mass of the model
- a_m : base acceleration in model
- $F_{f,m}$: force due to friction in the composite liner system in model
- μ_m : friction coefficient of the composite liner system in model
- A_m : base contact area of model
- P_m : base pressure of model
- m_m : mass of model
- g_m : acceleration of gravity in model
- ΔF_m : the differential force in model

Since,

$$a_m = a_p, \mu_m = \mu_p, g_m = g_p,$$

$$m_m^1 = \lambda_m^1 \times m_p^1 \quad (\lambda_m^1 : \text{scale factor for participated mass})$$

$$m_m = \lambda_m \times m_p \quad (\lambda_m : \text{scale factor for mass})$$

So,

$$\Delta F_m = (\lambda_m^1 \times m_p^1 \times a_p) - (\mu_p \times \lambda_m \times m_p \times g_p)$$

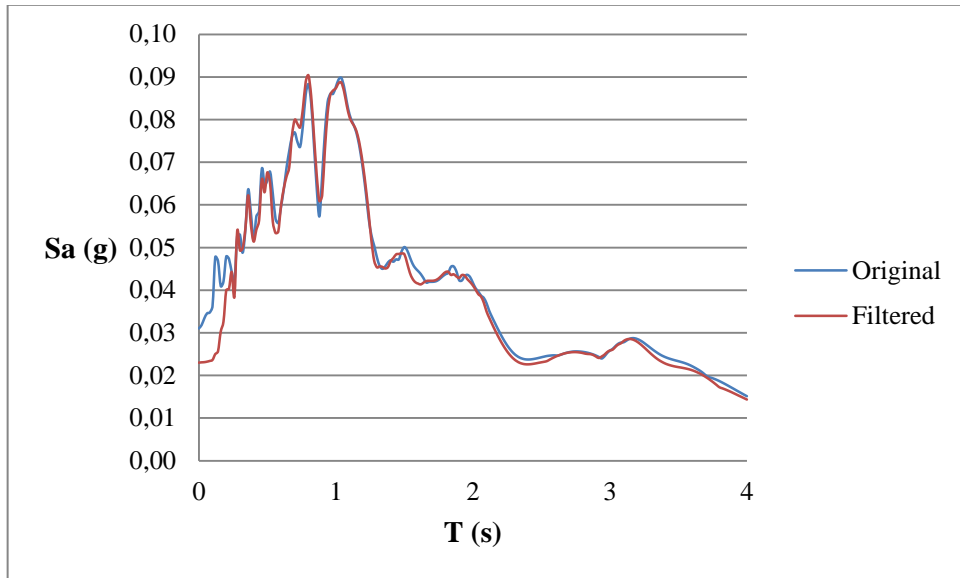
Assuming $\lambda_m^1 = \lambda_m$, the equation becomes:

$$\Delta F_m = \lambda_m [(m_p^1 \times a_p) - (\mu_p \times m_p \times g_p)] = \lambda_m \times \Delta F_p$$

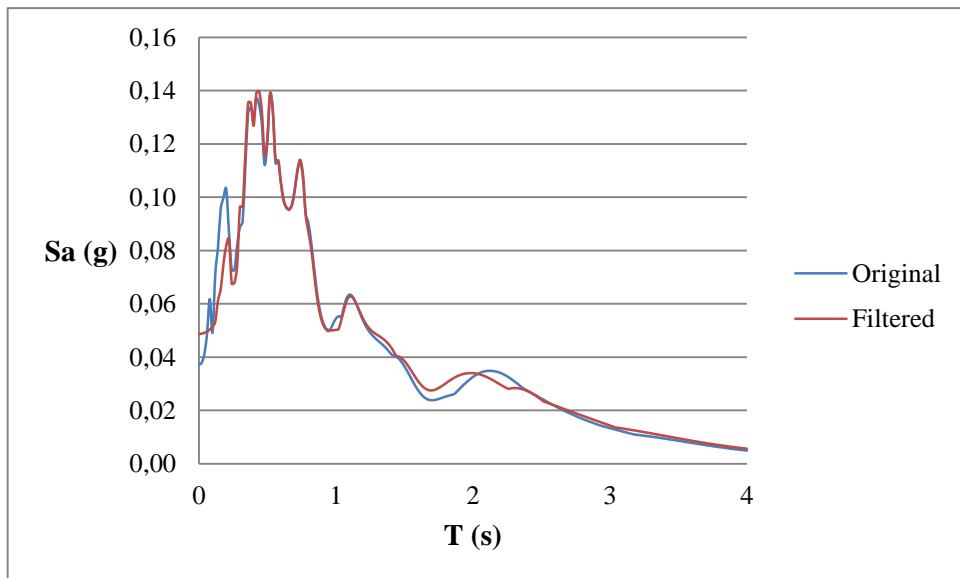
This means that the force difference which causes the slip displacement is scaled with same factor used for mass. So, the slip displacements obtained for the models are expected to be comparable with those of the corresponding prototypes.

APPENDIX C

RESPONSE and FOURIER AMPLITUDE SPECTRA OF ORIGINAL AND FILTERED STRONG MOTIONS

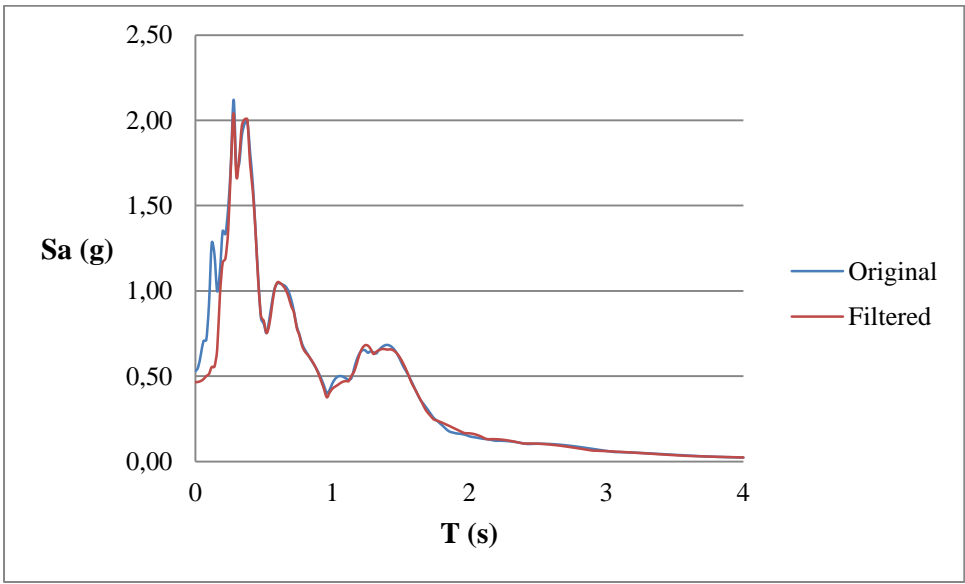


a. Landers earthquake



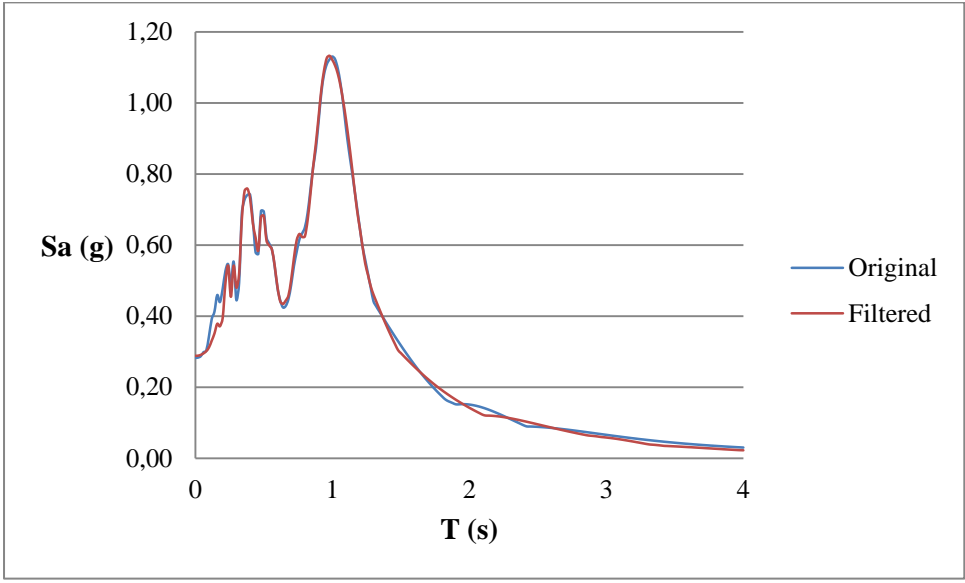
b. Chalfant Valley earthquake

Fig. C.1 Response spectra for strike-slip earthquakes



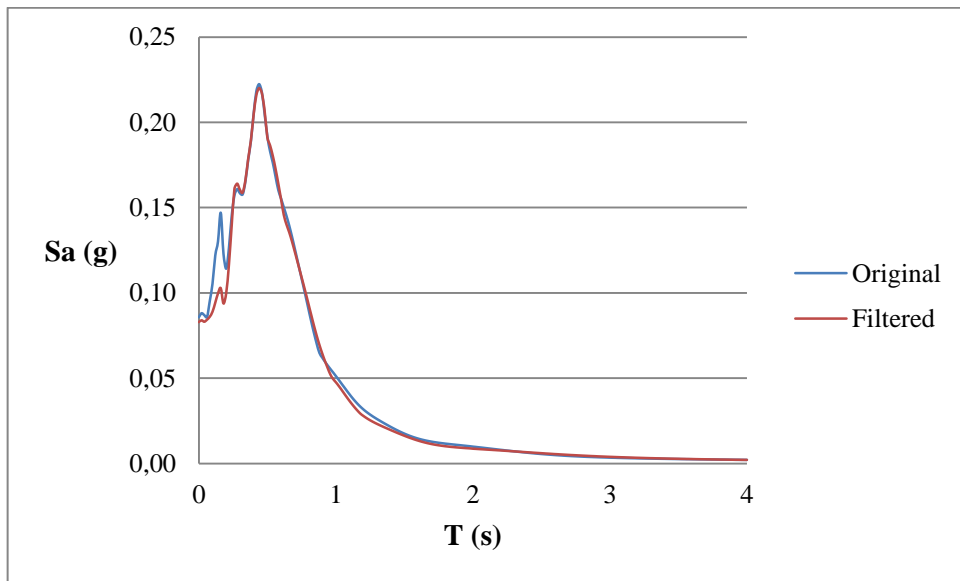
c. Lome Prieta earthquake

Fig. C.1 Response spectra for strike-slip earthquakes (continued)

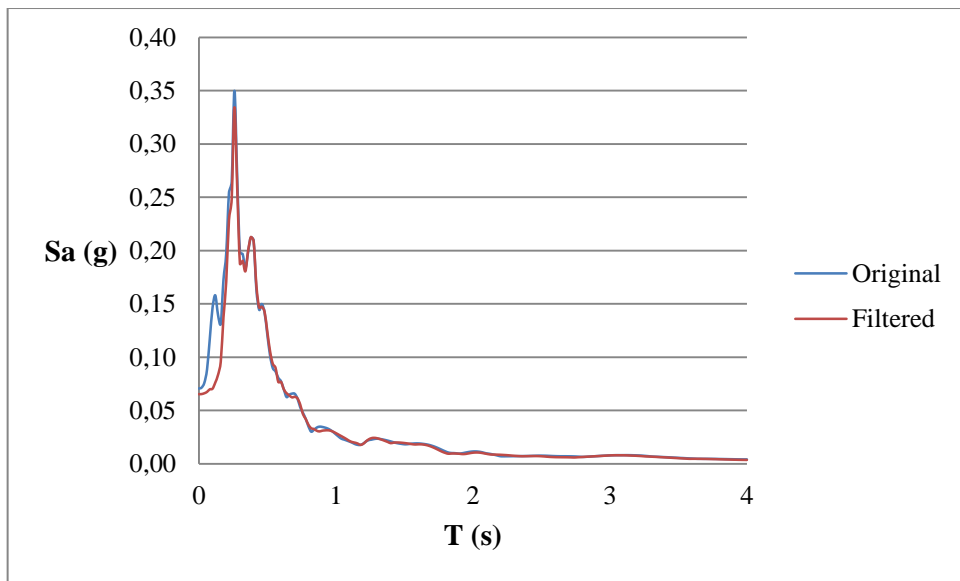


a. Coalinga earthquake

Fig. C.2 Response spectra for reverse fault earthquakes

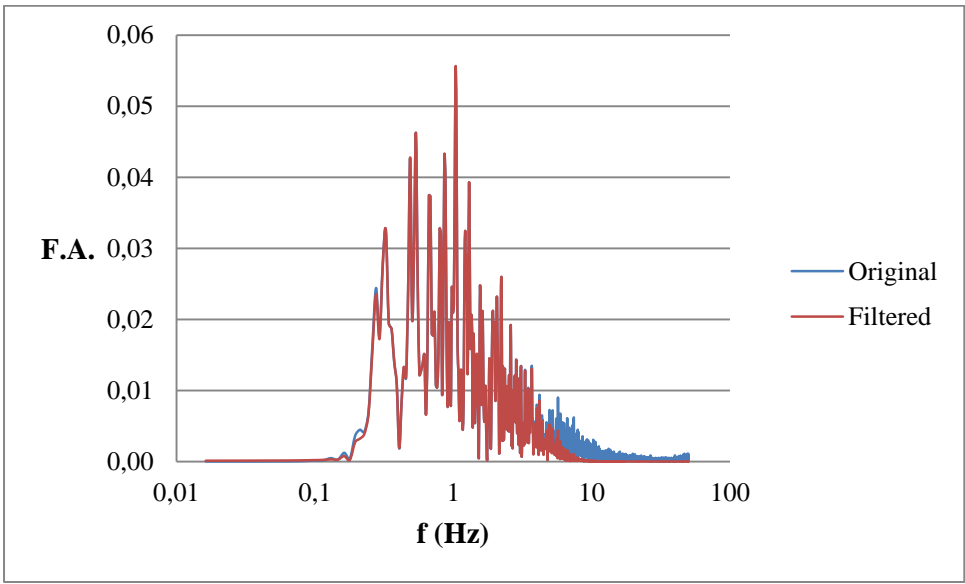


b. Northridge earthquake

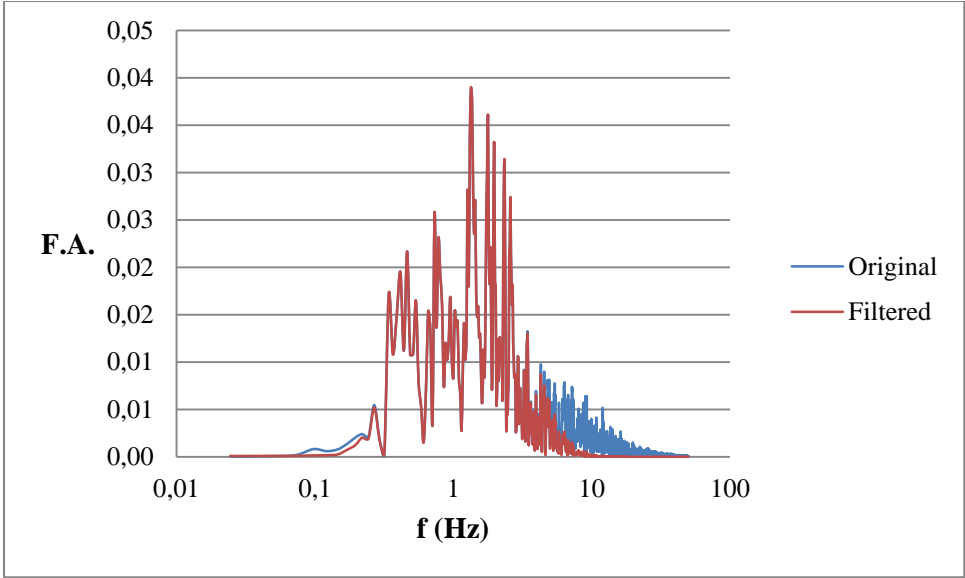


c. San Fernando earthquake

Fig. C.2 Response spectra for reverse fault earthquakes (continued)

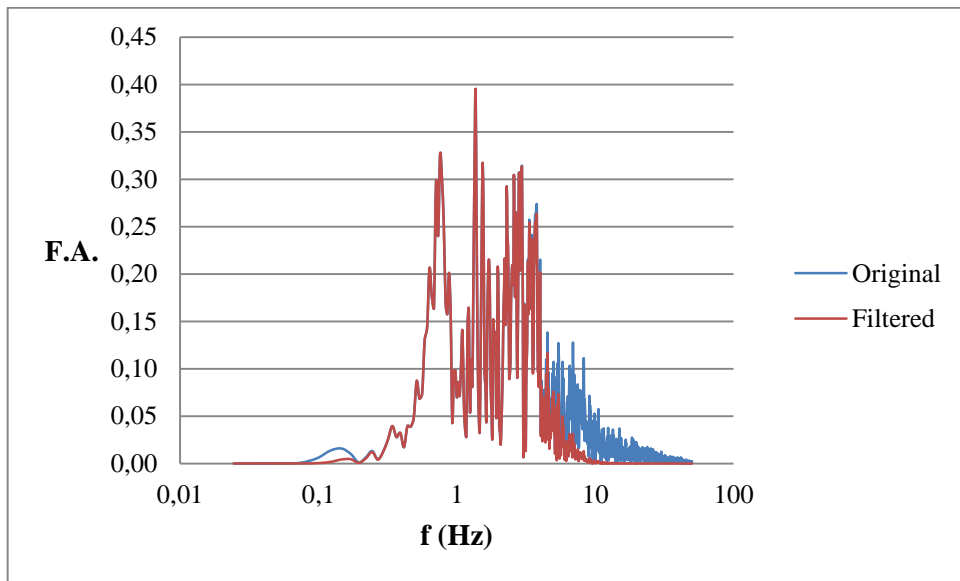


a. Landers earthquake



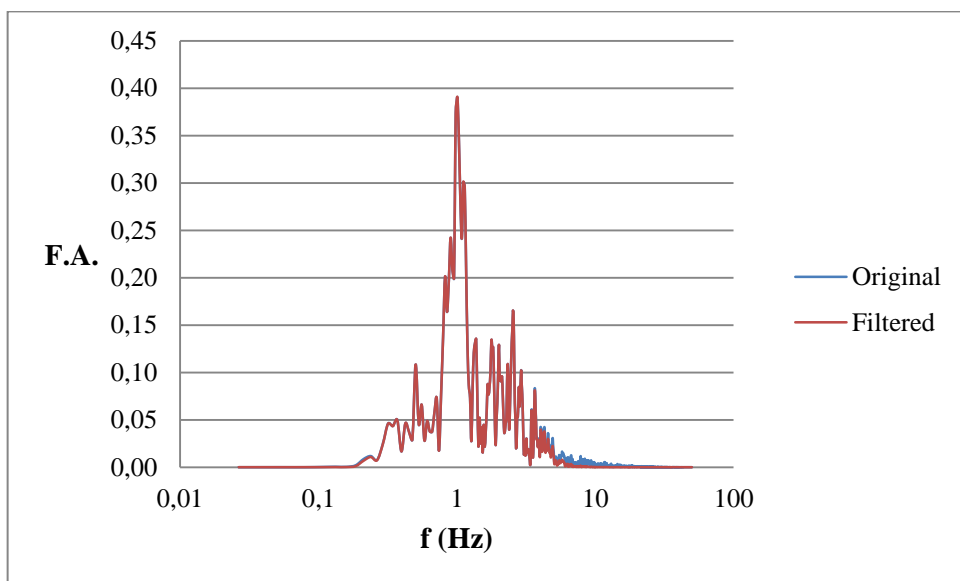
b. Chalfant Valley earthquake

Fig. C.3 Fourier amplitude spectra for strike-slip earthquakes



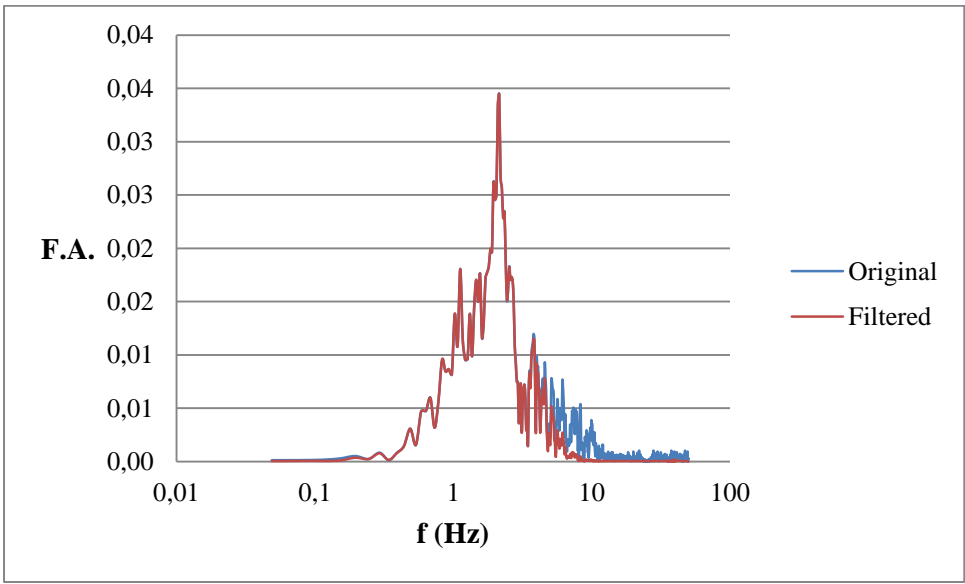
c. Loma Prieta earthquake

Fig. C.3 Fourier amplitude spectra for strike-slip earthquakes (continued)

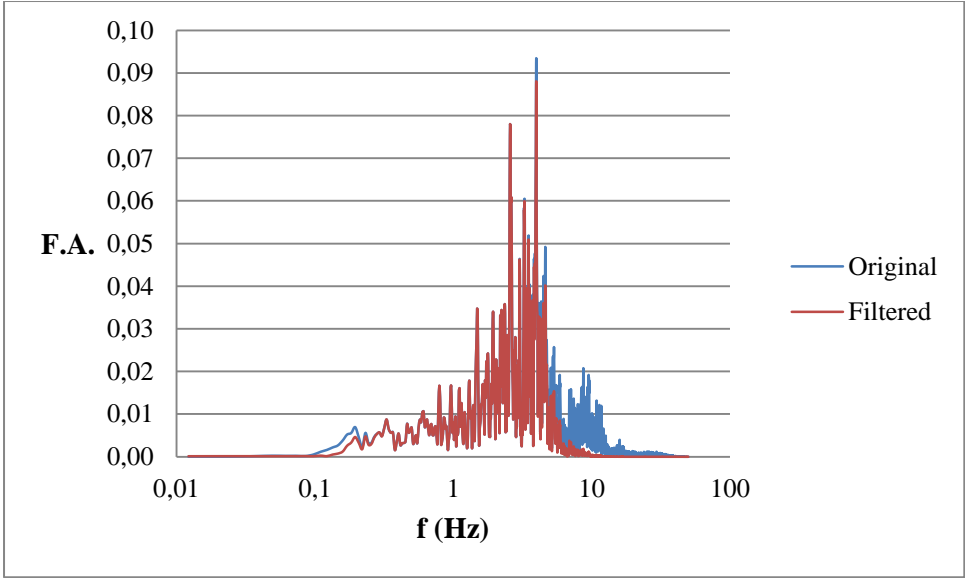


a. Coalinga earthquake

Fig. C.4 Fourier amplitude spectra for reverse fault earthquakes



b. Northridge earthquake

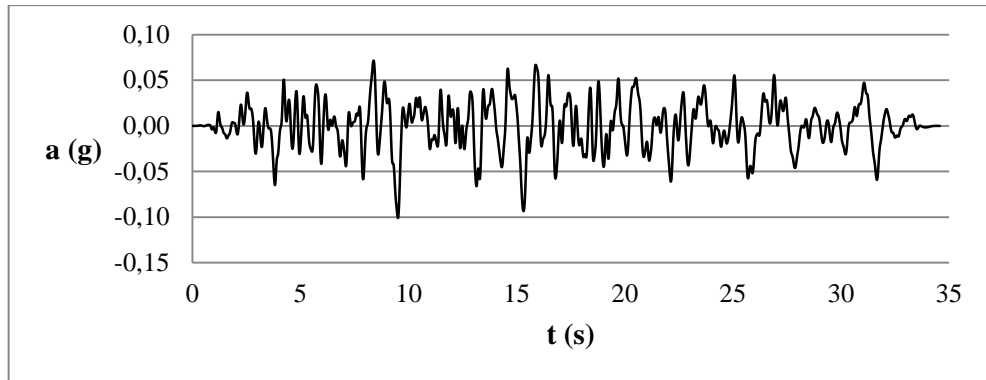


c. San Fernando earthquake

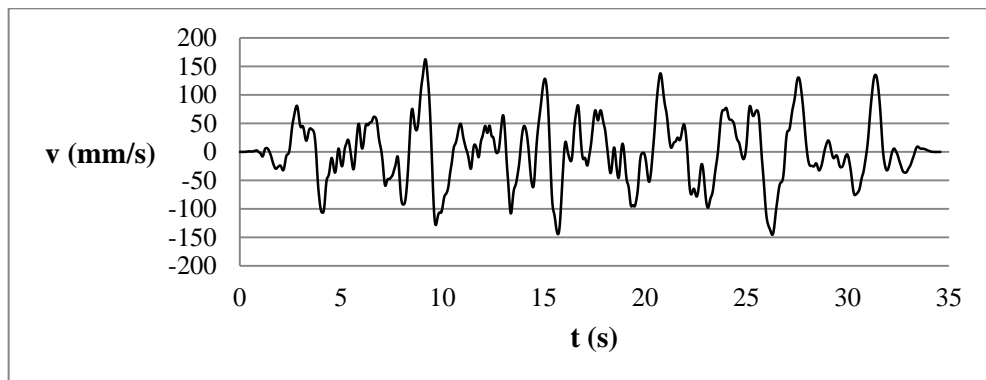
Fig. C.4 Fourier amplitude spectra for reverse fault earthquakes (continued)

APPENDIX D

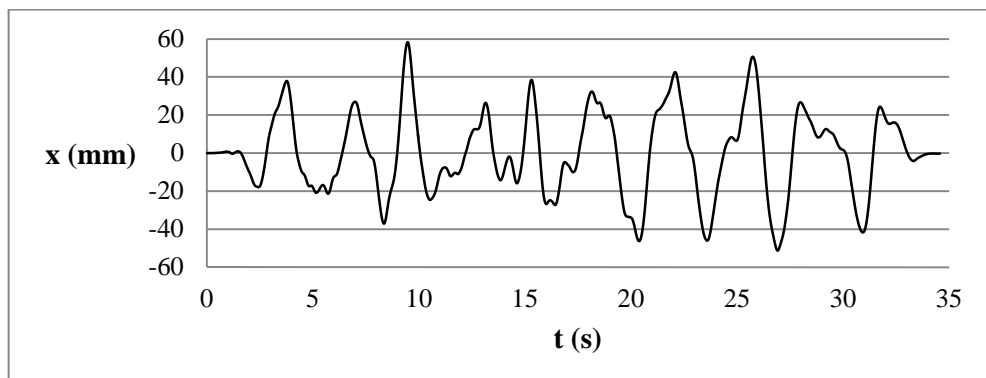
TIME HISTORIES OF UTILIZED RANDOM MOTIONS



a. a-t plot

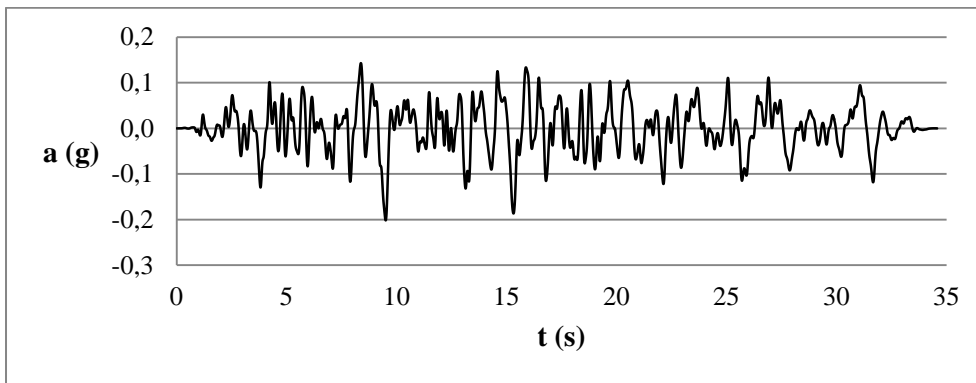


b. v-t plot

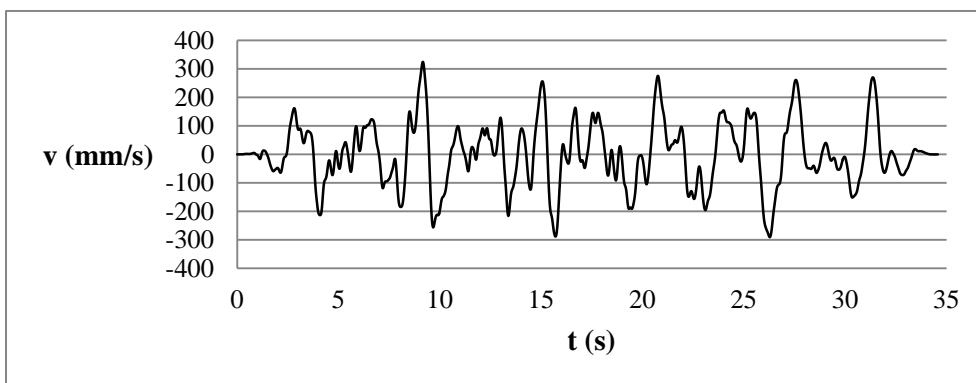


c. x-t plot

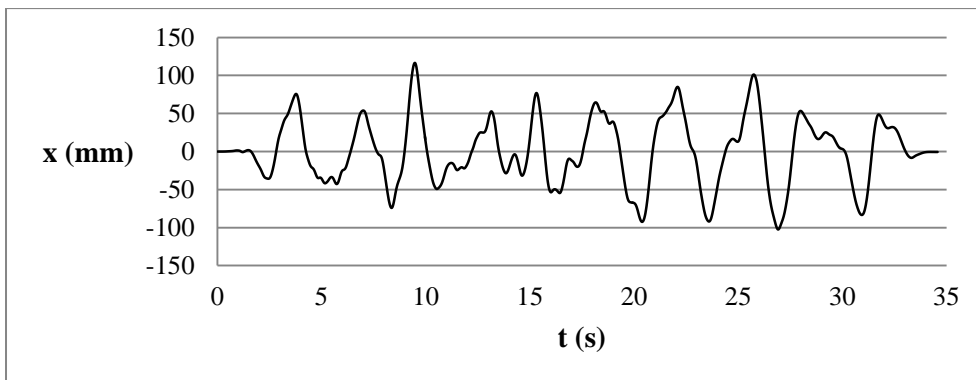
Fig. D.1 Time histories for S1_0.1 motion



a. a-t plot

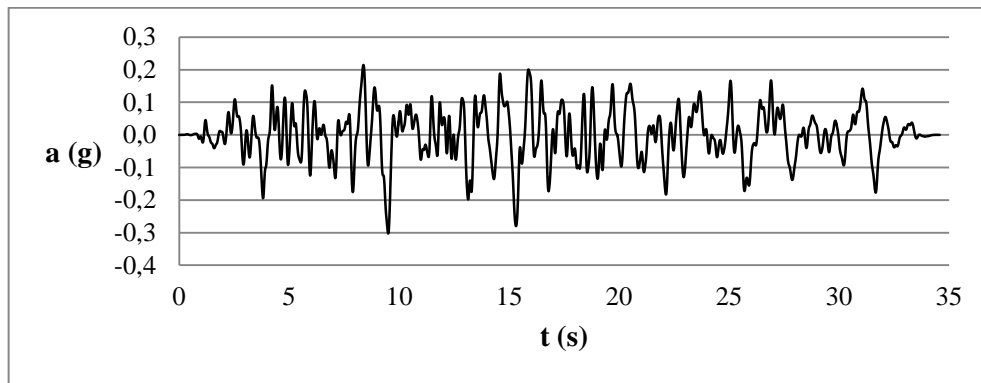


b. v-t plot

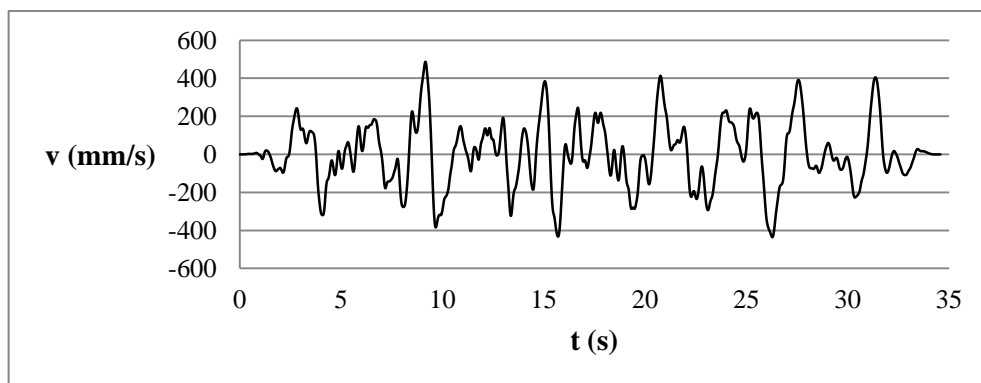


c. x-t plot

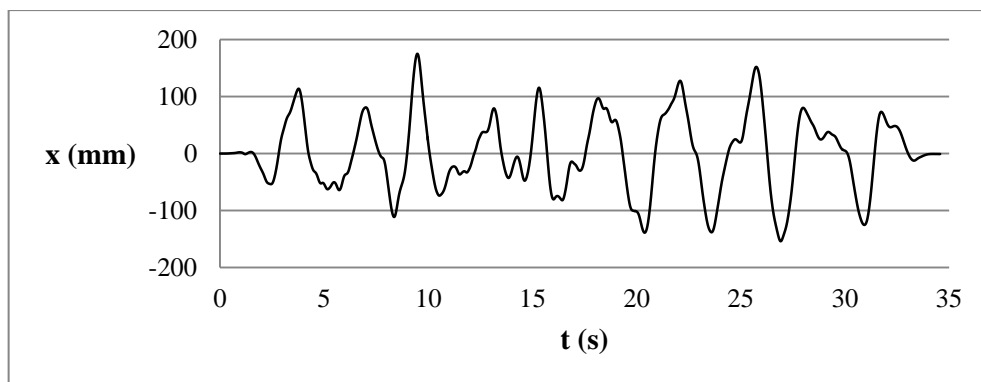
Fig. D.2 Time histories for S1_0.2 motion



a. a-t plot

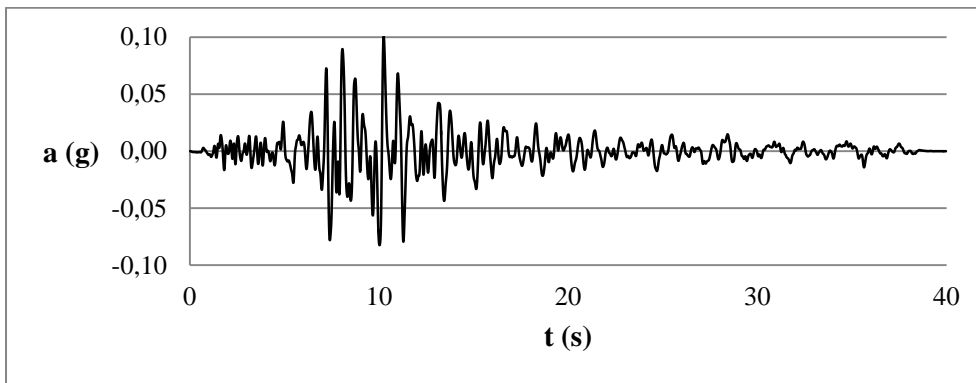


b. v-t plot

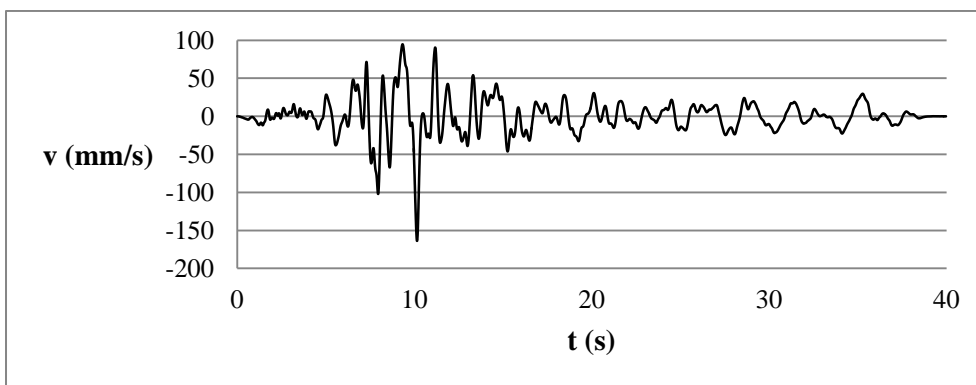


c. x-t plot

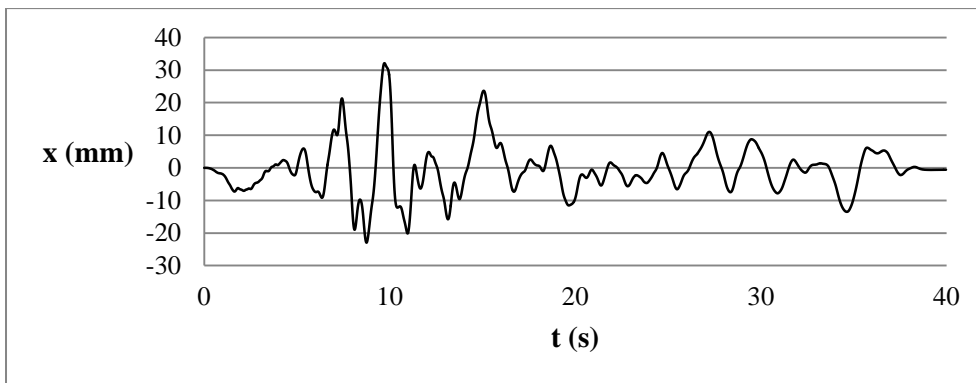
Fig. D.3 Time histories for S1_0.3 motion



a. a-t plot

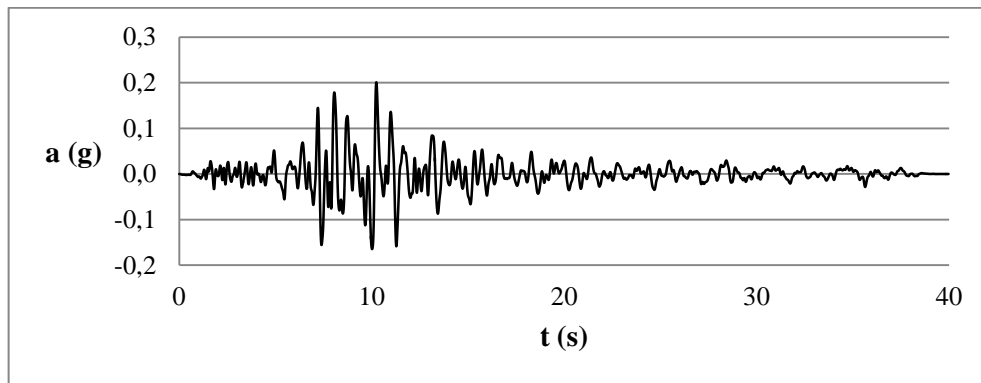


b. v-t plot

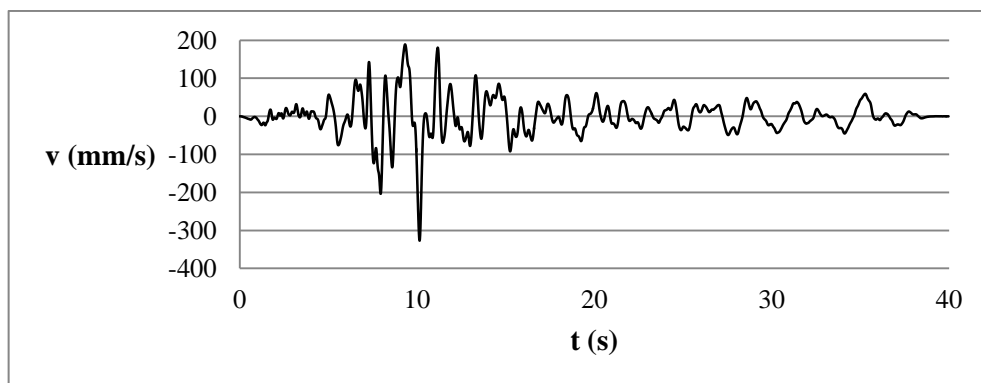


c. x-t plot

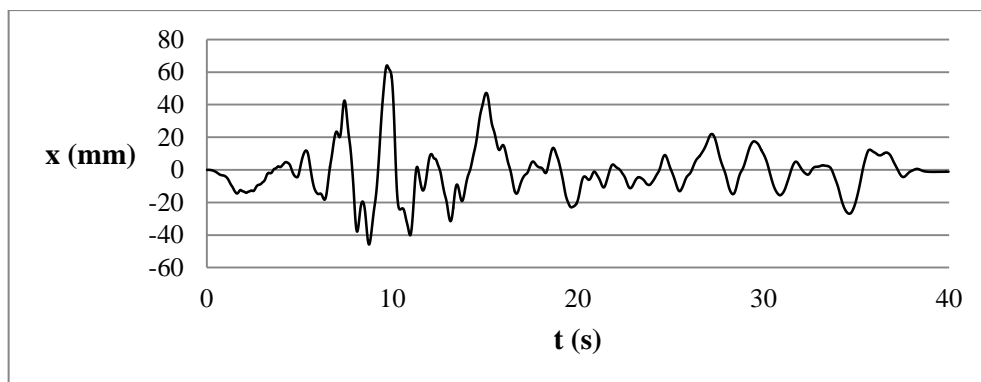
Fig. D.4 Time histories for S2_0.1 motion



a. a-t plot

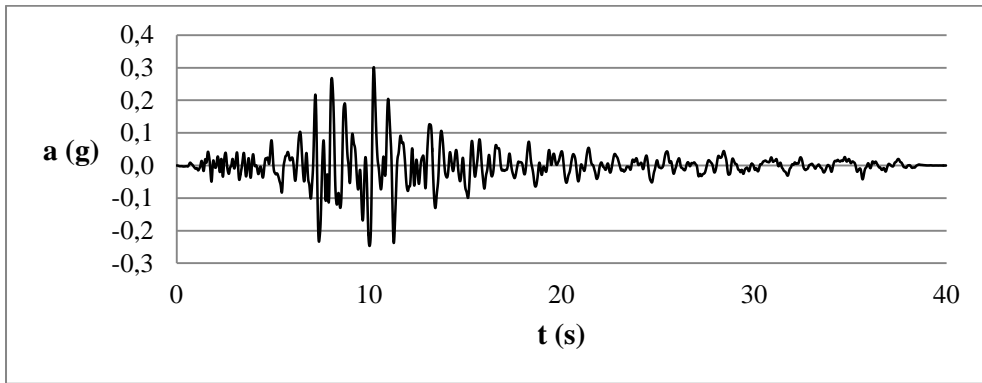


b. v-t plot

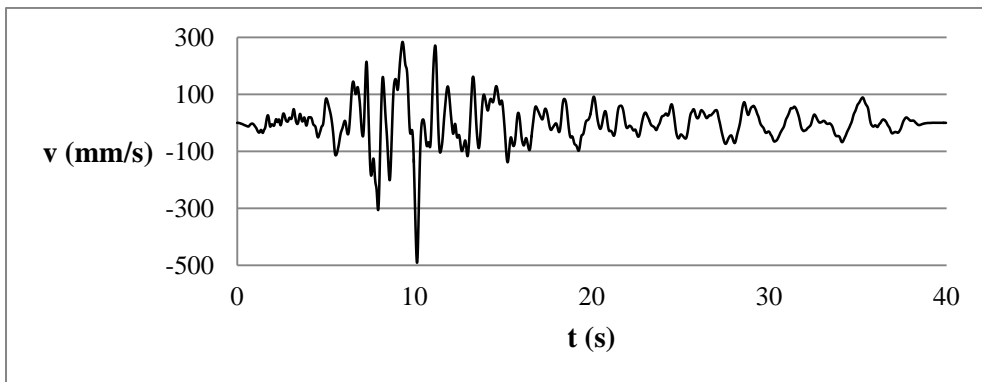


c. x-t plot

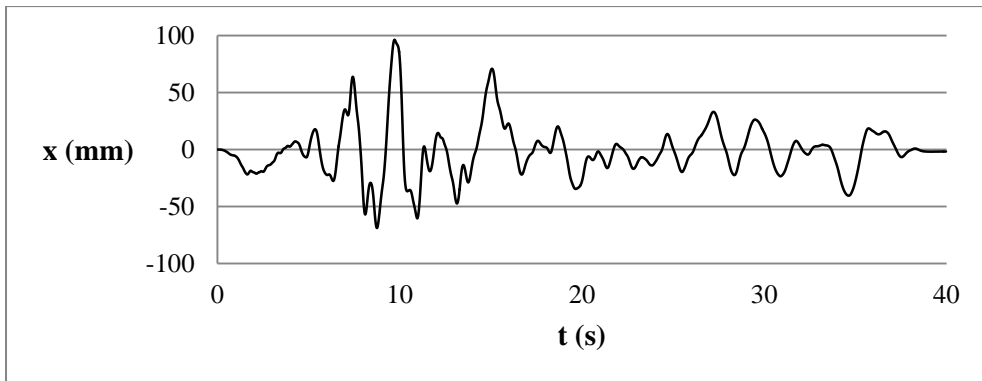
Fig. D.5 Time histories for S2_0.2 motion



a. a-t plot

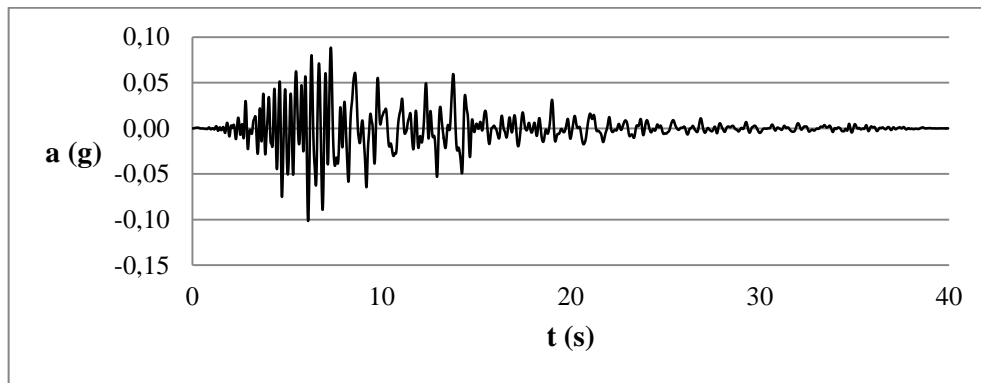


b. v-t plot

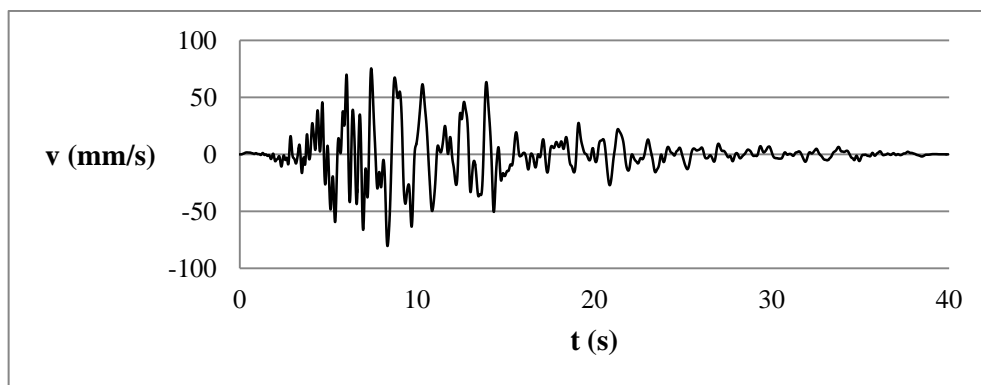


c. x-t plot

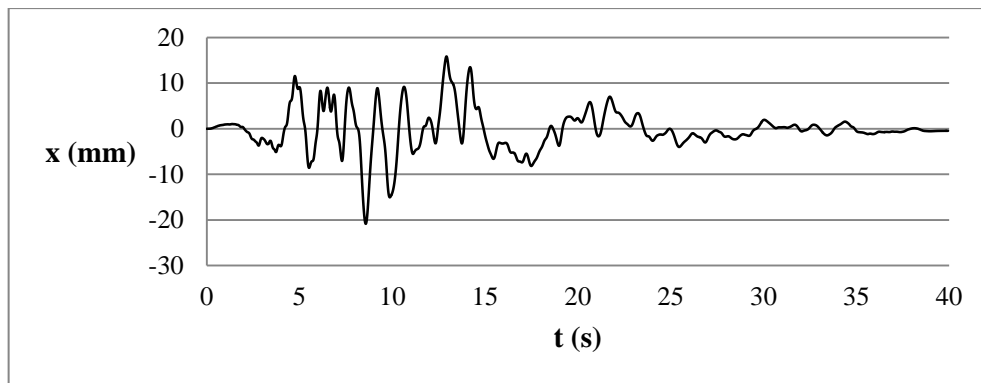
Fig. D.6 Time histories for S2_0.3 motion



a. a-t plot

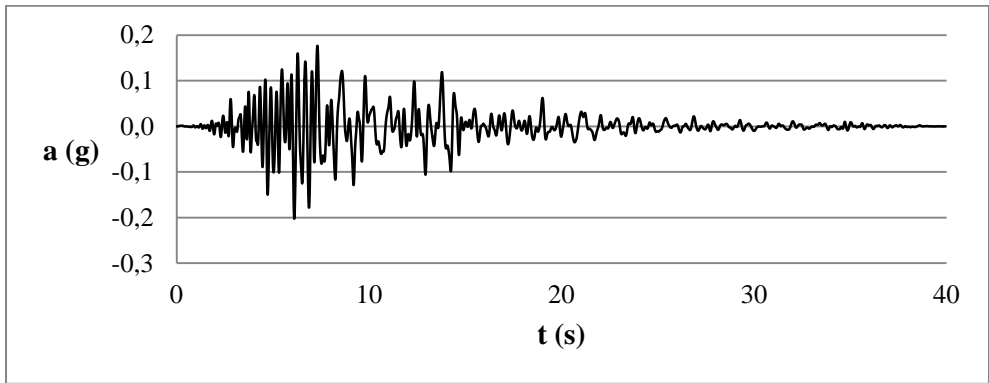


b. v-t plot

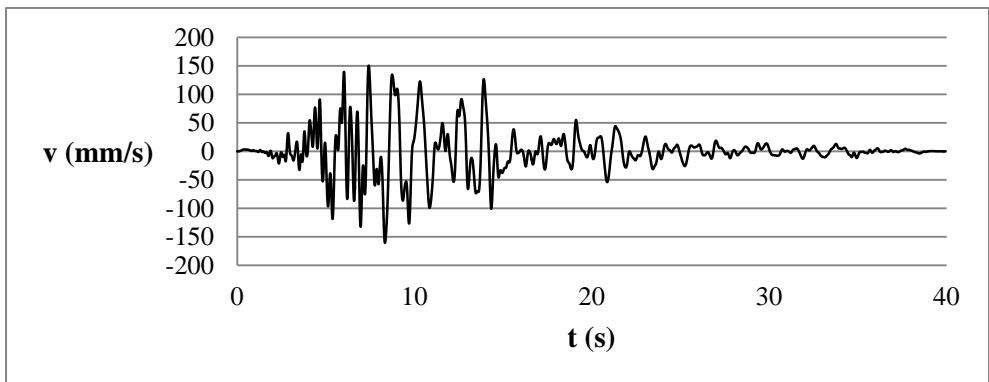


c. x-t plot

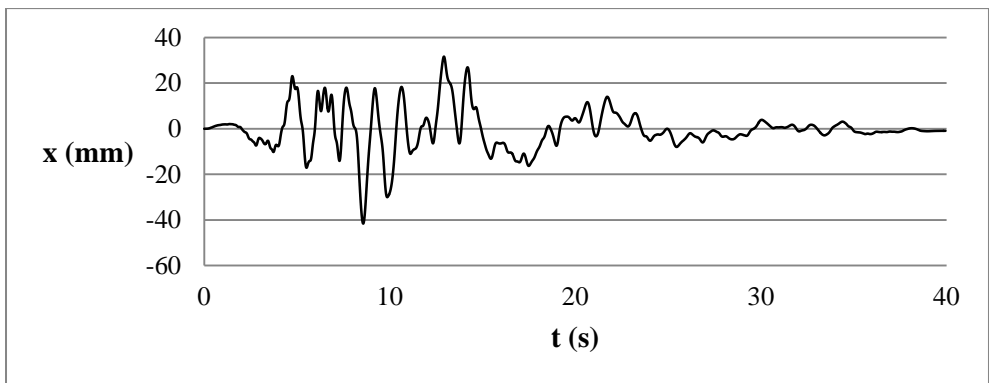
Fig. D.7 Time histories for S3_0.1 motion



a. a-t plot

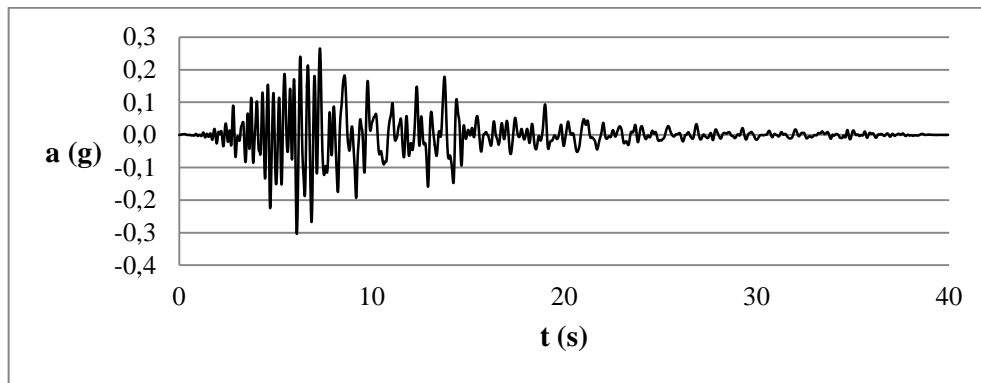


b. v-t plot

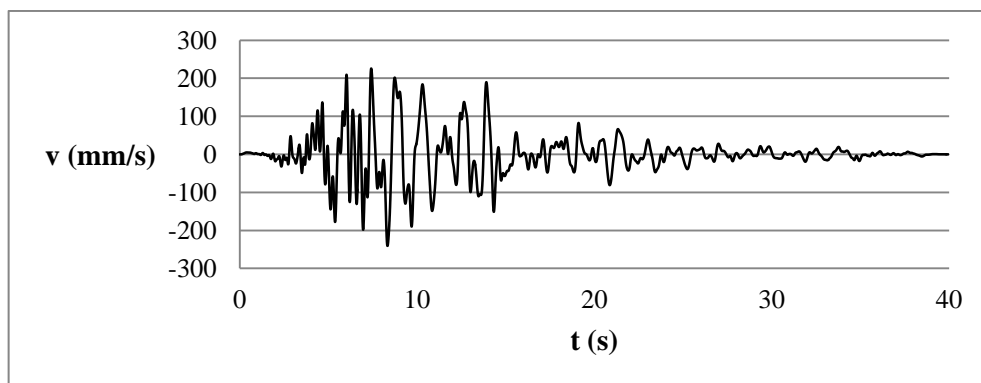


c. x-t plot

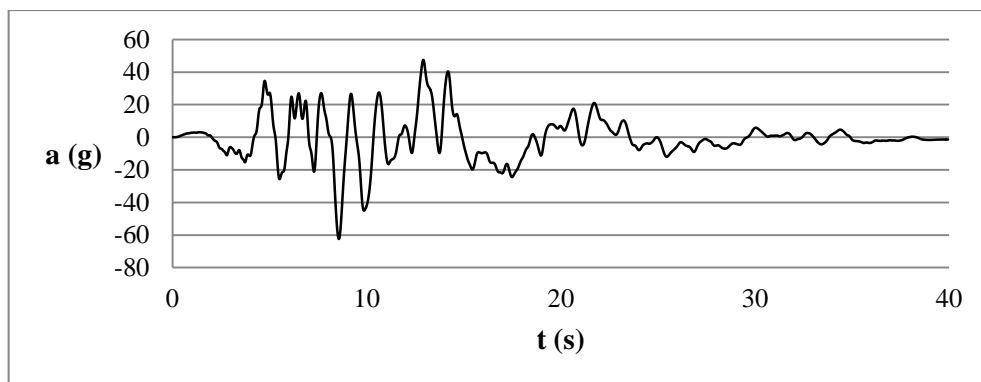
Fig. D.8 Time histories for S3_0.2 motion



a. a-t plot

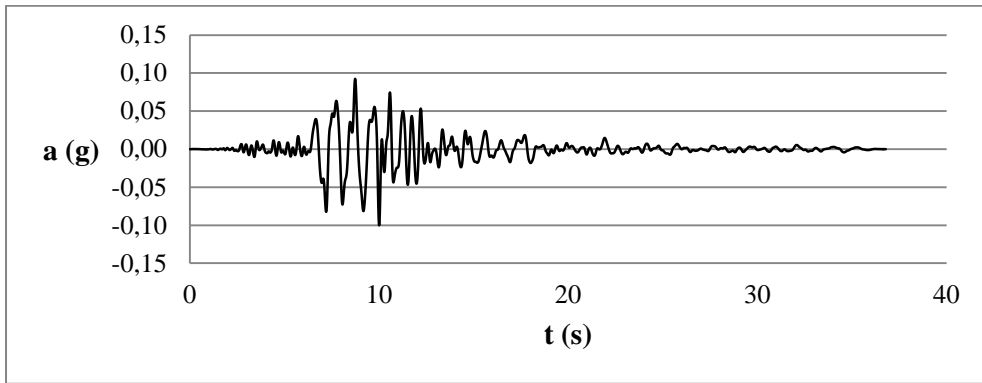


b. v-t plot

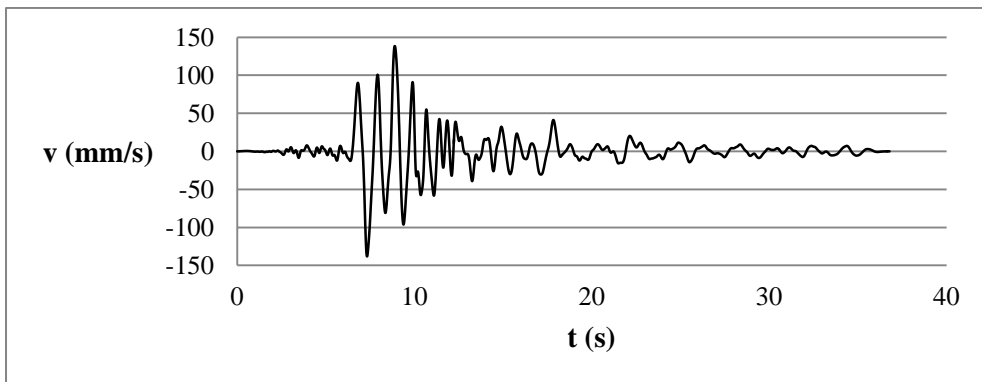


c. x-t plot

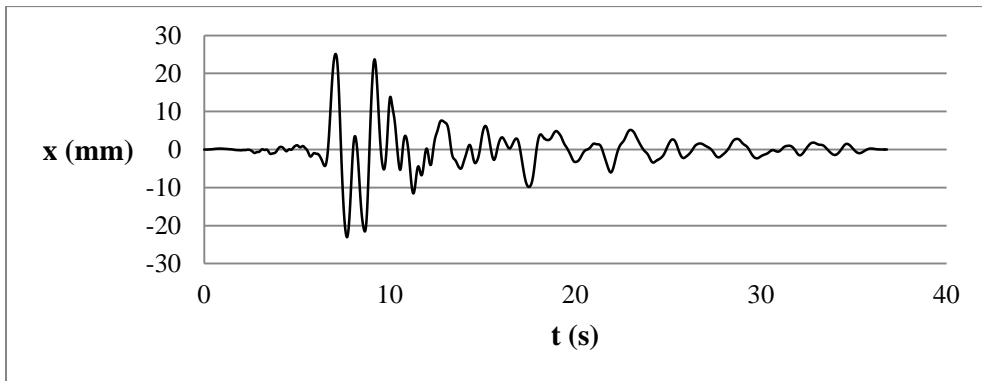
Fig. D.9 Time histories for S3_0.3 motion



a. a-t plot

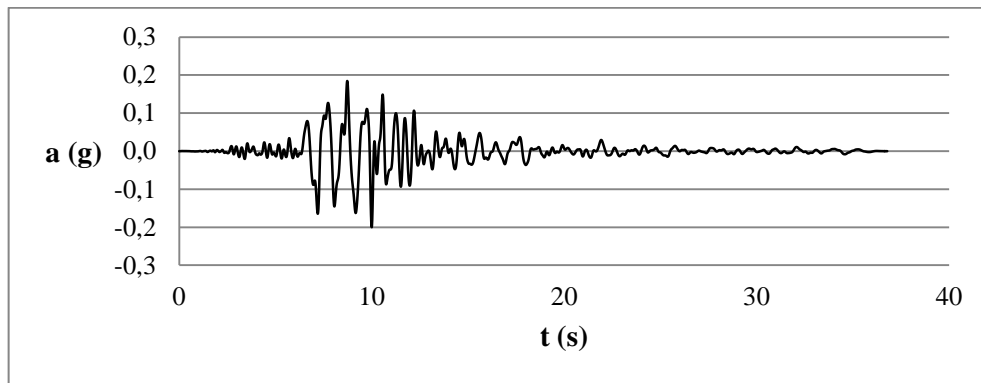


b. v-t plot

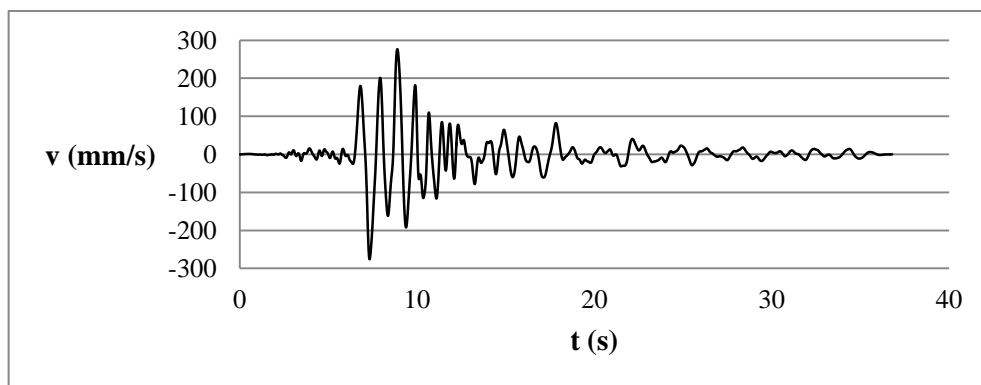


c. x-t plot

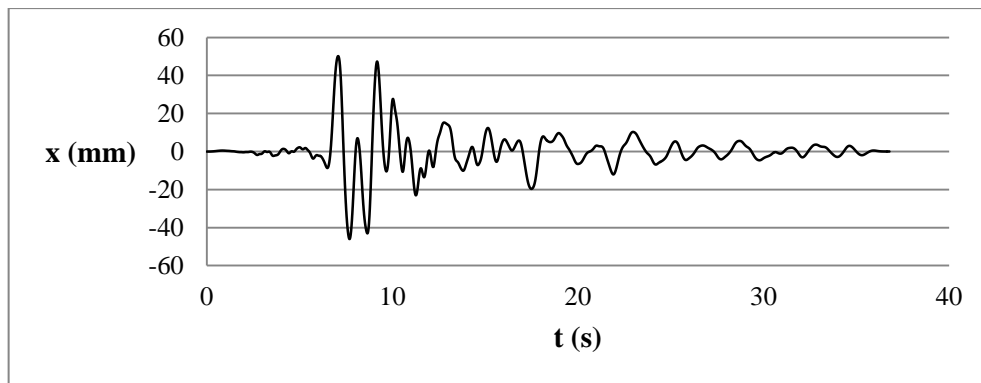
Fig. D.10 Time histories for R1_0.1 motion



a. a-t plot

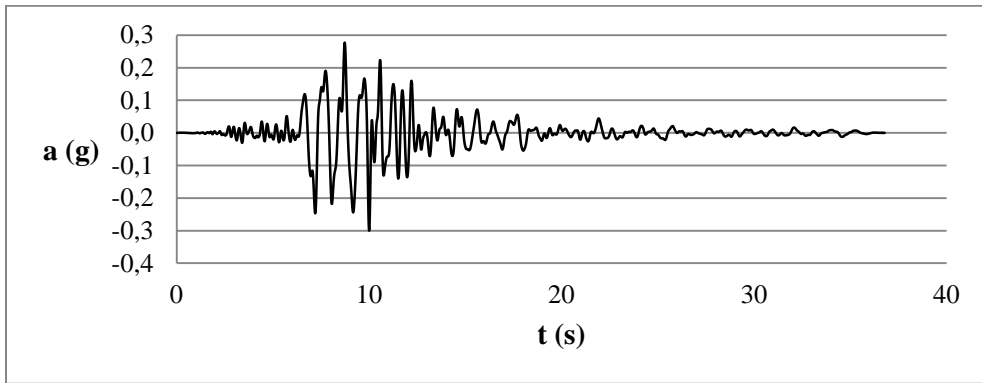


b. v-t plot

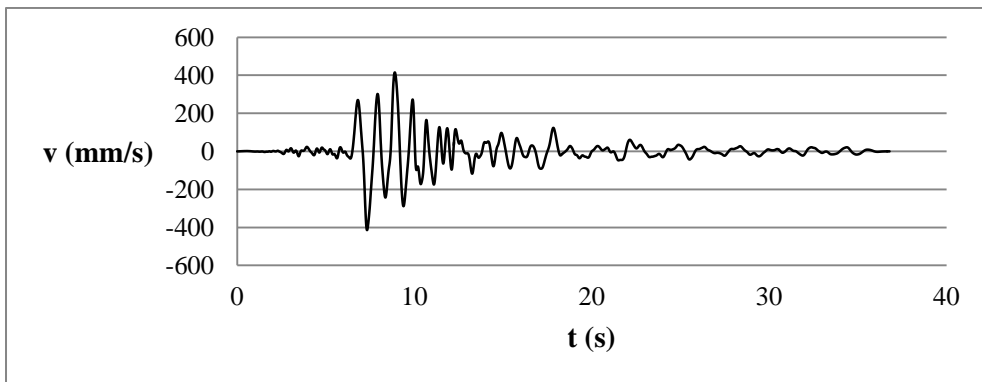


c. x-t plot

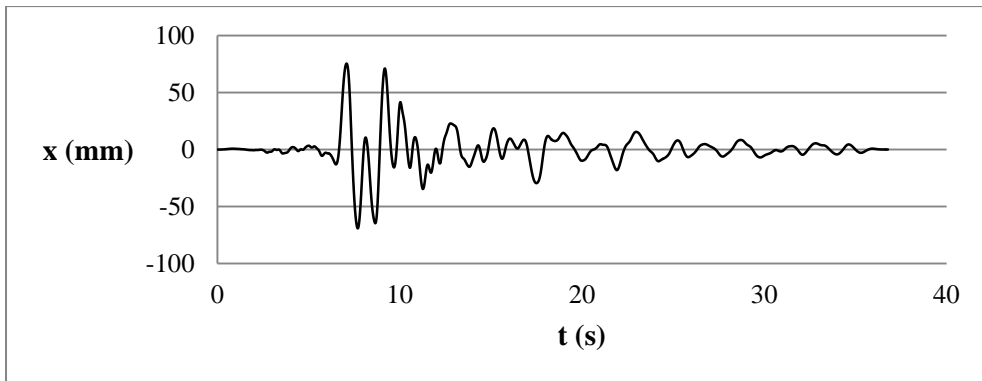
Fig. D.11 Time histories for R1_0.2 motion



a. a-t plot

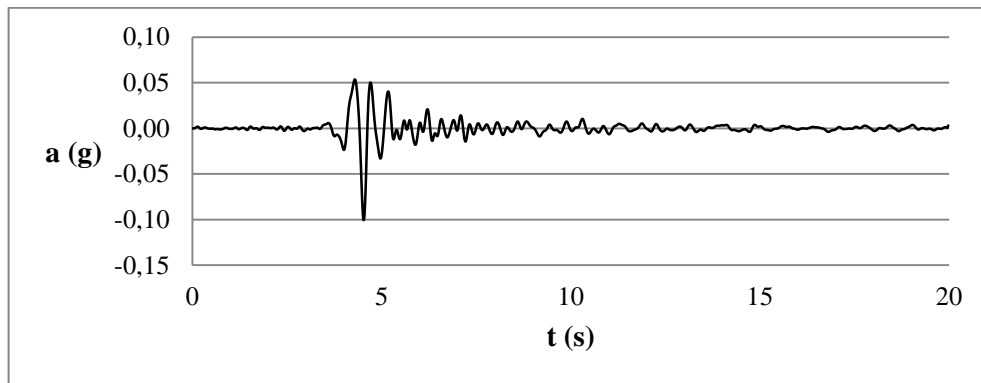


b. v-t plot

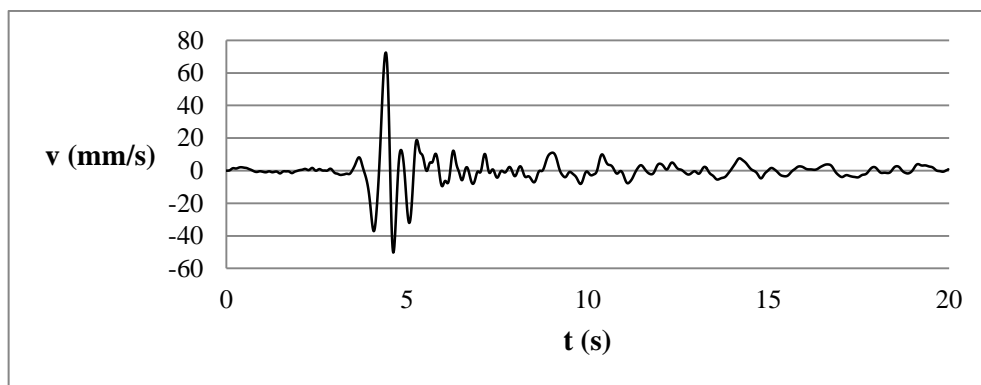


c. x-t plot

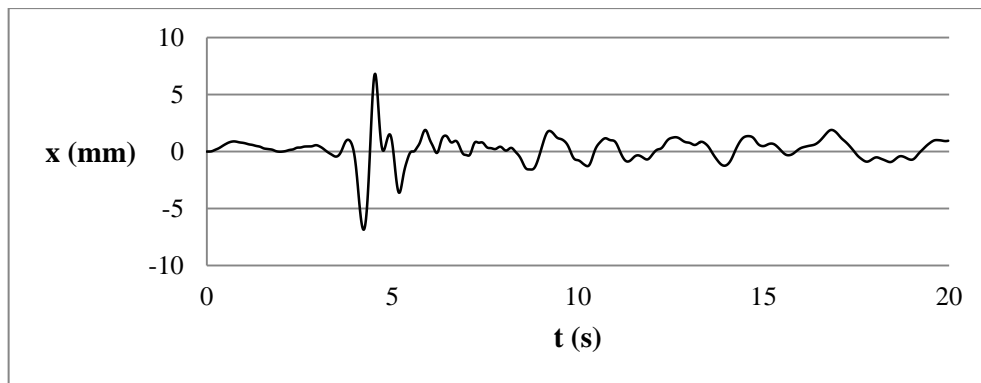
Fig. D.12 Time histories for R1_0.3 motion



a. a-t plot

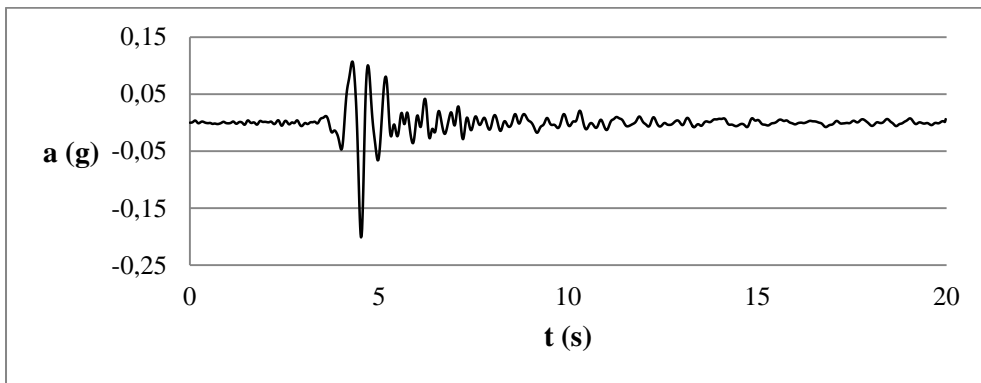


b. v-t plot

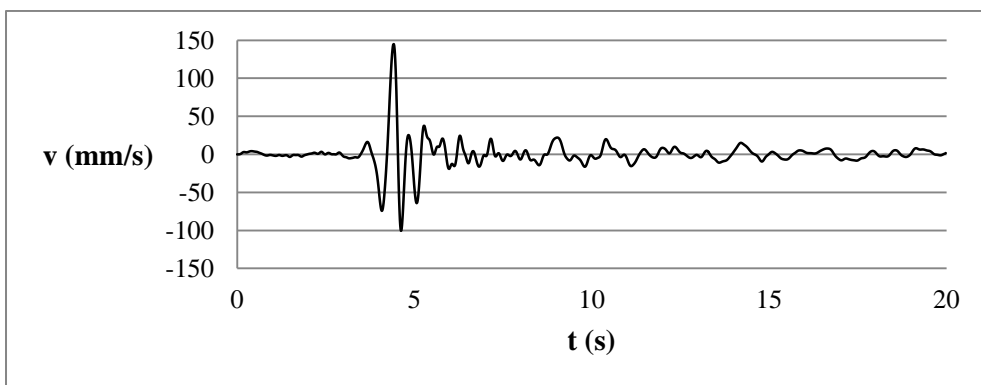


c. x-t plot

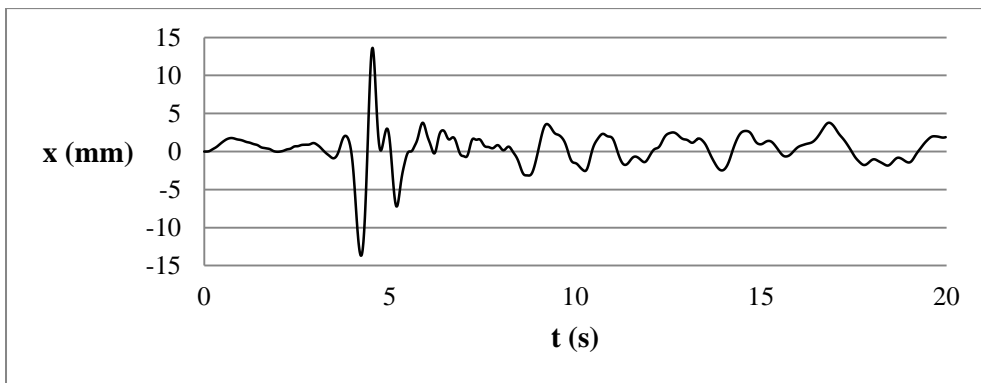
Fig. D.13 Time histories for R2_0.1 motion



a. a-t plot

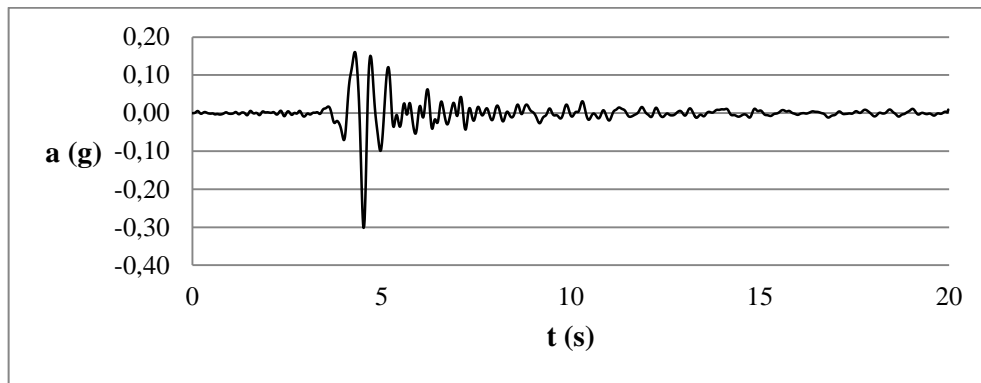


b. v-t plot

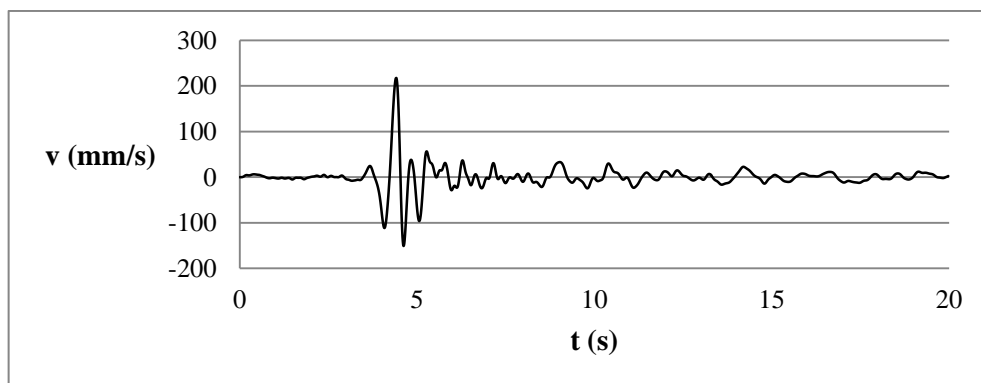


c. x-t plot

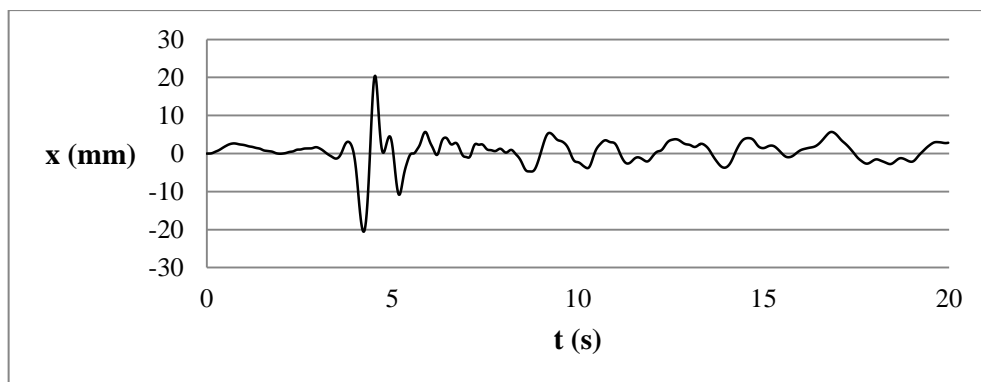
Fig. D.14 Time histories for R2_0.2 motion



a. a-t plot

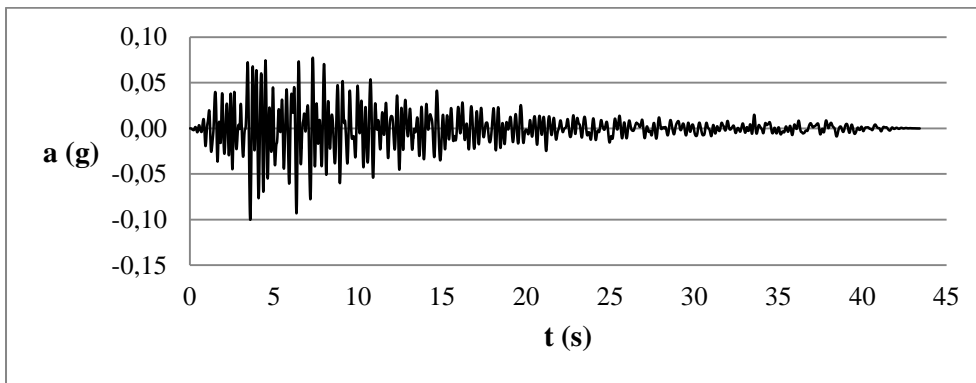


b. v-t plot

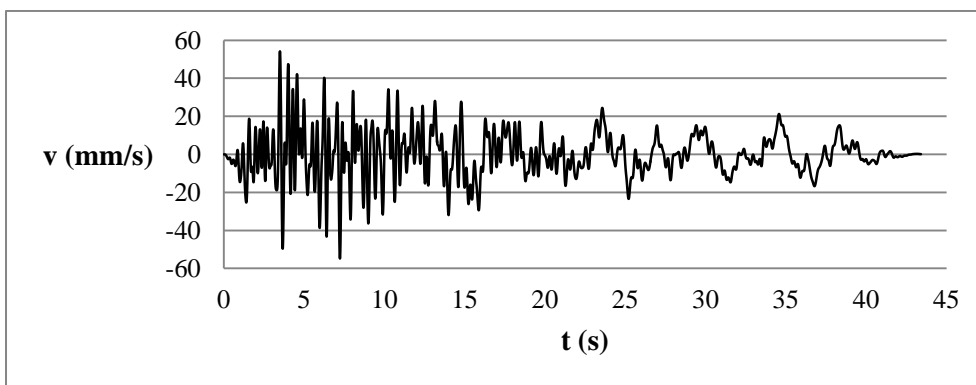


c. x-t plot

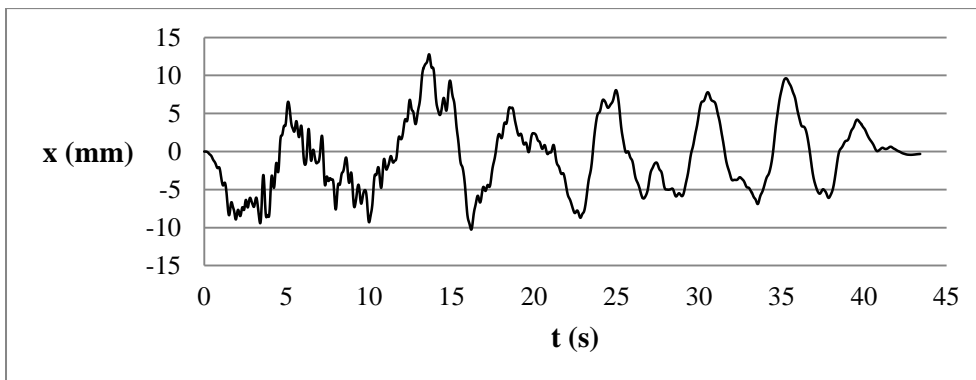
Fig. D.15 Time histories for R2_0.3 motion



a. a-t plot

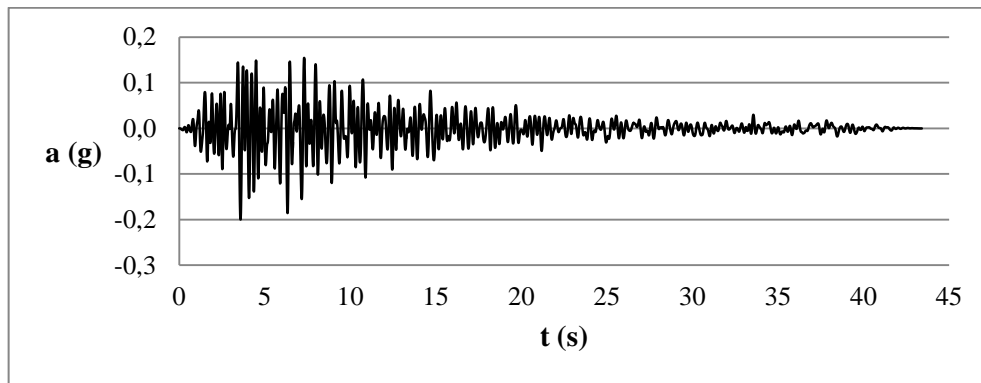


b. v-t plot

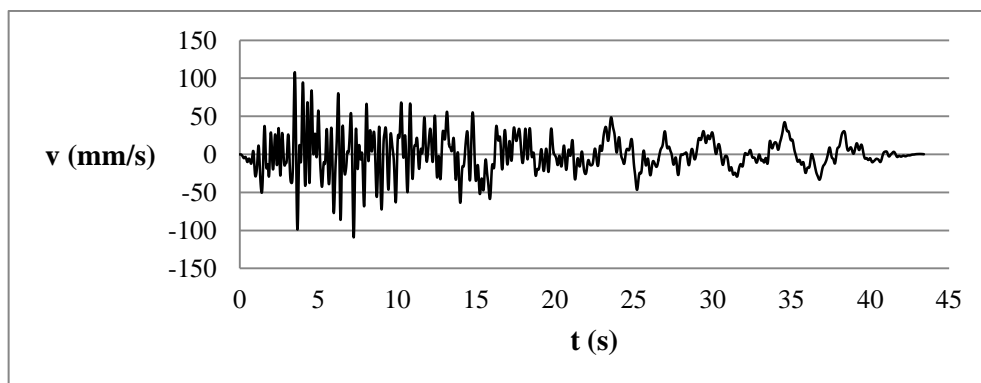


c. x-t plot

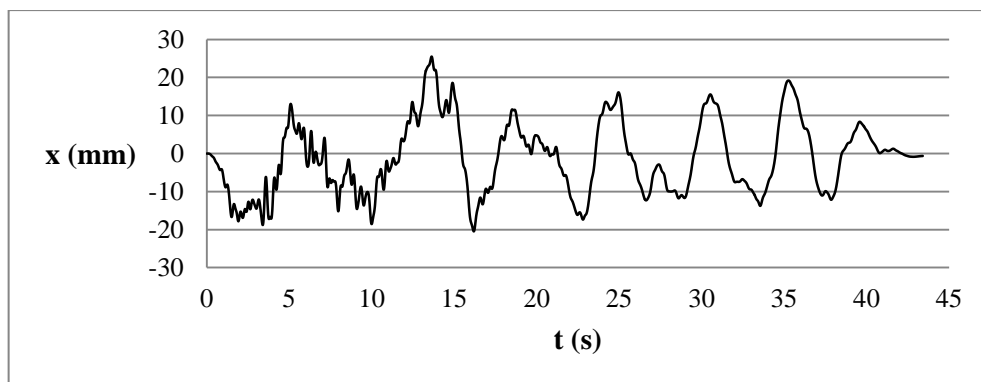
Fig. D.16 Time histories for R3_0.1 motion



a. a-t plot

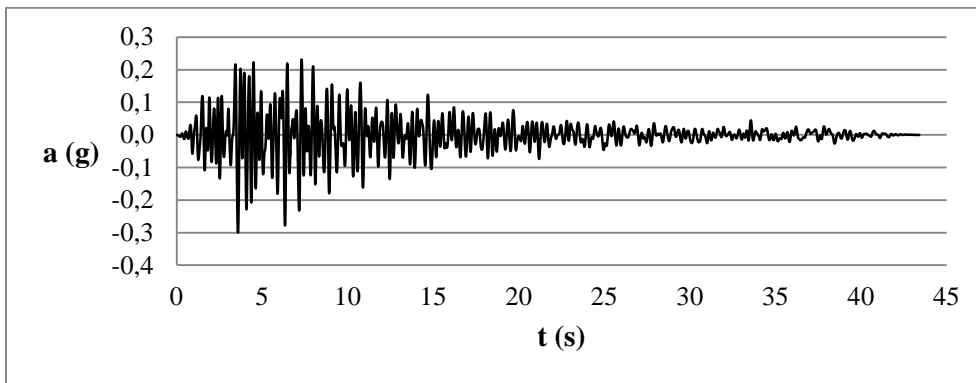


b. v-t plot

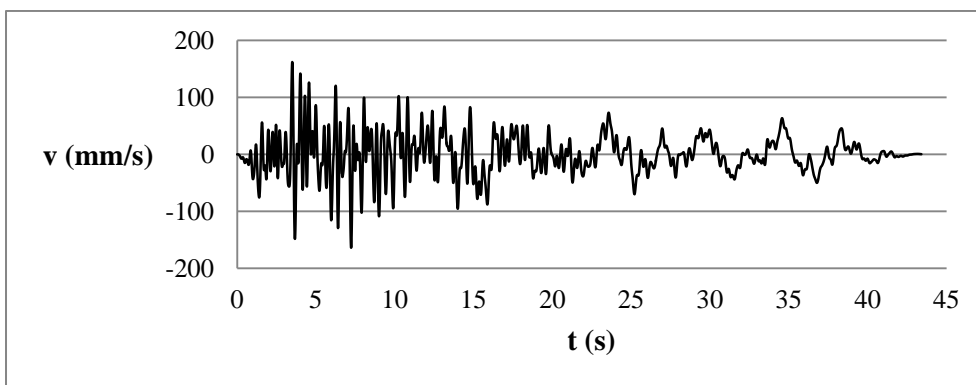


c. x-t plot

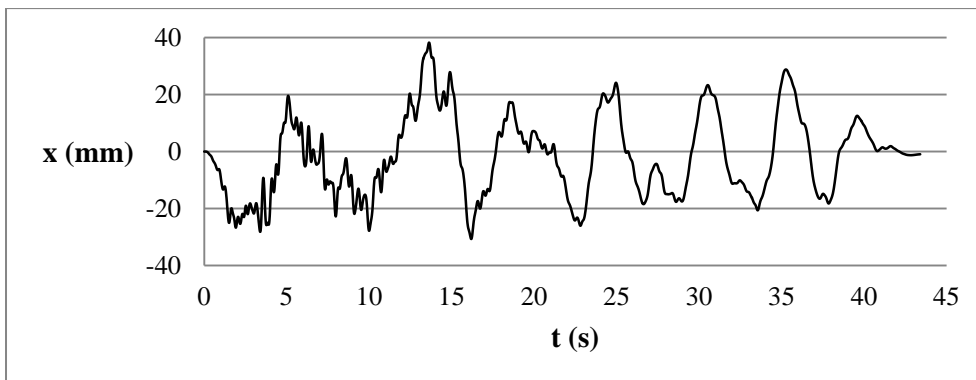
Fig. D.17 Time histories for R3_0.2 motion



a. a-t plot



b. v-t plot

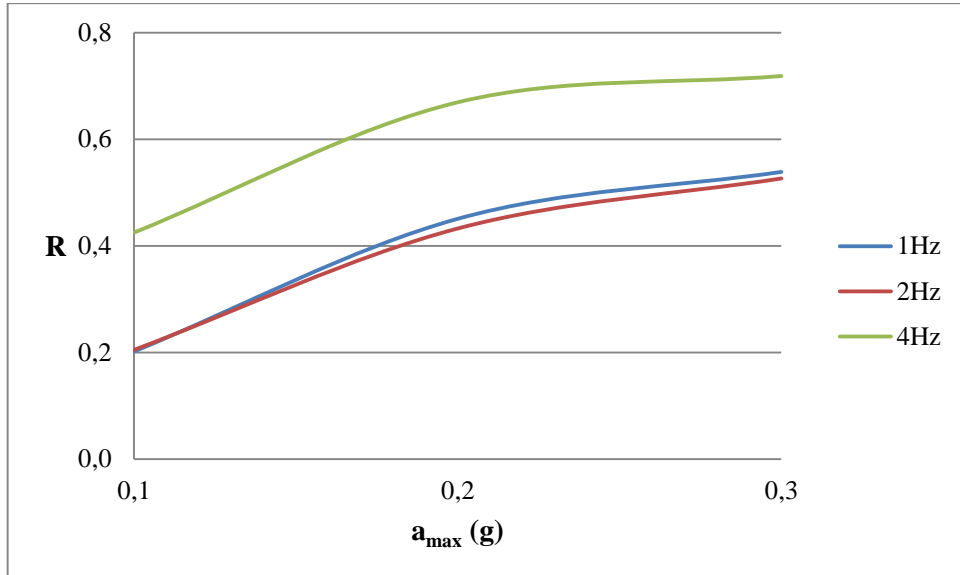


c. x-t plot

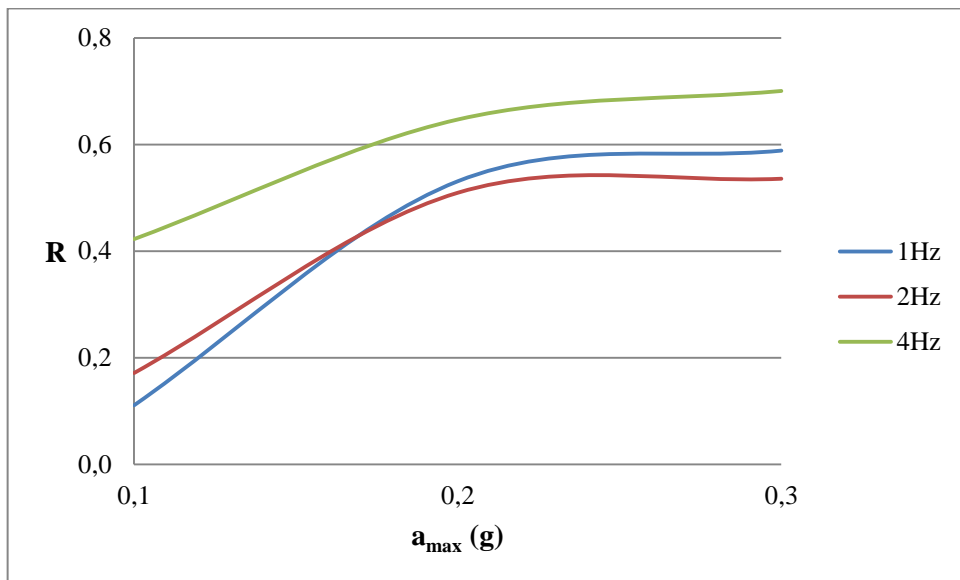
Fig. D.18 Time histories for R3_0.3 motion

APPENDIX E

REDUCTIONS IN MID-STOREY ACCELERATIONS
FOR 3-STOREY MODEL

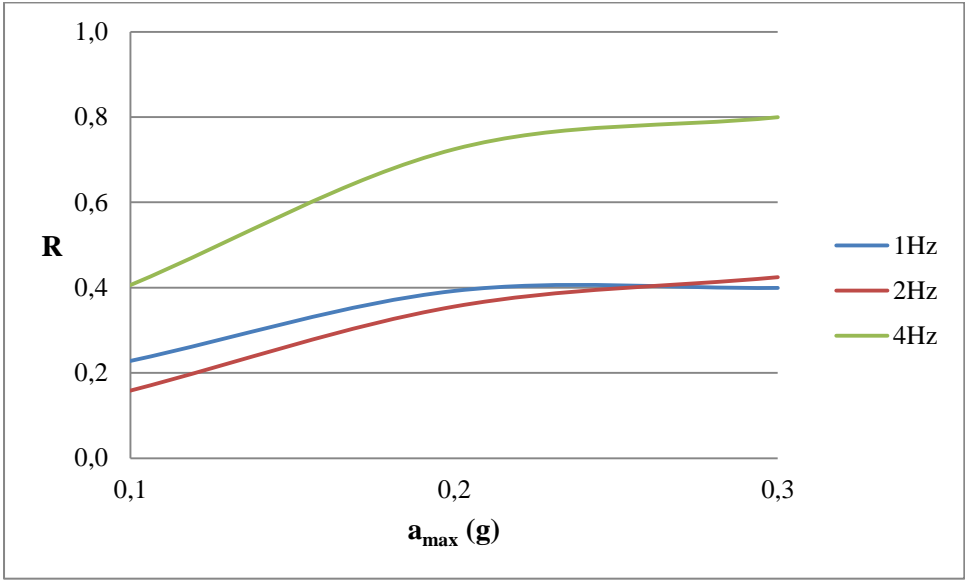


a. "R" for second storey

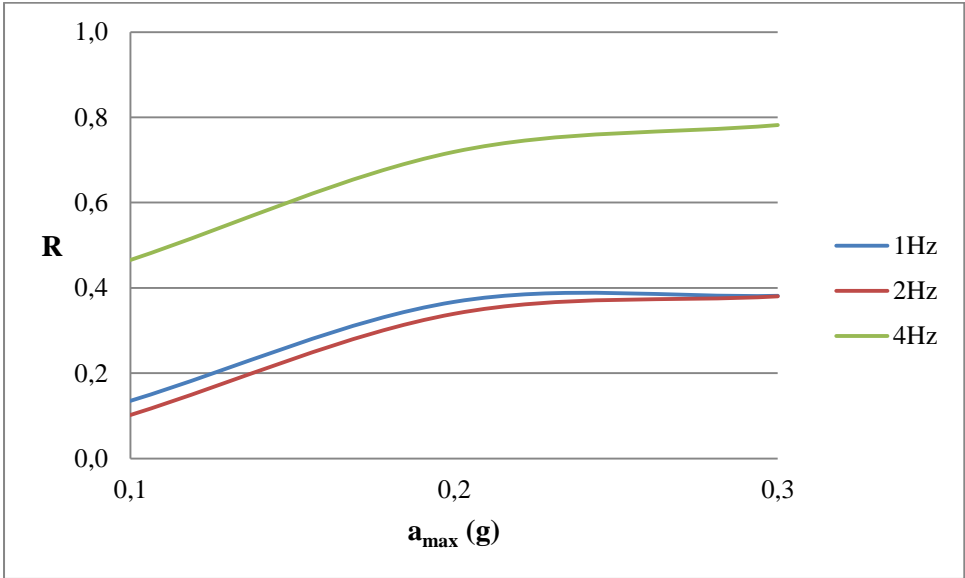


b. "R" for third storey

Fig. E.1 Acceleration reductions (R) in mid-storeys for S1, S2 and S3 motions



a. "R" for second storey

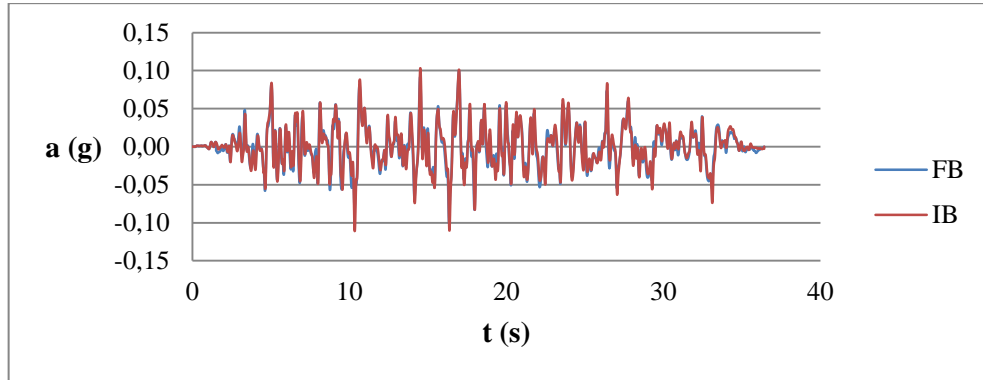


b. "R" for third storey

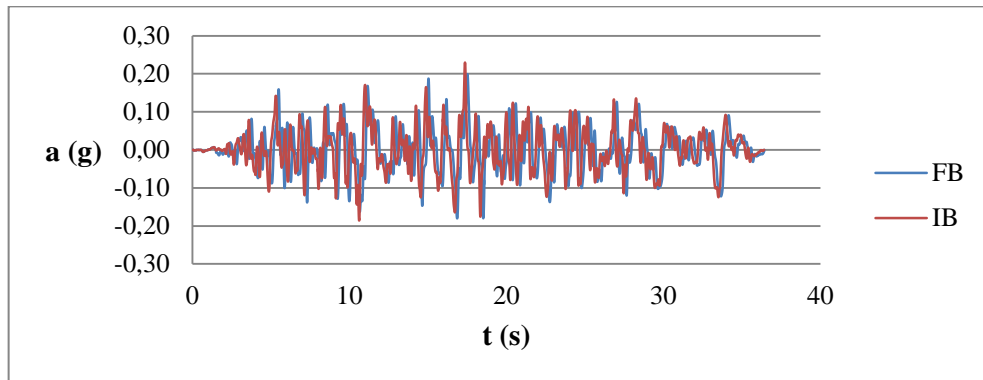
Fig. E.2 Acceleraton reductions (R) in mid-storeys for R1, R2 and R3 motions

APPENDIX F

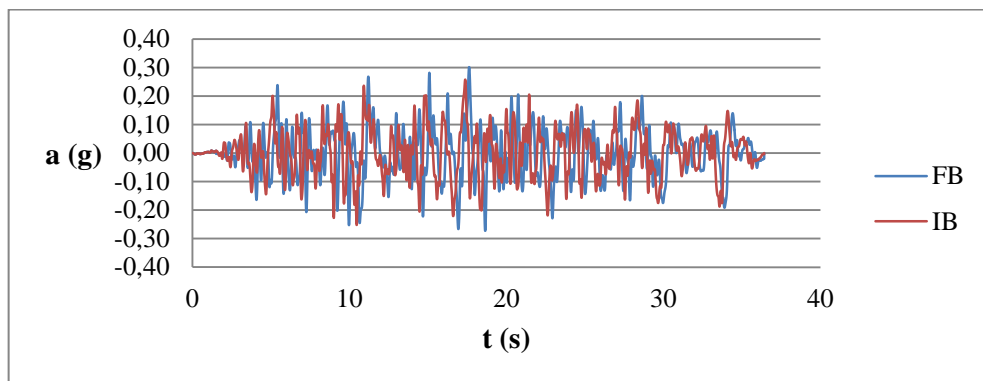
ACCELERATION TIME HISTORIES FOR BASE OF 3-STOREY MODEL
FOR “FB” AND “IB” CONDITIONS



a. $a_{\max} = 0.1g$

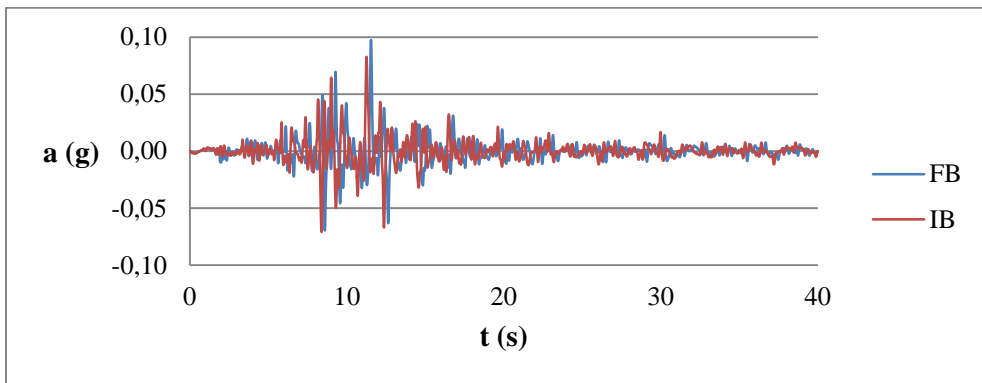


b. $a_{\max} = 0.2g$

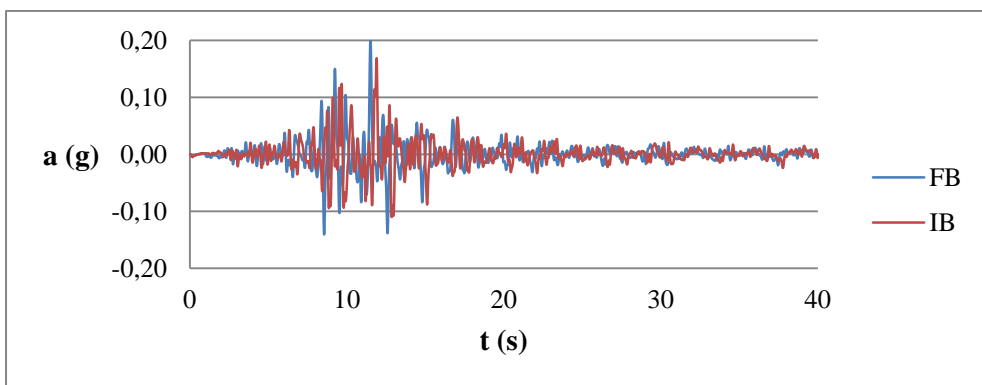


c. $a_{\max} = 0.3g$

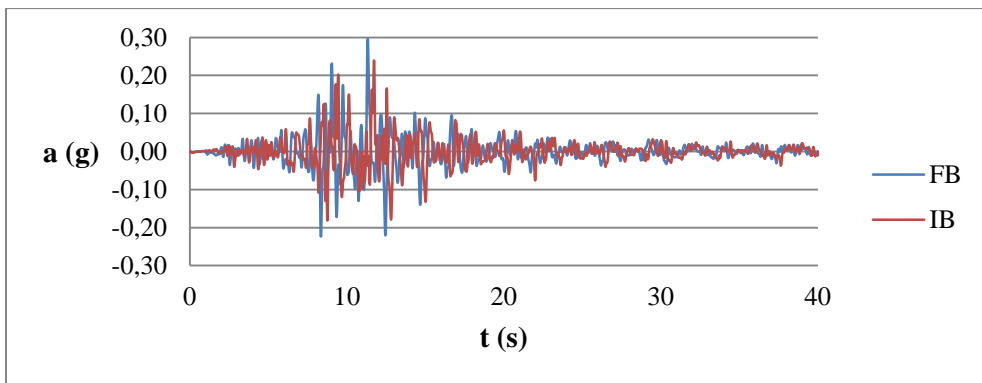
Fig. F.1 Acceleration-time histories for tests under S1 motion



a. $a_{\max} = 0.1g$

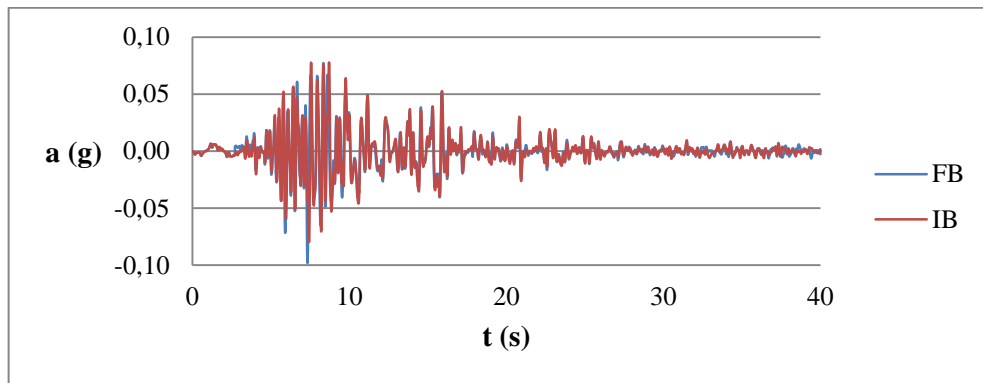


b. $a_{\max} = 0.2g$

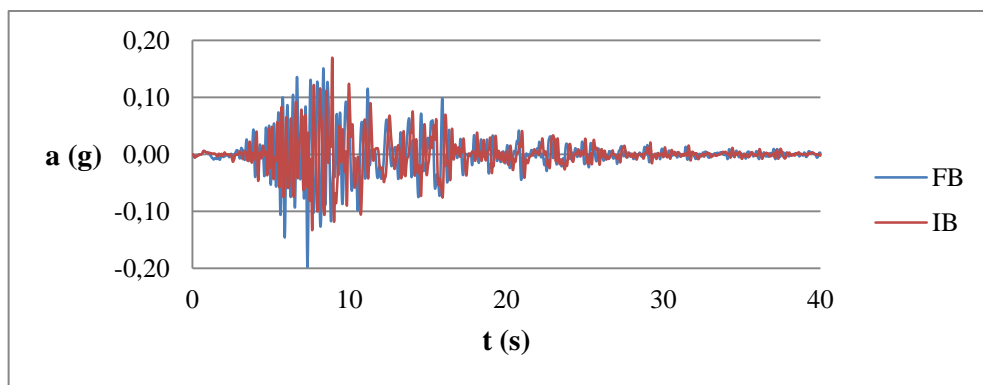


c. $a_{\max} = 0.3g$

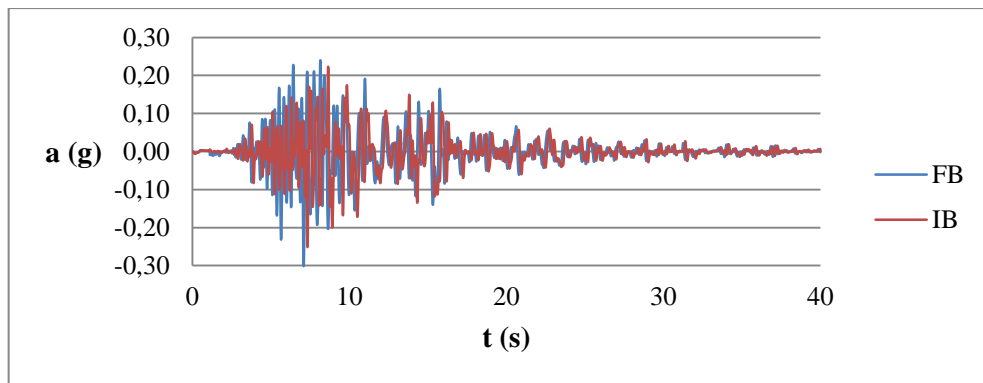
Fig. F.2 Acceleration-time histories for tests under S2 motion



a. $a_{\max} = 0.1g$

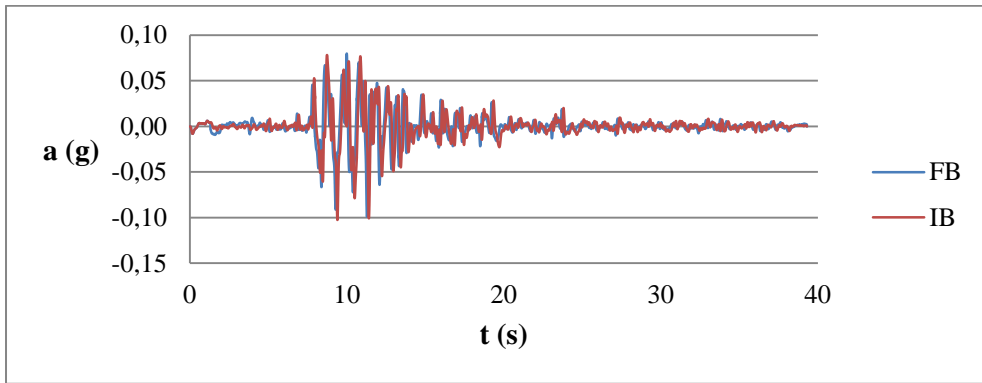


b. $a_{\max} = 0.2g$

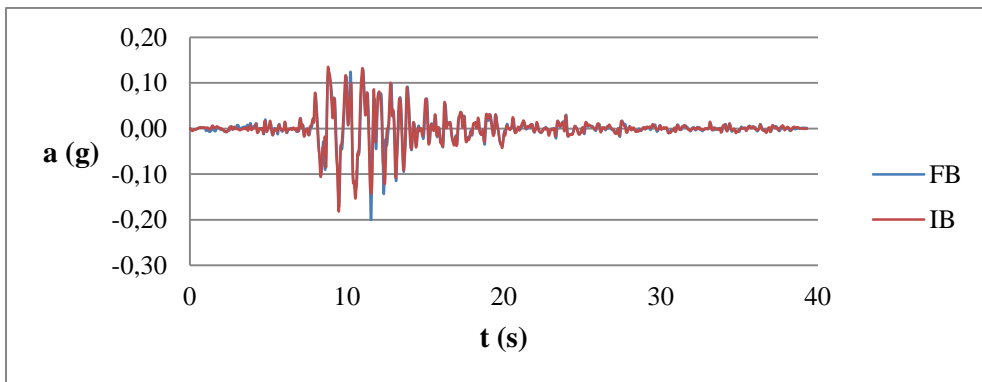


c. $a_{\max} = 0.3g$

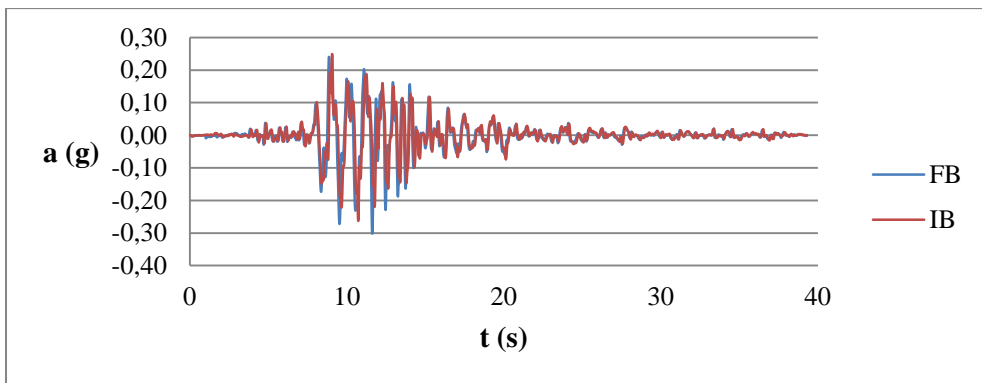
Fig. F.3 Acceleration-time histories for tests under S3 motion



a. $a_{\max} = 0.1g$

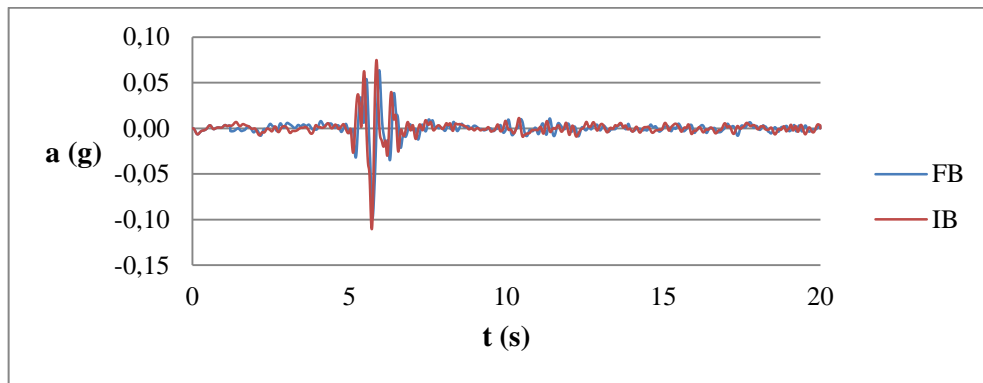


b. $a_{\max} = 0.2g$

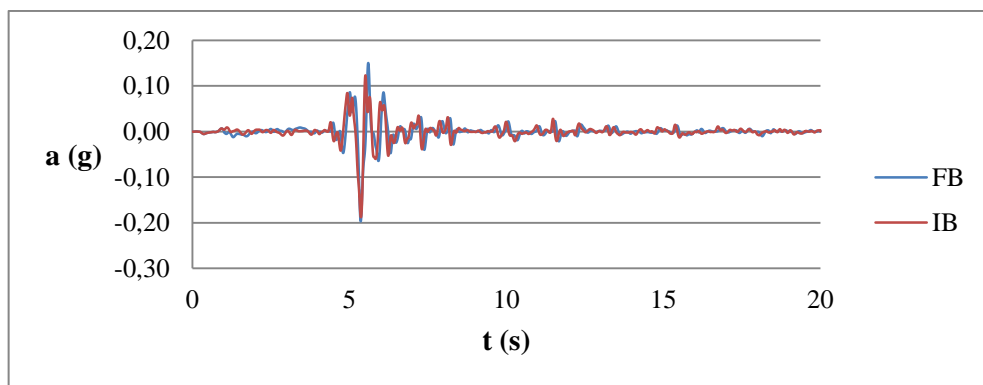


c. $a_{\max} = 0.3g$

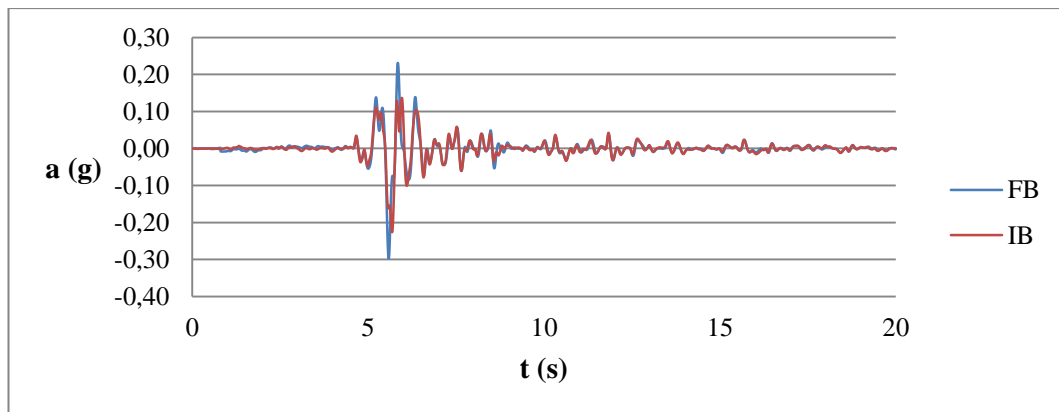
Fig. F.4 Acceleration-time histories for tests under R1 motion



a. $a_{\max} = 0.1g$

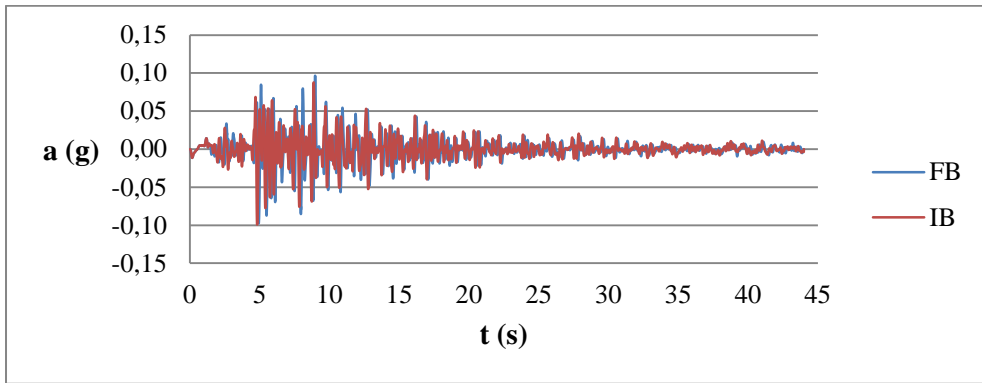


b. $a_{\max} = 0.2g$

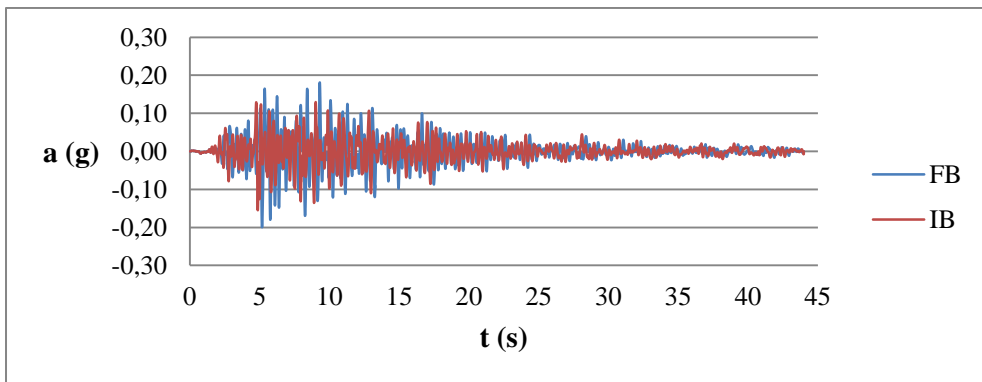


c. $a_{\max} = 0.3g$

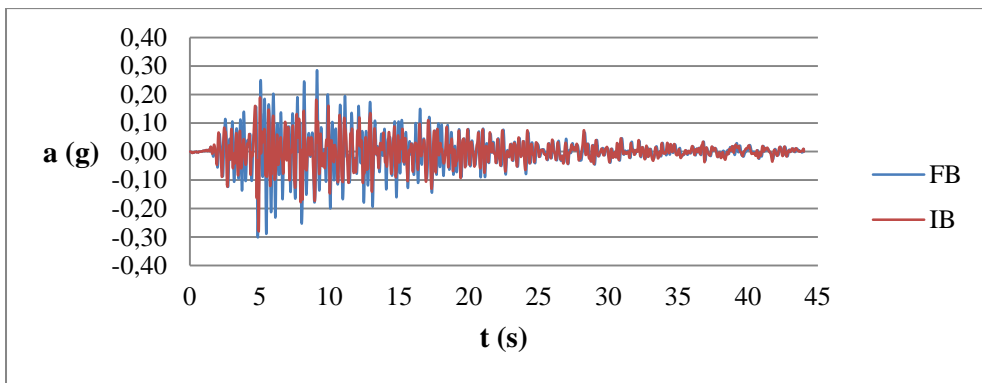
Fig. F.5 Acceleration-time histories for tests under R2 motion



a. $a_{\max} = 0.1g$



b. $a_{\max} = 0.2g$



c. $a_{\max} = 0.3g$

Fig. F.6 Acceleration-time histories for tests under R3 motion

APPENDIX G

RESPONSE SPECTRA FOR 3-STOUREY MODEL UNDER D = 5% DAMPING

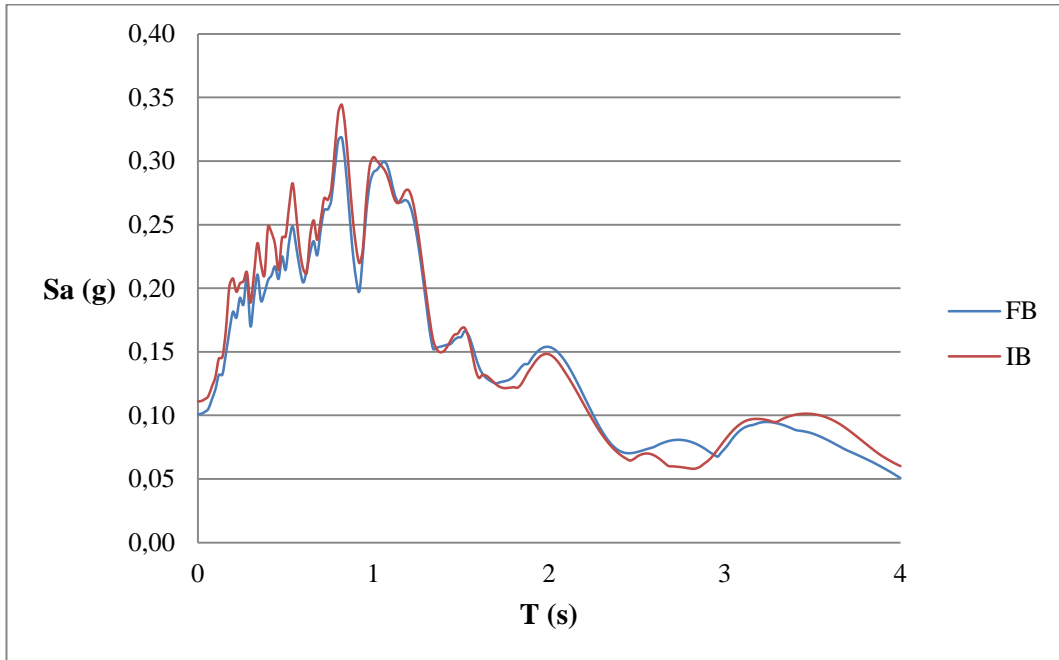


Fig. G.1 Response spectra for S1_0.1 motion (D = 5%)

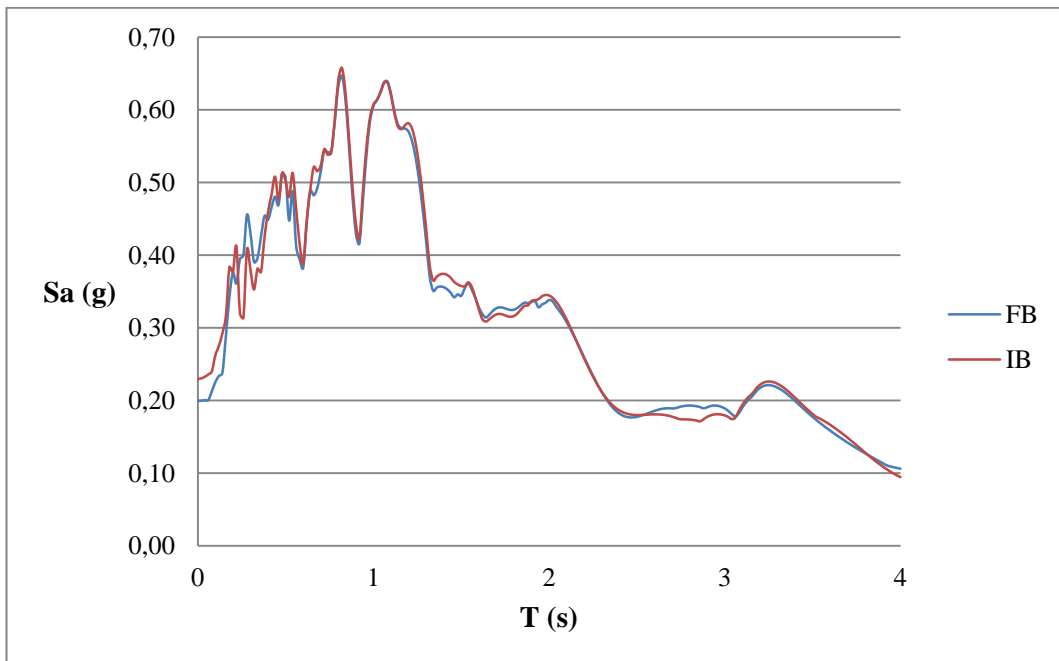


Fig. G.2 Response spectra for S1_0.2 motion (D = 5%)

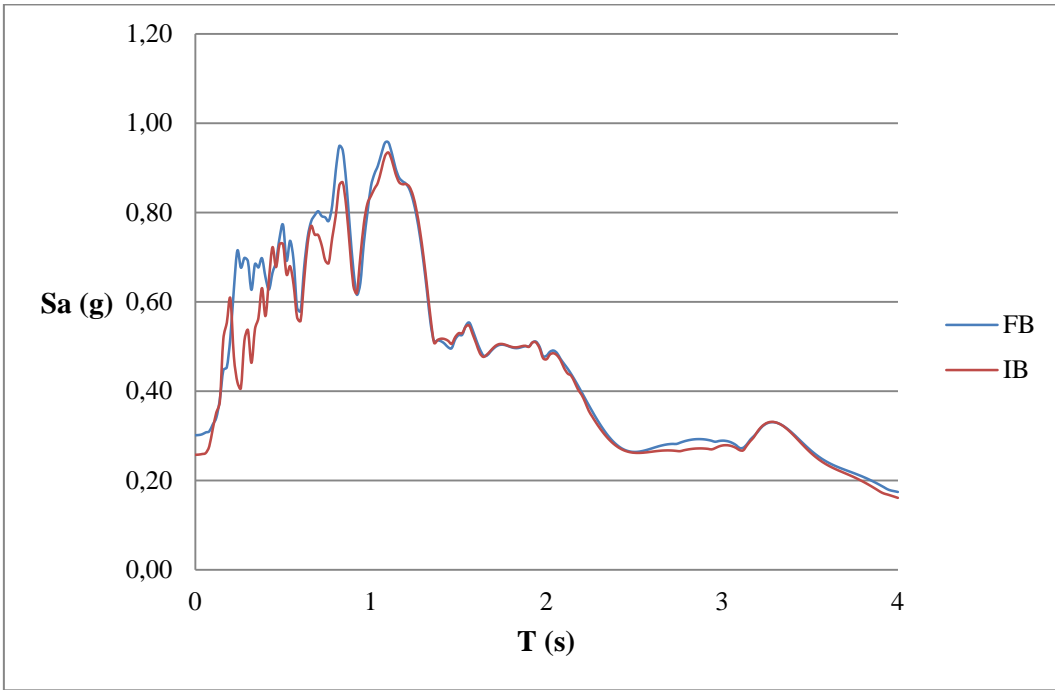


Fig. G.3 Response spectra for S1_0.3 motion (D = 5%)

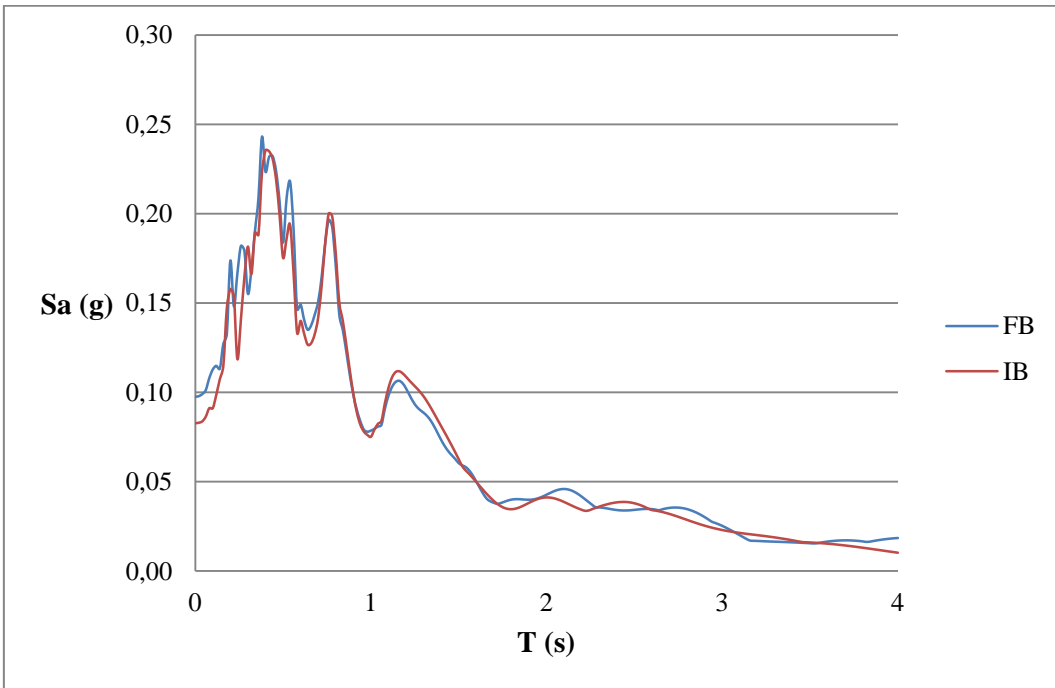


Fig. G.4 Response spectra for S2_0.1 motion (D = 5%)

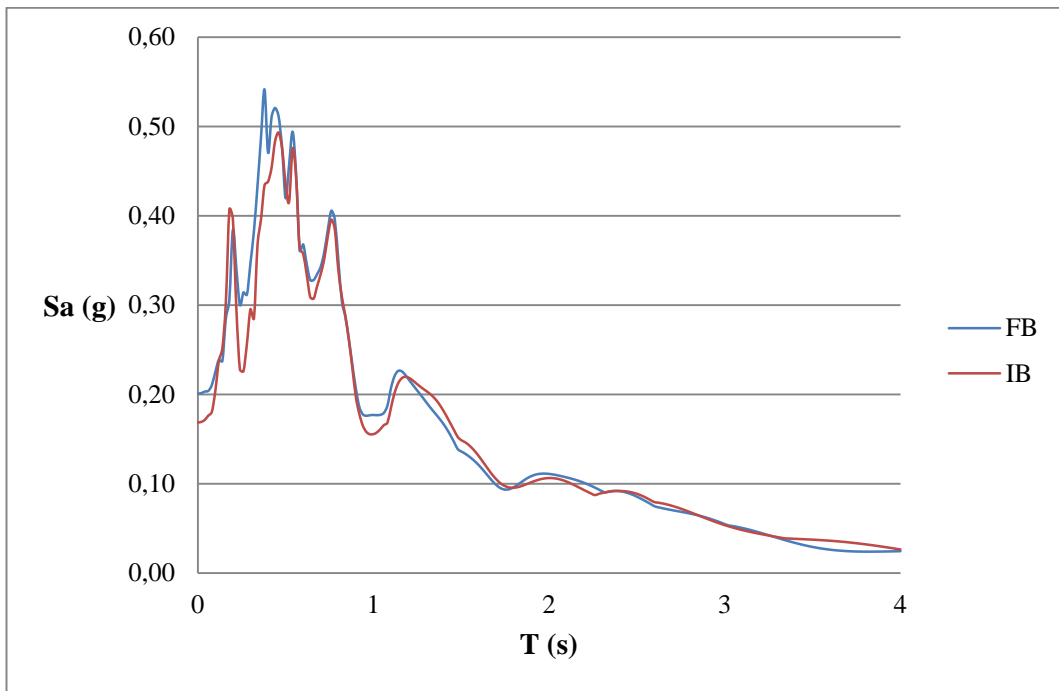


Fig. G.5 Response spectra for S2_0.2 motion (D = 5%)

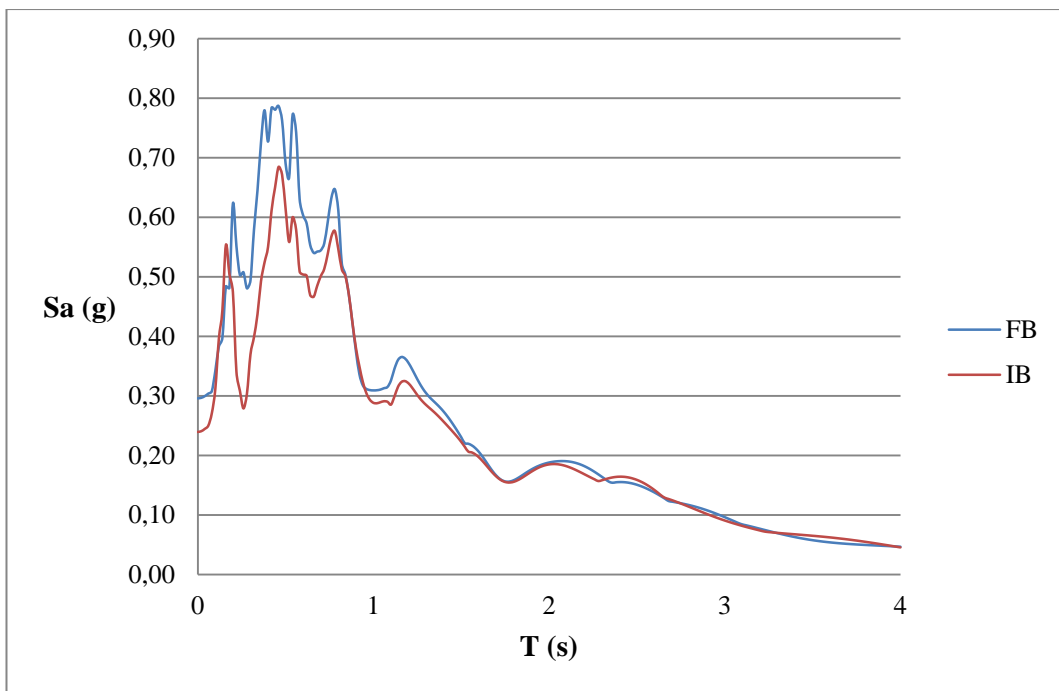


Fig. G.6 Response spectra for S2_0.3 motion (D = 5%)

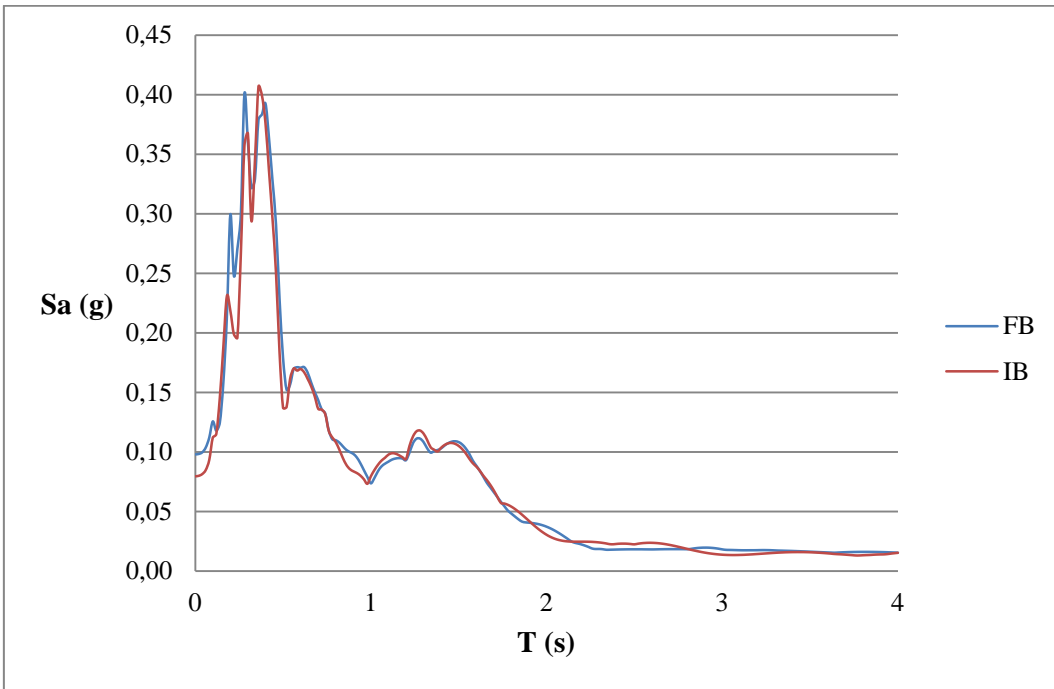


Fig. G.7 Response spectra for S3_0.1 motion (D = 5%)

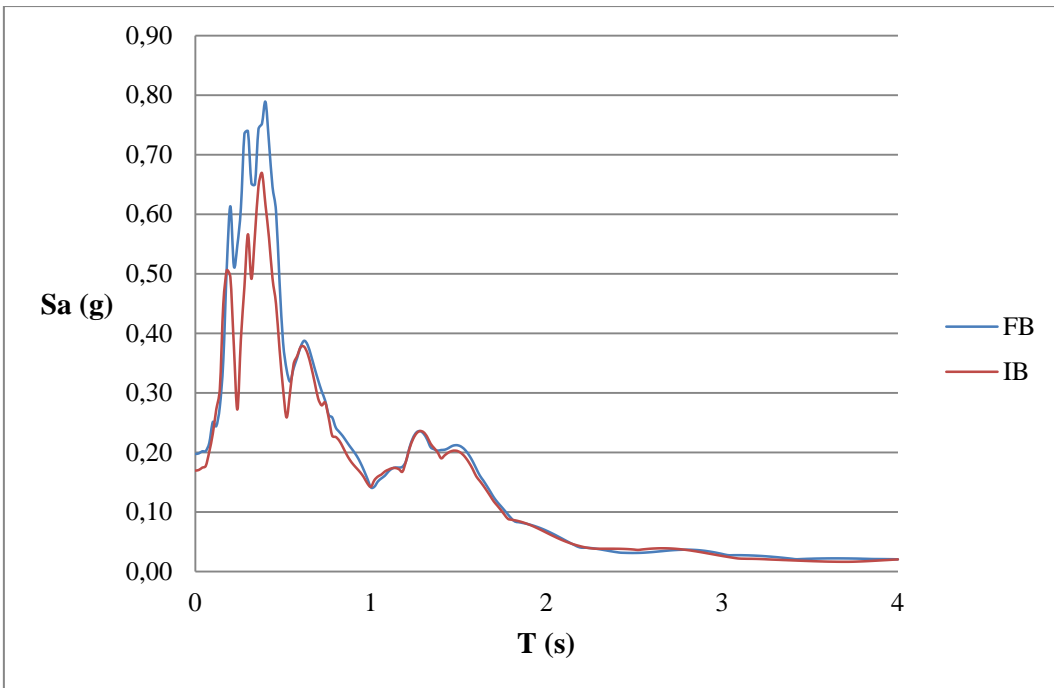


Fig. G.8 Response spectra for S3_0.2 motion (D = 5%)

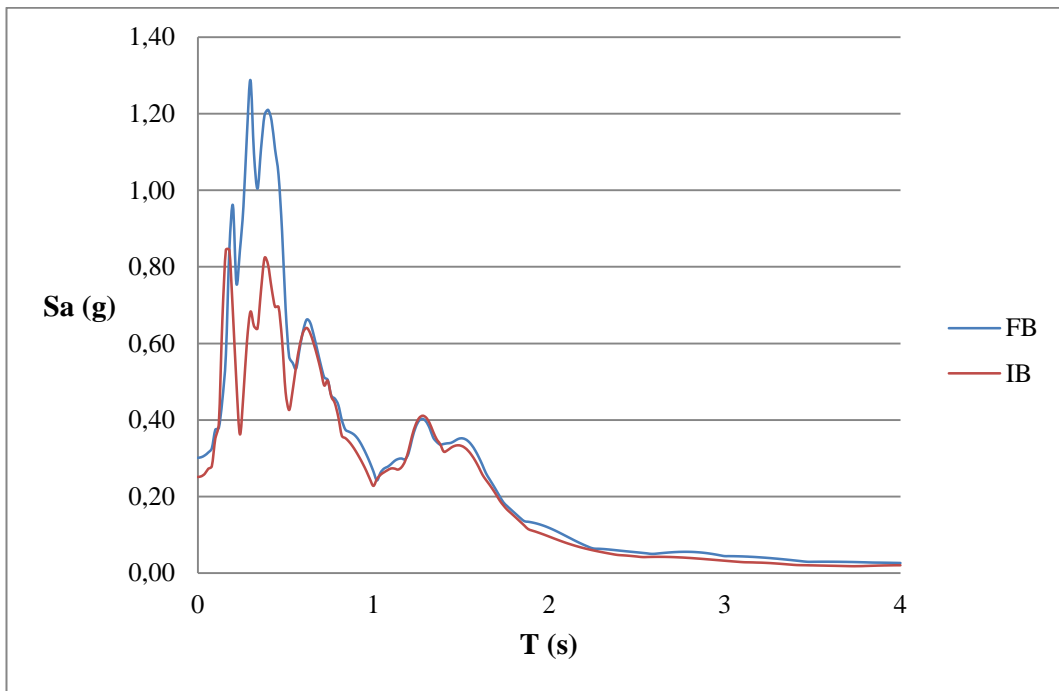


Fig. G.9 Response spectra for S3_0.3 motion (D = 5%)

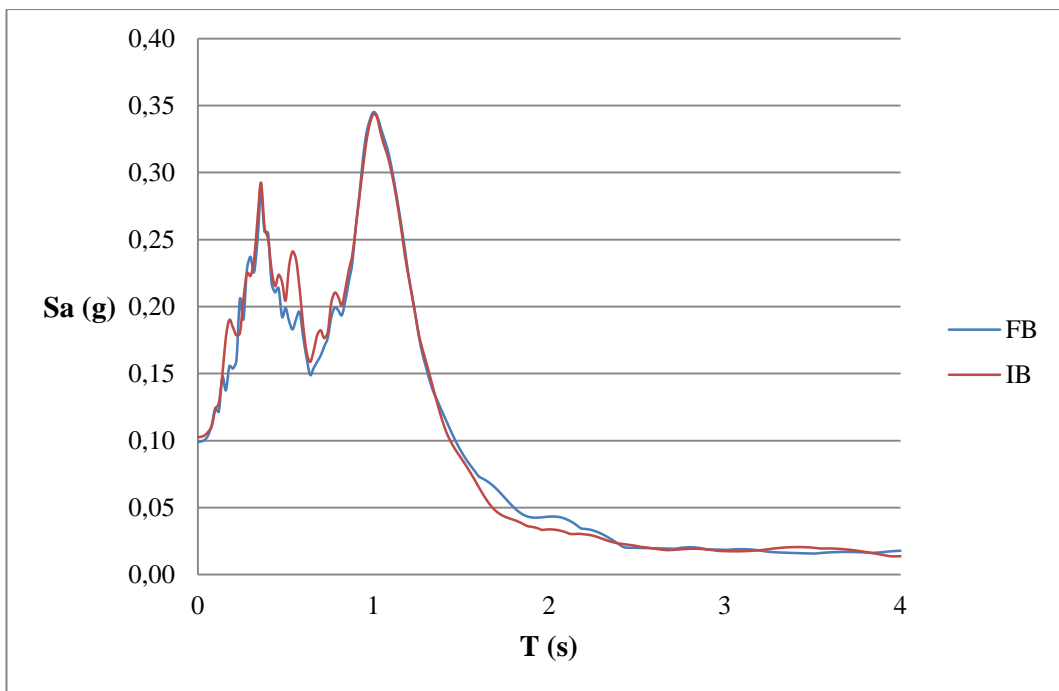


Fig. G.10 Response spectra for R1_0.1 motion (D = 5%)

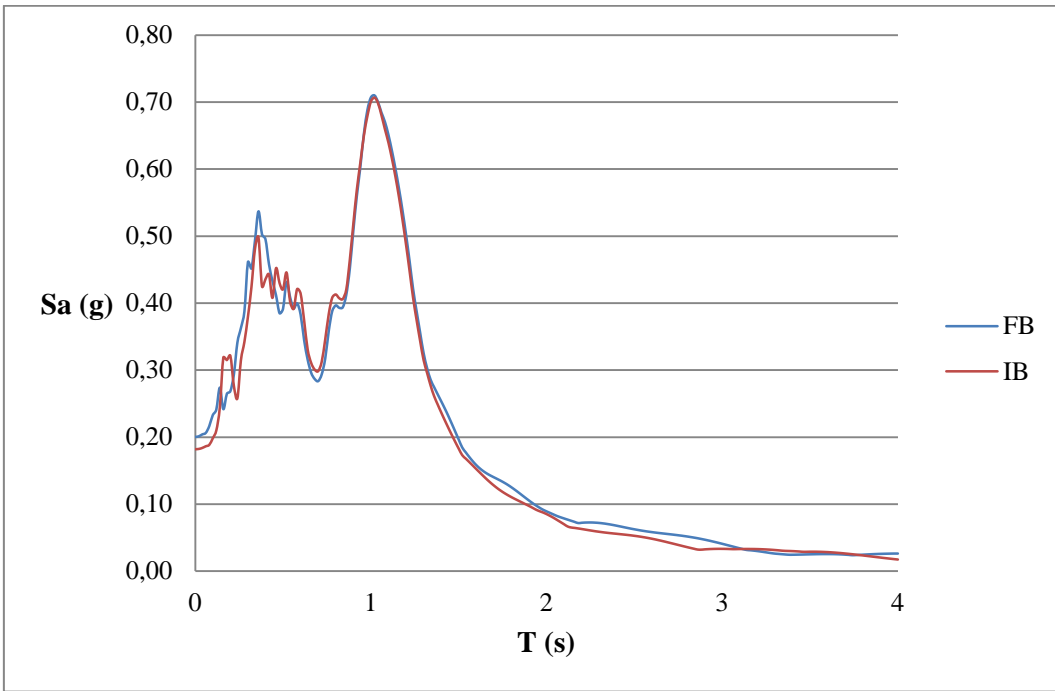


Fig. G.11 Response spectra for R1_0.2 motion (D = 5%)

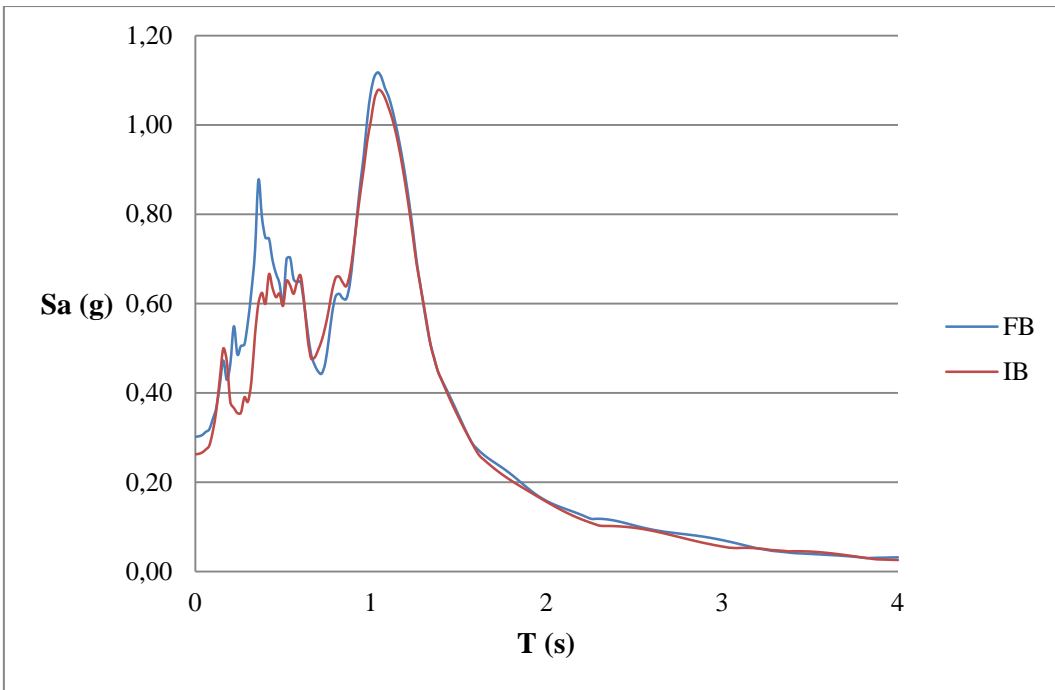


Fig. G.12 Response spectra for R1_0.3 motion (D = 5%)

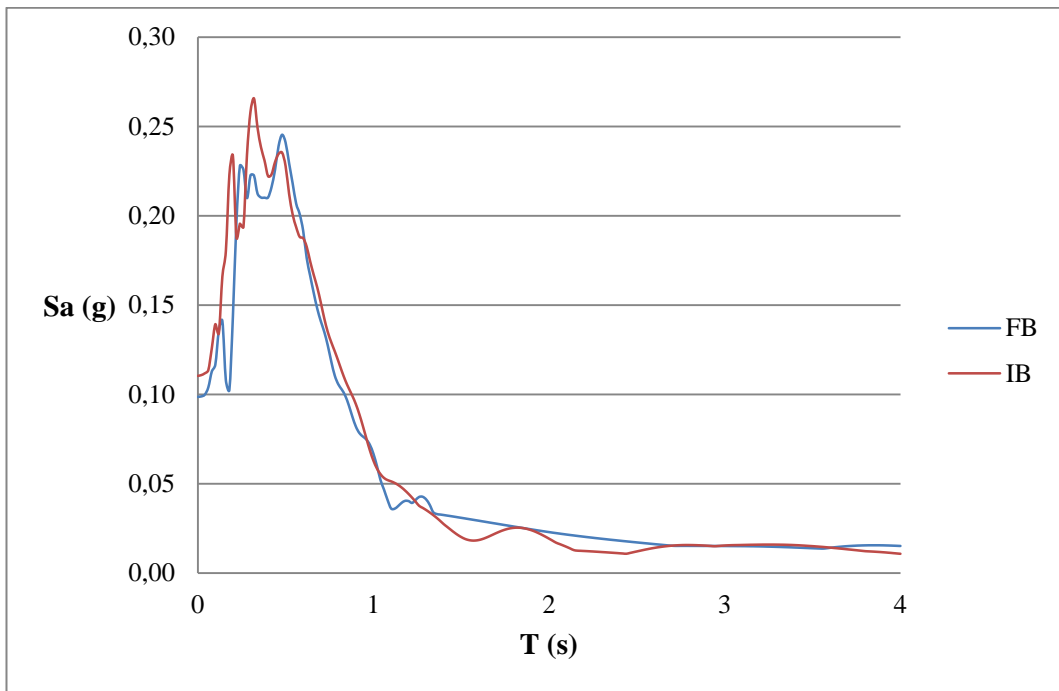


Fig. G.13 Response spectra for R2_0.1 motion (D = 5%)

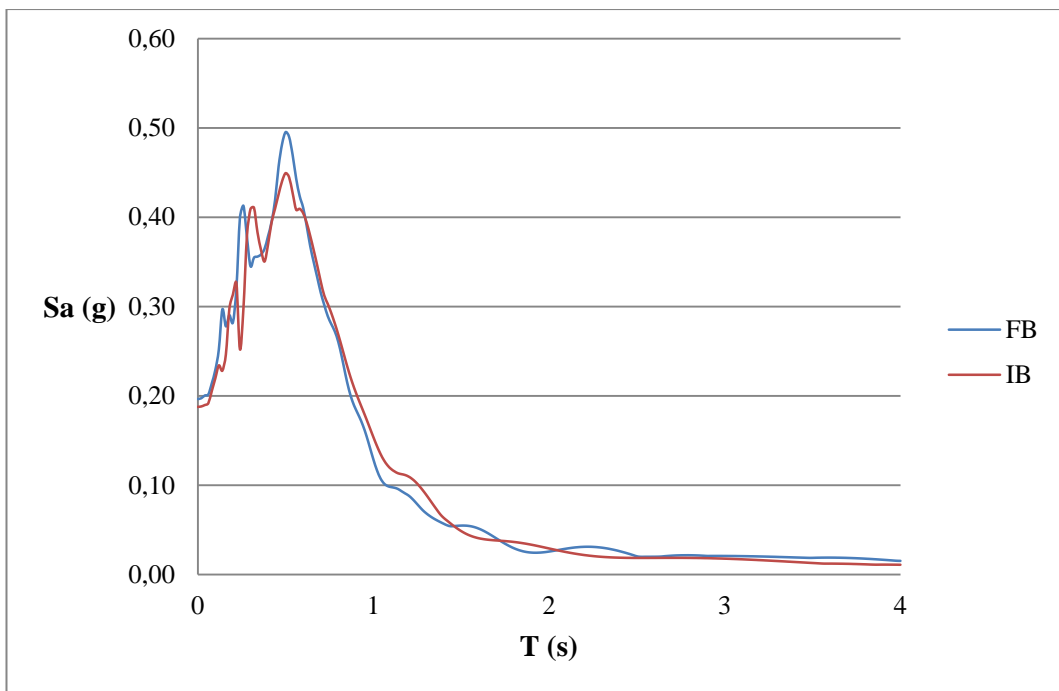


Fig. G.14 Response spectra for R2_0.2 motion (D = 5%)

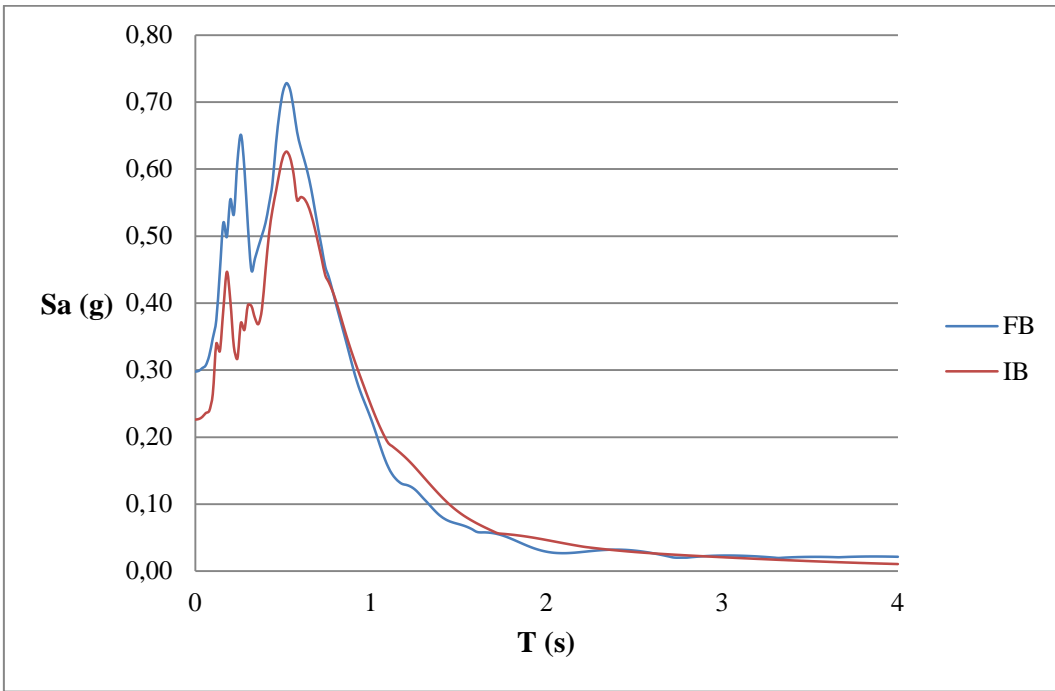


Fig. G.15 Response spectra for R2_0.3 motion (D = 5%)

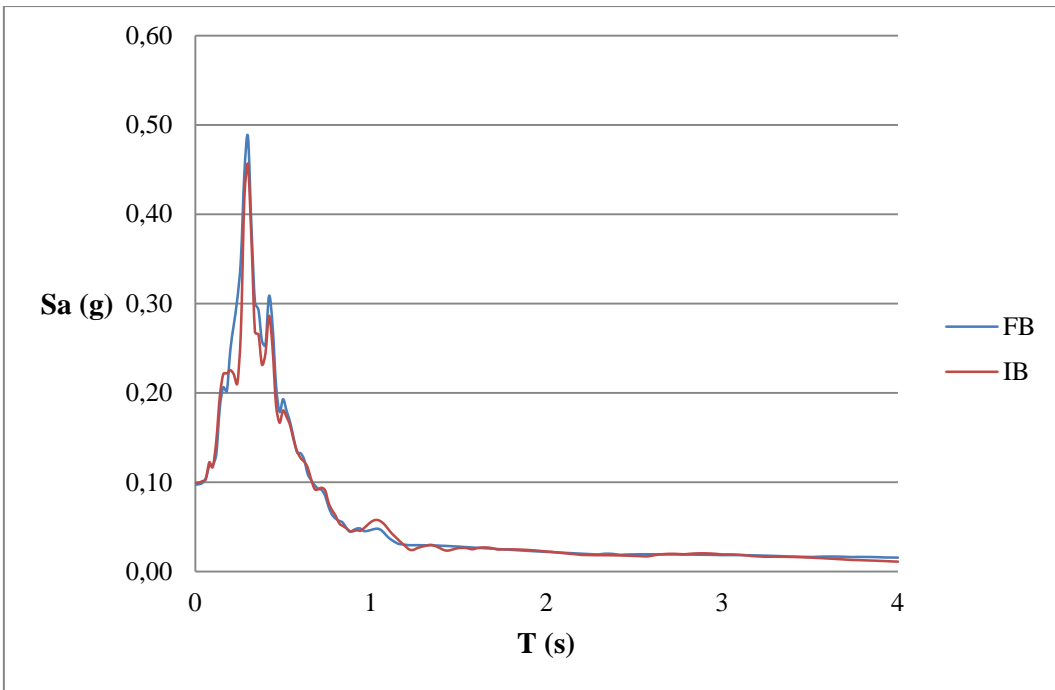


Fig. G.16 Response spectra for R3_0.1 motion (D = 5%)

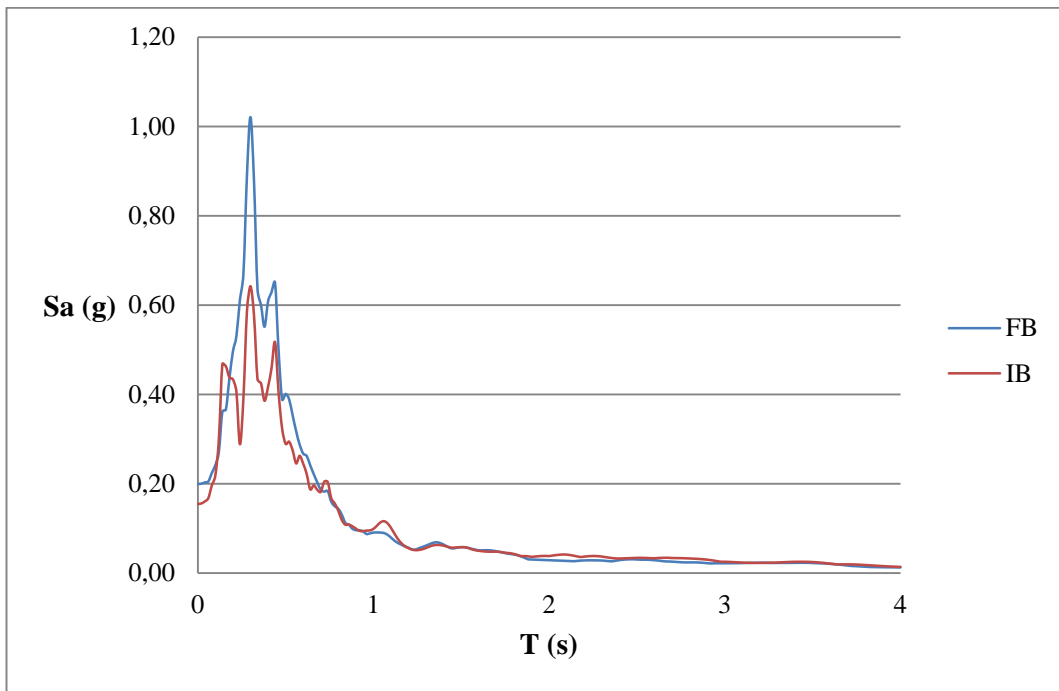


Fig. G.17 Response spectra for R3_0.2 motion (D = 5%)

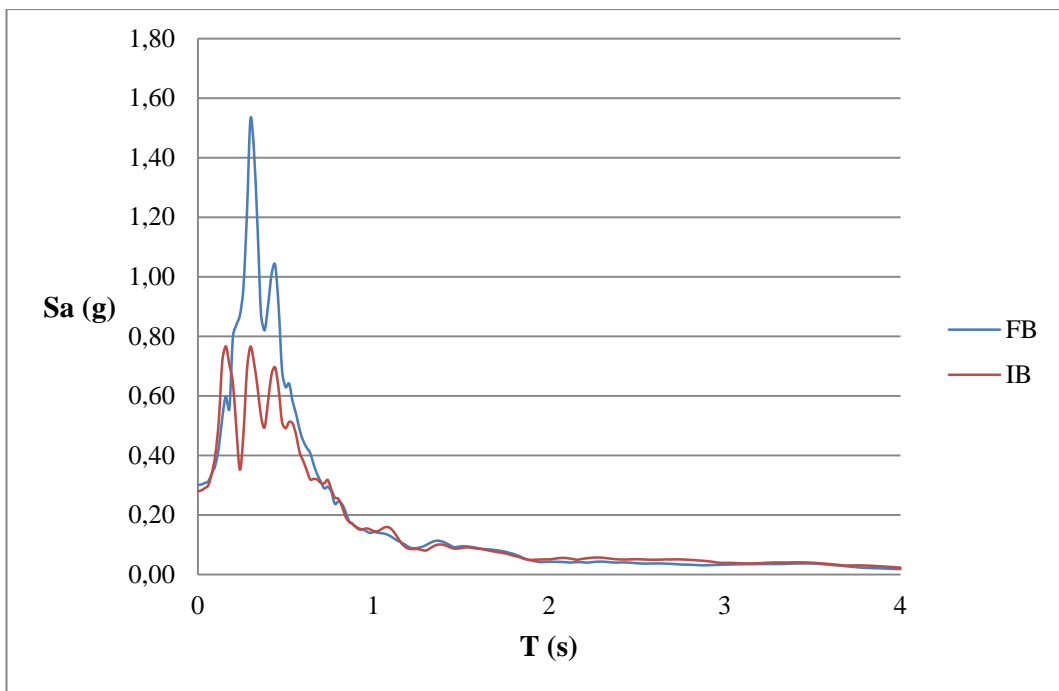
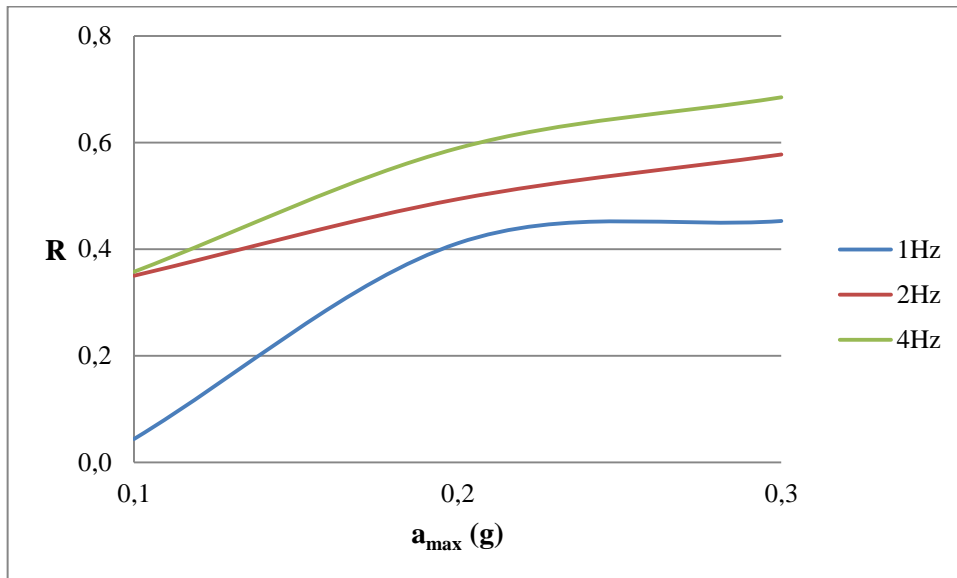


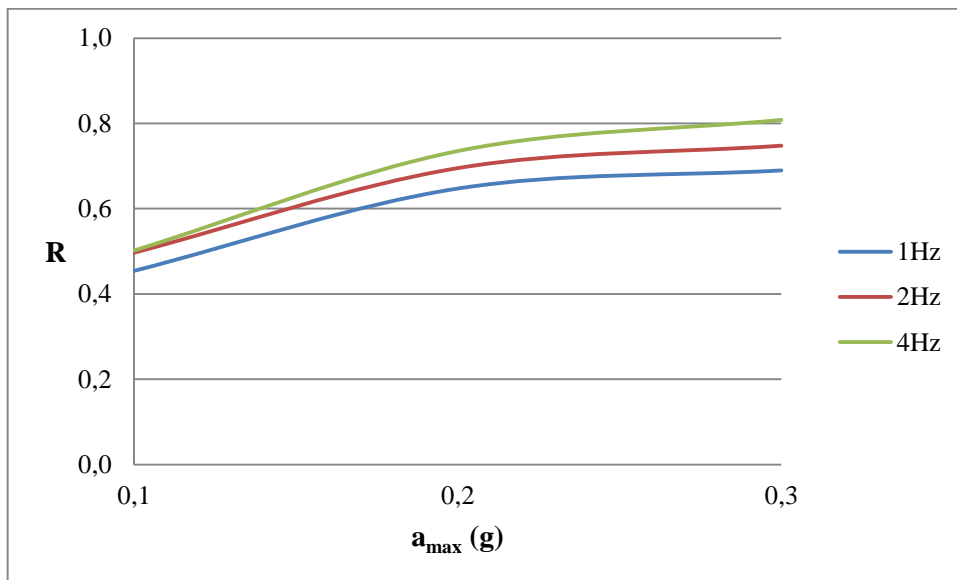
Fig. G.18 Response spectra for R3_0.3 motion (D = 5%)

APPENDIX H

REDUCTIONS IN MID-STOREY ACCELERATIONS FOR 5-STOREY MODEL

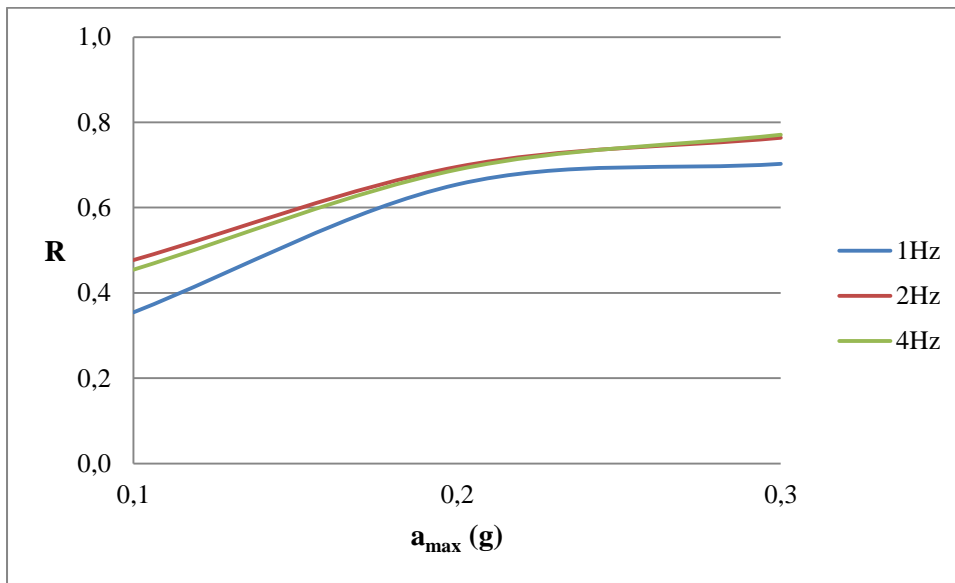


a. "R" for second storey

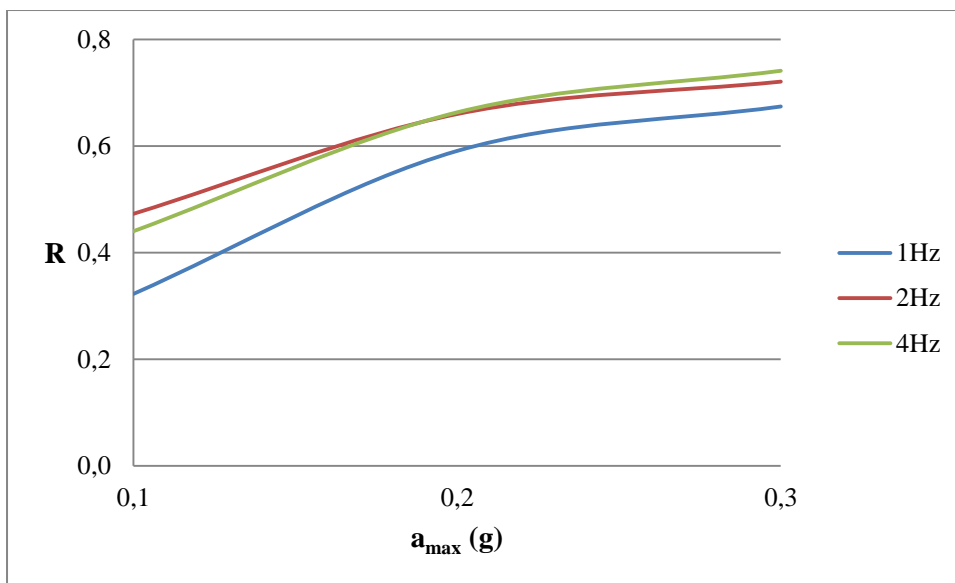


b. "R" for third storey

Fig. H.1 Acceleration reductions (R) in mid-storeys for S1, S2 and S3 motions

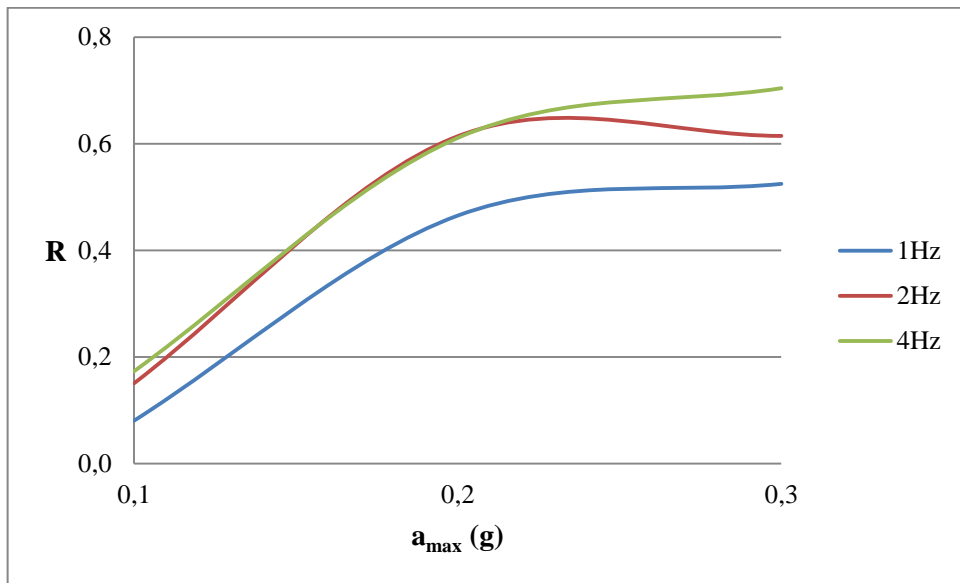


c. "R" for fourth storey

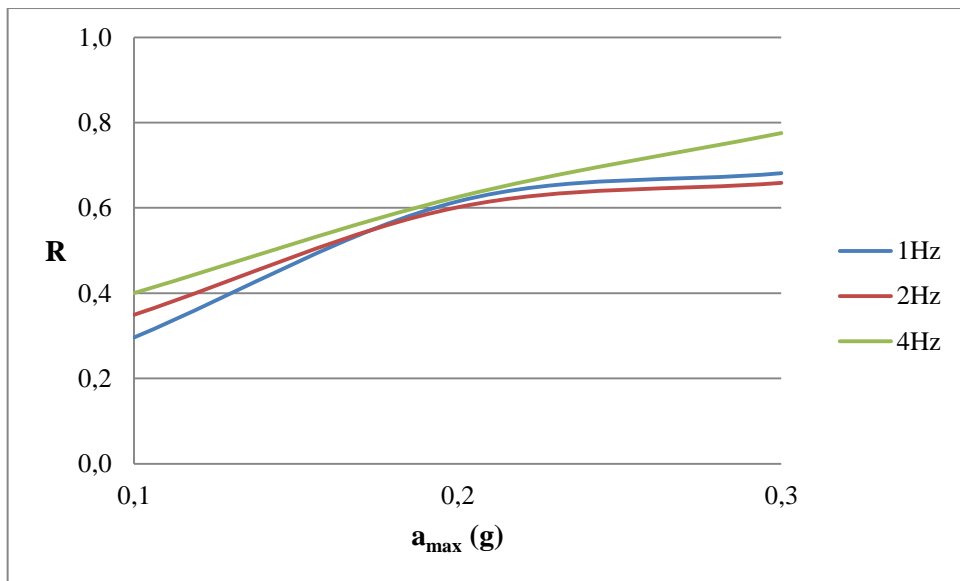


d. "R" for fifth storey

Fig. H.1 Acceleration reductions (R) in mid-storeys for S1, S2 and S3 motions (continued)

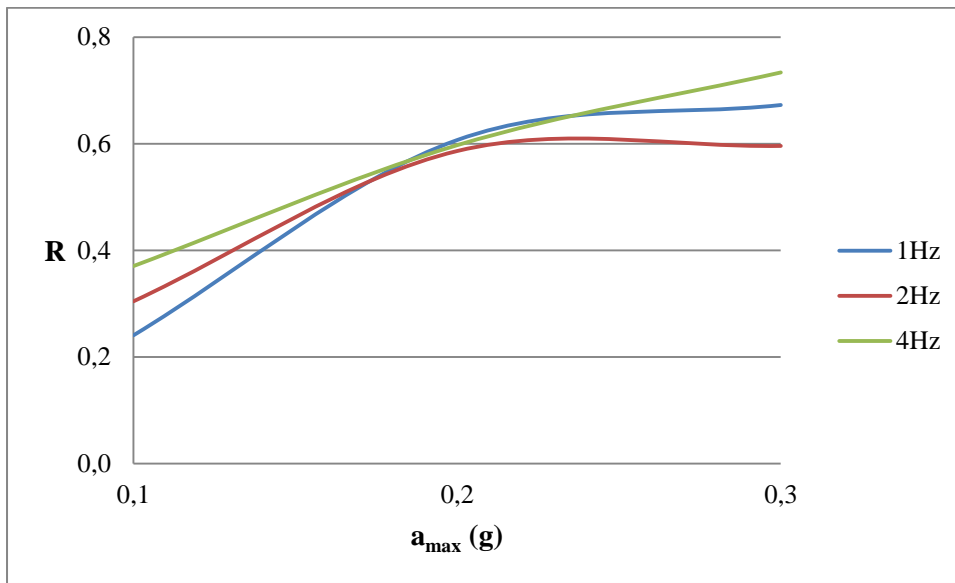


a. "R" for second storey

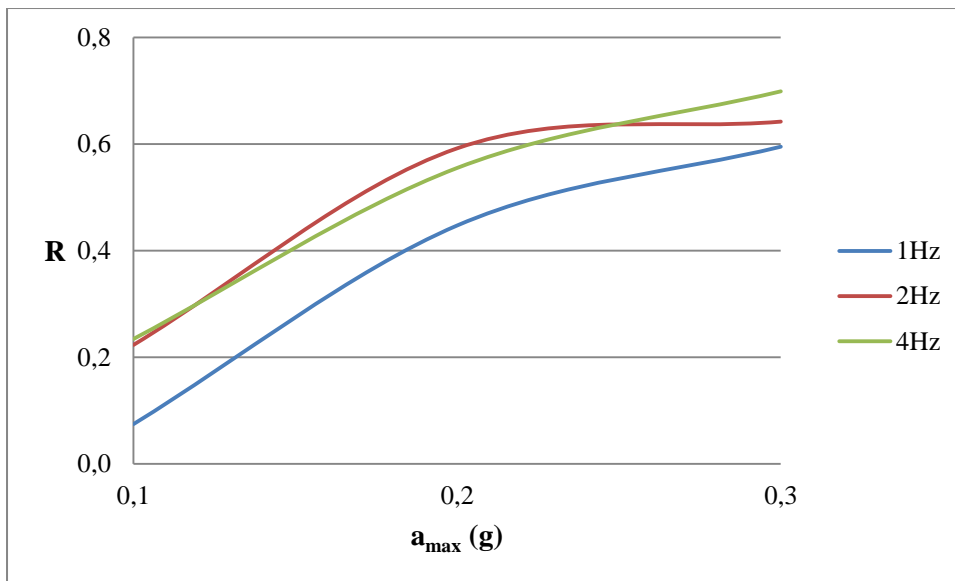


b. "R" for third storey

Fig. H.2 Acceleraton reductions (R) in mid-storeys for R1, R2 and R3 motions



c. "R" for fourth storey

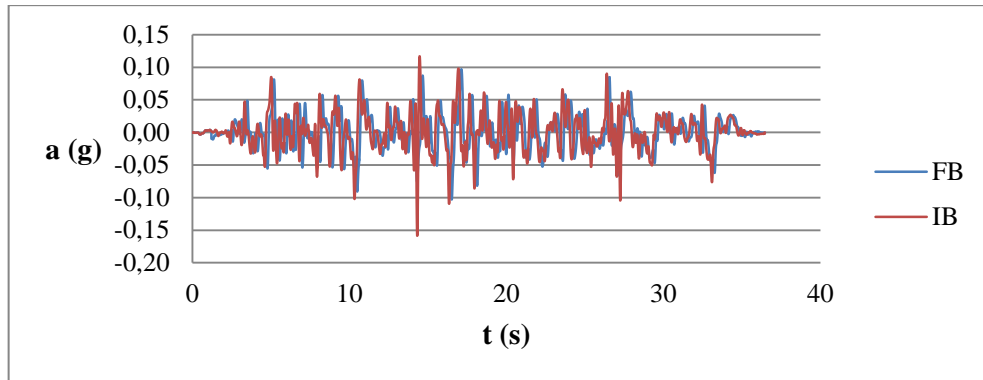


d. "R" for fifth storey

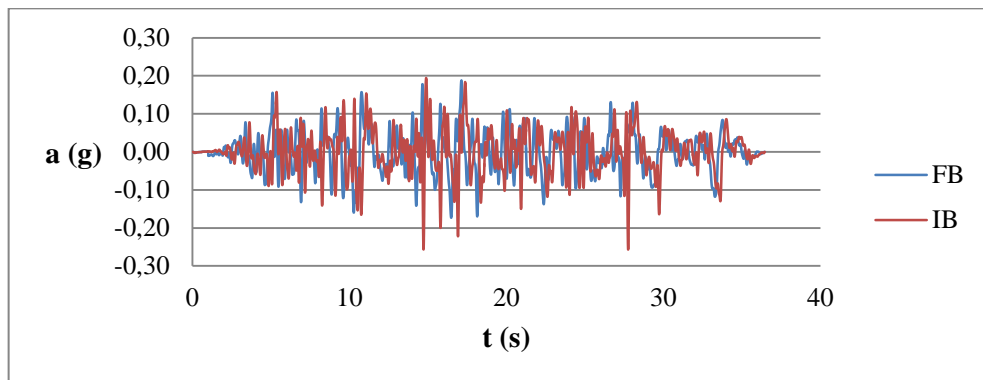
Fig. H.2 Acceleraton reductions (R) in mid-storeys for R1, R2 and R3 motions (continued)

APPENDIX I

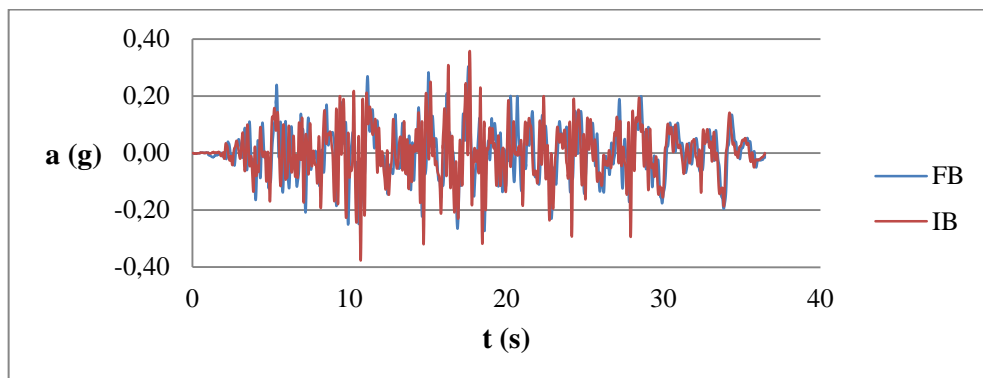
ACCELERATION TIME HISTORIES FOR BASE OF 5-STOREY MODEL
FOR "FB" AND "IB" CONDITIONS



a. $a_{\max} = 0.1g$

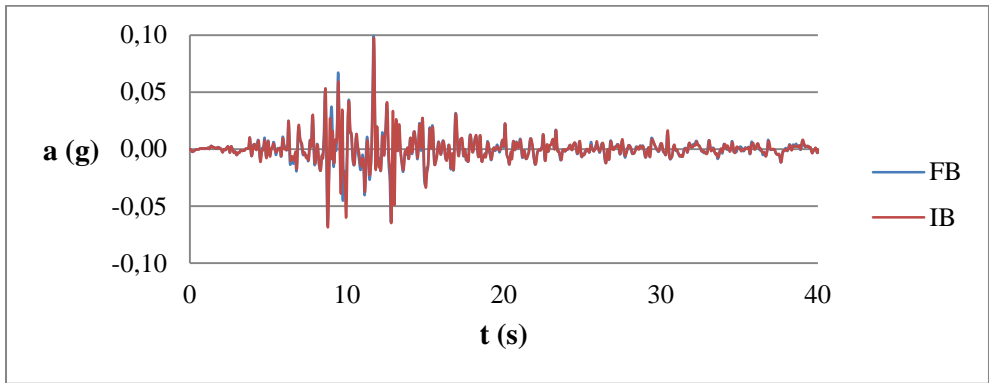


b. $a_{\max} = 0.2g$

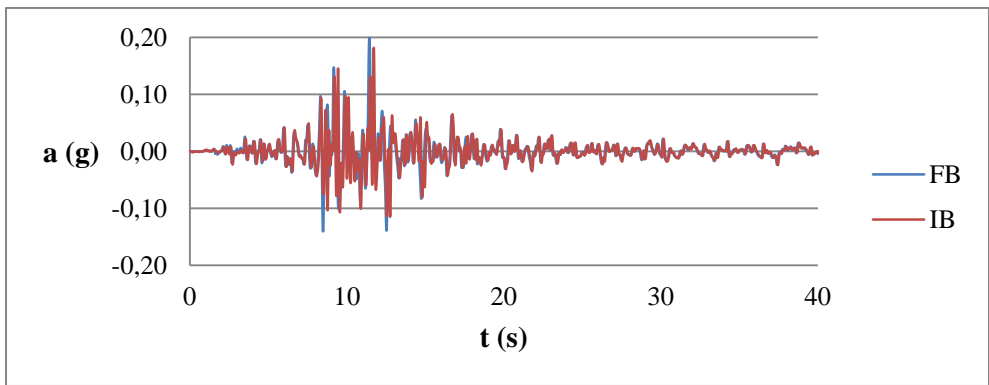


c. $a_{\max} = 0.3g$

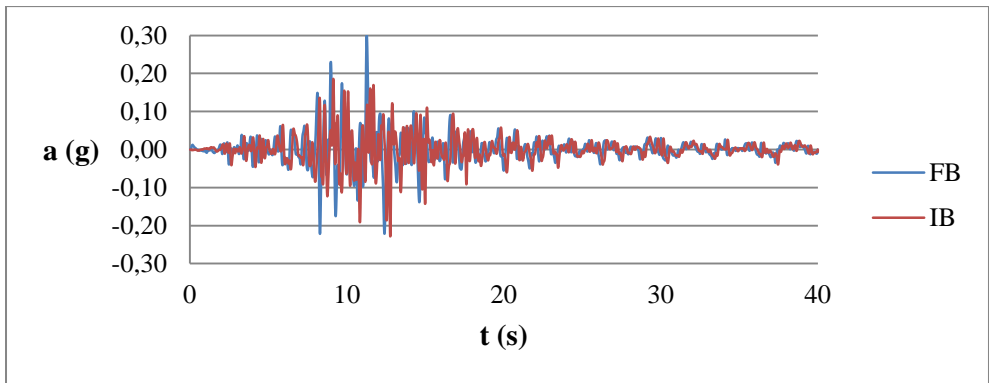
Fig. I.1 Acceleration-time histories for tests under S1 motion



a. $a_{\max} = 0.1g$

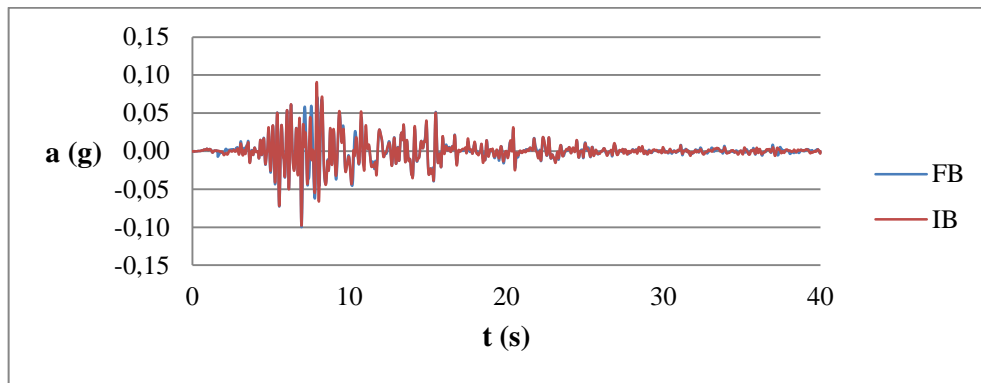


b. $a_{\max} = 0.2g$

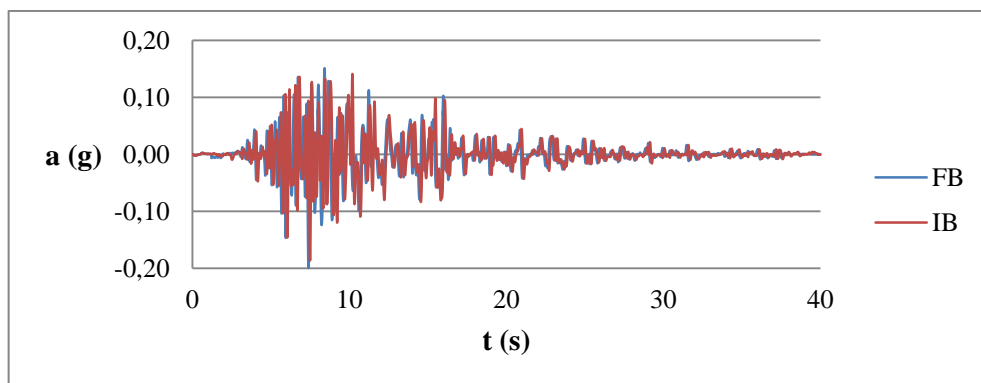


c. $a_{\max} = 0.3g$

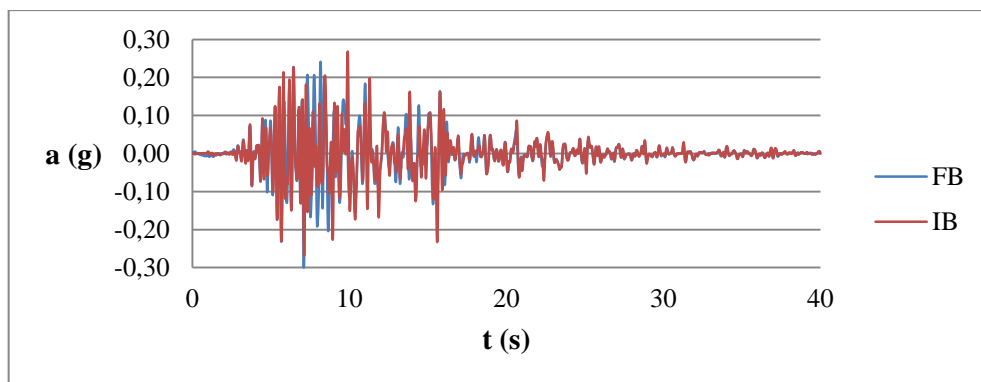
Fig. I.2 Acceleration-time histories for tests under S2 motion



a. $a_{\max} = 0.1g$

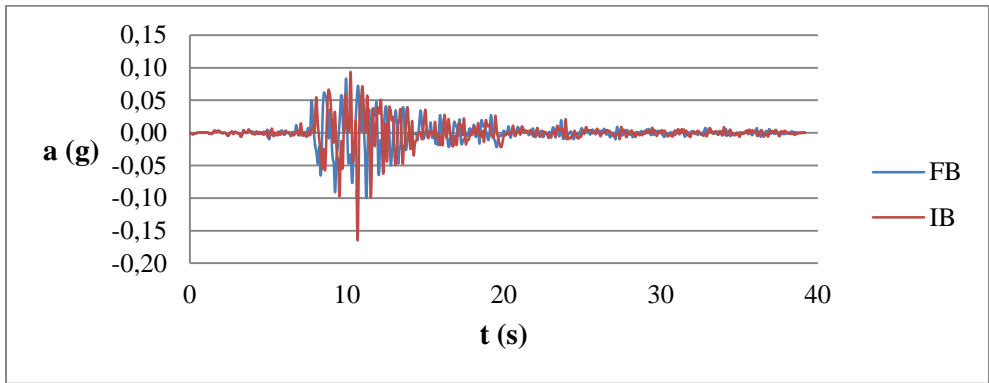


b. $a_{\max} = 0.2g$

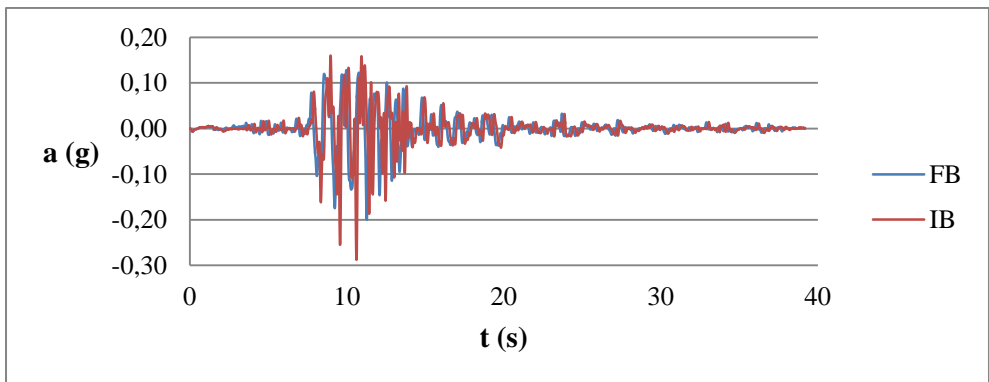


c. $a_{\max} = 0.3g$

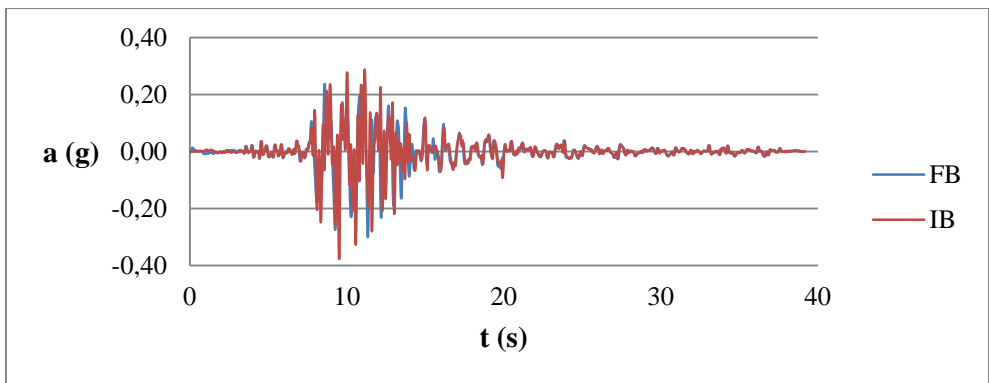
Fig. I.3 Acceleration-time histories for tests under S3 motion



a. $a_{\max} = 0.1g$

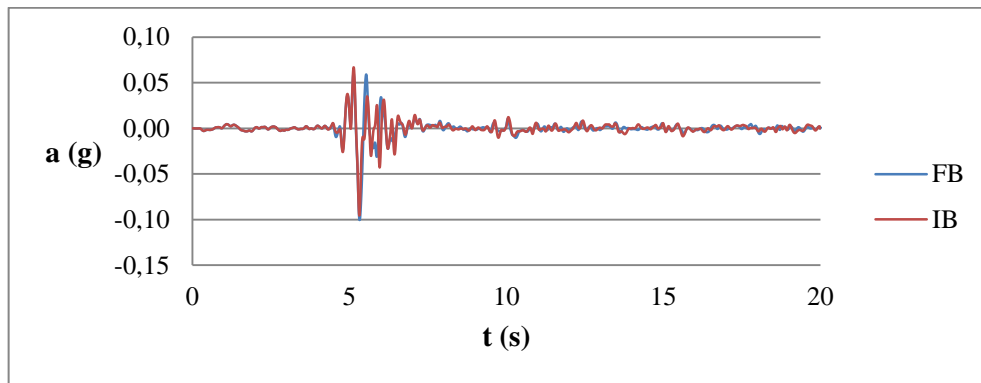


b. $a_{\max} = 0.2g$

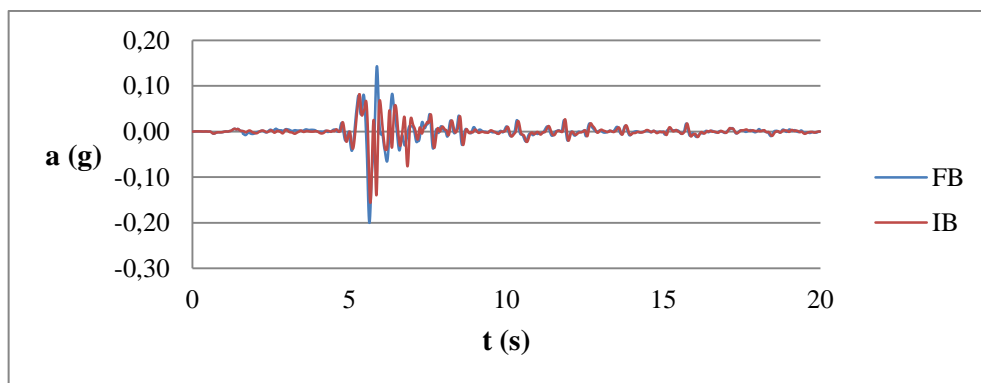


c. $a_{\max} = 0.3g$

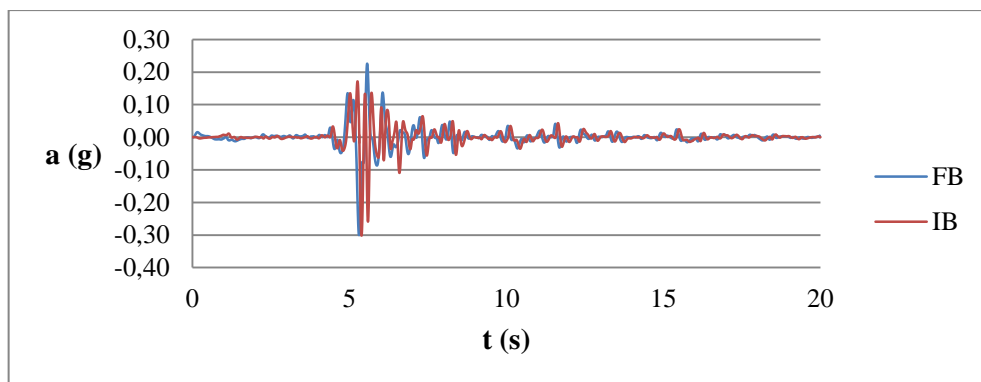
Fig. I.4 Acceleration-time histories for tests under R1 motion



a. $a_{\max} = 0.1g$

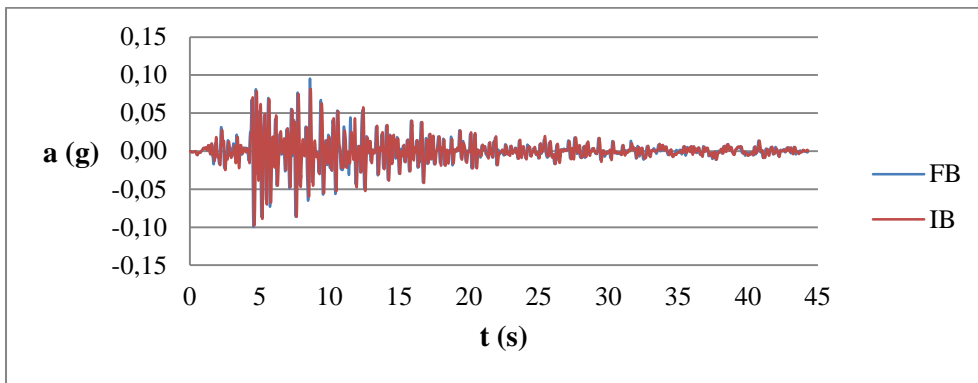


b. $a_{\max} = 0.2g$

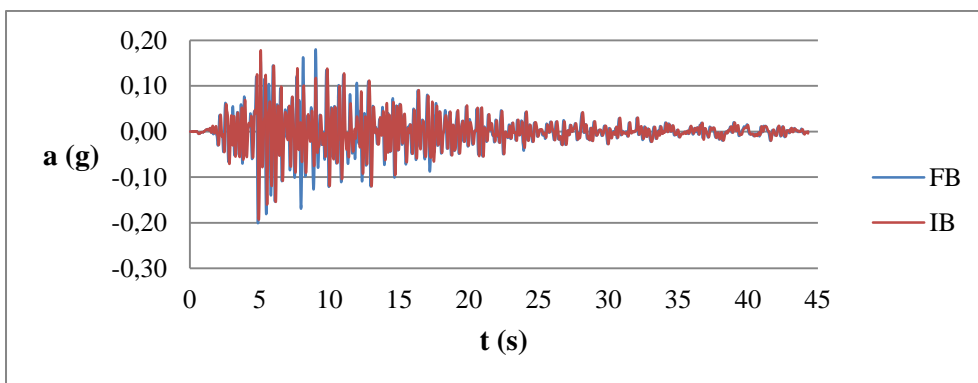


c. $a_{\max} = 0.3g$

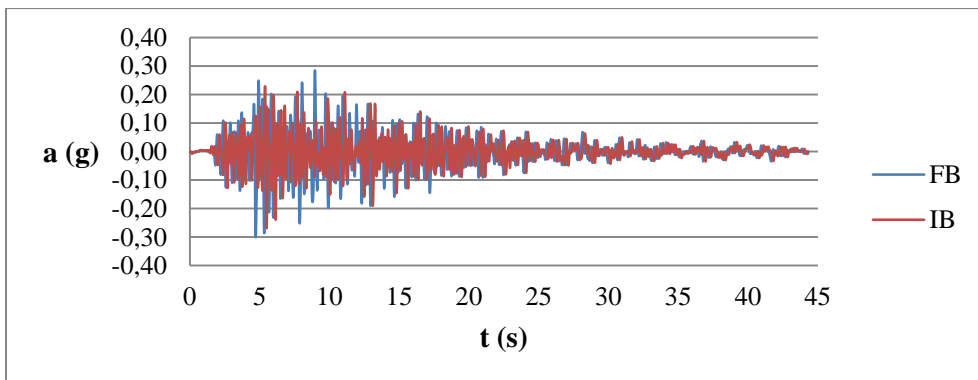
Fig. I.5 Acceleration-time histories for tests under R2 motion



a. $a_{\max} = 0,1g$



b. $a_{\max} = 0,2g$



c. $a_{\max} = 0,3g$

Fig. I.6 Acceleration-time histories for tests under R3 motion

APPENDIX J

RESPONSE SPECTRA FOR 5-STOUREY MODEL UNDER D = 5% DAMPING

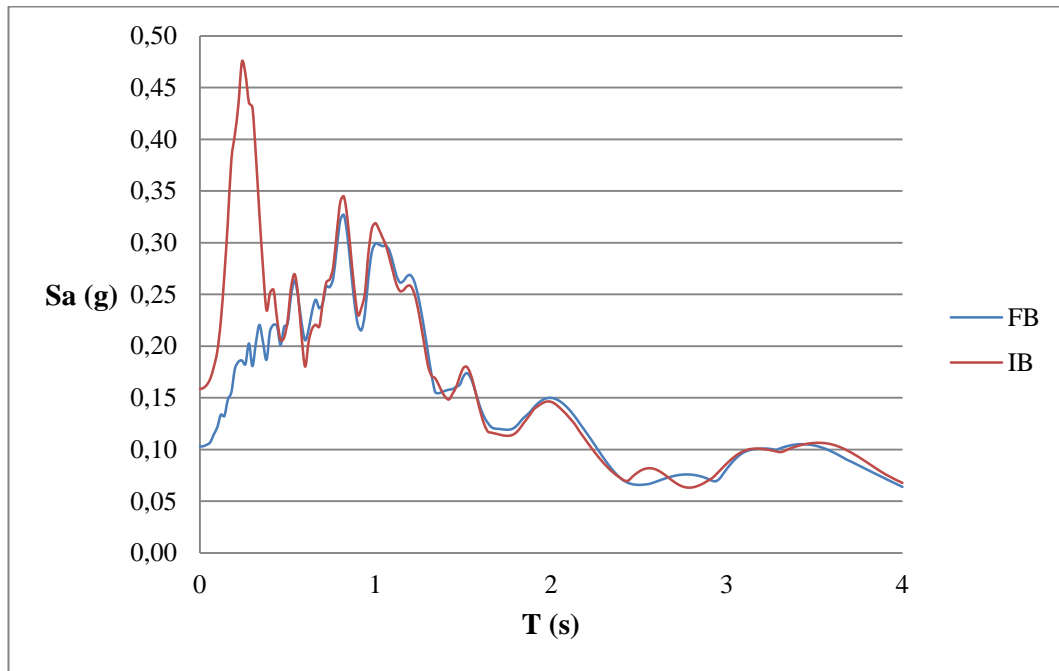


Fig. J.1 Response spectra for S1_0.1 motion (D = 5%)

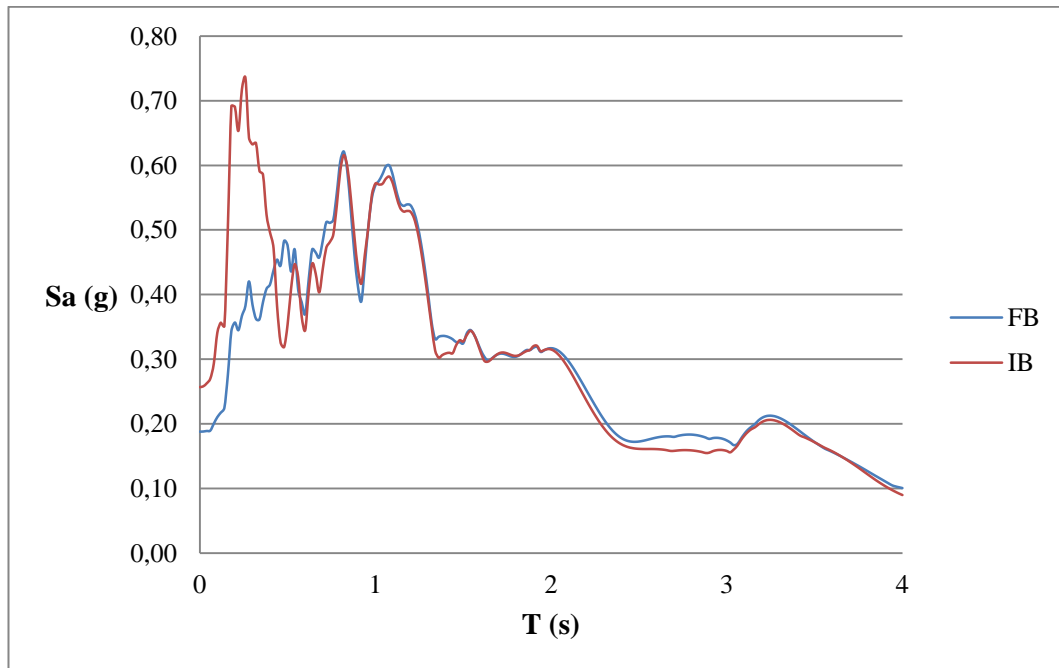


Fig. J.2 Response spectra for S1_0.2 motion (D = 5%)

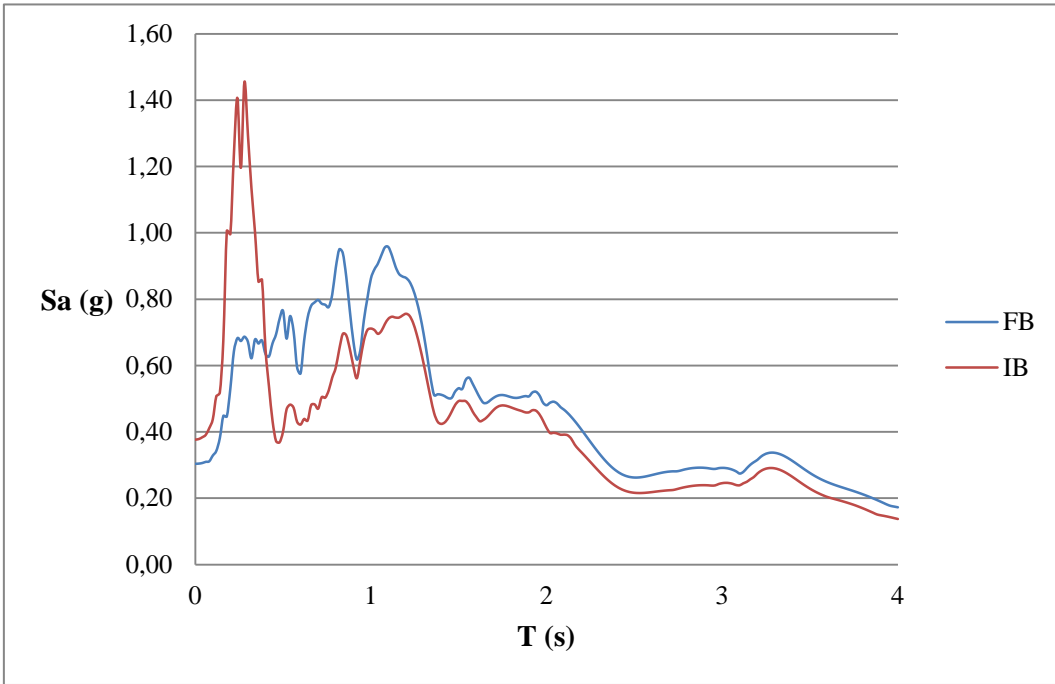


Fig. J.3 Response spectra for S1_0.3 motion (D = 5%)

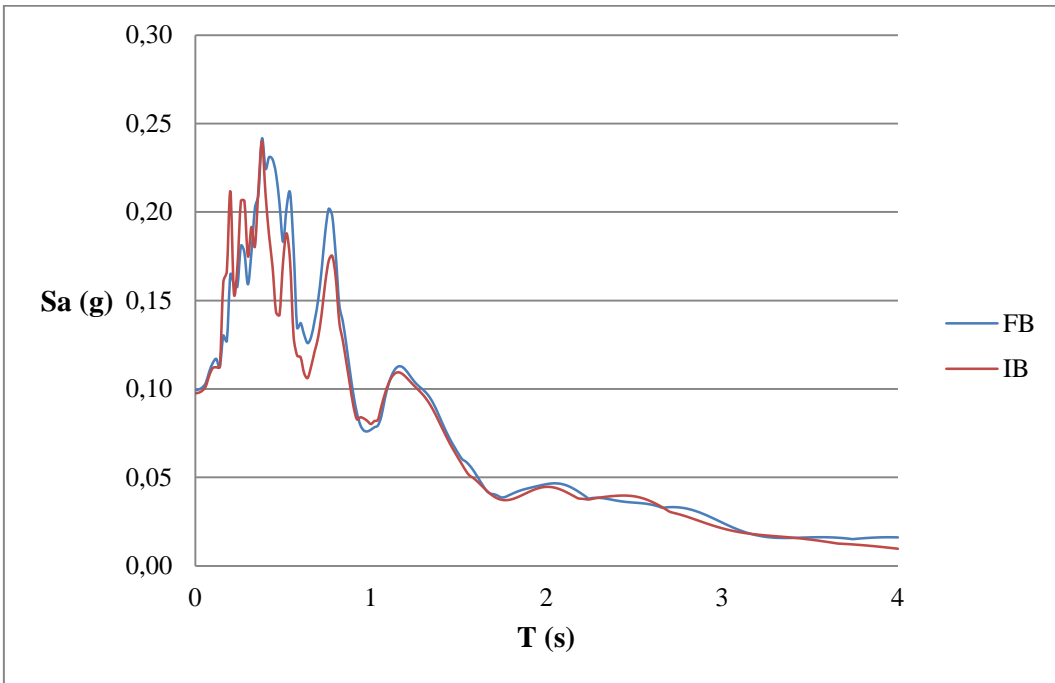


Fig. J.4 Response spectra for S2_0.1 motion (D = 5%)

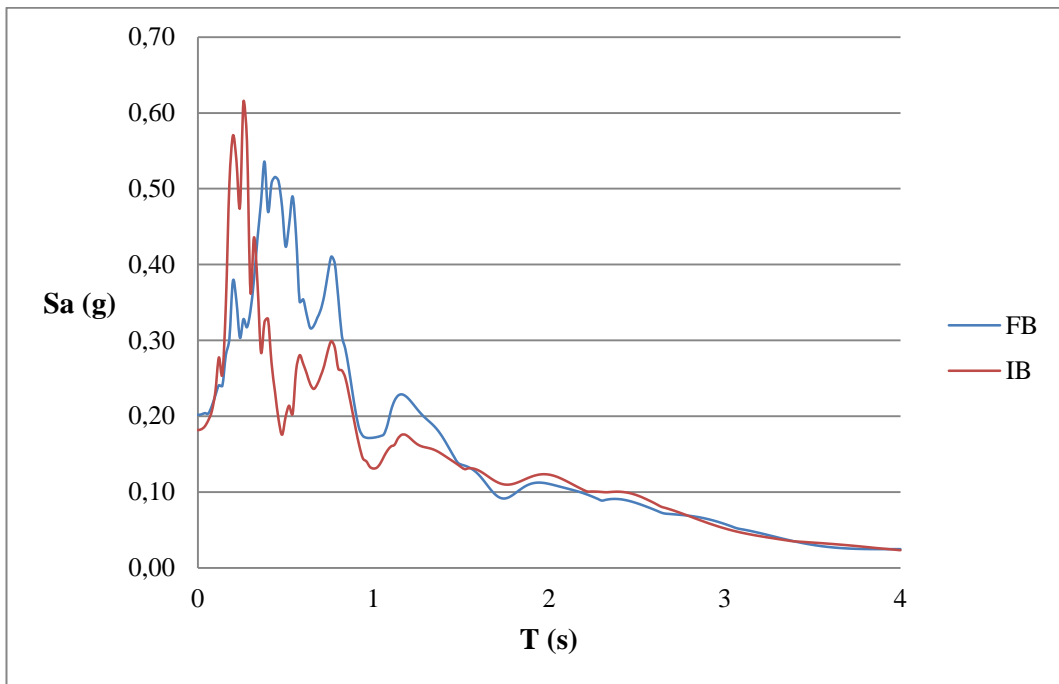


Fig. J.5 Response spectra for S2_0.2 motion (D = 5%)

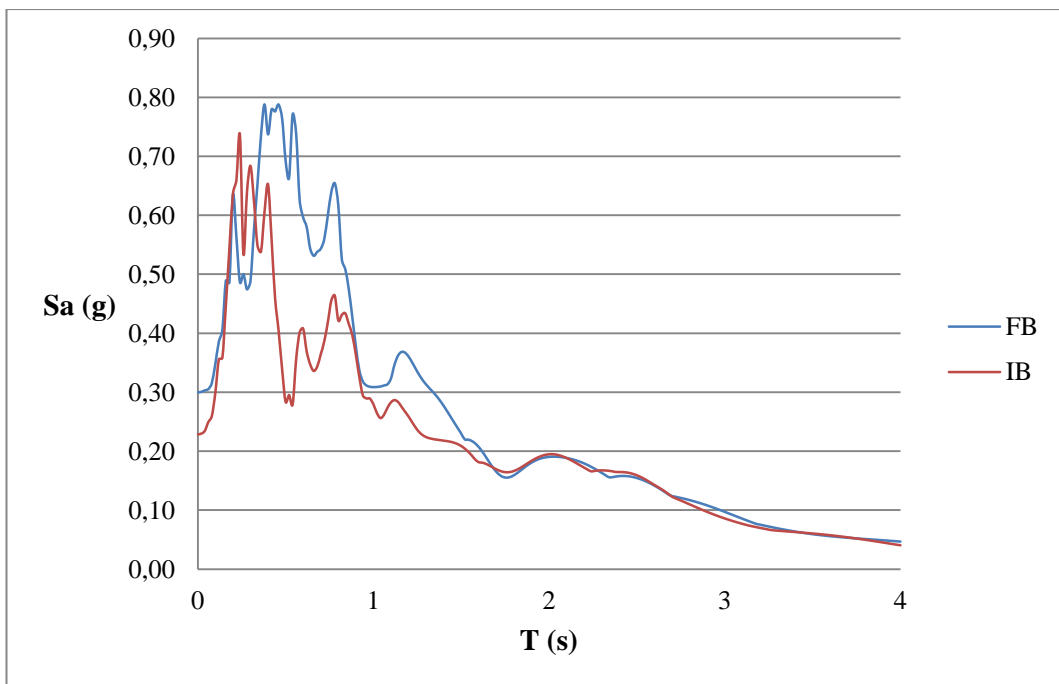


Fig. J.6 Response spectra for S2_0.3 motion (D = 5%)

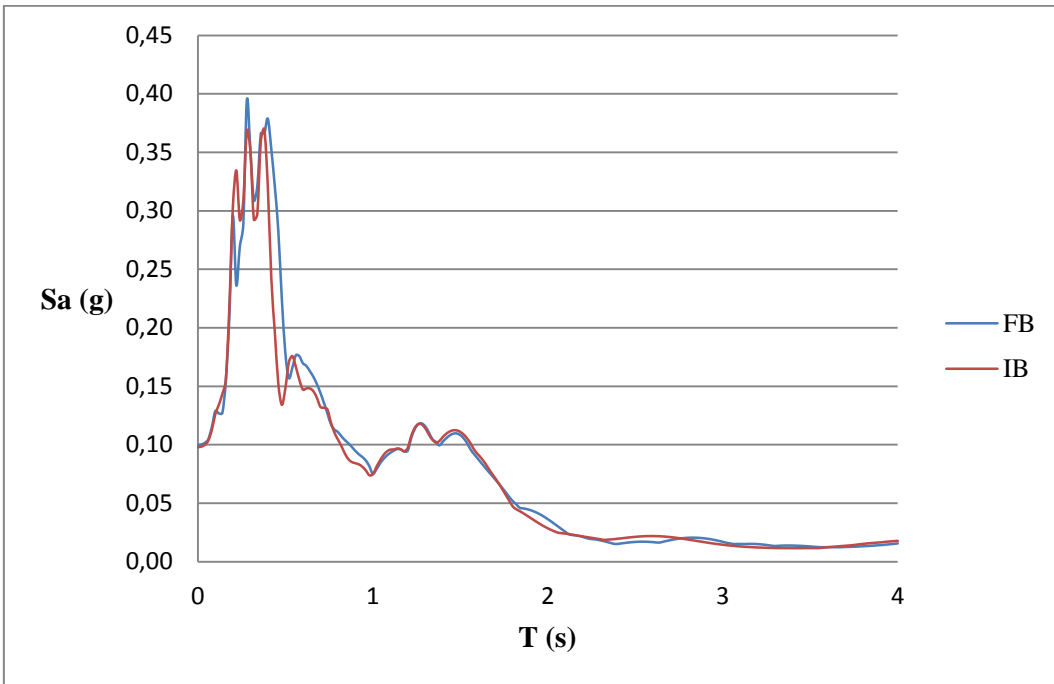


Fig. J.7 Response spectra for S3_0.1 motion (D = 5%)

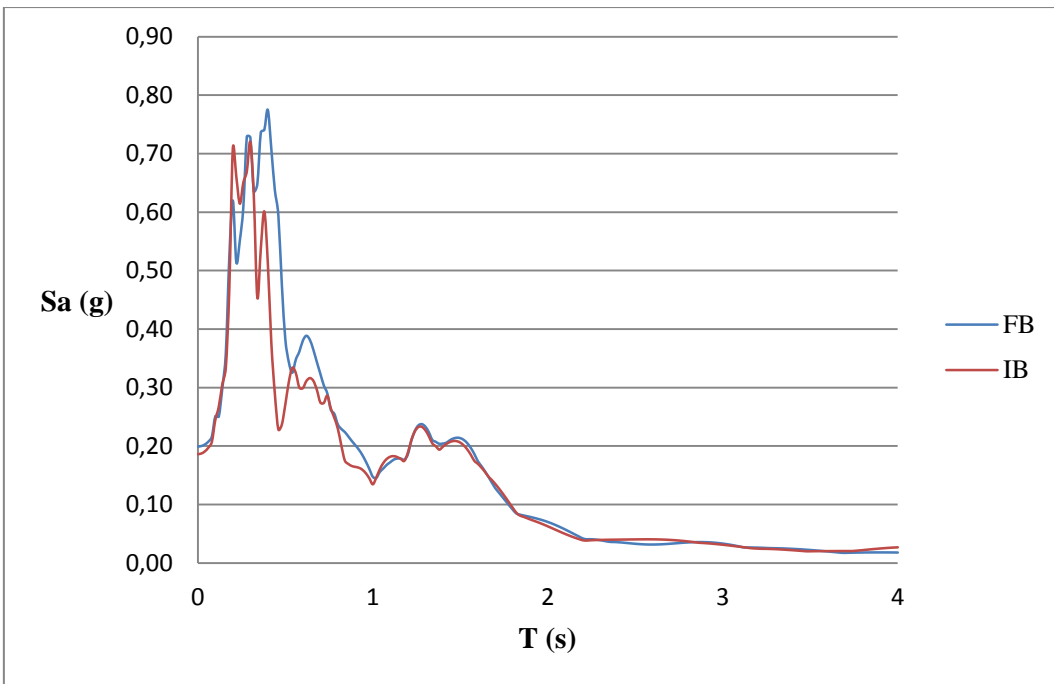


Fig. J.8 Response spectra for S3_0.2 motion (D = 5%)

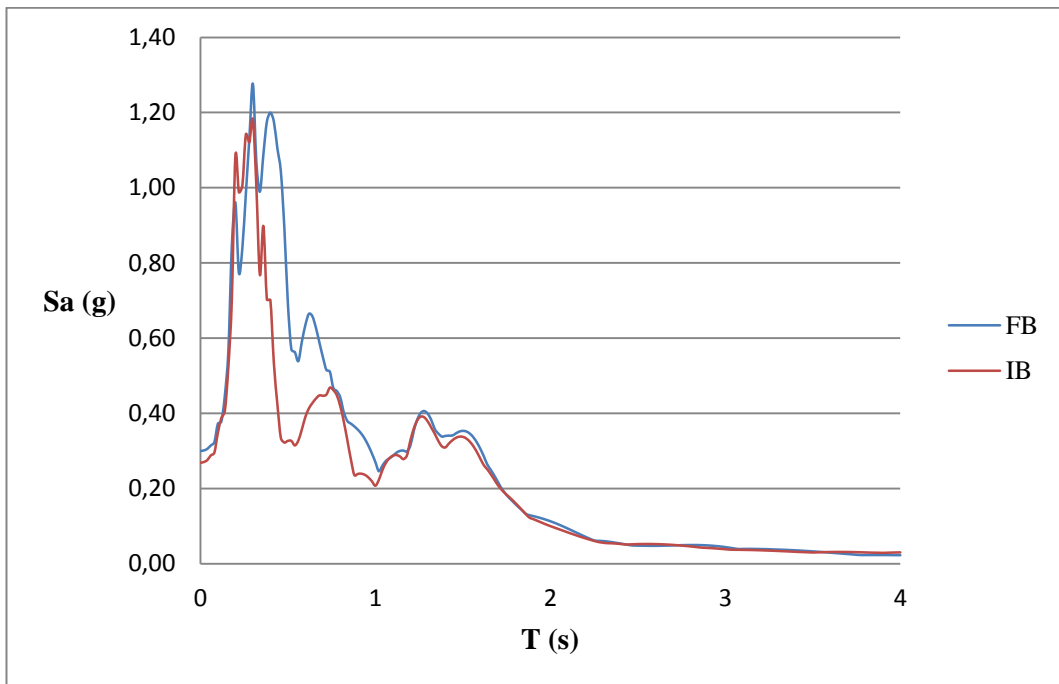


Fig. J.9 Response spectra for S3_0.3 motion (D = 5%)

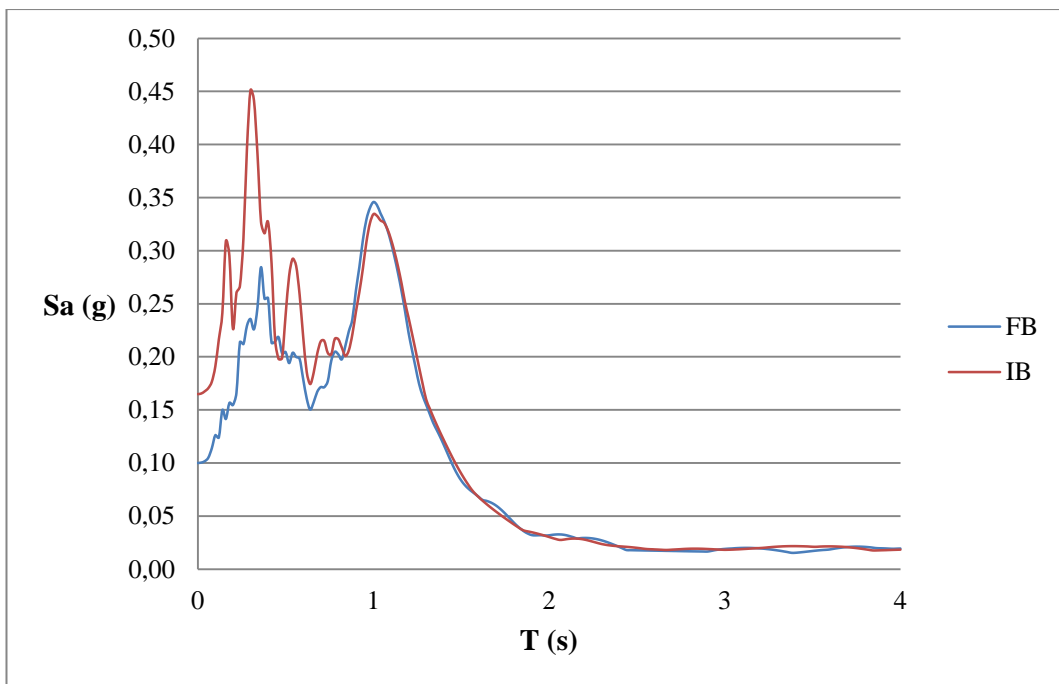


Fig. J.10 Response spectra for R1_0.1 motion (D = 5%)

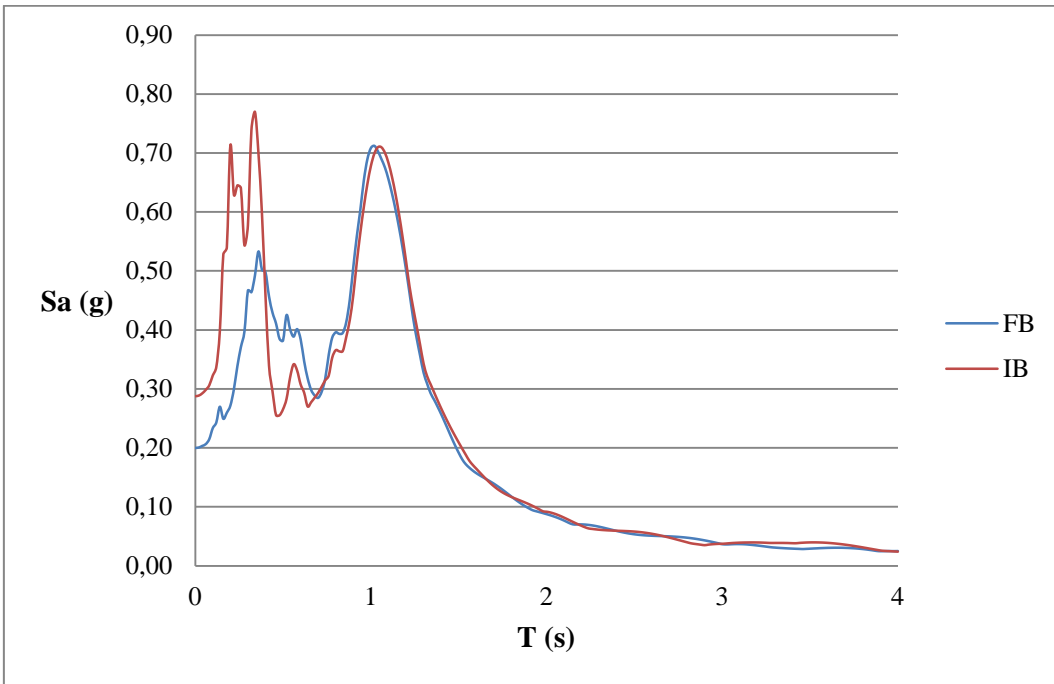


Fig. J.11 Response spectra for R1_0.2 motion (D = 5%)

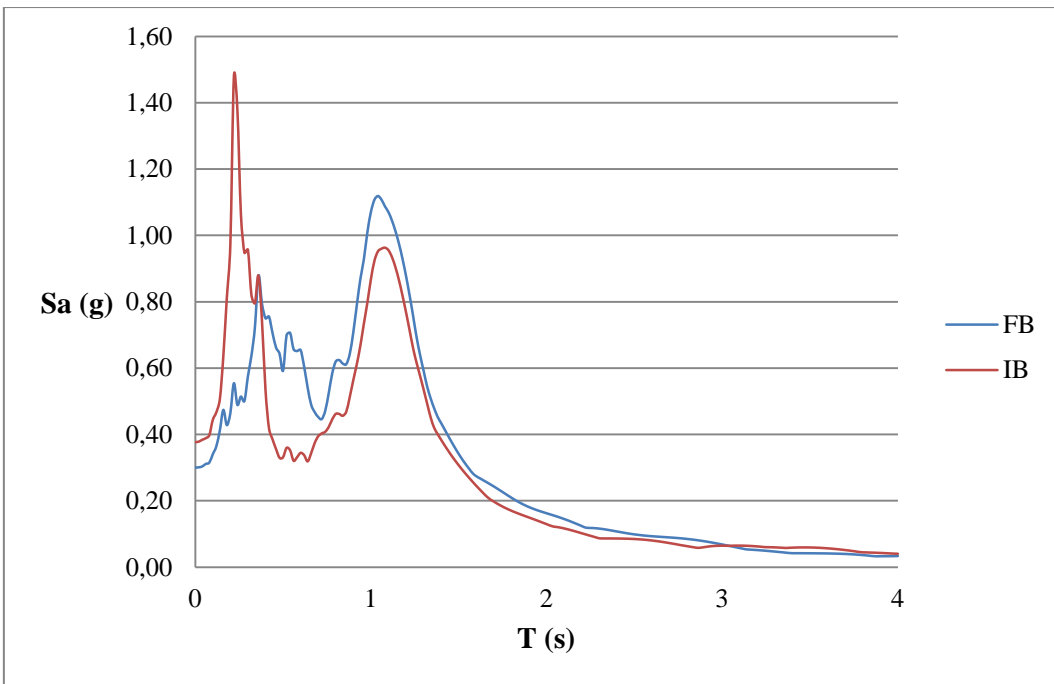


Fig. J.12 Response spectra for R1_0.3 motion (D = 5%)

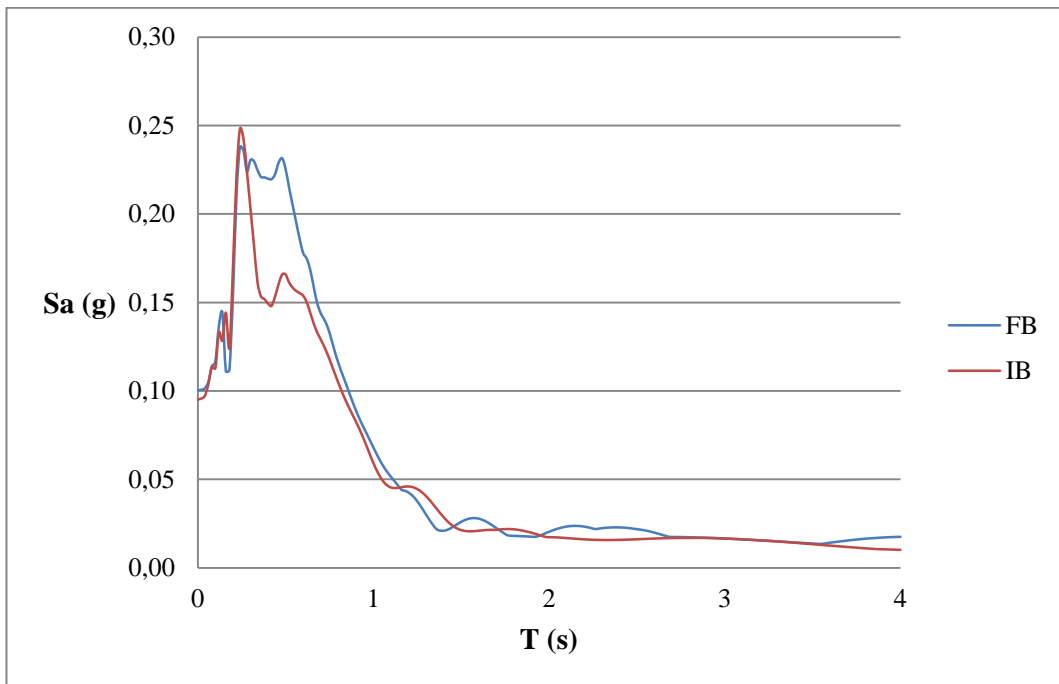


Fig. J.13 Response spectra for R2_0.1 motion (D = 5%)

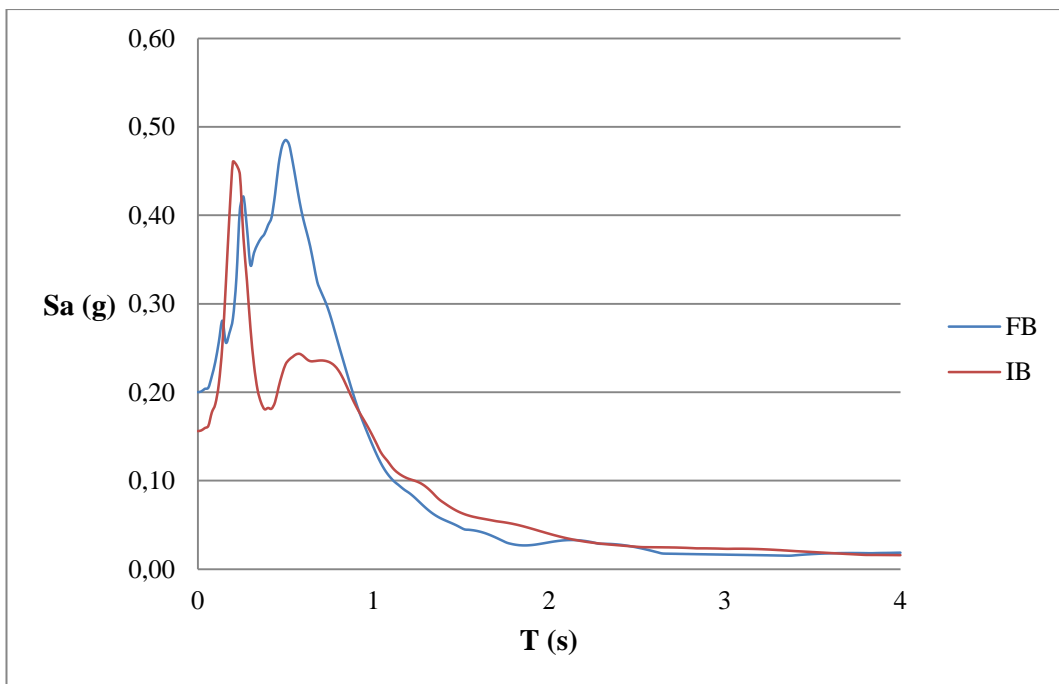


Fig. J.14 Response spectra for R2_0.2 motion (D = 5%)

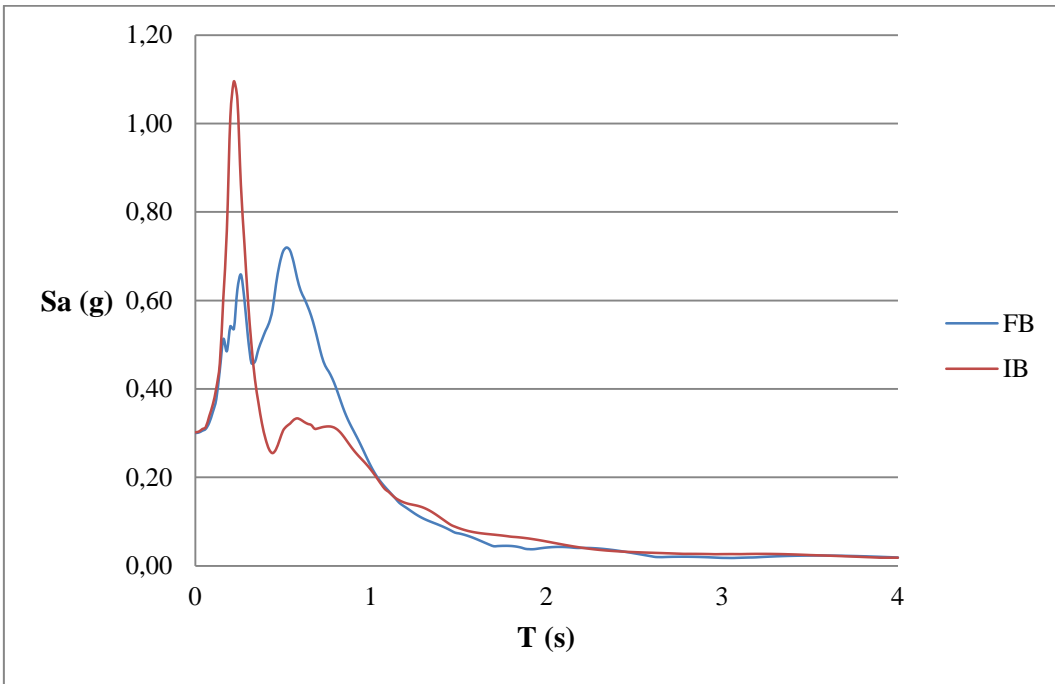


Fig. J.15 Response spectra for R2_0.3 motion (D = 5%)

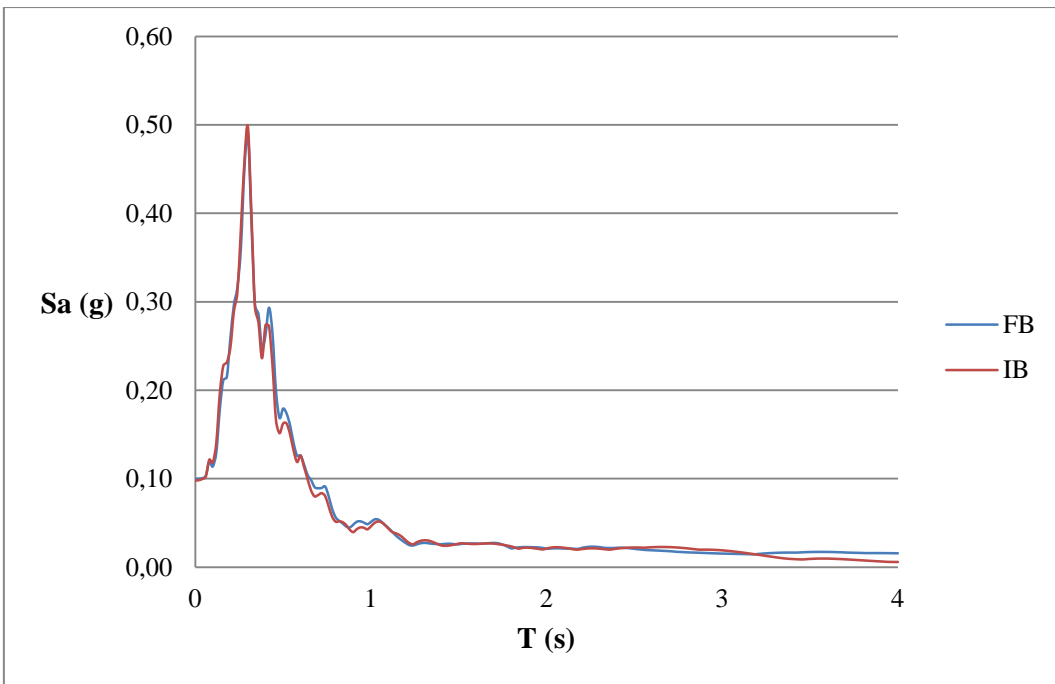


Fig. J.16 Response spectra for R3_0.1 motion (D = 5%)

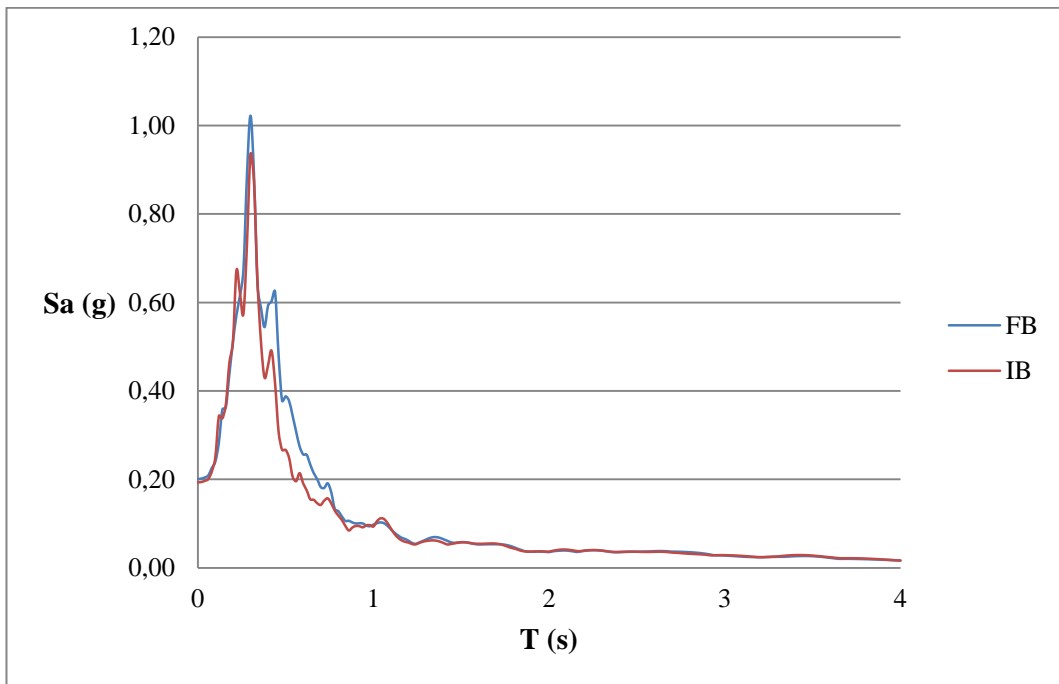


Fig. J.17 Response spectra for R3_0.2 motion (D = 5%)

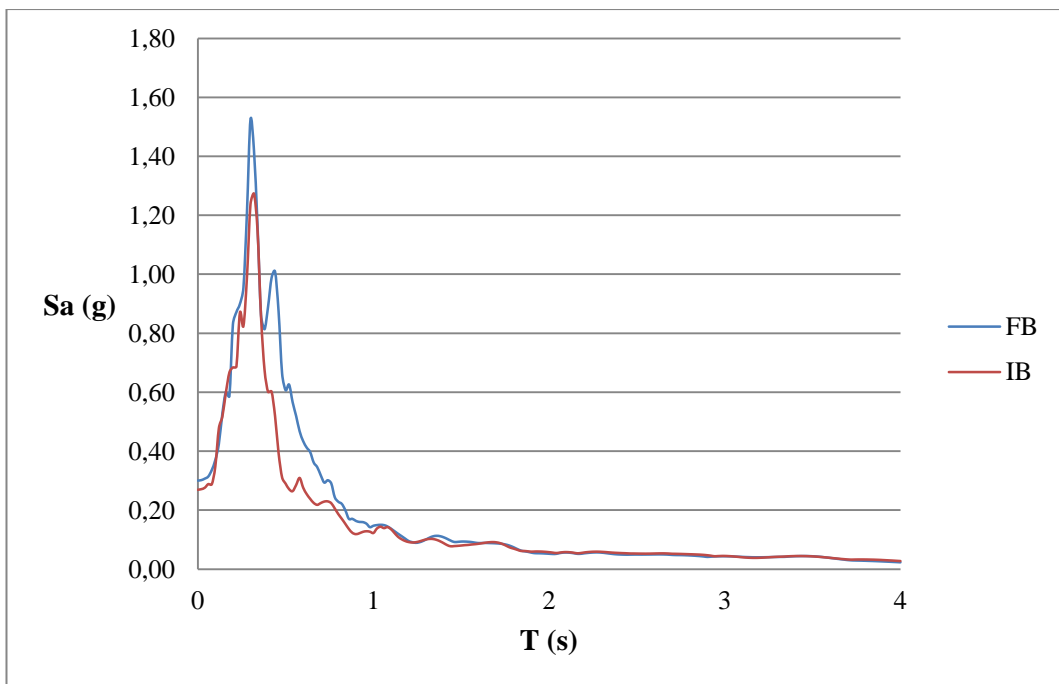


Fig. J.18 Response spectra for R3_0.3 motion (D = 5%)

CURRICULUM VITAE

PERSONAL INFORMATION

Surname, Name: Kalpakcı, Volkan
Nationality: Turkish (TC)
Date and Place of Birth: 28 July 1984, Konya
Phone: +90 312 210 54 69
Fax: +90 312 210 54 01
Mobile: +90 532 473 68 26
e-mail: kvolkan@metu.edu.tr

EDUCATION

Degree	Institution	Year of Graduation
MS	METU Civil Engineering	2009
BS	METU Civil Engineering	2007
High School	Karatay Anatolian High School, Konya	2002

WORK EXPERIENCE

Year	Place	Enrollment
2009 – present	METU Department of Civil Engineering	Research Assistant

FOREIGN LANGUAGES

Advanced English, Fluent German

PUBLICATIONS

1. Kalpakcı, V., and Ozkan, M.Y. (2012). A simplified approach to the settlement estimation of piled rafts. *Acta Geotechnica Slovenica*, Vol.9, 77 – 85.

HOBBIES

Classical Turkish Music, Playing Lavta and Baglama, Motor Sports